

2011

Seismic Performance Evaluation and Effective Design of Precast Concrete Diaphragm Connections

Ruirui Ren
Lehigh University

Follow this and additional works at: <http://preserve.lehigh.edu/etd>

Recommended Citation

Ren, Ruirui, "Seismic Performance Evaluation and Effective Design of Precast Concrete Diaphragm Connections" (2011). *Theses and Dissertations*. Paper 1307.

This Dissertation is brought to you for free and open access by Lehigh Preserve. It has been accepted for inclusion in Theses and Dissertations by an authorized administrator of Lehigh Preserve. For more information, please contact preserve@lehigh.edu.

**Seismic Performance Evaluation and Effective Design of
Precast Concrete Diaphragm Connections**

by

Ruirui Ren

A Dissertation

Presented to the Graduate Research Committee

of Lehigh University

in Candidacy for the Degree

of Doctor of Philosophy

in

Structural Engineering

Lehigh University

Bethlehem, PA

September 2011

Approved and recommended for acceptance as a dissertation in partial fulfillment of the requirements for the degree of Doctor of Philosophy.

Date

Dr. Clay J. Naito
Dissertation Advisor

Accepted Date

Committee Members:

Dr. Richard Sause
Committee Chairman

Dr. James M. Ricles
Committee Member

Dr. Shamim N. Pakzad
Committee Member

Dr. Robert B. Fleischman
External Committee Member

Acknowledgements

This research presented here served as the doctoral dissertation of the author, under supervision of the doctoral committee. The study is part of a multi-university project supported by National Science Foundation (NSF), the Precast/Prestressed Concrete Institute (PCI), the Pennsylvania Infrastructure Technology and the contributions of the Charles Pankow Foundation, JVI, and the Meadow Burke Co.

The author would like to thank Dr. Clay J. Naito, the dissertation advisor, for his invaluable attention, guidance, encouragement, and support throughout her graduate studies, and Dr. Richard Sause, the committee chairman, for his constructive advices on the research direction. The author would like to extend great appreciations to Dr. Robert B. Fleischman for establishing a clear objective and organizing research activities throughout the project term, Dr. James Ricles and Dr. Shamim Pakzad for their technical advice, comments and support during this study. A special thank you is extended to the DSDM advisory board for their review and consultation and the graduate students working on the project, Dr. Liling Cao and Dr. Dichuan Zhang for their assistance and help.

The author would like to express her sincere thanks to John Hoffner, Roger Moyer, Carl Bowman, Thomas Marullo and Adam Kline for their help and contributions

throughout the three years experimental program. Suggestions provided by Dr. Ben T. Yen and the computer technical support provided by Peter Bryan are greatly appreciated.

The author would like to thank her ATLSS fellows for their friendship and generous help over the years.

The author would like to express her gratitude to her family for their love, warm support and encouragement. A special thank you goes out to her fiancé Zhipeng, for his love, understanding, encouragement and support.

Table of Contents

Acknowledgements.....	iii
Table of Contents	v
List of Figures	xiii
List of Tables	xxiii
Abstract.....	1
Chapter 1 Introduction	4
1.1 Overview	4
1.2 Research Objectives and Scope.....	9
1.3 Organization of Dissertation	12
1.4 References	14
Chapter 2 Background	16
2.1 Precast Concrete Diaphragm Floor Systems	16
2.1.1 Precast Hollow Core Floor Systems	17
2.1.2 Precast Double Tee (DT) Floor Systems	20

2.2	Precast Concrete Double-tee Diaphragm Connections	22
2.2.1	Chord Connection	23
2.2.2	Web Connection	24
2.2.3	Collector/Anchorage Reinforcement Details.....	26
2.3	Current Seismic Design Method of Precast Concrete Diaphragm	27
2.3.1	Diaphragm Seismic Design Force	28
2.3.2	Diaphragm Connection Details Design	31
2.4	Recent Diaphragm Seismic Behavior Research	33
2.4.1	Diaphragm Performance in 1994 Northridge Earthquake	33
2.4.2	Previous Research on Seismic Behavior of Diaphragm System	36
2.4.3	Previous Research on Seismic Behavior of Diaphragm Connection.....	37
2.5	New Proposed Diaphragm Seismic Design Methodology	38
2.5.1	Basic Design Option	40
2.5.2	Elastic Design Option	41
2.5.3	Relaxed Design Option.....	42
2.6	References	43
Chapter 3 An Evaluation Method for Precast Concrete Diaphragm Connectors Based on		
	Structural Testing.....	47
3.1	Background	48
3.1.1	Simplified Analytical Approaches.....	49
3.1.2	Existing Experimental Methods	52

3.2 Proposed Evaluation Method for Precast Concrete Diaphragm Connections Based on Structural Testing.....	58
3.2.1 Scope.....	59
3.2.2 Test Module	59
3.2.3 Test Setup	61
3.2.4 Instrumentation	61
3.2.5 Loading Protocols	62
3.2.6 Tension Tests	71
3.2.7 Shear Tests	71
3.2.8 Testing Observations and Acquisition of Data.....	72
3.2.9 Backbone Approximation.....	73
3.2.10 Data Reduction	78
3.2.11 Multiple Tests Approach	80
3.2.12 Test Report.....	81
3.3 Summary	83
3.4 References	83
Chapter 4 Experimental Studies of Improved Double Tee Connections	87
4.1 Subassembly Details.....	87
4.2 Ductile Connection Specimens	88
4.2.1 Ductile Ladder Connector.....	90
4.2.2 Ductile Ladder with Hairpin Connector	91
4.2.3 Carbon Dry Chord Connector.....	92

4.2.4	Stainless Dry Chord Connector	92
4.3	Material Properties	93
4.4	Test Setup	95
4.5	Loading Protocols.....	96
4.6	Test Matrix	97
4.7	Experimental Tension Behavior	98
4.7.1	Experimental Tension Results	98
4.7.2	Comparative Tension Behavior	98
4.8	Experimental Shear Behavior.....	114
4.8.1	Experimental Shear Results	115
4.8.2	Comparative Shear Behavior	120
4.9	References	144
Chapter 5 Database of Precast Diaphragm Connections		145
5.1	Precast DT Connection Details Database.....	146
5.1.1	Database of Connection Details in Previous Research.....	148
5.1.2	Connection Details Database Extension.....	150
5.2	Connection Performance Database	151
5.2.1	Previous Connection Performance Database	152

5.2.2	Discussion on Previous Connection Performance Database	155
5.2.3	New Developed Comprehensive Connection Performance Database	157
5.2.4	Performance Database Usage	160
5.3	References	167
Chapter 6 Response Estimation Approach of Diaphragm System based on Performance		
	Database	171
6.1	Precast DT Diaphragm Joint	171
6.2	Simplified Diaphragm Response Estimation Approach.....	172
6.2.1	Joint Flexure/Shear Response.....	176
6.2.2	Diaphragm Flexure/Shear Response.....	177
6.3	Numerical Examples	178
6.4	References	183
Chapter 7 Experimental Program of Precast Concrete Diaphragm Critical Joint with		
	Multiple Connections.....	184
7.1	Test Setup	185
7.2	Test Specimen	187
7.2.1	Scaling of Specimens.....	188
7.2.2	Flexure Joint Specimen Design	192
7.2.3	Shear Joint Specimen Design	195

7.3	Material Properties	196
7.4	PDH Test of Diaphragm Critical Flexural Joint.....	197
7.4.1	Instrumentation	198
7.4.2	Loading Control Algorithm	200
7.4.3	Flexure Joint Performance	202
7.5	Simplified Estimation of Joint Performance	206
7.6	Hybrid Test of Diaphragm Critical Shear Joint.....	207
7.6.1	Instrumentation	207
7.6.2	Control Algorithm	208
7.6.3	Shear Joint Performance	209
7.7	References	212
Chapter 8 Design and Development of Ductile Dry Chord Connection		214
8.1	Background	215
8.1.1	Experimental Performance of Conventional Dry Chord Connection.....	216
8.1.2	Performance Evaluation of Enhanced Dry Chord Connection.....	219
8.2	Design Concept	223
8.3	Design Goal.....	224
8.4	Design Detail.....	225

8.4.1	Standard Module.....	225
8.4.2	New Connection Layout.....	227
8.4.3	Design Details.....	228
8.5	Expected Performance.....	235
8.6	References	236
Chapter 9 Analytical Studies of New Proposed Precast Concrete Dry Chord Connection		
	238
9.1	Simplified Models	239
9.1.1	PCI Truss/Spring Model.....	239
9.1.2	DSDM Connection Model.....	240
9.1.3	Previous 2D FE Connection Model.....	242
9.2	3D FE Connection Model.....	243
9.2.1	Model Geometry.....	243
9.2.2	Material Models and Properties.....	247
9.2.3	Mesh and Elements.....	249
9.2.4	Interface Contact Modeling	251
9.2.5	Boundary and Loading Conditions.....	254
9.2.6	Iteration Methods.....	255
9.2.7	Analyses.....	256
9.3	Analytical Tension Behavior.....	257
9.3.1	Deformed Shape	259

9.3.2	Stress State.....	260
9.3.3	Global Force-displacement Performance	274
9.3.4	Discussion.....	276
9.3.5	Summary of Tension Behavior.....	279
9.4	Design Recommendation	281
9.5	References	282
Chapter 10 Conclusions and Future Work.....		283
10.1	Summary	283
10.2	Conclusions	288
10.3	Unique Contribution.....	297
10.4	Future Work	299
Vita.....		300

List of Figures

Figure 2.1. Precast hollow core planks	18
Figure 2.2. Precast hollow core planks with cast-in-place topping	18
Figure 2.3. Connection details for the precast hollow-core floor systems (PCI 2010).....	19
Figure 2.4. Embedded reinforcing bars across the joint (Cao 2006)	19
Figure 2.5. Serrated hollow-core slab edge profile (Menegotto and Monti 2005)	20
Figure 2.6. Precast DT Panel and A parking garage with DT floors (PCI 2010)	21
Figure 2.7. Precast topped and pre-topped DT Panel	21
Figure 2.8. Precast DT structural system (PCI 2010)	22
Figure 2.9. Reinforcements in a typical diaphragm system.....	23
Figure 2.10. Typical chord connection details.....	24
Figure 2.11. Typical web connection details	25
Figure 2.12. Continuous reinforcing bars in cast-in-place topping served as collectors ..	26
Figure 2.13. Flange connector welded to stud groups served as anchorage reinforcement	27

Figure 2.14. Threaded insert between pour strip and spandrel served as anchorage reinforcement	27
Figure 2.15. Equivalent lateral force demands	29
Figure 2.16. Analogous beam design of a diaphragm	32
Figure 2.17. Collapsed parking garage (Iverson and Hawkins 1994).....	34
Figure 2.18. Precast panels collapsed and structural walls remained intact	34
Figure 2.19. Diaphragm cracking and connection failure.....	35
Figure 2.20. Basic Design Option (Zhang 2010)	40
Figure 2.21. Elastic Design Option (Zhang 2010)	42
Figure 2.22. Relaxed Design Option (Zhang 2010)	43
Figure 3.1. In-plane force of double-tee connection.....	50
Figure 3.2. Out of plane vertical force of double-tee connection	51
Figure 3.3. Potential in-plane failure modes in diaphragm connections.....	58
Figure 3.4. Test module plan view of half	60
Figure 3.5. Multi-directional test fixture.....	62

Figure 3.6. Shear loading protocol.....	66
Figure 3.7. Tension/Compression loading protocol.....	67
Figure 3.8. Monotonic shear with proportional tension (ratio of 2.0 shown).....	69
Figure 3.9. Cyclic envelope determination	74
Figure 3.10. Simplified multi-linear backbone curve	74
Figure 3.11. Deformation curve types	77
Figure 4.1. Supplemental reinforcement layout and construction details.....	88
Figure 4.2. Enhanced ductile connector specimen details	89
Figure 4.3. Ductile ladder connector.....	90
Figure 4.4. Ductile ladder with hairpin connector	91
Figure 4.5. Pre-topped carbon chord connector.....	92
Figure 4.6. Pre-topped stainless chord connector	93
Figure 4.7. Multi-directional test setup.....	95
Figure 4.8. Monotonic tension response	100
Figure 4.9. Cyclic tension response	101

Figure 4.10. Damage state at 2.5-in tensile opening.....	105
Figure 4.11. Damage state at 3.0-in tensile opening.....	106
Figure 4.12. Ductile ladder (DL) tensile data	106
Figure 4.13. Damage state at 2.0-in tensile opening.....	107
Figure 4.14. Ductile ladder w/ hairpin (DL&HP) connector tensile data.....	108
Figure 4.15. Damage state at 5.0-in tensile opening.....	110
Figure 4.16. Damage state at 0.39-in tensile opening.....	110
Figure 4.17. Carbon chord connector tensile data	111
Figure 4.18. Damage state at 0.5-in tensile opening.....	112
Figure 4.19. Damage state at 2.0-in tensile opening.....	113
Figure 4.20. Stainless chord connector tensile data.....	114
Figure 4.21. Monotonic shear response	117
Figure 4.22. Cyclic shear response	120
Figure 4.23. Damage state at 0.49-in shear opening.....	125
Figure 4.24. Damage state at 0.33-in shear opening.....	126

Figure 4.25. Damage state at 0.59-in shear opening.....	127
Figure 4.26. Damage state at 0.77-in shear opening.....	128
Figure 4.27. Ductile ladder (DL) shear data	131
Figure 4.28. Damage state at 0.55-in shear opening.....	132
Figure 4.29. Damage state at 1.0-in shear opening.....	132
Figure 4.30. Damage state at 1.08-in shear opening.....	133
Figure 4.31. Ductile ladder with hairpin connector (DL&HP) shear data.....	134
Figure 4.32. Damage state at 0.75-in shear opening.....	135
Figure 4.33. Shear & Axial force vs. shear displacement.....	136
Figure 4.34. Damage state at 3.5-in shear opening.....	136
Figure 4.35. Damage state at 3.5-in shear opening.....	137
Figure 4.36. Damage state at 1.98-in shear opening.....	138
Figure 4.37. Carbon Chord shear data	139
Figure 4.38. Damage state at 0.75-in shear opening.....	140
Figure 4.39. Damage state at 4.5-in shear opening.....	140

Figure 4.40. Damage state at 2.15-in shear opening.....	141
Figure 4.41. Damage state at 0.80-in shear opening.....	142
Figure 4.42. Damage state at 1.60-in shear opening.....	142
Figure 4.43. Stainless Chord shear data.....	143
Figure 5.1. Typical diaphragm plan layout and connections.....	146
Figure 5.2. Hairpin connection details.....	148
Figure 5.3. Simplified lineal curve used in previous database.....	152
Figure 5.4. Normalized data of stiffness, strength and deformation.....	160
Figure 6.1. Typical double tee diaphragm joints.....	172
Figure 6.2. Flexural deflection/shear sliding response of diaphragm.....	176
Figure 6.3. Prototype structure diaphragms and joint design cases.....	179
Figure 6.4. Joint moment-rotation and shear-sliding responses.....	181
Figure 6.5. Diaphragm resistance-deformation response.....	182
Figure 7.1. Multi-directional test fixture.....	186
Figure 7.2. Field welding of connections between panels.....	187

Figure 7.3. Scaling of DT Section	189
Figure 7.4. Full scale and half scale unbonded chord connection	190
Figure 7.5. Full scale and half scale JVI Vector	191
Figure 7.6. Critical flexural joint in a typical parking structure	192
Figure 7.7. Flexural joint specimen plan view & side elevation	194
Figure 7.8. Shear joint specimen plan view & side elevation.....	196
Figure 7.9. PDH test program	198
Figure 7.10. Instrumentation layout of PDH test.....	199
Figure 7.11. Control system of video Camera	200
Figure 7.12. Flexure joint performance	206
Figure 7.12. Instrumentation layout of hybrid test	208
Figure 7.13. Control algorithm of hybrid test	209
Figure 8.1. Dry chord connection in typical precast diaphragm.....	216
Figure 8.2. Test specimen detail of conventional dry chord connection	217
Figure 8.3. Tension performance of conventional dry chord connection	218

Figure 8.4. Shear performance of conventional dry chord connection.....	218
Figure 8.5. Failure mechanisms of conventional dry chord connections	219
Figure 8.6. Development and improvements of dry chord connection.....	220
Figure 8.7. Test specimen details of typical enhanced dry chord connections.....	221
Figure 8.8. Ductile design concept	224
Figure 8.9. Detail of standard casting module	226
Figure 8.10. Lay out of new developed dry chord connection	227
Figure 8.11. A typical panel-to-panel 3-Bar chord connection	228
Figure 8.12. Slots location on the tube	233
Figure 8.13. Location of faceplate to slug weld.....	235
Figure 8.14. Tabs prefabricated with the faceplate to locate slug	235
Figure 9.1. Idealized truss/Spring model	240
Figure 9.2. DSDM connection model [Wan, G. and Fleischman, R.B 2006]	241
Figure 9.3. 2D FE dry chord model (Cao 2006).....	243
Figure 9.4. Partial concrete panel region around connector (6x12x4-in)	244

Figure 9.5. Chord connector with slug and slug weld	245
Figure 9.6. Tube and plug welds.....	246
Figure 9.7. Chord connector embedded in the concrete panel.....	246
Figure 9.8. Constitutive steel model	247
Figure 9.9. Constitutive material model for casting steel, rebar, slug and welds	248
Figure 9.10. Modified second-order element C3D10M (ABAQUS, 2009)	249
Figure 9.11. Meshes of the dry chord connector and surrounding concrete panel	250
Figure 9.12. Interactive action in the FE model of connector and concrete panel	251
Figure 9.13. Normal “hard” contact pressure-overclosure relationship (ABAQUS, 2009)	254
Figure 9.14. Model boundary and loading conditions	255
Figure 9.15. Location of faceplate-to-welds in various cases.....	258
Figure 9.16. Undeformed and deformed shape comparison of connector in various cases	260
Figure 9.17. Maximum principal stress contour of concrete panel in various cases	263

Figure 9.18. Von Mises stress contour of casting modular system in various cases	266
Figure 9.19. Von Mises stress contour of anchorage bar in various cases	267
Figure 9.20. Von Mises stress contour of tube-to-rebar plug weld in various cases	269
Figure 9.21. Von Mises stress contour of faceplate-to-slug fillet weld in various cases at a joint opening of 1.2-in.....	271
Figure 9.22. Von Mises stress contour of faceplate-to-slug fillet weld in various cases at a joint opening of 0.6-in.....	272
Figure 9.22. Von Mises stress contour of slug in various cases	274
Figure 9.23. Axial force-displacement performance of a pair of dry chord connector ..	275
Figure 9.25. Performance of connector at same time step in various cases.....	278

List of Tables

Table 3.1. Evaluation methodologies of precast concrete diaphragm connections	53
Table 3.2. Deformation category range	79
Table 4.1. Material Properties.....	94
Table 4.2. Test Matrix.....	97
Table 4.3. Connector Capacity Formulation Estimates	102
Table 4.4. Connector Capacity Experimental Results	103
Table 4.5. Capacity Formulation Estimates.....	122
Table 4.6. Connector Capacity Experimental Results	123
Table 5.1. Summary of precast concrete diaphragm connection details in previous research	148
Table 5.2. Precast concrete diaphragm connection details summary	150
Table 5.3. Previous DT/DT web connector performance database (Cao 2006).....	153
Table 5.4. New developed DT/DT web connector performance	162

Table 6.1. Joints design with different tension category connectors	180
Table 7.1. Half scale connector strength hierarchy.....	191
Table 7.2. Critical flexural joint design	193
Table 7.3. PDH test sequence	201
Table 7.4: Chord connection response of PDH test.....	203
Table 7.5: JVI Vector connection response of PDH test	205
Table 7.6: Chord connection response of hybrid test	210
Table 7.7: JVI Vector connection response of hybrid test.....	211
Table 8.1: Enhanced dry chord connection failure mechanisms	222
Table 9.1. Material properties of connector model.....	249

Abstract

Precast concrete double-tee connections are extensively used to ensure structural integrity and force transfer within a precast diaphragm system. An experimental and analytical study is conducted on the precast concrete diaphragm double tee connections to evaluate their in-plane seismic behavior and develop effective connection details to achieve a desired ductile performance. The dissertation research is carried out in five phases.

In the first phase, an experimental evaluation approach for assessing the stiffness, strength and deformation properties of embedded connections used in conventional precast concrete panel systems is developed. Adherence to this evaluation method allows connection properties to be determined in a repeatable, reproducible, and consistent manner so that existing and new connections can be quantified and utilized effectively in the diaphragm system.

In the second phase, an experimental program is conducted to categorize stiffness, strength and deformability of four improved web and chord connections under in-plane tension, shear and combined tension with shear deformation in accordance with the evaluation approach. The enhanced design details are found to be effective in improving the connector deformability in few cases. However, the majority of connections are unable to achieve ductile mechanism due to premature failure of field welds.

In the third phase, over 200 tests are conducted on thirty-eight types of existing diaphragm chord and web connections. The force-deformation responses of all the connections are incorporated into a comprehensive connection performance database to provide stiffness, strength capacity, deformation capacity, and deformation category of each connector detail examined for design and modeling purposes. A simplified pushover modeling approach is developed to estimate the diaphragm flexural and shear resistance-deformation responses based on database information. The application of this approach is illustrated by a numerical example with three cases of diaphragm system designed with web connectors in LDE, MDE and HDE categories.

As part of the collaborative DSDM project, an experimental program associated with integrated experimental and analytical evaluation of the seismic behavior of critical multi-connection joints of precast concrete diaphragm system is conducted in the fourth phase. A full scale multi-direction test fixture which allows simultaneous control of shear, axial and bending deformations exhibited at the panel joint during earthquake simulations is developed to evaluate the performance of critical flexural and shear multi-connection joints. The critical flexural joint is evaluated under predetermined displacement histories and the critical shear joint is evaluated using hybrid testing techniques in collaboration with project members in University of Arizona. The performance of the critical flexure and shear joints are discussed.

The findings related to the experimental study of conventional dry chord and improved dry chord connection indicates that these connections cannot achieve their

strength capacities and the connections fail with limited or moderate ductility due to premature weld failure. To meet the ductile design demands of diaphragm system in high seismic zone the fifth phase is focused on development of an innovative dry chord connection with high ductility at a low cost. A standard module system which serves as the connection piece between faceplate and anchorage bars is used instead of conventional weld technique to develop high ductility and avoid the premature weld failure. A three dimensional (3D) finite element (FE) detailed chord connection model is developed to evaluate the performance and further improve the design details. Design recommendations are provided according to the analytical study.

Chapter 1 Introduction

1.1 Overview

Precast concrete roof and floor diaphragms are commonly used in buildings and parking structures due to the rapid field construction and reliable quality control which is not available in cast-in-place concrete construction. In addition to providing support for gravity loads of structures and its contents, the precast floor system also serve as the horizontal elements of the lateral force resisting system (LFRS). It plays a key role in transferring the inertial forces to the lateral load resisting systems under earthquake events. To ensure the structural integrity, individual precast double tee panel are usually connected through either a mechanical connector embedded in the precast element or cast-in-place topping slabs.

In current building codes, the vertical elements of precast concrete structural systems are assumed to yield first and limit system response, while the precast diaphragm is designed to remain elastic as it collects and transfers loads to the vertical elements. A force-based horizontal beam model is used in current seismic design practice to determine the diaphragm connection details between the precast panels. Chord connections at diaphragm boundaries are designed to carry in-plane flexural load and discrete web connections along the joints are designed to carry in-plane shear force.

The actual response of the diaphragm system under extreme earthquake excitations, however, is complex and not well represented by the current code design methodology. It was observed that severe damage occurred to floor diaphragm systems in precast concrete parking structures following the 1994 Northridge California earthquake. In most structures which collapsed during the Northridge earthquake, the vertical elements of lateral force resisting systems such as shear walls performed well while the floor and roof diaphragm systems were very vulnerable to the earthquake events. The observed damage of diaphragm system included buckling of diaphragm chord connections and brittle rupture of web connections (Iverson and Hawkins 1994). The researchers have found out that the reasons could have caused or contributed to the collapses are as follows: underestimation of diaphragm forces, insufficient web connection in the key regions, nonductile failure of diaphragm chord and web connections not intended for inelastic deformation, large lateral drifts of gravity system columns due to the high diaphragm flexibility.

The poor performance of the precast concrete diaphragm system during the 1994 Northridge earthquake demonstrated an inconsistency between the intended failure mode and the seismic design provisions used (Fleischman et al. 1998), which suggested the need for development of rational diaphragm seismic design methodology and further diaphragm connection details and performance improvements. A collaboration of three university teams consisting of University of Arizona, University of California San Diego and Lehigh University, together with the Precast/Prestressed Concrete Institution (PCI) has conducted a PCI-NSF funded research project “DSDM” (Development of a Seismic

Design Methodology) (Fleischman et al. 2005a) to develop a framework of new seismic design procedure for precast concrete floor systems (Hawkins, N.M., 2008).

The new proposed seismic diaphragm design procedure involves specifying: (1) the performance level for which the precast concrete diaphragm should be designed in terms of forces, displacements and deformations; (2) the precast concrete diaphragm connection details that must be used to provide this performance; and (3) the required stiffness of the precast concrete diaphragm relative to the stiffness of the lateral force resisting system. The work performed for this dissertation represents a part of this research project.

As specified previously, the performance of precast concrete diaphragm connections is an important portion of this new seismic diaphragm design procedure. It ensures the desired performance of the diaphragm and integrity of precast concrete systems. Unfortunately, the diaphragm connection details in current practice have been developed and specified without full considerations of the required deformation capacity.

To ensure the desired diaphragm performance under the seismic demand, the behavior of current connection details must be well understood. During the past 30 years, a number of experimental studies have been conducted on conventional precast double-tee connections. The first published research was conducted in 1968, which focused on hairpin connectors under shear demands. Research continued on a number of different connectors with recent studies focused on a variety of proprietary connections. Although these previous research identifies the shear characteristics of a number of connectors, the

breadth of experimental evaluation is limited. The majority of studies have focused on the shear response of web connectors. Furthermore, the objective of the majority of research was to determine the monotonic load carrying capacity of the connector, limited data was provided on the effects of cyclic loading and the ultimate displacement capacity of connectors.

In order to better understand the behavior of precast concrete double tee connections in shear and tension, a previous graduate researcher, Liling Cao at Lehigh University, continued the research on the performance of precast concrete diaphragm connections (Cao 2006). Her work established a quantitative database of previously published connection test results, and included an experimental and analytical evaluation of the discrete web and chord connections used by the precast industry. In addition, improved details for the pre-topped chord connector targeting at achieving the desired ductile mechanism were developed. The experimental results indicated that a number of common connectors were unable to meet their expected design strengths. Failures included pullout of the connector legs, weld tearing, and concrete crushing. The connectors that did achieve their capacity did so with very limited ductility. The research findings by Cao (2006) provided important and useful information on performance of discrete chord and web connections.

However, the experimental studies conducted by Cao (2006) were limited to six commonly used discrete conventional connections, most of which exhibited limited ductility and failed to meet expected design force capacity. In addition, the loading

protocols adopted in the experimental method were solely based on displacement control and most of the tests were limited to monotonic loading condition. So the experimental methods need to be improved to accommodate combined deformation and force demands and further examine the cyclic loading effect. The enhanced design details were developed based on a two dimensional (2D) FE model, which may not be able to properly model the multi-directional failure modes that occur. Therefore, the advantages of enhanced ductile design details need to be experimentally verified and further extended to a more extensive range of diaphragm web connections with potential high deformation capacity. As a result, additional research is needed to evaluate seismic performance of discrete connections and multi-connection joints and further develop effective design details.

To address this need a comprehensive experimental and analytical research on discrete ductile connections and multi-connection joints is conducted. Based on the experimental results, most of enhanced connection designs do improve the ductile performance of conventional connections. However, the dry chord connection is not able to achieve expected ductile performance and force capacity with premature weld failure. This undesirable failure mode is also validated in the shake table testing performed at UCSD as part of the DSDM project (Schoettler et al. 2009). To eliminate non-ductile weld failure of diaphragm connections, an innovative ductile dry chord connection for high seismic zone is developed based on analytical studies.

1.2 Research Objectives and Scope

The primary objective of this dissertation work is to develop standard experimental evaluation method, evaluate the seismic performance of enhanced ductile connection details, develop diaphragm connection performance database and develop a ductile dry chord connection for high seismic zone. In order to achieve this goal, the following specific objectives are established:

Objective 1: Development of experimental evaluation approach for precast concrete diaphragm connections

An experimental evaluation approach for assessing the mechanical properties of existing embedded connections or/and any new developed connections used in conventional precast concrete panel systems is developed. In addition a series of performance levels are defined which can be used to categorize the connector based on the measured response.

Objective 2: Experimental evaluation of enhanced discrete precast concrete diaphragm connections

The control method used in previous research is modified to allow for an improved characterization of the precast diaphragm connectors under prescribed force demands instead of using pure displacement demands. Full scale experimental investigation of discrete chord and web diaphragm connectors with enhanced details is

conducted to determine the connection stiffness, strength and deformation properties, and further to evaluate the effectiveness of enhanced design. Both monotonic and cyclic tests are performed and compared for each connection to study the effect of load reversals. The connection failure mechanism under each loading pattern is investigated.

Objective 3: Development of a comprehensive database of connection performance

A large number of experiments have been conducted in this research. A comprehensive database of measured diaphragm connection performance is developed to provide stiffness, strength and deformation properties of each connector detail examined. The measured responses are tied to performance levels which are used to categorize connectors in accordance with the new seismic design methodology for precast diaphragms.

Objective 4: Estimation modeling approach of diaphragm system based on database information

A simplified pushover modeling approach is developed to estimate the maximum midspan flexural deflection and shear sliding of a diaphragm subjected to a statically applied uniform load. Estimation of flexural and shear responses of diaphragm designed with connectors in LDE, MDE and HDE categories are conducted as examples.

Objective 5: Experimental Program of precast concrete diaphragm joint with multiple connections

A multi-directional diaphragm test fixture is developed to investigate the critical multiple connection joints subjected to complex loading condition. The PDH (Predefined Displacement History) and Hybrid tests are conducted on the specimens that are designed for critical flexural and shear joints.

Objective 6: Design of new ductile dry chord connection

A new design of ductile dry chord connection is proposed since both the conventional and enhanced dry chord connections cannot achieve expected performance. Casting steel material is selected to improve the ductility of conventional dry chord connection. The detailed profile of connection is presented.

Objective 7: Analytical studies of new precast concrete dry chord connection

Appropriate modeling techniques are established to characterize the behavior of concrete, weld and casting steels. Detailed 3D FE connection models are developed to represent proposed chord connection subassemblies. Connection behavior is examined through FEM analysis to ensure the formation of a yield mechanism in the targeted region with predictable strength and deformation capacity.

1.3 Organization of Dissertation

The dissertation work is organized and presented in ten chapters as follows.

Chapter ONE introduces the overview, dissertation objectives and the organization of the dissertation.

Chapter TWO provides a background on precast concrete floor system, the connections used in a typical floor diaphragm, the current seismic diaphragm design, recent research on diaphragm behavior and the emerging seismic design methodology proposed by DSDM research team.

Chapter THREE presents the experimental evaluation approaches for existing and new developed precast concrete diaphragm connections. Simplified analytical approaches and existing experimental methods are discussed. A standard experimental approach is proposed to assess the in-plane strength, stiffness, and deformation capacity of precast concrete diaphragm connections.

Chapter FOUR presents the enhanced ductile connection specimens used for the experimental study. The connection details are discussed. Test matrix of the experimental studies is presented. The tension and shear behavior of representative diaphragm connections are discussed. The experimental program identifies the initial stiffness, strength and deformation capacity of each tested connection under tension, shear and

combined tension with shear. The effectiveness of the enhanced details is evaluated through the comparison with the conventional connections. The measured strength is compared to the design estimates and failure mechanism in each connection detail is investigated.

Chapter FIVE presents a comprehensive evaluation of precast concrete diaphragm connections currently used in US construction. A previous connection detail database is presented and extended by incorporating all the connections evaluated in this dissertation research. Previous and recent research on connection performance is discussed. The results of over 200 experimental tests conducted in this dissertation research are incorporated into a comprehensive performance. In addition, the database usage is also presented.

Chapter SIX describes the precast concrete diaphragm multi-connection joints, and a simplified estimation modeling approach is developed to evaluate flexural and shear force-displacement response by using the database information.

Chapter SEVEN presents the experimental program used to evaluate performance of multi-connection joint. Specimens of critical flexural and shear joint are described. The material properties, test matrix, instrumentation and control algorithm for predefined history (PDH) test and hybrid are presented.

Chapter EIGHT summarizes the performance of conventional dry chord connection and enhanced dry chord connection. The limited ductility of these connections

indicates the necessity to develop a new dry chord connection. The design concept, connector layout, design detail and expected strength and ductility capacity are presented.

Chapter NINE presents the background of three simplified modeling approaches: PCI truss/spring model, DSDM connection model and previous 2D FE connection model. A detailed 3D FE connection model is developed to simulate the geometry, material, boundary condition and interactions of the new dry chord connection. The analytical studies of the new proposed dry chord connection under tension loading are presented, design recommendations based on the analytical study are proposed.

Chapter TEN presents a summary of this investigation and conclusions on the experimental and analytical studies. Future work for this dissertation work is discussed.

1.4 References

1. Iverson, J.K., Hawkins, N.M., “Performance of Precast/Prestressed Concrete Building Structures During Northridge Earthquake”, *PCI Journal*, Vol.39, No.2, 1994, pp.38-55
2. Fleischman, R.B., Sause, R., Pessiki, S., and Rhodes, A.B., “Seismic Behavior of Precast Parking Structure Diaphragms,” *PCI Journal*, V. 43, No.1, January-February 1998, pp.38-53
3. Fleischman, R., Naito, C., Restrepo, J., Sause, R., Ghosh, S., “Precast Diaphragm Seismic Design Methodology (DSDM) Project, Part 1: Design Philosophy and Research Approach,” *PCI Journal*, Vol. 50, No. 5, Sept.-Oct., 2005, pp. 68-83.

4. Building Seismic Safety Council, Committee TS-4. (2009). "Seismic design methodology for precast concrete floor diaphragms," Part III, 2009 NEHRP Recommended Seismic Provisions, Federal Emergency Management Agency, Washington, D.C.
5. Cao, L., "Effective Design of Precast Concrete Diaphragm Connections Subjected to In-Plane Demands", Ph.D. dissertation, Dec 2006
6. Schoettler, M.J., Belleri, A., Zhang, D., Restrepo, J., and Fleischman, R.B. (2009). "Preliminary results of the shake-table testing for development of a diaphragm seismic design methodology." *PCI Journal*, 54 (1), 100-124.

Chapter 2 Background

This chapter gives an overview of precast concrete diaphragm floor systems, connection details, previous research on design method and seismic behavior of diaphragm connections, and the seismic diaphragm design methodology being proposed by the DSDM project.

2.1 Precast Concrete Diaphragm Floor Systems

Precast concrete construction is commonly used for buildings and parking structures throughout United States because it allows for fast construction and good quality control. In precast construction, the floor and roof systems is termed as “diaphragms”, which serves as the horizontal elements of the lateral force resisting systems (LFRS) to transmit the horizontal force to vertical lateral force resisting structural members. The action of load transfer to the vertical elements is referred to as “diaphragm action”.

The precast concrete diaphragm systems are classified as untopped or topped diaphragm (PCI Design Handbook 2010). An untopped diaphragm refers to a floor system comprised only of precast units. In this case, diaphragm action must be provided by the precast units (often pretopped) and the mechanical connections in-between. A topped diaphragm possesses a cast-in-place topping on the precast units. The diaphragm action on the topped diaphragm system depends on the different types. For a non-

composite topped diaphragm (ACI 2005), the lateral forces are transferred by the cast-in-place topping slab alone, while the lateral forces are transmitted through composite action of precast units and the cast-in-place topping slab for a composite topped diaphragm. For both topped and untopped diaphragm, the joint between the precast units is regarded as planes of weakness. It contributes significantly to diaphragm flexibility in the elastic state and concentrates inelastic deformation capacity in the post-yield state.

While precast and prestressed concrete can be manufactured in a variety of sizes and shapes, precast floor diaphragm systems are commonly constructed from double-tee (DT) panels or hollow-core panels.

2.1.1 Precast Hollow Core Floor Systems

Precast hollow-core planks (Figure 2.1) are typically 4 to 8-ft wide and 6 or 8 inches thick depending on the desired span. As the name implies, they have evenly spaced cores running the length of the slab reducing the weight of the panels and can function as a chase for electrical and mechanical utilities. Most systems are reinforced with prestressing wires between the cores. They are manufactured in large precast plants and transported to the site by truck and placed on the supporting walls with a crane. In some cases a cast-in-place topping is placed over the planks.

To provide structural integrity, the precast hollow core planks are usually connected by grouting the joint, referred to as a grouted shear key (Figure 2.3a), to resist the in-plane diaphragm shear demands. At the locations between the slab and inverted

beams, reinforcements are placed in the joint and designed to resist the shear based on (ACI 318-05 11.7) shear-friction principles (Figure 2.3b).



Figure 2.1. Precast hollow core planks

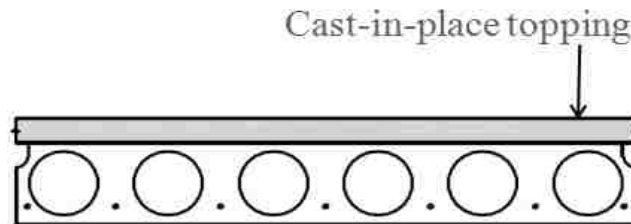


Figure 2.2. Precast hollow core planks with cast-in-place topping

As an alternative to grouted shear keys, embedded reinforcing bars can be used across the joint and grouted into the slab cores or steel plates are embedded in the slabs and connected by welding a cover plate (Figure 2.4).

Both of these connections can serve as chord and web connections to provide tension and shear resistances to the lateral diaphragm demand at the panel-to-panel and panel-to-wall joints.

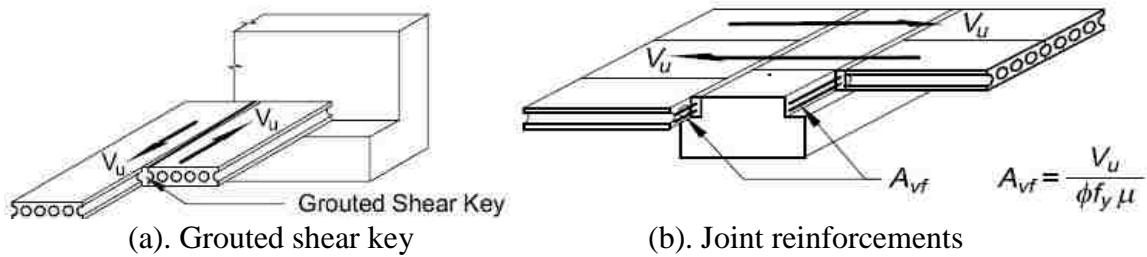


Figure 2.3. Connection details for the precast hollow-core floor systems (PCI 2010)

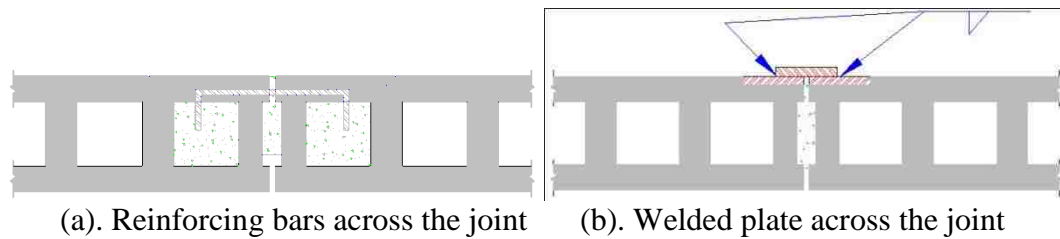


Figure 2.4. Embedded reinforcing bars across the joint (Cao 2006)

In low seismic regions, sufficient shear strength can be provided by the grouted shear keys to resist the demands. In high seismic regions, however, a sliding mechanism may occur at the key due to loss of adhesion. To ensure the structural integrity under seismic demands, a special waved shear key has been developed by recent research (Menegotto and Monti 2005). The shear key has a sinusoidal waved profile along the edge as shown in Figure 2.5. The profile is obtained by special wheels attached to the casting extruder. The wave length is approximately 2-in. and the amplitude is 0.1-in.

This particular geometry prevents the shear key from slipping. Thus the diaphragm constructed from this hollow-core slab configuration can provide good performance with high strength and ductility (Menegotto and Monti 2005).

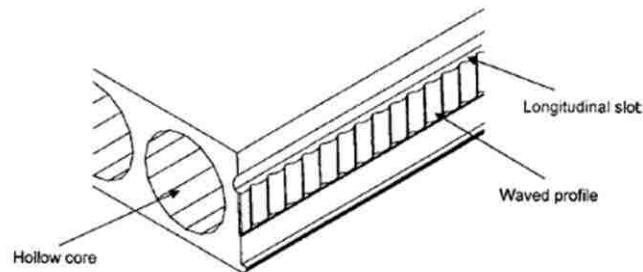


Figure 2.5. Serrated hollow-core slab edge profile (Menegotto and Monti 2005)

2.1.2 Precast Double Tee (DT) Floor Systems

The precast concrete double tee (DT) panels (Figure 2.6) are typically 8 to 16-ft. wide and used to span 40-ft to 80-ft using depths of 24 -in. to 34-in., respectively, although longer spans are possible with deeper sections. The DT panels are commonly fabricated with a 2-in thick flange and topped with cast-in-place concrete topping after erection or pre-topped with a 4-in. thick flange during precast operations (Figure 2.7). The geometry of cross section and prestressing levels are designed to resist gravity loads. Individual DT panels are usually connected through discrete mechanical connectors embedded in flange or cast-in-place topping to ensure structural integrity and transfer in-plane lateral diaphragm demands. In addition to primary precast DT panels, the DT diaphragm system typically contains inverted-tee beams spanning from column to

column to support the floor units internally; spandrel beams to support these units externally and walls (Figure 2.8).



Figure 2.6. Precast DT Panel and A parking garage with DT floors (PCI 2010)

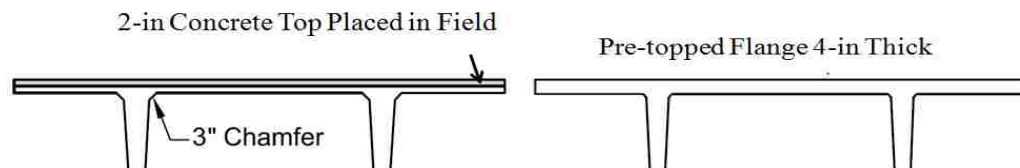


Figure 2.7. Precast topped and pre-topped DT Panel

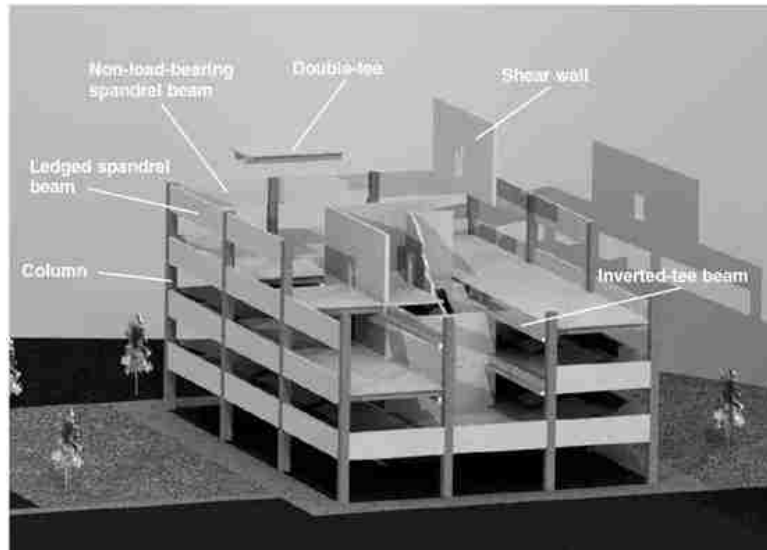


Figure 2.8. Precast DT structural system (PCI 2010)

2.2 Precast Concrete Double-tee Diaphragm Connections

In precast concrete double-tee diaphragm systems, individual precast panels are connected together by using mechanical connections embedded in flange or cast-in-place topping. These diaphragm connections are used to provide resistance to diaphragm response under lateral loads and also assist with leveling the two adjacent panels. A typical precast diaphragm system consists of three primary connection types to ensure structural integrity: chord connection, web connections and collectors/anchorage (Figure 2.9).

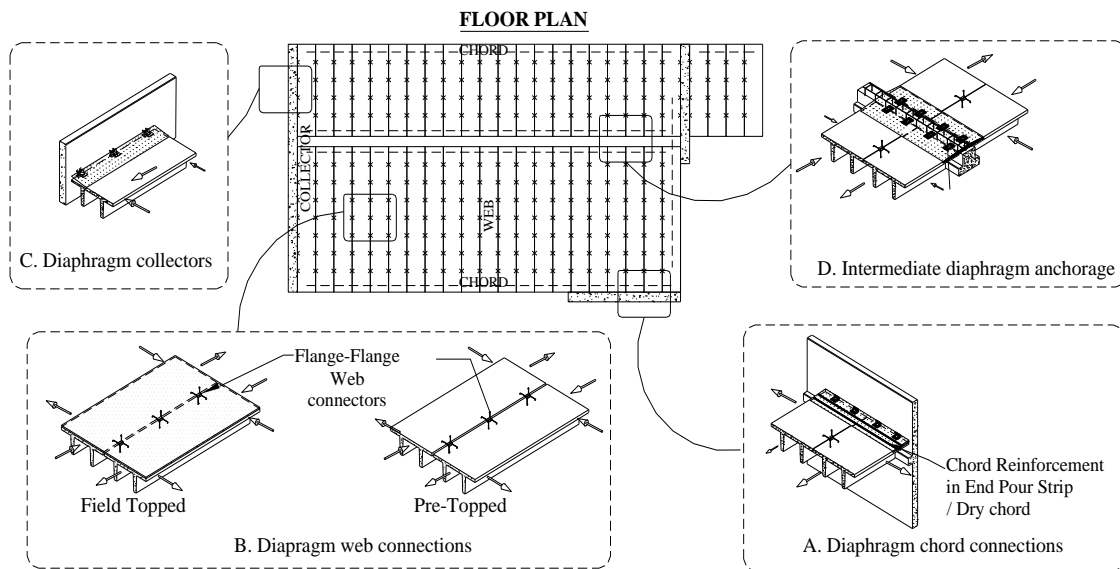
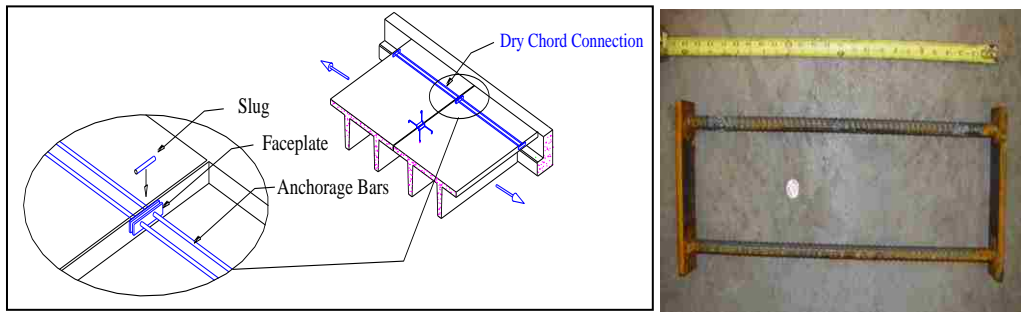


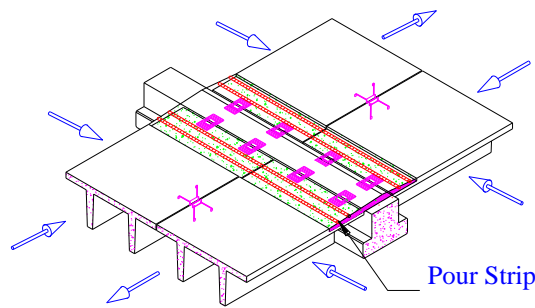
Figure 2.9. Reinforcements in a typical diaphragm system

2.2.1 Chord Connection

Diaphragm chord connections are located at extreme edges of the diaphragm to provide flexural resistance through a tension-compression couple at both edges. In pre-topped systems, the chord connection is referred to as a “dry” chord because the connection is embedded in the panel during precast operation and does not require cast-in-place concrete to complete its anchorage (Figure 2.10a). In topped systems, chord connections are typically continuous bars placed in cast-in-place topping slabs. Alternatively, continuous bars can be placed in reduced flange thickness section at the end of each DT panel and then topped by cast-in-place concrete creating an elevated strip region referred to as a “pour-strip” as shown in Figure 2.10b.



(a). Dry chord connection in pre-topped diaphragm system

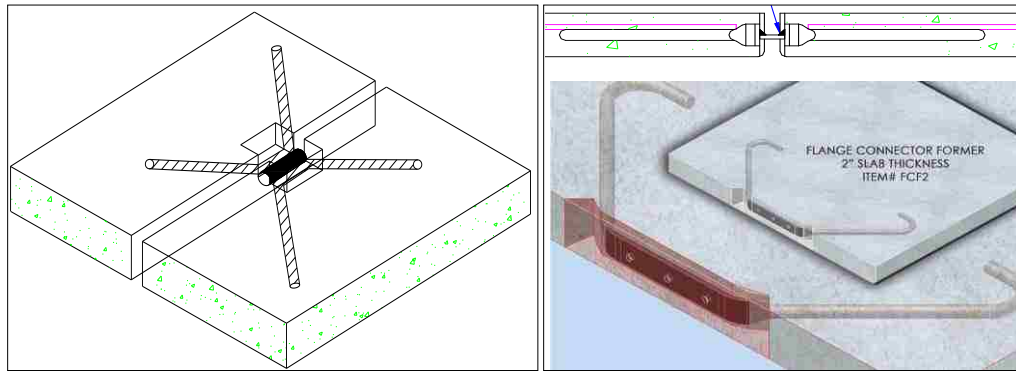


(b). Pour strip in topped diaphragm system

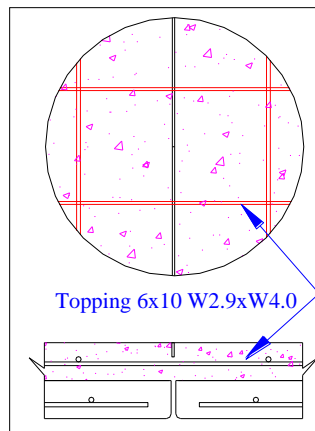
Figure 2.10. Typical chord connection details

2.2.2 Web Connection

Diaphragm web connections, also called shear connectors, are placed along diaphragm joints to resist in-plane shear loads. In pre-topped systems, web connections



(a). Web connection in pre-topped diaphragm system



(b). Web connection in topped diaphragm system

Figure 2.11. Typical web connection details

are referred as discrete flange to flange mechanical connectors embedded in precast panels (Figure 2.11a). In topped systems, web connections can be provided by welded wire reinforcements or reinforcing bars installed across the joint in the topping (Figure 2.11b).

2.2.3 Collector/Anchorage Reinforcement Details

Collectors, as the name implies, usually exist between the diaphragm panel and vertical elements of lateral force resisting systems (LFRS) to “collect” the diaphragm lateral force to anchorage reinforcement. The collector detail is continuous bars in the cast-in-place topping slabs (Figure 2.12), pour strip or precast panels. The anchorage reinforcement is used to transfer diaphragm lateral forces to the primary (vertical plane) elements of LFRS. In most cases, the diaphragm anchorage reinforcement detail is constructed by welding a cover plate connector embedded in the precast flange to the stud groups in the wall (Figure 2.13). The anchorage reinforcement detail may also be provided by threaded insert (Figure 2.14) placed in pour strips (in pre-topped systems) and topping slabs (in topped systems).

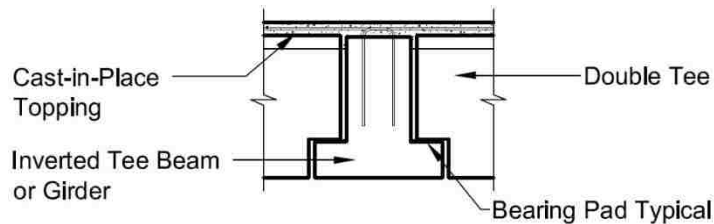


Figure 2.12. Continuous reinforcing bars in cast-in-place topping served as collectors

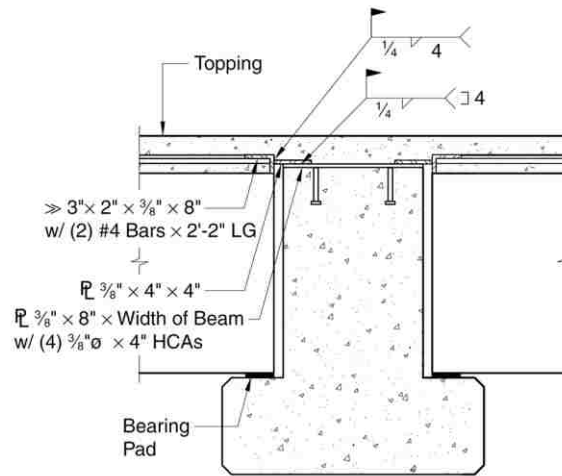


Figure 2.13. Flange connector welded to stud groups served as anchorage reinforcement

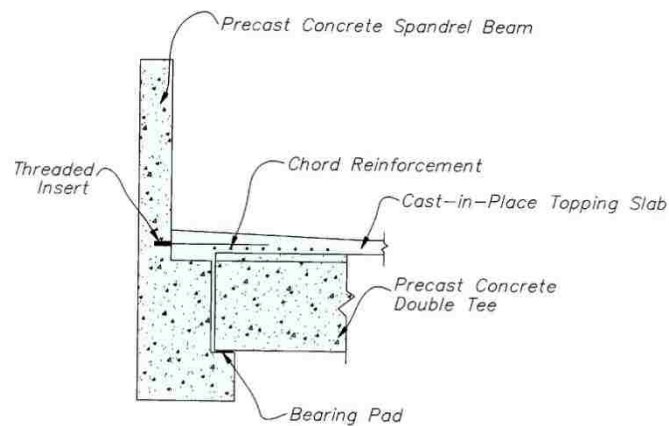


Figure 2.14. Threaded insert between pour strip and spandrel served as anchorage reinforcement

2.3 Current Seismic Design Method of Precast Concrete Diaphragm

Current seismic design codes assume elastic diaphragm behavior and rely on the inelastic deformation capacity of structural walls to sustain the earthquake excitation. In

the practice, the diaphragm is designed to maintain the elastic behavior while ductile inelastic deformation requirements are imposed on the vertical elements of lateral force resisting systems. The diaphragm design force, F_{px} , is determined by Equivalent Lateral Force (ELF) procedures introduced in IBC code (IBC 2006). This force is in turn used to design the primary diaphragm reinforcement details: chord connection, web connection, collector and anchorage reinforcement details.

2.3.1 Diaphragm Seismic Design Force

In current practice, the lateral force-resisting system and the floor diaphragm of buildings are designed to resist the seismic demands based on ELF approach. This seismic design procedure is introduced in IBC code (IBC 2006) in accordance with (ASCE7-05). In ELF procedure, the maximum expected lateral force due to seismic ground motion at the base of a structure, termed “base shear”, V_b , is determined in accordance with Eq. 2-1.

$$V_b = C_s W \quad \text{Eq. 2-1}$$

where W is the effective seismic weight of the structure, and C_s is the seismic response coefficient determined from Eq. 2-2 or Eq. 2-3.

$$C_s = \frac{S_{DS}}{(R/I)} \leq \frac{S_{D1}}{T(R/I)} \quad \text{for } T \leq T_L \quad \text{Eq. 2-2}$$

$$C_s = \frac{S_{D1} T_L}{(R/I) T^2} \quad \text{for } T \geq T_L \quad \text{Eq. 2-3}$$

Where S_{DS} is the design spectral response acceleration parameter in the short period range, and S_{DI} is the design spectral response acceleration parameter at a period of 1.0-s determined from section 11.4.4 in ASCE 7-05, I is the occupancy importance factor in accordance with section 11.5.1 in ASCE 7-05, T is the fundamental period of the structure determined from section 11.4.5 in ASCE 7-05 and T_L is the long period transition period. R is the response modification factor determined from Table 12.2-1 (ASCE 7-05). This factor represents the inherent ductility capacity and overstrength of lateral force resisting systems.

In addition, the value of C_s should not be less than 0.01. For structures located where S_I is equal to or greater than 0.6g, C_s should not be less than $\frac{0.5S_I}{(R/I)}$, where S_I is the mapped maximum considered earthquake spectral response acceleration parameter determined from section 11.4.1 in ASCE 7-05.

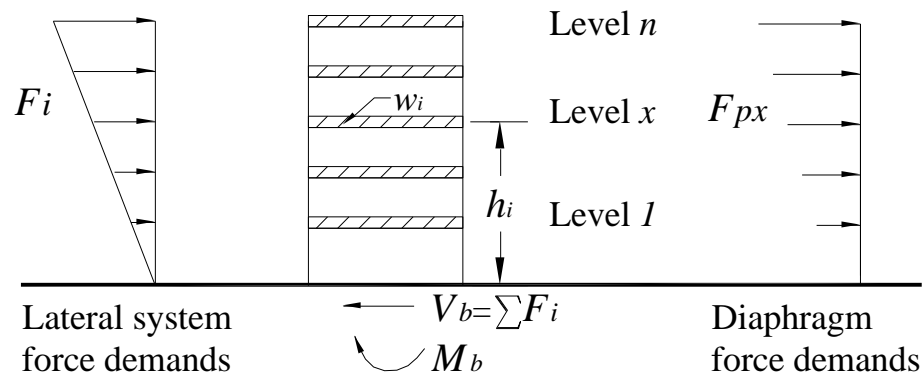


Figure 2.15. Equivalent lateral force demands

As shown in Figure 2.15, the base shear V_b is distributed over the height of the structure to each floor level as F_i based on the first mode vibration pattern of a cantilever structure. These forces are used for design of vertical elements of the lateral force resisting systems. The Seismic demands on the diaphragm, F_{px} , are calculated based on the equivalent lateral force distribution as shown in Eq. 2-4:

$$F_{px} = \left(\frac{\sum_{i=x}^n F_i}{\sum_{i=x}^n w_i} \right) w_{px} \quad \text{Eq. 2-4}$$

where w_{px} is the tributary element weight of diaphragm at floor level x and w_{ix} is the tributary element weight of diaphragm at floor level i . This equation assumes that the seismic demand on the individual diaphragm does not occur simultaneously. As a consequence, this approach gives the maximum value of the diaphragm design force at each level. This force distribution leads to an increase of diaphragm force demand as the floor height increases. The diaphragm design force is also limited within the range from the lower bound Eq. 2-5 to the upper bound Eq. 2-6.

$$F_{px} \geq 0.2S_{DS} I w_{px} \quad \text{Eq. 2-5}$$

$$F_{px} \leq 0.4S_{DS} I w_{px} \quad \text{Eq. 2-6}$$

It is noted that although the current building code recommends inverse triangle distribution of F_{px} , recent research (Fleischman and Farrow 2001) show that the rectangular distribution of diaphragm inertia force is more reasonable under seismic loading due to the high mode effect and diaphragm flexibility.

2.3.2 Diaphragm Connection Details Design

Due to the relatively high stiffness of the double tee and hollow core panels, the critical conditions occurs in the joints between precast units under lateral loads, as these locations represent planes of weakness in the building floor system. Then the majority of diaphragm inelastic deformations are concentrated at the connections between precast units under lateral loads. Therefore adequate diaphragm reinforcements across these joints are required to ensure the safe diaphragm design.

In the current design practice (PCI Design Handbook 2006), the diaphragm design force, F_{px} , is applied as a distributed in-plane load along the diaphragm span length (Figure 2.16). Then in-plane diaphragm internal forces are determined based on the horizontal beam model (PCI 2006).

In this model, the diaphragm is assumed to act as a deep horizontal beam simply supported by vertical elements of LFR system. Under distributed lateral loads, the in-plane flexural moment is induced through tension and compression force couple which are carried by chord connections at the extreme edges. The in-plane shear demand is generated along the diaphragm joint with the maximum at diaphragm boundary ends.

Discrete web connections with equal spacing along the joint are assumed to resist an equal portion of the maximum diaphragm shear demand at first joint. In current practice, the spacing of connections varies from 5 to 8ft and is usually maintained constant to simplify construction. In addition, shear anchorage connectors which are designed to resist the “beam shear flow” (VQ/I) (Figure 2.16) are installed between DT panel and their interior support beam.

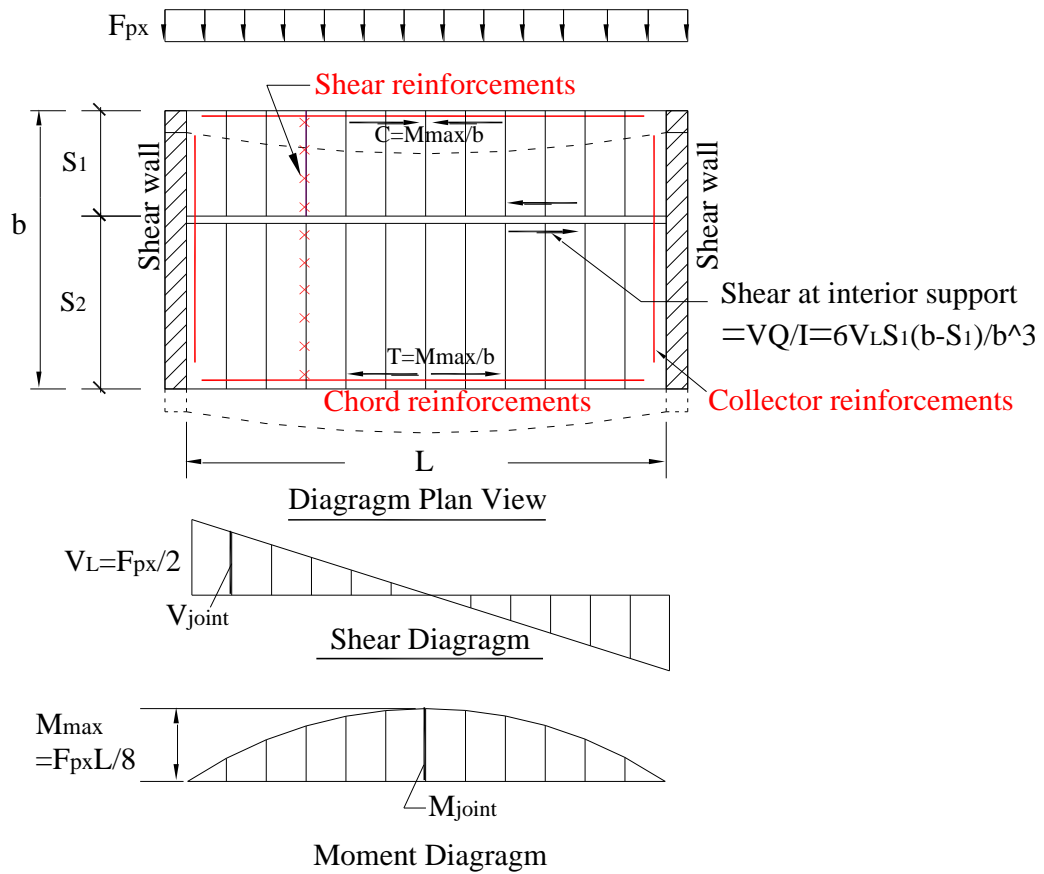


Figure 2.16. Analogous beam design of a diaphragm

2.4 Recent Diaphragm Seismic Behavior Research

Precast concrete structures with large plan areas showed poor performance in the 1994 Northridge earthquake, California (Iverson and Hawkins 1994). It is revealed that significant improvements are required in the current design practice for precast diaphragms. A good amount of research has been done on this subject to improve the diaphragm performance after the Northridge earthquake. This section presents the poor diaphragm performance in 1994 Northridge earthquake and summarizes the recent research has been done on the seismic behavior of diaphragm and connection.

2.4.1 Diaphragm Performance in 1994 Northridge Earthquake

The precast parking structures were subjected to severe damages (Figure 2.17) in the 1994 Northridge earthquake (Iverson and Hawkins 1994). In most collapsed structures, the precast elements of diaphragm systems were damaged while the vertical elements of lateral force resisting systems such as shear walls performed well (Figure 2.18). The cracking of diaphragm system was observed along the wall-to-panel and panel-to-panel joints in topped diaphragms (Figure 2.19).



Figure 2.17. Collapsed parking garage (Iverson and Hawkins 1994)



Figure 2.18. Precast panels collapsed and structural walls remained intact

(Iverson and Hawkins 1994)

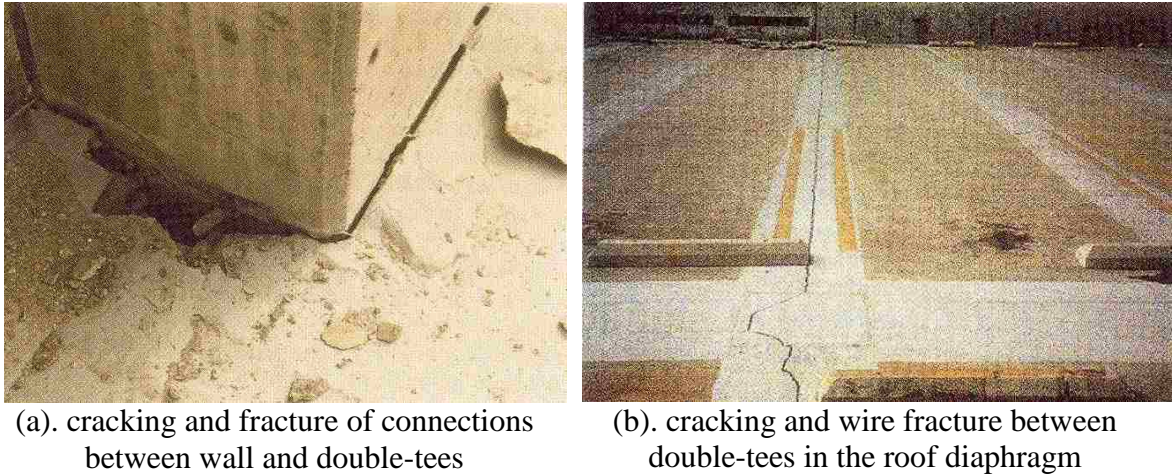


Figure 2.19. Diaphragm cracking and connection failure

(Iverson and Hawkins 1994)

The observed failure modes of connections in the diaphragm due to the shear and flexural demands included failure of web connections between DT panels, rupture of welded wire fabric cross joint in the topping, buckling of chord connections, and failure of diaphragm-to-wall anchorage connections.

These observed damages in precast concrete diaphragms and connections demonstrated that the diaphragm plays an important role in lateral load resisting system, and it is necessary to develop a safe diaphragm design to ensure ductile diaphragm response under strong ground motion.

2.4.2 Previous Research on Seismic Behavior of Diaphragm System

Due to the poor performance of diaphragm systems in the 1994 Northridge earthquake, several changes (Ghosh and Hawkins 2000) were made to building codes such as the 1997 UBC (ICB 1997), the 2000 IBC (IBC 2000) and the 1999 ACI (ACI-318 1999). For example, in the 1997 UBC and IBC 2000, the collector elements of diaphragms, their splices and their connections to seismic-force-resisting elements were required to be designed by using a factor Ω_o times the code-prescribed diaphragm design force, where Ω_o is a system overstrength factor. The ACI 318-99 required using a lower shear strength reduction factor and a larger minimum transverse spacing of topping wire (10 in.) to ensure more deformation capacity across the joints in the diaphragm.

While some changes had been made to building codes after the 1994 Northridge earthquake, it is generally agreed among researchers and practitioners that additional research studies need be conducted on precast diaphragm seismic behavior to further improve the current design practices (Nakaki 2000). This section summarizes the research conducted on this subject since that time.

Wood et al. (1995 and 2000) investigated the failures of parking garage structures during 1994 Northridge earthquake. Fleischman et al. (1998) also studied the damages of these structures. Their studies showed that the inadequate diaphragm strength and stiffness might be the main reasons led to the collapses.

Rodriguez et al. (2002) carried out floor acceleration analysis of the building with rigid diaphragm under earthquake. It is identified that the diaphragm design forces underestimate the actual forces. A method of determining amplified design force based on modal response was proposed.

Fleischman and Farrow (2001 and 2002) investigated the seismic response of building with flexible diaphragm. The study showed that current ELF design procedure may significantly underestimate diaphragm inertia forces. The critical seismic force level may not occur at the roof level as predicted from equivalent lateral force distribution. Instead, the lower level diaphragm of the building may be subjected to the maximum inertial force. Therefore the diaphragm design forces based on current ELF procedure underestimate the actual seismic floor force demands. Thus an appropriate diaphragm design force pattern should be developed to accommodate critical seismic force demands.

2.4.3 Previous Research on Seismic Behavior of Diaphragm Connection

To predict the diaphragm response under the seismic demand, common connection details should be identified and performance of the diaphragm connections must be well understood. A significant amount of research has been conducted on the performance of diaphragm connections under in-plane demands for past 40 years.

Published studies initiated in 1968 with tests on hairpin connectors conducted by Venuti (Venuti 1968) and have continued to the present with work by Oliva, Shaikh and others (Oliva 2000, Shaikh 2002, Pincheira, J.A. et.al 2005). Most of the earlier research

focused on hairpin connectors under shear demands while more recent studies focused on a variety of proprietary connections.

While the previous research identifies the shear characteristics of a number of connectors, the majority of studies have focused on the monotonic shear response of web connectors. Most tests were focusing on the strength of connections because of current force based design recommendations. The displacement capacity of connections was not quantified.

To better understand the behavior of both chord and web connections in shear and tension. Cao (2006), a previous research on DSDM project, conducted an experimental and analytical research on representative connections. It is identified that majority of conventional connection details are failed in brittle failure modes. Enhanced connection details were proposed to improve the performance of typical connections.

2.5 New Proposed Diaphragm Seismic Design Methodology

A new seismic design methodology was proposed for precast concrete diaphragms (BSSC TS4 2009) as part of the activities of the overall DSDM project. The research reported in this dissertation has been focused on evaluating existing connections and developing appropriate connection details to ensure desirable diaphragm performance, which is part of the new proposed diaphragm seismic design methodology.

The new design methodology is performance-based and addresses four key aspects of diaphragm behavior which are not treated adequately in previous seismic design provisions of precast concrete diaphragm system. The new method is aimed to specify: (1) more accurate seismic design forces of diaphragm systems developed during earthquake events. (2) The precast concrete diaphragm connection details that must be used to provide inelastic deformation capacity; and (3) Protection of potentially non-ductile elements in the precast concrete diaphragm through the use of capacity design concepts; and, (4) Explicit inclusion of diaphragm flexibility in drift limits checks.

The new proposed methodology provides the designers three options, which can be used to meet different requirements. The options include: (1) a basic design option (BDO); (2) an elastic design option (EDO); and (3) a relaxed design option (RDO). Each of these design options is associated with different performance targets which specify a different diaphragm design force and deformation capacity requirement. These design forces and deformation capacity requirements are highly dependent on several design parameters determined by building geometry, construction and seismic hazard level. In general, the diaphragm force levels and required deformation capacity determined by the performance targets are higher than current diaphragm design force levels. Developing connection details that can satisfy the ductile diaphragm performance target is part of this dissertation work.

2.5.1 Basic Design Option

A diaphragm force-deformation “pushover” curve of the Basic Design Option (BDO) is shown in Figure 2.20. The BDO is targeted in providing elastic diaphragm response in the design basis earthquake (DBE). Therefore, an increase in current diaphragm force levels, F_{px} , is required for this design option. In this approach, a diaphragm force amplification factor Ψ_d is used to increase the current diaphragm design force along the height of the structure.

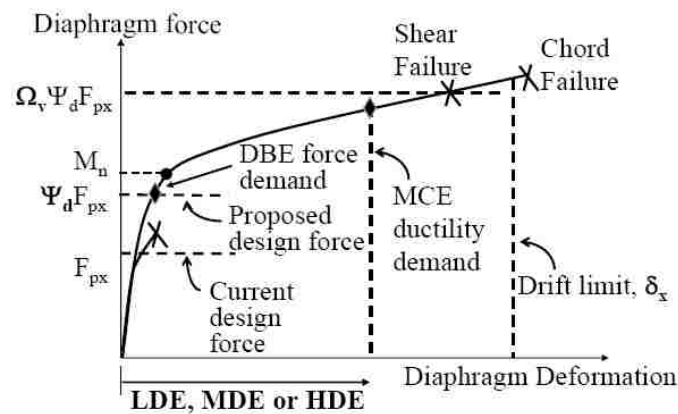


Figure 2.20. Basic Design Option (Zhang 2010)

As shown in Figure 2.20, the pushover curve represents the strength and deformation capacity of the diaphragm. Estimated seismic demand levels such as DBE and MCE are also indicated. Inelastic deformation demands are expected in a maximum considered earthquake (MCE) for diaphragm system. Therefore, the connection details used in diaphragm are required to have sufficient deformation capacity.

In order to use appropriate connection details for different deformation demands, the diaphragm connections are classified as LDE (low deformability element), MDE (moderate deformability element) or HDE (high deformability element). For typical BDO design, the connection details with the deformation capacity in MDE category are used in the diaphragm system.

In addition, to develop the desirable ductile failure modes in the diaphragm system, the shear and anchorage overstrength factors, Ω_v and Ω_a respectively, are used for shear and anchorage connections to ensure elastic response of these potentially non-ductile elements.

2.5.2 Elastic Design Option

A diaphragm force-deformation “pushover” curve of the Elastic Design Option (EDO) is shown in Figure 2.21. The EDO is targeted in providing elastic diaphragm response in the maximum considered earthquake (MCE). Thus a larger increase in current diaphragm force, F_{px} , is required compared with that of the BDO, an amplification factor Ψ_e is used as indicated in Figure 2.21.

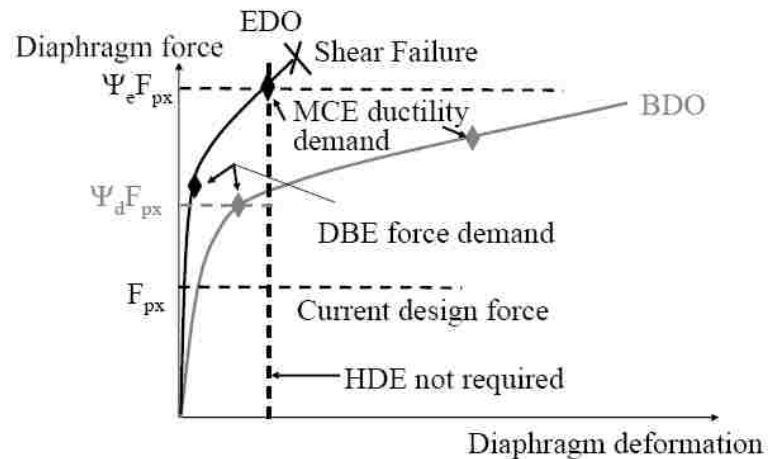


Figure 2.21. Elastic Design Option (Zhang 2010)

With the uneconomical and potential unsafe issue inherent in this design option, it is primarily used for low aspect ratio diaphragm system in lower seismic zone. For the typical EDO design, LDE connection details are usually used because of no significant inelastic deformation demands required in this option.

2.5.3 Relaxed Design Option

The relaxed design option (RDO) is as indicated in Figure 2.21. The RDO is usually used for longer span diaphragm systems in high seismic zone, in which condition BDO design is not practical. Limited inelastic diaphragm response is allowed at the DBE level for this option. A smaller increase in current diaphragm force, F_{px} , is required compared with that of the BDO, an amplification factor Ψ_r is used as indicated in Figure 2.21. To provide more inelastic deformation at MCE level, the HDE connection details are usually required for the typical RDO design.

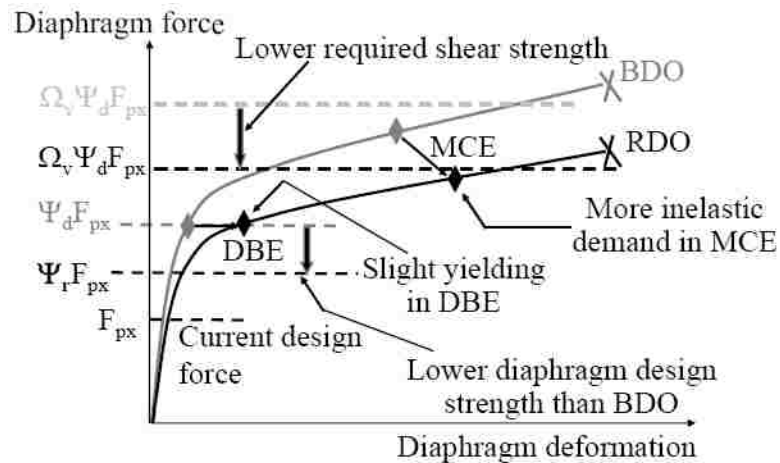


Figure 2.22. Relaxed Design Option (Zhang 2010)

2.6 References

1. Precast/Prestressed Concrete Institution. (2010). “*PCI design handbook: precast and prestressed concrete.*” Seventh Edition, Chicago IL.
2. ACI Committee 318 (2005). *Building Code Requirements for Structural Concrete and Commentary*, American Concrete Institute, Farmington Hills, MI.
3. Cao, L. (2006). “Effective Design of Precast Concrete Diaphragm Connections Subjected to In-Plane Demands”, Ph.D dissertation, Lehigh University, Bethlehem, PA
4. Menegotto, M., and Monti, G. (2005). “Waved Joint for Seismic-Resistant Precast Floor Diaphragms.” *J. Struct. Engrg.*, 131(10), 1515-1525.
5. IBC (2006). *International Building Code, 2006 Edition*. International Code Council, Inc., Falls Church, VA.

6. ASCE/SEI 7-05, *Minimum Design Loads for Buildings and Other Structures*, 2005 with Supplement 1. American Society of Civil Engineers, Reston, VA.
7. Fleischman, R. B., and Farrow, K. T. (2001) "Dynamic Response of Perimeter Lateral-System Structures with Flexible Diaphragms", *Journal of Earthquake Engineering & Structural Dynamics*, V.30, No. 5, May, pp. 745-763.
8. Iverson, J.K., Hawkins, N.M. (1994). "Performance of Precast/Prestressed Concrete Building Structures during Northridge Earthquake." *PCI Journal*, 39 (2), 38-55.
9. Ghosh, S. K., Hawkins, Neil M., "Proposed Revisions to 1997 NEHRP Recommended Provisions for Seismic Regulations for Precast Concrete Structures: Part 1-Introduction," *PCI Journal*, Vol. 45, No. 3, May-June 2000.
10. ICBO, *Uniform Building Code*, 1997 Edition, International Conference of Building Officials, Whittier, CA, May 1997.
11. Nakaki, S. D. "Design guidelines for precast and cast-in-place concrete diaphragms" Technical Report, *EERI Professional Fellowship*, Earthquake Engineering Research Institute, 2000, April.
12. Wood, S. L., Stanton, J. F., and Hawkins, N. M. (1995), "Performance of precast parking garages during the 1994 Northridge earthquake", Proceedings, *XIII ASCE Structures Congress*, Restructuring: America and Beyond, 1, New York, NY, pp. 563-566.
13. Wood, S. L., Stanton, J. F., and Hawkins, N. M., "New Seismic Design Provisions for Diaphragms in Precast Concrete Parking Structures," *PCI Journal*, 2000, 45 (1), Jan-Feb: 50-65.

14. Fleischman, R.B., Sause, R., Pessiki, S., and Rhodes, A.B. (1998). "Seismic Behavior of Precast Parking Structure Diaphragms." *PCI Journal*, 43(1), 38-53.
15. Rodriguez, M.E., Restrepo, J.I., and Carr, A.J. (2002). "Earthquake-induced floor horizontal accelerations in buildings." *Earthquake Engineering & Structural Dynamics*, 31(3), 693-718.
16. Fleischman, R.B. Farrow, K.T. Eastman, K. (2002). "Seismic response of perimeter lateral-system structures with highly flexible diaphragms." *Earthquake Spectra*, 18(2), 251-286.
17. Venuti, W. J. (1970). "Diaphragm Shear Connectors between Flanges of Prestressed Concrete T-Beams." *PCI Journal*, 15(1), 67-78.
18. Oliva, M.G. (2000). "Testing of the JVI Flange Connector for Precast Concrete Double-tee Systems." *Test Report*, Structures and Materials Test Laboratory, University of Wisconsin, Milwaukee, Illinois.
19. Shaikh, A.F., and Feile, E.P. (2002). "Testing of JVI Vector Connector." *Test Report*, Structural Engineering Laboratory, Milwaukee, Illinois.
20. Pincheira, J.A., Oliva, M.G., and Zheng, W. (2005). "Behavior of Double-Tee Flange Connectors Subjected to In-Plane Monotonic and Reversed Cyclic Loads" *PCI Journal*, 50(6), 32-54.
21. Building Seismic Safety Council, Committee TS-4. (2009). "Seismic design methodology for precast concrete floor diaphragms," Part III, 2009 NEHRP Recommended Seismic Provisions, Federal Emergency Management Agency, Washington, D.C.

22. Zhang, D. (2010). "Examination of precast concrete diaphragm seismic response by three-dimensional nonlinear transient dynamic analyses", Ph.D dissertation, the University of Arizona, Tucson, AZ.

Chapter 3 An Evaluation Method for Precast Concrete Diaphragm Connectors Based on Structural Testing

As discussed in Chapter 2, the Precast/Prestressed Concrete Institute in coordination with researchers from the University of Arizona, Lehigh University and the University of California San Diego have completed a comprehensive research project “DSDM” on the development of a seismic design methodology for precast concrete diaphragms. Unlike conventional force-based diaphragm design the new performance-based approach requires knowledge of the diaphragm connector stiffness, deformation capacity, and strength to effectively and efficiently design the diaphragm system for seismic forces. To meet this need it is critical that the connector properties be determined in a repeatable, reproducible, and consistent manner so that existing and new connections can be utilized effectively in the diaphragm system. This chapter proposes an experimental evaluation approach for assessing the mechanical properties of embedded connections used in conventional precast concrete panel systems. The measured responses are tied to performance levels which are used to categorize connectors in accordance with the new seismic design methodology for precast diaphragms.

The section 3.1 presents the background information including the simplified analytical approaches and existing experimental methods. The proposed evaluation method for precast concrete diaphragm connectors based on structural testing is presented in section 3.2.

3.1 Background

Precast concrete floor diaphragms are a popular form of construction in the United States for parking structures, residential and commercial facilities. The floor diaphragms are comprised of large precast concrete panels connected to each other through discrete embedded connections. These connections act to transfer vertical and in-plane demands between panels. Vertical force demands are limited to 3 kips in accordance with ASCE 7(ASCE 2010). Assurance of connector vertical capacity can be achieved through standard strength testing. Under seismic events the floor system is subject to in-plane inertial demands which subject the discrete connections to combinations of in-plane shear, tension and compression (Fleischman et. al. 1998).

Proper performance of connection details is critical for the effective design and safety of precast concrete building and bridge systems. Many types of mechanical connector details are used in precast concrete diaphragm systems to ensure integrity. Due to the large variation in details used it is not practical to assess performance based on generalized analytical response formulations.

Using traditional diaphragm design approaches, adequate in-plane force capacity is required for each connection to safely support the expected earthquake demands. Simplified diaphragm modeling methods are provided in the *PCI Design Handbook* to determine the required shear and tension demand in each connection. Subsequent force-based connection design approaches such as those outlined in the *PCI Connection*

Manual for Precast and Prestressed Concrete Construction can be followed to size the connection required. In addition, a significant amount of experimental research has been conducted evaluating response of diaphragm connectors under in-plane demands. This section presents the simplified analytical approach and existing experimental approaches.

3.1.1 Simplified Analytical Approaches

Simplified analytical methods for adequacy of connections have been developed and are described in PCI Design Handbook (PCI 2010). There are several approaches for determining the vertical shear, horizontal shear, and horizontal tension capacity of reinforcing bar-based connections in design of precast concrete connections. Current formulation for in-plane strength determination of a connection is based on a general design criteria presented in section 3.8.1.1 of the PCI Design Handbook (PCI 2010). The assumption in this formulation is that the connection resists in-plane shear and tension through the tension and/or compression of the steel anchorage legs. The resistance of the concrete is not explicitly accounted for in the approach. The connectors with splayed legs are designed assuming that each anchor leg reaches yield as shown in Figure 3.1.

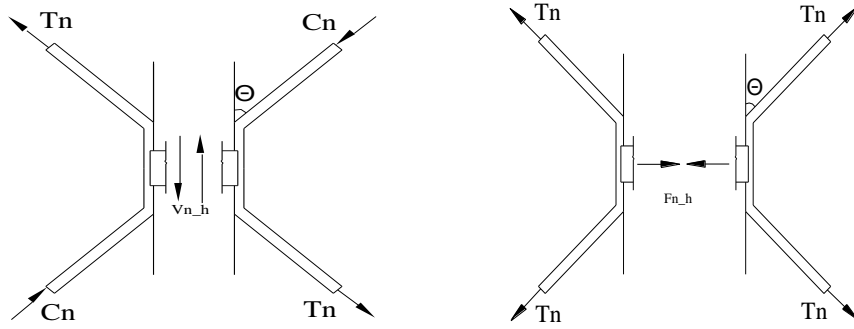


Figure 3.1. In-plane force of double-tee connection

Based on this assumed mechanism, the following equations (Eq. 3-1, Eq. 3-2, Eq. 3-3) are used for determining the nominal horizontal shear capacity, $V_{n,h}$, and the nominal horizontal tension capacity, $F_{n,h}$, of the connector.

$$C_n = T_n = A_s f_y \quad \text{Eq. 3-1}$$

$$V_{n,h} = (T_n + C_n) \cos \theta \quad \text{Eq. 3-2}$$

$$F_{n,h} = 2T_n \sin \theta \quad \text{Eq. 3-3}$$

Where T_n is the normal tension force, C_n is the normal compression force, $F_{n,h}$ is normal horizontal tension force, $V_{n,h}$ is the normal horizontal shear force, f_y is the yield strength of reinforcing bar, A_s is the cross section area of reinforcing bar, θ is the angel of reinforcing bar from faceplate.

The PCI Connection Manual for Precast and Prestressed Concrete Construction (PCI Connection Details Committee, 2008) provides an analytical method for the determination of the nominal vertical shear capacity (Figure 3.2) of the connection. It

accounts for two possible failure modes: the first controlled by steel yielding V_{n_v1} , and the second controlled by concrete shear failure V_{n_v2} .

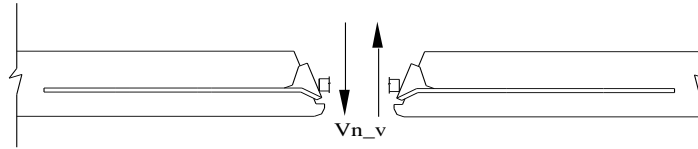


Figure 3.2. Out of plane vertical force of double-tee connection

The nominal vertical shear capacity, V_{n_v} , can be determined through the following equations (Eq. 3-4, Eq. 3-5 and Eq. 3-6)

$$V_{n_v1} = 2A_s f_y \quad \text{Eq. 3-4}$$

$$V_{n_v2} = 2.8\sqrt{f'_c} A_{cr} \quad \text{Eq. 3-5}$$

$$V_{n_v} = \text{Min}(V_{n_v1}, V_{n_v2}) \quad \text{Eq. 3-6}$$

Where A_s is the cross section area of reinforcing bar, f_y is the yield strength of reinforcing bar, A_{cr} is the area of assumed concrete crack interface, f'_c is the compressive strength of concrete, V_{n_v} is the normal vertical force, V_{n_v1} is the normal vertical force limited by steel, V_{n_v2} is the Normal vertical force limited by concrete.

These simplified analytical methods can be used to evaluate strength capacities of reinforcing bar based connections. While the majority of connections are configured similar to the splayed connector previously discussed, the actual strength of the connection is dependent on the details of the connector, amount of embedment, and

welding techniques used to attach the two connectors. Therefore, these methods can only accommodate a small amount of specific connection types for strength capacity evaluation.

3.1.2 Existing Experimental Methods

A significant amount of experimental research had been conducted on evaluating response of diaphragm connectors under in-plane and out-of-plane demands. Initial experiments on shear mechanical connector were conducted in 1968 when Venuti (Venuti 1970) examined 68 rebar connections. Since 1968 many studies have been conducted to qualify the performance of flange to flange connectors (CTC 1974; Spencer and Neille 1976; Aswad 1977; Spencer 1986; Kallros 1987; Pincheira et al. 1998; Oliva 2000; Oliva 2001; Shaikh and Feile 2002; WJE Associates Inc 2002; Shaikh and Feile 2003; Shaikh and Feile 2004; Pincheira et al. 2005; Shaikh and Gehlhoff 2005). These existing Experimental Methods are summarized in chronological order as illustrated in Table 3.1.

Connections were evaluated under in-plane shear loading, in-plane tension loading, and combined in-plane shear and tension demands. Studies were conducted both monotonically and cyclically. Most test fixtures from 1970 to 1980 were developed to examine the connector performance under monotonic in-plane shear strength through force control. This approach is unable to capture post-peak behavior and deformation capacity. In addition, most studies utilized half the connection to ease installation and lower testing cost. Research has shown that the level of axial restraint significantly

affects the measured shear capacity (Naito et al. 2006). These systems were connected to a stiff loading beam to artificially restrain the connector; unfortunately for most cases the axial restraint provided by the loading beam was not measured. With these shortcomings, the previous experimental approaches have limited ability to correctly quantify both the strength and deformation properties of diaphragm connections under in-plane demands.

Table 3.1. Evaluation methodologies of precast concrete diaphragm connections		
Ref.	Test Setup	Loading Protocol
Venuti, W. 1970		MV (Deformation control)
CTC. (1974)		MV (Force control)

Table 3.1. Evaluation methodologies of precast concrete diaphragm connections

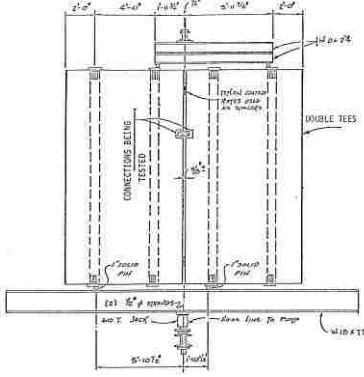
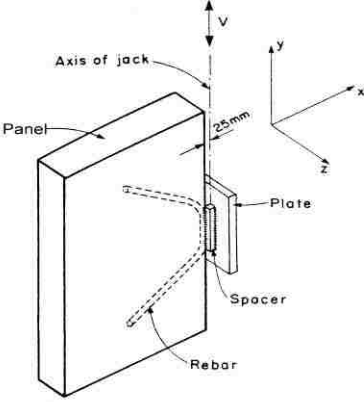
Ref.	Test Setup	Loading Protocol
Aswad (1977)		CV(3 Cycles)&MV (Force control)
		MV&OV (Force control)
		MV (Force control)
		MT (Force control)
R. Spencer (1986)		CV (Force control)
		MV (Force control)

Table 3.1. Evaluation methodologies of precast concrete diaphragm connections

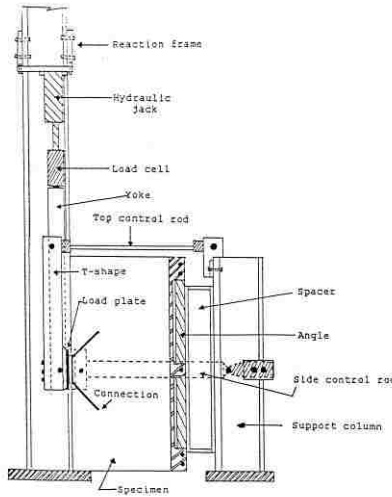
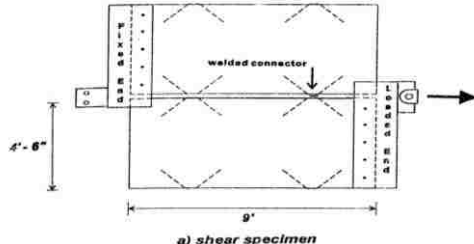
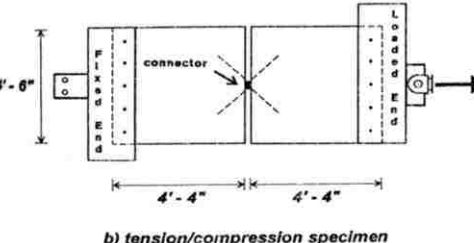
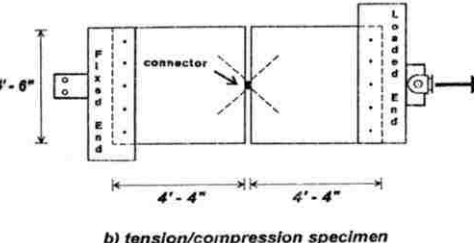
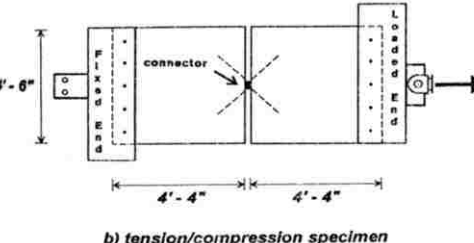
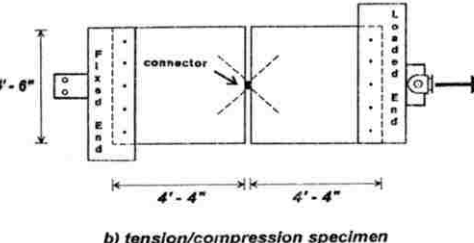
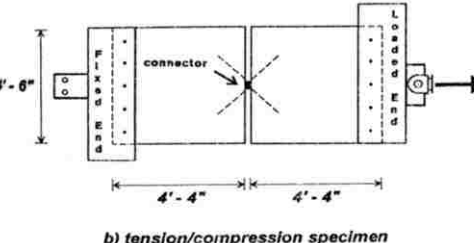
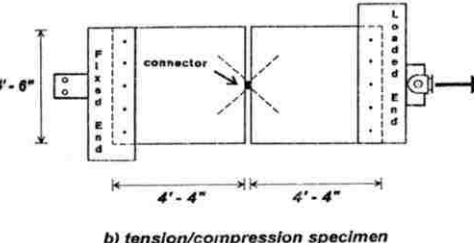
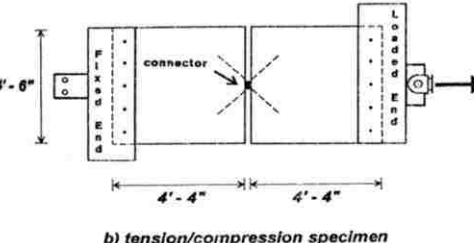
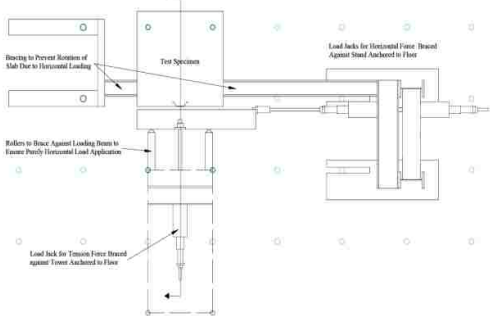

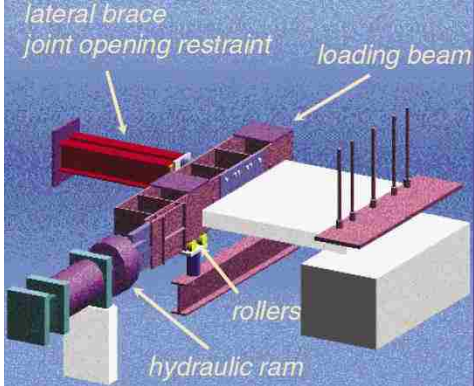
Ref.	Test Setup	Loading Protocol
Kallros (1987)		CV (Force control)
		MV (Force control)
Pincheira (1998)	 <p>a) shear specimen</p>	MV (Force control & Displacement Control)
	 <p>b) tension/compression specimen</p>	CV (Displacement Control)
	 <p>b) tension/compression specimen</p>	MT (Force control & Displacement Control)
	 <p>b) tension/compression specimen</p>	CT (Displacement Control)
	 <p>b) tension/compression specimen</p>	MVT-V (Force control & Displacement Control)
	 <p>b) tension/compression specimen</p>	MVT-T (Force control & Displacement Control)
	 <p>b) tension/compression specimen</p>	CVT-V (Displacement Control)
 <p>b) tension/compression specimen</p>	CVT-T (Displacement Control)	

Table 3.1. Evaluation methodologies of precast concrete diaphragm connections

Ref.	Test Setup	Loading Protocol
JVI (2000,2002,2003,2004,2005)		MV (Force & Displacement Control)
		CV (Displacement Control)
		OV (Force & Displacement Control)
		MT (Force & Displacement Control)
		MVT (Force & Displacement Control)
		CVT (Displacement Control)
Dayton (2002)		MV (Force control)
		MT (Force control)
		MVT (Force control)
		CV (Displacement Control)
		CVT (Displacement Control)
Pincheira (2005)		MV (Force control)
		MT (Force control)
		MVT (Force control)
		CV (Displacement Control)
		CVT (Displacement Control)
Note: M-Monotonic, C-cyclic, T-tension, V-shear, O-Vertical, VT-combined shear and tension		

As discussed previously the new performance-based formulation for precast diaphragms relies not only on the strength of the connections used but also on the stiffness and deformation capacities. Under the proposed design methodology the choice of connection type is tied to the flexure and shear over-strength factors needed by the diaphragm to meet the required level of seismic performance. While the methodology is complex, in essence the use of connections with limited deformation capacity could result in higher required design forces while ductile connections could allow for lower design forces. To choose the appropriate over-strength factor thus requires knowledge on the deformation capacity of each connection type used in the diaphragm.

Due to the variety of connections in use, analytical determination of the expected deformability is not trivial. Connection deformation capacity under in-plane tension and shear is contingent on a series of inelastic failure modes. These include concrete breakout, yield of the anchorage bars, flexure or torsion of the faceplate, yield of the slug or jumper plate, fracture of the welds, or fracture of the faceplate or anchorage as illustrated in Figure 3.3.

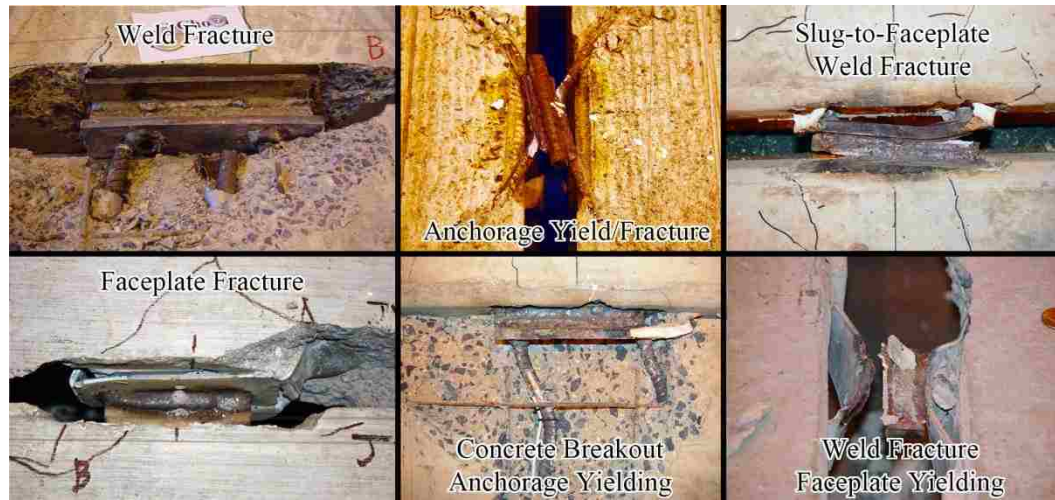


Figure 3.3. Potential in-plane failure modes in diaphragm connections

The occurrence of each of these conditions is difficult to accurately predict even with finite element methods. Furthermore each connection type exhibits variations in these modes of failure. Consequently proper determination of the deformation capacity of connections is best determined through experimental evaluation. A proposed experimental evaluation method for assessing the stiffness, strength capacity and deformation capacity of embedded connections used in conventional precast concrete diaphragm systems is as presented in the following section.

3.2 Proposed Evaluation Method for Precast Concrete Diaphragm Connections Based on Structural Testing

An experimental approach is provided to assess the in-plane strength, stiffness, and deformation capacity of precast concrete diaphragm connections. The methodology is developed specifically for diaphragm flange-to-flange connections. Similar procedures

can be used for collector elements however these methods have not been verified as part of this dissertation work.

3.2.1 Scope

This recommendation is intended to meet ACI Code 318-08 requirements for precast concrete connections (ACI 2008). As defined in Section 16.6.1.1 the adequacy of connections to transfer forces between members shall be determined by analysis or by test. This recommendation provides test procedures for assessing both strength and deformation capacity.

Under seismic demands connections between adjacent precast concrete diaphragms elements are subject to combinations of shear, tension and compression. The relative combinations of these deformation or force components are dependent on the location within the diaphragm and the presence of discontinuities. The testing method independently determines the shear and tension performance of connections. Alternate procedures are also provided for determination of combined interactions of shear and tension.

3.2.2 Test Module

To evaluate the performance of a precast concrete connection a test module representing the connection and the precast concrete element it is embedded in shall be fabricated and tested. A separate test module shall be used for each characteristic of

interest. At a minimum, one in-plane shear test module, and one in-plane tension test module shall be evaluated. It is strongly recommended to conduct multiple tests to assess repeatability and consistency.

Modules shall be fabricated at full scale unless reduced scale connectors are available. For reduced scale specimens appropriate reductions in maximum aggregate size should be accounted for and laws of similitude should be followed. Full scale modules shall include a tributary concrete section of at least 2 ft. Since the test module represents only a small portion of a precast concrete panel, potential confinement effects are not provided and the panel may be subjected to premature cracking. Additional reinforcement shall be used to prevent premature failure of the test module. The additional reinforcement shall not be placed in a way that would alter the performance of the connector. Example reinforcing strategy for the 2 ft by 4 ft $\frac{1}{2}$ test module is illustrated in Figure 3.4. The connections should be installed and welded in the test module in accordance with the intended guidelines.

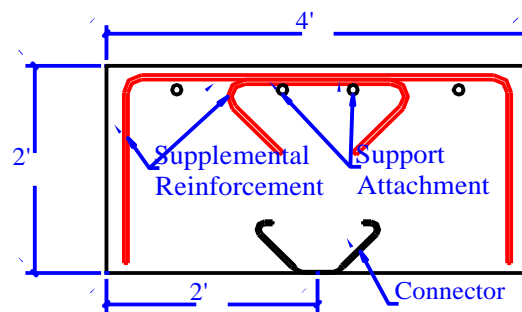


Figure 3.4. Test module plan view of half

3.2.3 Test Setup

For each connection test a multi-directional test fixture shall be used to allow for the simultaneous control of shear, axial, and potential bending deformations at the panel joint. A possible setup is illustrated in Figure 3.5. The fixture is composed of three independently controlled actuators, two providing axial displacement and one providing shear displacement to the connection. Demand shall be applied through displacement control of each of the three actuators. The test specimen shall be connected to restraint beams on either end of the panel, slip between the test module and beams shall be minimized. One support beam shall be fastened to the laboratory floor, providing a fixed end, while the other beam rests on a low friction movable support. Vertical movement of the panel shall be restricted by providing support under the center of each panel.

3.2.4 Instrumentation

At a minimum instrumentation shall consist of displacement and force transducers. Force shall be measured in line with each actuator to quantify shear and axial demands on the connection. To accommodate displacement control of the actuators feedback transducers shall be incorporated into each actuator. Connection deformation shall be measured directly on the test module (use of actuator transducers is not recommended due to potential slip in the test fixture). A minimum of two axial transducers shall be used to determine the average axial opening and closing at the connection. Shear deformation shall be determined from measurements taken at the location of the connection. Placement of the transducers on the test module shall be at an

adequate distance from the connection to minimize damage to the transducer supports during the test history. A possible arrangement of transducers is illustrated in Figure 3.5.

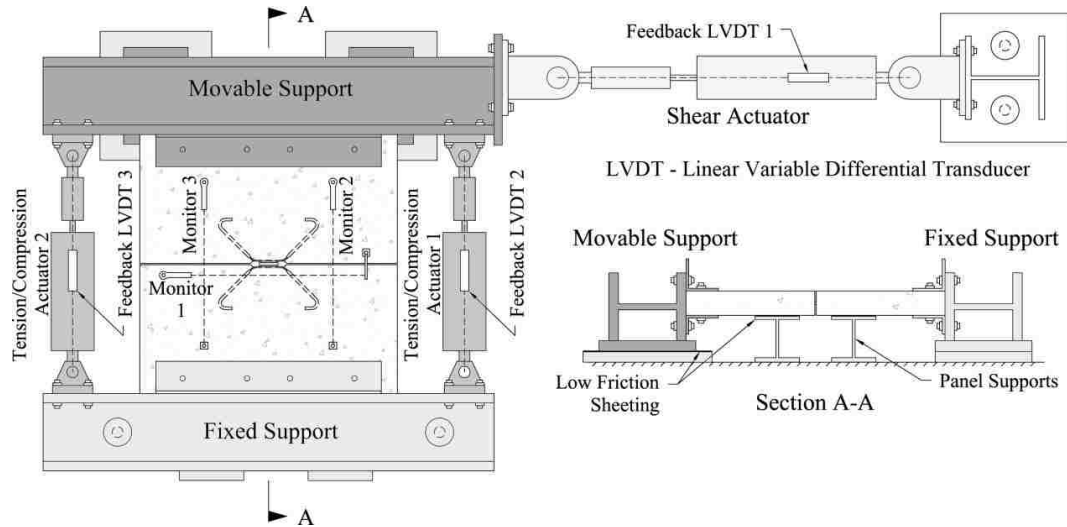


Figure 3.5. Multi-directional test fixture

3.2.5 Loading Protocols

The connections shall be evaluated for in-plane shear, tension, and combinations of shear with tension. Tests shall be conducted under displacement control using quasi-static rates less than 0.05 in. / sec or through an enhanced mixed displacement and force control. All test modules shall be tested until the specimen capacity approaches zero.

Under seismic demands a floor diaphragm system is subjected to a spectrum of relative motions. Analytical studies on the precast concrete diaphragm response to seismic demands have shown that the connection displacement history is dependent on the location within the diaphragm (Cao 2006). Connections located at the mid-span of the

diaphragm are subjected to high flexural demands while connections located at the boundaries are subjected to high shear demands with minimal tensile opening. Connections located in intermediate diaphragm regions are subjected to combined shear and tensile deformation demands with a common shear-to-tension deformation ratio of 2.0. To encompass these possible motions, six displacement protocols are proposed to assess the performance of diaphragm connectors subjected to seismic demands. They include:

- ***Monotonic Shear*** – For determination of connection shear yield and associated reference deformation for use in the cyclic loading protocol. Monotonic tests shall be eliminated if connection yield deformation can be estimated.
- ***Cyclic Shear*** – For determination of connector shear stiffness, strength, deformation limits, and modes of failure.
- ***Monotonic Tension*** – For determination of connection tension yield and associated reference deformation for use in the cyclic loading protocol. Monotonic tests shall be eliminated if connection yield deformation can be estimated.
- ***Cyclic Tension and Compression*** – For determination of connector tension stiffness, strength, deformation limits, and modes of failure.

- ***Monotonic Shear with Proportional Tension*** – Alternate protocol to assess influence of combined tension and shear.
- ***Cyclic Shear with Axial Force Control*** – Alternate protocol to assess influence of axial confinement on shear performance.

3.2.5.1 Monotonic Protocols

Monotonic shear and tension loading protocol consists of three preliminary cycles to 0.01 in to verify control and instrumentation operation. Following verification of the system the test module shall be loaded under a monotonically increasing displacement until failure. The monotonic test shall be used to determine the reference deformation of the connection if a reference is not available. The reference deformation represents the effective yield of the test module.

Reference Deformation

Experimental determination of the reference deformation, Δ , shall be based on a monotonic test of a connection test module. The reference deformation represents the effective yield deformation of the connector. It shall be computed by taking the intercept of a horizontal line at the maximum tension force (T_{max}) or shear force (V_{max}) and a secant stiffness line at 75% of the maximum measured load (Figure 3.6). As an alternate to the monotonic test, analytical determination of the reference deformation is allowed in accordance with section 3.2.6 and 3.2.7.

3.2.5.2 Cyclic Protocols

To assess the performance of diaphragm connections for use in seismic applications, evaluation shall be conducted with cyclically increasing demands. The cyclic demand shall be applied relative to the reference deformation of the connection to ensure that an appropriate number of elastic and inelastic cycles are applied.

Cyclic loading protocols in accordance with Precast Seismic Structural Systems (PRESSSS) program are recommended (Priestley, M. J. N. 1992.). Testing with three preliminary cycles to 0.01 in. shall be conducted to evaluate control and acquisition accuracy. The remaining protocol consists of groups of three symmetric cycles at increasing deformation levels. Each level is based on a percentage of a reference deformation computed from the corresponding monotonic tests.

Cyclic Shear Protocol

Cyclic shear protocol consists of three preliminary cycles to 0.01 in. to verify control and instrumentation operation. Following verification of the system the test module shall be loaded in increasing sets of shear deformation as illustrated as in Figure 3.6. The tension deformation across the joint shall be maintained at a constant level during the shear history through adjustment of the tension/compression actuators 1 and 2. The axial deformation shall be maintained at zero or at a tension opening of 0.1 in.

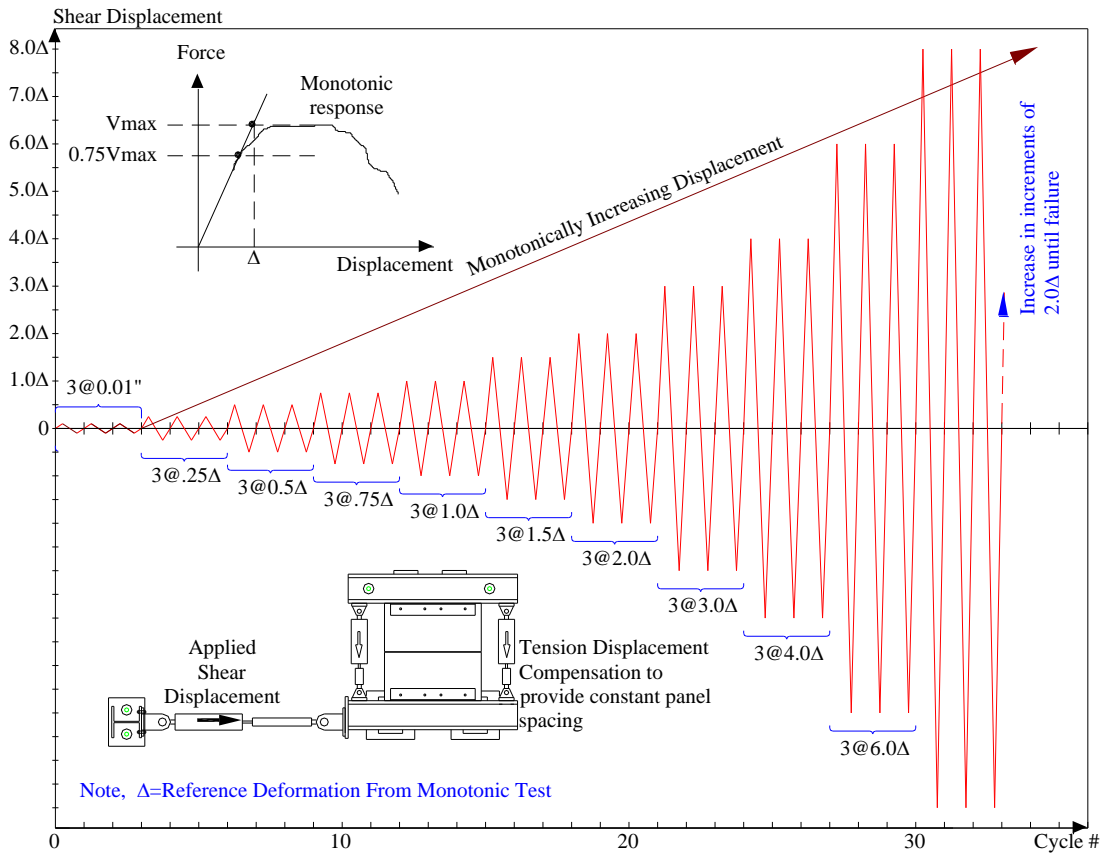


Figure 3.6. Shear loading protocol

Cyclic Tension / Compression Protocol

Cyclic tension / compression protocol consists of three preliminary cycles to 0.01 in. to verify control and instrumentation operation. Following verification of the system, the test module shall be loaded in increasing sets of tension deformation as illustrated as in Figure 3.7. Due to the high compression stiffness of connections the compression portion of each cycle shall be force limited. Each compression half cycle shall consist of

an increasing compression deformation until a force limit is reached. The force limit for each cycle shall be equal to the max force of the preceding tension half cycle. The shear deformation shall be maintained at zero through adjustment of the shear actuator. As an alternate, the shear actuator may be disconnected from the setup prior to loading allowing for zero shear force during the cyclic tension/compression history.

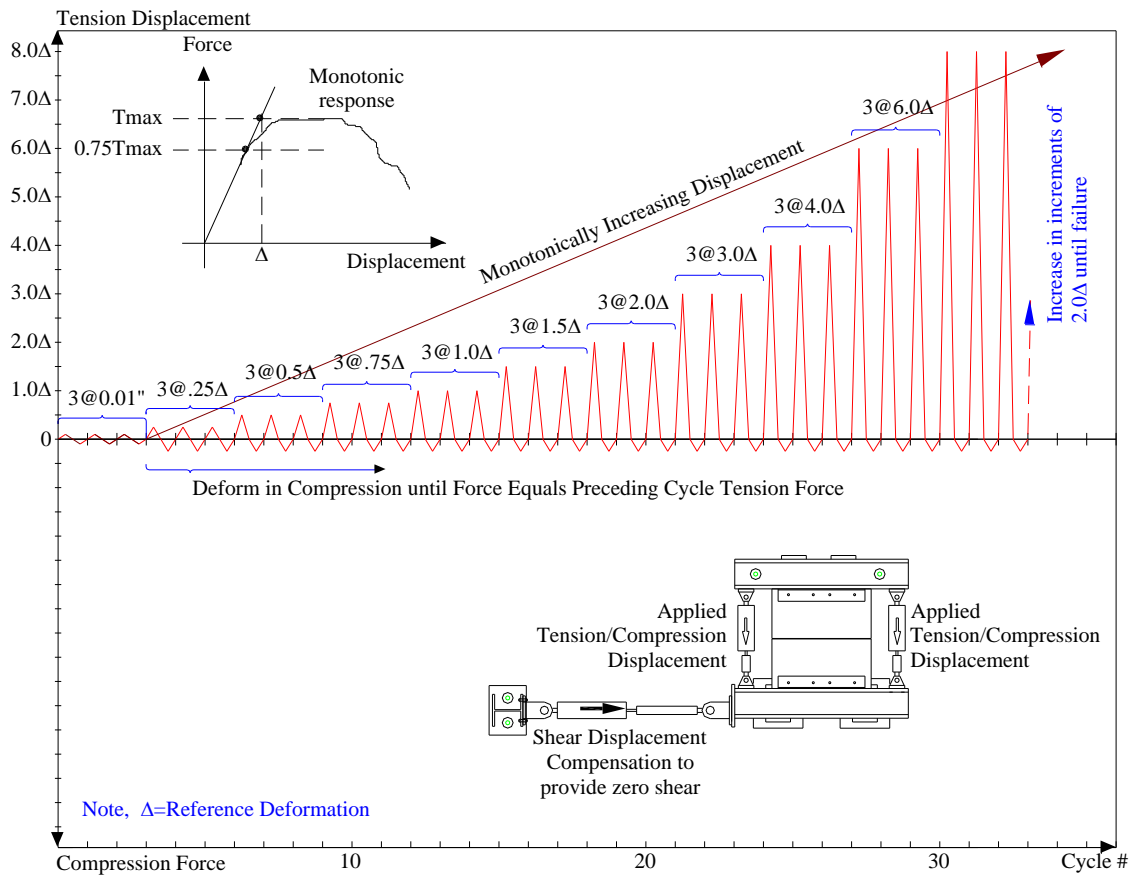


Figure 3.7. Tension/Compression loading protocol

3.2.5.3 Alternate Protocols

For cases where additional connector performance is needed, two alternative loading protocols can be used.

Monotonic Shear with Proportional Tension

Diaphragm connections may be subject to combinations of shear and tension due to their location in the diaphragm. A shear to tensile deformation ratio of 2.0 is recommended for web connections used in shear dominated regions of the diaphragm. A ratio of 0.5 is recommended for chord connections in tension dominated regions of the diaphragm. The monotonic shear with tension test consists of three cycles of 0.01 in. in shear and a proportional tension/compression deformation (Figure 3.8). The shear and tension deformations are increased proportionally using the chosen constant shear-to-tension deformation ratio. The test shall be paused at each 0.1 in. of shear deformation for observations.

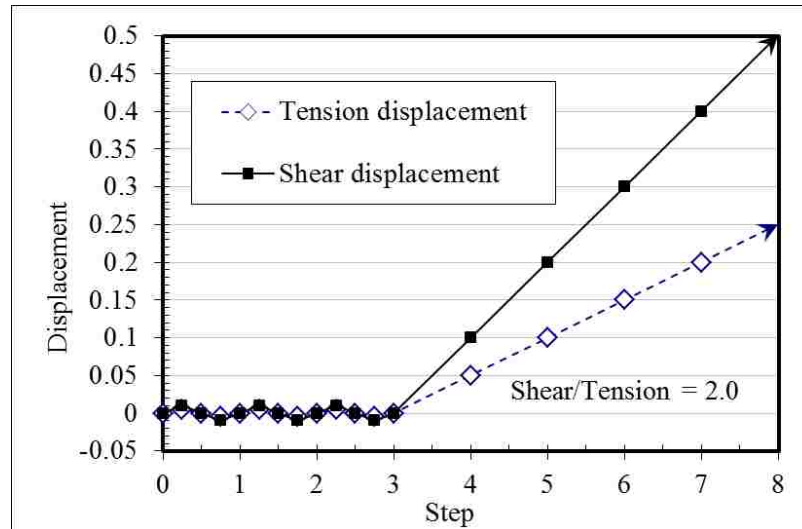


Figure 3.8. Monotonic shear with proportional tension (ratio of 2.0 shown)

Monotonic/Cyclic Shear with Axial Force Control

Enhanced displacement based control protocols may be used to evaluate the connections under in-plane shear. Standard shear displacement based protocols hold the joint opening at a fixed opening which may result in the build-up of large axial forces. The enhanced protocols are developed to examine the shear performance of connections under fixed levels of axial force. These test protocols provide information that can be used to model the shear resistance of connections at various locations in the floor diaphragm. This includes regions of high compression, tension or areas where zero axial loads are present.

All tests shall be conducted at quasi-static rates under mixed displacement and force control. The control shall be achieved using an inner control loop and an outer control loop. The outer loop conforms to the deformation based shear protocols shown in

Figure 3.6. Each displacement step shall be divided into small sub-steps of approximately 0.001 in. Each sub-step shall be applied in the inner control loop. The inner loop is controlled in a mixed load and displacement manner. After the application of each inner loop shear sub-step, the force in the axial actuators shall be measured. If the sum of the forces is greater than the target axial load, the actuators shall be extended an equal amount until the axial force equals the target. If the axial force is less than the target axial load, the actuators shall be retracted until the axial force equals the target. An error tolerance of 500 lbf to 1000 lbf shall be used for acceptance. Following this procedure the next sub-step shall be applied and the axial inner loop shall be repeated. This process shall be continued until the full outer shear step is applied. Then next shear step would be applied and the process would be repeated.

The algorithm of applying shear deformation with zero axial load is as follows:

1. Apply shear deformation step to shear actuator;
2. Read force in compression/tension actuators 1 and 2, F_1 and F_2 ;
3. Compute Total force, $F_t = F_1 + F_2$;
 - a. If, $F_t > 0$, Extend actuators 1 and 2 until $F_t = 0$
 - b. If, $F_t < 0$, Retract actuators 1 and 2 until $F_t = 0$
4. Go to Step 1 until target shear displacement is reached.

3.2.6 Tension Tests

- A monotonic tension test shall be conducted to determine the initial reference deformation for use in the cyclic tension tests. Two alternative (non-experimental) methods may be used for determination of the reference deformation.
 - (1) The reference deformation may be based on an analytical estimate of the yield deformation of the connection.
 - (2) The reference deformation may be based on a desired deformation capacity for the connection. For this method, the deformation category of the connection may be used as the reference deformation.
- In-plane cyclic tension tests shall be conducted to failure to determine stiffness, strength capacity and deformation capacity of connection under tension loading. The measured tension deformation capacity shall be used to establish the performance category of the connection.

3.2.7 Shear Tests

- A monotonic shear test shall be conducted to determine the initial reference deformation for use in the cyclic shear tests. Two alternative (non-experimental) methods may be used for determination of the reference deformation.
 - (1) The reference deformation may be based on an analytical estimate of the shear yield deformation of the connection.

(2) The reference deformation may be based on a desired deformation capacity for the connection.

- In-plane cyclic shear tests (with a constant 0.1 in. axial opening) shall be conducted to failure to determine stiffness and strength capacity of connection under shear loading. .
- In-plane monotonic shear with proportional tension tests may also be conducted for the connections used in intermediate diaphragm regions. In-plane cyclic shear with a target axial load tests could be conducted if needed.

3.2.8 Testing Observations and Acquisition of Data

Data shall be recorded from the test such that a quantitative, as opposed to qualitative, interpretation can be made of the performance of the test module. A continuous record shall be made of the force versus deformation. For in-plane tests the axial and shear force, and deformations should be recorded. Data shall be recorded at a minimum rate of 1.0 cycle/second. Photographs shall be taken to illustrate the condition of the test module at the initiation and completion of testing as well as points through the testing history. Ideally photos should be taken at the end of each group of cycles. Test history photos taken at points of interest, such as cracking, yield, ultimate load and post-test, are adequate for most evaluations.

3.2.9 Backbone Approximation

The experimentally measured performance shall be categorized in accordance with the procedures outlined in ASCE/SEI 41-06 Seismic Rehabilitation of Existing Buildings (ASCE/SEI 41-06). Each connection shall be classified as deformation-controlled (ductile) or force-controlled (non-ductile). This assessment shall be determined based on the backbone curve of the response.

An envelope of the cyclic force deformation response shall be constructed from the points making up the peak displacement applied during the first cycle of each increment of loading (or deformation) as indicated in ASCE/SEI 41-06. This method provides a higher estimate of strength than alternate methods outlined in FEMA 356, in which the envelope is defined by drawing through the intersection of the first cycle curve for all the $(i)th$ deformation step with the second cycle curve of $(i-1)th$ deformation step (FEMA 2000). The difference between the two methods is illustrated in Figure 3.9 for a ladder connection.

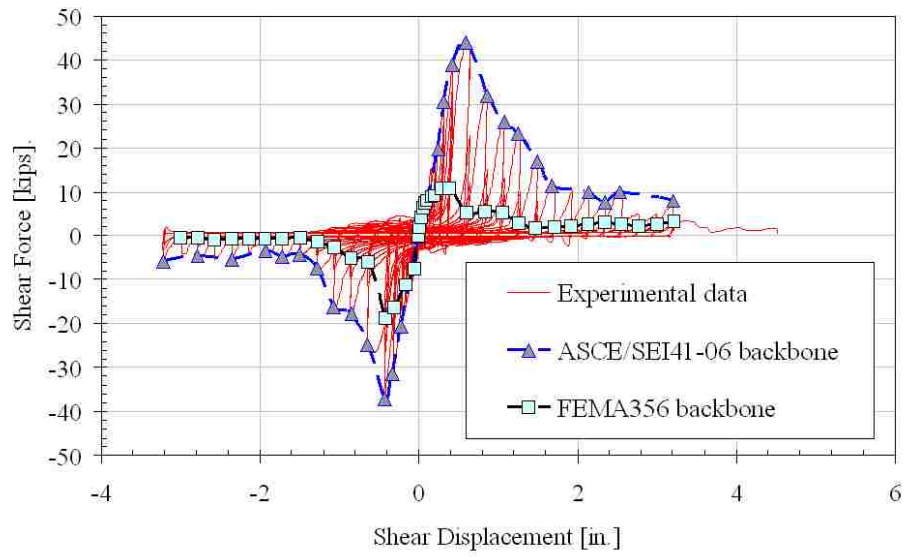


Figure 3.9. Cyclic envelope determination

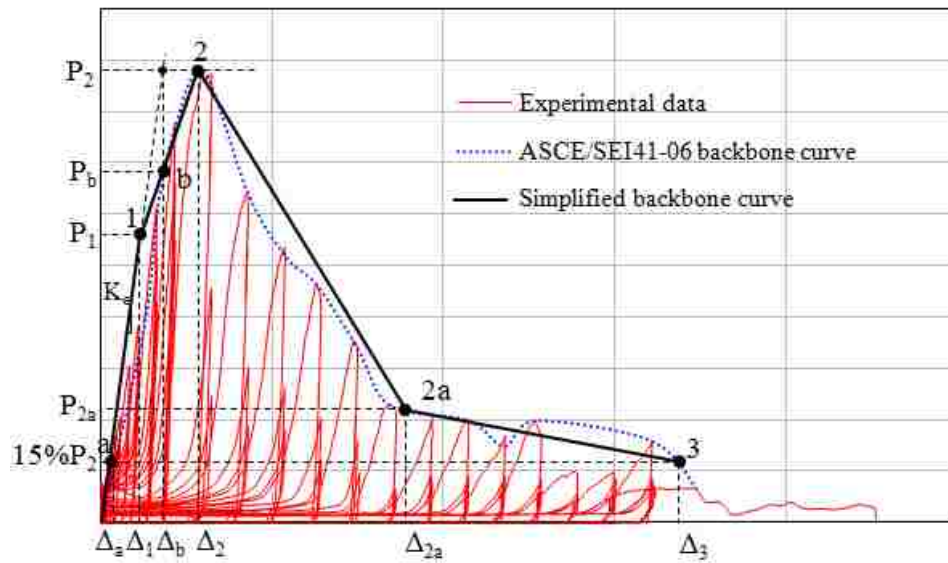


Figure 3.10. Simplified multi-linear backbone curve

The cyclic envelope shall be further simplified to a multi-segment backbone curve. The backbone curve shall consist of a four point (Point '1', '2', '2a', '3') multi-linear curve as illustrated in Figure 3.10.

The backbone curve is adopted to represent a simplistic approximation of the load-deformation response of the connection. Point '2' represents the peak envelope load. Point 'a' is defined as the point where the strength first achieves 15% of peak load. Initial elastic stiffness is calculated as the secant of strength-displacement relationship from origin to point 'a'. Point 'b' is the point on the envelope curve at a displacement Δ_b . The deformation Δ_b is the intersection of a horizontal line from the max envelope load and the initial elastic stiffness line at 15% of the max load. Point '1' represents the occurrence of yield, which is defined by drawing a line between point '2' and 'b' and extending back to intersect the initial elastic stiffness line at 15% of the max load. Point '3' is defined as the point where the strength is less than 15% of the peak load. Point '2a' is defined as the point where the deformation is 50% of the summation of deformations at point '2' and '3'. The points are defined in terms of the resistance P_a , P_1 , P_b , P_2 , P_{2a} , and P_3 , and the displacements Δ_a , Δ_1 , Δ_b , Δ_2 , Δ_{2a} and Δ_3 . The initial elastic stiffness K_e is the secant at point a. The procedure of determination of these points is shown as follows:

1. Determine the force at Point 2, $P_2 = P_{max}$
2. Determine the force at point a, $P_a = 15\% * P_{max}$

Determine the deformation at point a, Δ_a from original data.

3. Determine the initial elastic stiffness, K_e using the following equation(Eq. 3-7):

$$K_e = \frac{P_a}{\Delta_a} \quad \text{Eq. 3-7}$$

4. Determine the deformation at point b using Eq. 3-8:

$$\Delta_b = \frac{P_2}{K_e} \quad \text{Eq. 3-8}$$

Determine the force at point b, P_b from the original data.

5. Determine the deformation, Δ_1 , and force, P_1 at point 1 using the following equations (Eq. 3-9 and Eq. 3-10)respectively:

$$\Delta_1 = \frac{(P_b * \Delta_2 - P_2 * \Delta_b)}{K_e * (\Delta_2 - \Delta_b) - (P_2 - P_b)} \quad \text{Eq. 3-9}$$

$$P_1 = K_e * \Delta_1 \quad \text{Eq. 3-10}$$

6. Determine the force at point 3 using Eq. 3-11:

$$P_3 = 15\% * P_{\max} \quad \text{Eq. 3-11}$$

Determine the deformation at point 3, Δ_3 from original data.

7. Determine the deformation at Point 2a using Eq. 3-12

$$\Delta_{2a} = \frac{\Delta_2 + \Delta_3}{2} \quad \text{Eq. 3-12}$$

Determine the force at point 2a, P_{2a} , from the original data.

The backbone curve shall be classified as one of the types indicated in Figure 3.11. As depicted in Figure 3.11, the type 1 curve is representative of ductile behavior where there is an elastic range (point 0 to point 1 on the curve) and an inelastic range (point 1 to point 3 on the curve), followed by loss of force-resisting capacity. The type 2 curve is representative of ductile behavior where there is an elastic range (point 0 to point 1) and an inelastic range (point 1 to point 2 on the curve), followed by substantial loss of force-resisting capacity. Some connections may exhibit small peak strength with limited ductility. For these cases the alternate type 2 curve is recommended. The type 3 curve is representative of a brittle or non-ductile behavior where there is an elastic range (point 0 to point 1) followed by loss of strength. Deformation controlled elements shall conform to type 1 or type 2 response with $\Delta 2 \geq 2\Delta 1$. All other responses shall be classified as force-controlled.

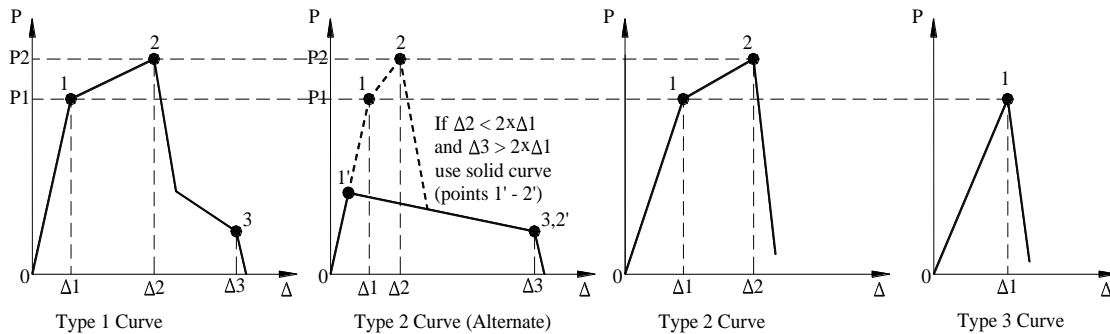


Figure 3.11. Deformation curve types

3.2.10 Data Reduction

The performance characteristics of the connector shall be quantified from the backbone response. The following values shall be quantified.

3.2.10.1 *Stiffness*

The initial elastic stiffness of the connection shall be determined from the secant to yield point 1. The previous formulation for K_e shall be used.

3.2.10.2 *Deformation Capacity*

The yield deformation shall be defined at Δ_1 , the max deformation at Δ_2 , and the residual deformation at Δ_3 . For deformation-controlled connections the *deformation capacity* shall correspond to Δ_2 . For force-controlled connections the *deformation capacity* shall correspond to Δ_1 . When multiple tests are conducted for repeatability the deformation capacity for each connection test shall be determined. The connection deformation capacity shall be determined as the mean value of each test deformation capacity for deformation-controlled elements and the mean minus one standard deviation for force-controlled connections.

3.2.10.3 *Deformation Category*

The connection shall be classified as a low-deformability element (LDE), a moderate-deformability element (MDE), or a high-deformability element (HDE) based

on its deformation capacity in tension. The deformation capacity as defined in previous section shall be used to classify the deformability category of the connector in accordance with Table 3.2. The category ranges were determined from the mean value of a database of diaphragm systems finite element analysis under a range of seismic demands (Building Seismic Safety Council Committee TS4, 2009). Alternate deformation limits can be used if supportive data is provided.

Table 3.2. Deformation category range	
Connection Deformability Category	Tension Deformation Limits, ΔT [in]
LDE	$0.00 < \Delta T \leq 0.15$
MDE	$0.15 < \Delta T \leq 0.50$
HDE	$\Delta T > 0.50$

3.2.10.4 Tension Force Capacity

The tension force capacity of the connection is defined as the maximum force, P_2 for deformation controlled connections and as P_1 for force controlled connections.

3.2.10.5 Shear Force Capacity

The intention is for the diaphragm system to remain elastic under shear demands. Consequently the inelastic shear force capacity of connections shall not be considered. The shear force capacity shall be computed at force level P_1 for all connections. Due to

the existence of low stiffness connections limits are placed on the allowable deformation at which the force capacity, P_I , can be determined.

- If the shear deformation Δ_I is less than 0.25 in., the shear force capacity shall be taken as the yield force P_I .
- If the shear deformation Δ_I is greater than 0.25 in., the shear force capacity shall be taken as the force value at 0.25 in. This shear force capacity can be computed as the stiffness, K_e , multiplied by 0.25 in.

3.2.11 Multiple Tests Approach

To provide accurate stiffness, strength, and deformation capacity multiple tests for shear and tension are recommended. The connection performance shall be tied to the number of tests conducted. The performance of the connector shall be based on the average of the tests if: a minimum of five tests are conducted, or at least three tests are conducted with none of the results varying more than 15 percent from the average of the three. Otherwise the lowest measured values shall be used. Additional requirements are recommended for determination of deformation capacity (see section 3.2.10.2).

When apply the multiple tests approach, it is noted that the average results are determined by averaging the simplified multi-linear curves of each type test for specific connection; The errors should be calculated by using the lower value as reference; In the

cases where tests are not conducted to failure, the highest load achieved for each test shall be assumed as ultimate.

3.2.12 Test Report

The test report must be sufficiently complete and self-contained for a qualified expert to be satisfied that the tests have been designed and carried out in accordance with the criteria previously described, and that the results satisfy the intent of these provisions. The test report shall contain sufficient evidence for an independent evaluation of the performance of the test module. As a minimum, all of the following information shall be provided:

- Details of test module design and construction, including engineering drawings.
- Specified materials properties used for design, and actual material properties obtained by testing.
- Description of test setup, including diagrams and photographs.
- Description of instrumentation, location, and purpose.
- Description and graphical presentation of applied loading protocol.
- Material properties of the concrete measured in accordance with ASTM C39 (ASTM 2008). The average of a minimum of three tests shall be used. The compression tests shall be conducted within 7 days of the connection tests or shall

be interpolated from compression tests conducted before and after the connection test series.

- Material properties of the connector, slug, and weld metal based on material testing or mill certification. As a minimum the yield stress, tensile stress, and the ultimate strain shall be reported.
- Description of observed performance, including photographic documentation, of test module condition at key loading cycles.
- Graphical presentation of force versus deformation response.
- The envelope and backbone of the load-deformation response.
- Yield strength, peak strength, and deformation capacity and connection category.
- Test data, report data, name of testing agency, report author(s), supervising professional engineer, and test sponsor.

Note: All the connections should be installed and welded in accordance with the manufacturer's published installation instructions. The results of the data generated shall be limited to connections built to the specified requirements.

3.3 Summary

An evaluation method for precast concrete diaphragm connectors based on structural testing is provided. The recommendation provides a detailed procedure for determination of stiffness, deformation capacity, and force capacity. Details on developing a test module, loading setup, load histories, instrumentation, data reduction, reporting and performance categorization is given. Adherence to the test method allows connection properties to be determined in a repeatable, reproducible, and consistent manner so that existing and new connections can be quantified and utilized effectively in the diaphragm system.

3.4 References

1. American Society of Civil Engineers (ASCE) 2010. *Minimum Design Loads for Buildings and Other Structures*. ASCE/SEI 7-10., Reston, VA.
2. Fleischman, R. B., R. Sause, S. Pessiki, and A. B. Rhodes. 1998. Seismic Behavior of Precast Parking Structure Diaphragms. *PCI Journal*, 43(1), 38–53.
3. Precast/Prestressed Concrete Institution. (2010). “*PCI design handbook: precast and prestressed concrete*.” Seventh Edition, Chicago IL.
4. PCI Connection Details Committee. 2008. *PCI Connection Manual for Precast and Prestressed Concrete Construction*. 1st ed. Chicago, IL: PCI.
5. Building Seismic Safety Council, Committee TS4. 2009. Seismic Design Methodology for Precast Concrete Floor Diaphragms, Part III. 2009 NEHRP

Recommended Seismic Provisions, Federal Emergency Management Agency, Washington, D.C.

6. Venuti, W. J. 1970. Diaphragm Shear Connectors between Flanges of Prestressed Concrete T-Beams. *PCI Journal*, 15(1), 67-78.
7. Concrete Technology Corporation. 1974. Tests of Shear Connectors Report. CTA-74-B8/9, 55-62.
8. Spencer, R. A., and Neille, D.S. 1976, Cyclic Tests of Welded Headed Stud Connectors, *PCI Journal*, 21(3), 70-83.
9. Aswad, A. 1977. Comprehensive Report on Precast and Prestressed Connectors Testing Program. *Research Report*, Stanley Structures, Inc, Denver, Colorado.
10. Pincheira, J. A., Oliva, M.G., and Kusumo-Rahardjo, F. I. 1998. Tests on Double Flange Connectors Subjected to Monotonic and Cyclic Loading. *PCI Journal*, 43(3) 82-96.
11. Pincheira, J.A., Oliva, M.G., and Zheng, W. 2005. "Behavior of Double-Tee Flange Connectors Subjected to In-Plane Monotonic and Reversed Cyclic Loads" *PCI Journal*, 50(6), 32-54.
12. Naito, C., Cao, L., Peter, W., 2009. Precast Double-Tee Floor Connectors Part I: Tension Performance. *PCI Journal*, 54(1), 49-66.
13. Cao, L., Naito, C., 2009. Precast Double-Tee Floor Connectors Part II: Shear Performance. *PCI Journal*, 54(2), 97-115.
14. Naito, C., W. Peter, L. Cao. 2006. Development of a Seismic Design Methodology for Precast Diaphragms - PHASE 1 SUMMARY REPORT. Advanced Technology

- for Large Structural Systems (ATLSS) Report No.06-03, ATLSS Center, Lehigh University.
15. American Concrete Institute (ACI) Committee 318. 2008. *Building Code Requirements for Structural Concrete (ACI 318-08) and Commentary (ACI 318R-08)*. Farmington Hills, MI: ACI.
 16. Cao, L. (2006). “Effective Design of Precast Concrete Diaphragm Connections Subjected to In-Plane Demands”, PhD dissertation, Lehigh University, Bethlehem, PA
 17. Priestley, M. J. N. 1992. The U.S.–PRESSS Program Progress Report. Third Meeting of the U.S. –Japan Joint Technical Coordinating Committee on Precast Seismic Structural Systems (JTCC-PRESSS), San Diego, CA, November 18-20.
 18. American Society of Civil Engineers (ASCE). 2007. *Seismic Rehabilitation of Existing Buildings*. ASCE/SEI 41-06. ASCE, Reston, VA.
 19. Federal Emergency Management Agency (FEMA). 2000. *NEHRP Commentary on the Guidelines for the Seismic Rehabilitation of Buildings*. FEMA 356, Washington, DC.
 20. Naito, C., Ren, R., Jones, C., Cullen, T., 2007, “Development of a Seismic Design Methodology for Precast Diaphragms – Connector Performance PHASE 1B,” Advanced Technology for Large Structural Systems (ATLSS) Report No.07-04, ATLSS Center, Lehigh University.

21. ASTM Standard C39, 2005, “Standard Test Method for Compressive Strength of Cylindrical Concrete Specimens,” ASTM International, West Conshohocken, PA, 2005, DOI: 10.1520/C0039_C0039M-05E01, www.astm.org.

Chapter 4 Experimental Studies of Improved Double Tee Connections

An experimental study of precast concrete diaphragm enhanced connections was conducted in accordance with the proposed evaluation method discussed in Chapter 3. This experimental program was conducted to examine the behavior of enhanced connection details under a series of loading patterns. Four discrete enhanced chord and web precast concrete diaphragm connection types were selected for full scale experimental evaluation. Full scale experimental investigation was conducted to determine the connection stiffness, strength and deformation properties, and further to evaluate the effectiveness of enhanced design. The connection failure mechanism under each loading pattern was investigated. This chapter discusses specific details of each connection. The experimental results of precast concrete diaphragm connections are presented. The experimental tension behavior is discussed in Section 4.7 and the experimental shear behavior is presented in Section 4.8.

4.1 Subassembly Details

According to the proposed evaluation method, a test module representing the connection and the precast concrete element it is embedded in was developed. This subassembly was developed assuming that the connectors are spaced at 4-ft and embedded in a double tee panel with a 2-ft distance from the DT web to the free flange

face. The subassemblies included two connectors embedded in a standard 2-in. or 4-in. pre-cast section. The panels were connected to form a 4ft square subassembly. Welded wire reinforcement (WWR) was included in each panel to meet ACI temperature and shrinkage reinforcement requirements (ACI 2008). In addition to the WWR conventional reinforcement was used to maintain integrity during testing. The bars were placed at the periphery of the panel to minimize influence on the connector response. To provide integrity at the boundary of the panels during testing, additional reinforcement was included in all test panels. The supplemental reinforcement is illustrated in Figure 4.1.

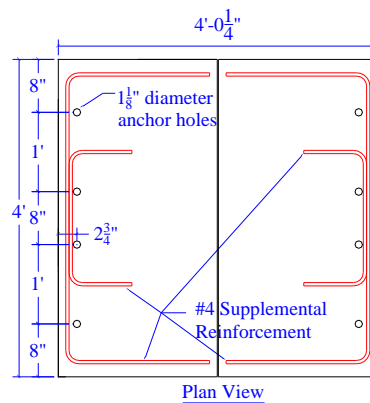
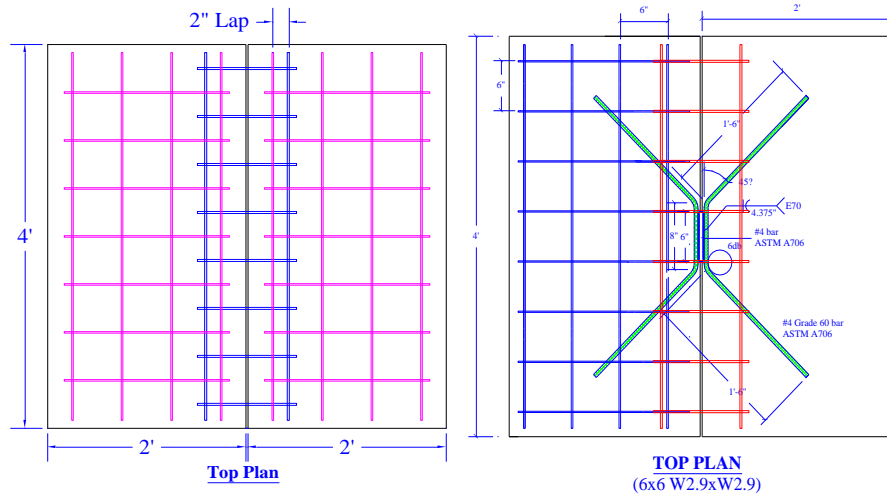


Figure 4.1. Supplemental reinforcement layout and construction details

4.2 Ductile Connection Specimens

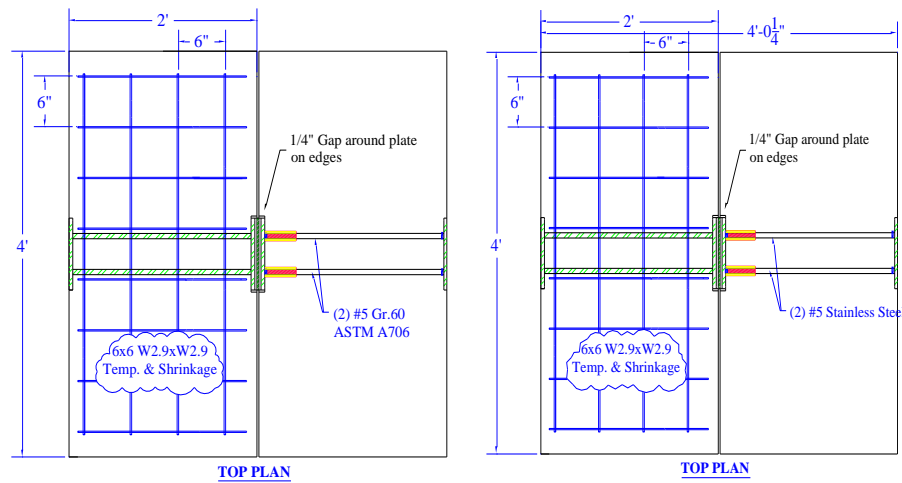
A series of experimental tests was conducted by recent research on conventional chord and web connection used in practice. Some enhanced details were proposed based on research finding to improve the connection behavior. These enhanced four ductile chord and web connections were selected for the experimental program (Figure 4.2). The

specific details were developed in collaboration with an industry advisory board to model current detailing techniques. Each specimen represented a diaphragm connection commonly used for pre-topped or topped diaphragm systems. Background information on each connection follows.



a. Ductile Ladder (DL)

b. Ductile Ladder with Hairpin (DL&HP)



c. Carbon Dry Chord

d. Stainless Dry Chord

Figure 4.2. Enhanced ductile connector specimen details

4.2.1 Ductile Ladder Connector

The ductile ladder connector was developed in coordination with Ivy Steel and Wire, Inc. The connector was fabricated from 1018 wire which has not been subject to the cold-rolling process. The welds were conducted at room temperature using a robotic welding process according to AWS specifications and ASTM standards. A special type of WWR 10x6 W4.9xW4.9 without cold-drawn process was placed across the joint in the 2-in filed placed topping. The connector would possess a high axial capacity and ductility as the “ladder” and wire configuration would act as a series of springs to resist the forces imposed on the diaphragm. The wire has a measured elongation of 30% which would lead to a predicted axial ductility of 3-in. across the 10-in. length of the ladder cross-members. The expected failure mode is fracture of the wires across the panel joint. The additional details of ductile ladder connector are illustrated in Figure 4.3.

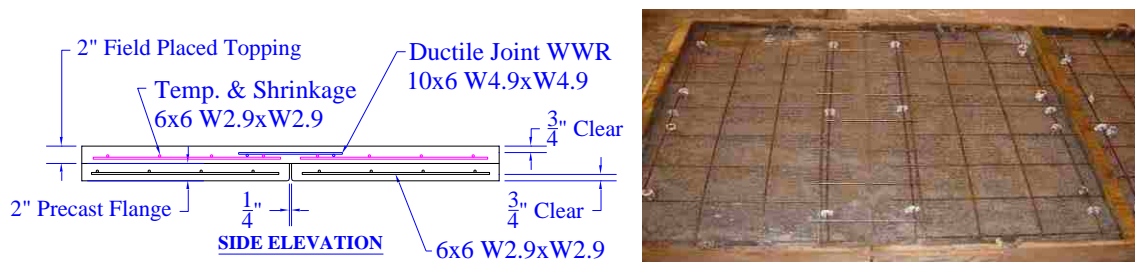


Figure 4.3. Ductile ladder connector

4.2.2 Ductile Ladder with Hairpin Connector

The Ductile Ladder with Hairpin connector was developed fabricated with ductile mesh in conjunction with a low cost “hairpin” connection fabricated from a bent #4 A706 reinforcing bar. Due to the low cost and ease of fabrication, the “hairpin” connector has been one of the most common shear connectors used in precast industry for 40 years. The specimen models a situation where a 2-in field placed topping was used over a double tee with 2-in. thick flange. The additional details of ductile ladder with hairpin connector are illustrated in Figure 4.4.

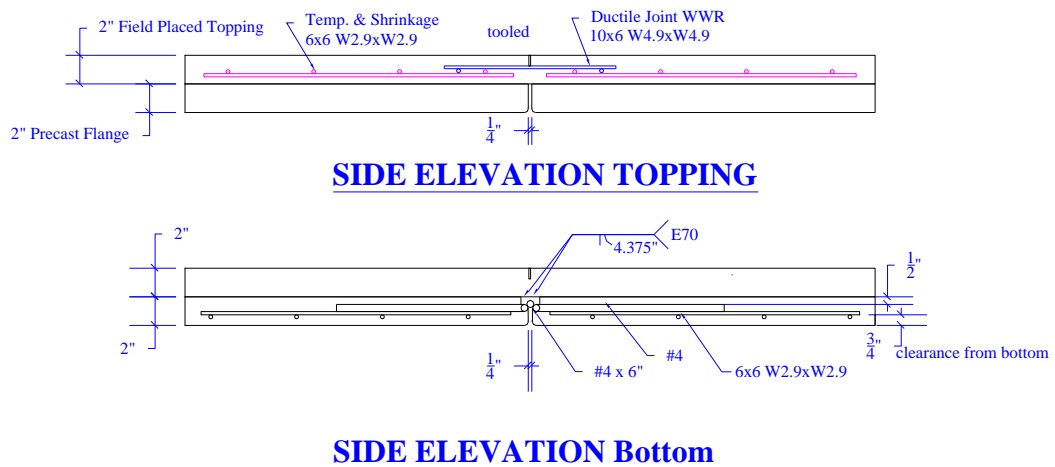


Figure 4.4. Ductile ladder with hairpin connector

4.2.3 Carbon Dry Chord Connector

The Pre-topped Carbon Chord Connector was developed in response to the poor performance of the conventional dry chord connection. The connection utilized an unbonded region to enhance the tension ductility of the connection and to allow for shear compliance (i.e., shear movement with low force resistance). The “Carbon” chord was fabricated from ASTM A36 plate and ASTM A706 reinforcement. All welds were conducted at room temperature using E7018 electrodes via the SMAW process. The welds were sized to produce failure of the reinforcement prior to the welds. The additional details of ductile ladder with hairpin connector are illustrated in Figure 4.5.

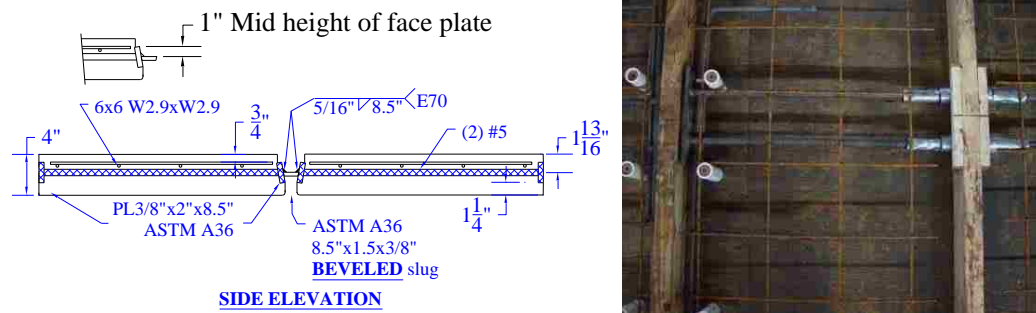


Figure 4.5. Pre-topped carbon chord connector

4.2.4 Stainless Dry Chord Connector

The Pre-topped Stainless Steel Chord Connector was also developed in response to the poor performance of the conventional dry chord connector. The connection utilized an unbonded region to enhance the tension ductility of the connection and to allow for shear compliance (i.e., shear movement with low force resistance). The

“Stainless” chord is an alternate to the Carbon steel chord examined. The stainless option can be used in regions where corrosion may be a concern. The connection was fabricated from type 304 Stainless plate, type 316LN reinforcing bar, and 308-16 weld electrodes. All welds were conducted at room temperature using the SMAW process in accordance with AWS procedures. The welds were sized to produce failure of the reinforcement prior to the welds. The additional details of ductile ladder with hairpin connector are illustrated in Figure 4.6.

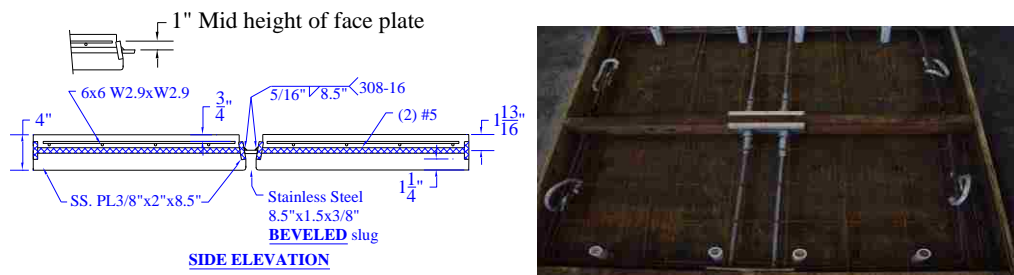


Figure 4.6. Pre-topped stainless chord connector

4.3 Material Properties

Materials used for fabrication of the test specimens replicated typical precast construction. Self-consolidating concrete with design strength of 7 ksi was used for the precast sections and a conventional 4 ksi ready mix concrete was used for the topping. These panels were built at High Concrete pre-cast facility under typical construction conditions. The average 28 day compressive strengths for each batch were determined from a series of 4-in. x 8-in. cylinder compressive tests conducted in accordance with ASTM C39. The material properties used for each connection are shown in Table 4.1.

Table 4.1. Material Properties						
Ductile Ladder	Concrete	Concrete Panel Type		Compressive Strength, f'c (psi) at time of test		
		2-in. base		5834 ± 235		
		2-in. topping		4558 ± 138		
	Steel	Size	Reinforcement Usage	Grade	Yield Stress(ksi)	Ultimate Strength (ksi)
10x6 W4.9XW4.9		Ductile Ladder	1018	54.2	76.6	
#4		Reinforcing Bars	A615 Gr. 60	67.7	105.4	
	6x6 W2.9XW2.9	Panel Mesh	A185 Gr.65	65.0*	108.5*	
Ductile Ladder with Hairpin	Concrete	Concrete Panel Type		Compressive Strength, f'c (psi) at time of test		
		2-in. base		7365 ± 576		
		2-in. topping		5764 ± 52		
	Steel	Size	Reinforcement Usage	Grade	Yield Stress(ksi)	Ultimate Strength (ksi)
		#4	Hairpin	A706	65.79	91.39
		#4	Reinforcing Bars	A615 Gr. 60	67.7	105.4
		6X6 W2.9XW2.9	Panel Mesh	A185 Gr. 65	65.00*	108.5
	10 X 6 W4.9XW4.9	Ductile Ladder	1018	54.2	76.6	
Carbon Dry Chord	Concrete	Concrete Panel Type		Compressive Strength, f'c (psi) at time of test		
		4-in.		5700 ± 367		
	Steel	Size	Reinforcement Usage	Grade	Yield Stress(ksi)	Ultimate Strength (ksi)
		#5	Anchorage Bar	A706	65.6	94.3
		PL 3/8" x 2" x 8.5"	Faceplate	A36	47.9	69.7
		PL 1" x 3/4" x 8.5"	Beveled Slug	A36	61.9	78.7
		#4	Reinforcing Bars	A615 Gr. 60	67.7	105.4
	6X6 W2.9XW2.9	Panel Mesh	A185 Gr. 65	65.00*	108.5	
Stainless Dry Chord	Concrete	Concrete Panel Type		Compressive Strength, f'c (psi) at time of test		
		4-in.		5700 ± 367		
	Steel	Size	Reinforcement Usage	Grade	Yield Stress(ksi)	Ultimate Strength (ksi)
		#5	Connector	316LN	98	118
		PL 3/8" x 2" x 8.5"	Faceplate	A304L	41.3	85.4
		PL 1" x 3/4" x 8.5"	Beveled Slug	A304L	41.3	85.4
		#4	Reinforcing Bars	A615 Gr. 60	67.7	105.4
	6X6 W2.9XW2.9	Panel Mesh	A185 Gr. 65	65.00*	108.5	

* Data unavailable, value assumed

4.4 Test Setup

A multi-directional test fixture was developed to allow for the simultaneous control of shear, axial, and bending deformations at the panel joint in accordance with Section 3.2.3. The fixture utilized three actuators, two in axial displacement and one in shear displacement as shown in Figure 4.7.



Figure 4.7. Multi-directional test setup

One edge of the panel was bolted onto the flange of a fixed restraining beam. The beam was welded to a base plate which was keyed into the lab floor. The other edge was attached to a low friction loading beam. The beam bears on Teflon sheets to reduce friction and was free to move in the horizontal plane. Control of the beam was made with a shear actuator and two tension-compression actuators. To provide vertical support to the test panels, two Teflon covered support beams were provided underneath the specimen. Tension and compression were applied to the connector through two 70 kip actuators, which were joined to the free-end load beam flange on both sides of the panel. Shear was applied with a 110 kip actuator attached to the movable load beam. Shear, tension, and compression loads were measured by load cells attached between the

hydraulic jack and free-end load beam. External LVDT's were used between each beam to control the applied deformation. The LVDT's were centered pin to pin of each actuator.

4.5 Loading Protocols

The specimens were tested under pure shear, pure tension, and combined shear with tension. All tests were conducted under quasi-static displacement control at a rate less than 0.05in/sec. The tests were continued until specimen capacity approaches zero. According to requirements defined in the new developed evaluation method (Section 3.2.5), six deformation protocols were used to represent the spectrum of demands a local diaphragm connector could experience under lateral loading:

- Monotonic Tension as defined in Section 3.2.5.1.
- Cyclic Tension and Compression as defined in Section 3.2.5.2.
- Monotonic Shear as defined in Section 3.2.5.1.
- Cyclic Shear as defined in Section 3.2.5.2.
- Monotonic Shear with Targeted Axial Force (0 kip) as defined in Section 3.2.5.3.
- Cyclic Shear with Targeted Axial Force (0 kip) as defined in Section 3.2.5.3.

4.6 Test Matrix

To identify the performance of enhanced precast concrete diaphragm ductile connections the experimental program incorporates twenty tests conducted on four connection specimens. Each connection was subjected to a series of loading patterns which were found critical in the seismic response of a regular diaphragm. Test matrix and loading protocols for the four specimens are summarized in Table 4.2.

Table 4.2. Test Matrix		
Test Specimen	ID	Loading Protocol
Topped Ductile Ladder(DL)	DL-1	Monotonic Shear with DT =0
	DL-2	Monotonic Shear with FT=0
	DL-3	Monotonic Tension with FV=0
	DL-4	Cyclic Shear with DT =0.1in
	DL-5	Cyclic Tension with FV=0
	DL-6	Cyclic Shear with FT=0
Topped Ductile Ladder with Hairpin(DL&HP)	DL&HP-1	Cyclic Tension with FV=0
	DL&HP-2	Cyclic Shear with DT =0.1in
	DL&HP-3	Cyclic Shear with FT=0
	DL&HP-4	Cyclic Shear with FT=0
Pre-topped Carbon Chord (CC)	CC-1	Monotonic Tension with FV=0
	CC-2	Monotonic Shear with DT =0
	CC-3	Monotonic Shear with FT=0
	CC-4	Cyclic Shear with DT =0
	CC-5	Cyclic Tension with FV=0
Pre-topped Stainless Chord(SC)	SC-1	Monotonic Shear with DT =0
	SC-2	Monotonic Tension with FV=0
	SC-3	Cyclic Tension with FV=0
	SC-4	Cyclic Shear with DT =0
	SC-5	Cyclic Shear with FT=0
Note: FV-Shear force, FT-Tension force, DT-Tension deformation, DV-Shear deformation		

4.7 Experimental Tension Behavior

To examine the in-plane tension response of the connections, a series of tension tests were applied on four enhanced ductile connections. Monotonic tension test (MT) was conducted on three connection specimen (ductile ladder, carbon chord and stainless chord) to obtain the reference deformation for cyclic tension test. The reference deformation of the connection specimen ductile ladder with hairpin was assumed to be the same as of ductile ladder connector. Cyclic tension test (CT) was conducted each connection specimen to examine the effect of load reversals. The performance of these connections under various tension loading patterns are presented in this section.

4.7.1 Experimental Tension Results

The connections exhibited a wide range of strength and ductility. The monotonic and cyclic tension response of each connection is summarized in Figure 4.8 and Figure 4.9. The measured response and a detailed response backbone curve are presented. The carbon chord and stainless chord connections provided relatively high tension resistance while the web connections ductile ladder and ductile ladder with hairpin provided a moderate resistance.

4.7.2 Comparative Tension Behavior

The measured experimental data was compared to the design strength and the expected ultimate tension strength. The design strengths were based on the expected yield

stress of the material. All ultimate strength estimates were computed using the tensile strengths of the connectors based on mill certified properties. The formulations were computed based on a simplified truss analogy in accordance with the PCI Design Handbook Section 4.8 (PCI 2010). This force-based method estimated the available capacities due to a ductile failure in the connector leg. It was assumed that the welds are adequately proportioned to resist the bar fracture strength and that forces were applied uniformly and concentrically to the connector.

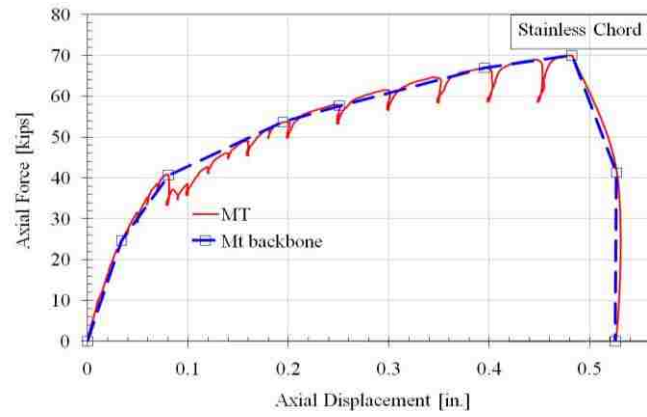
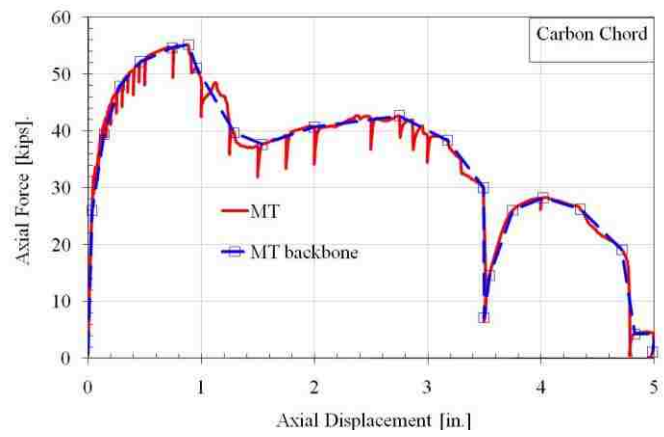
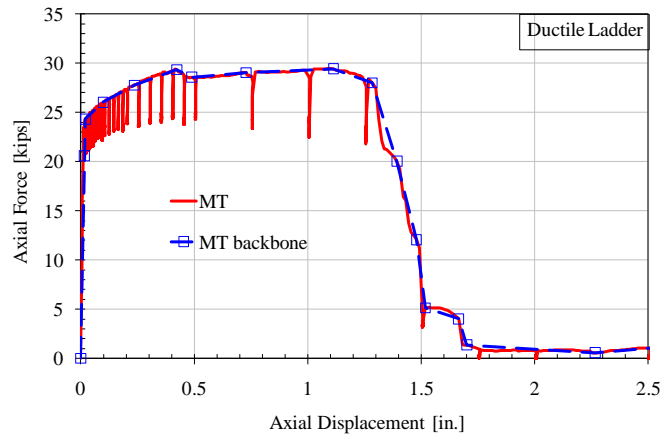


Figure 4.8. Monotonic tension response

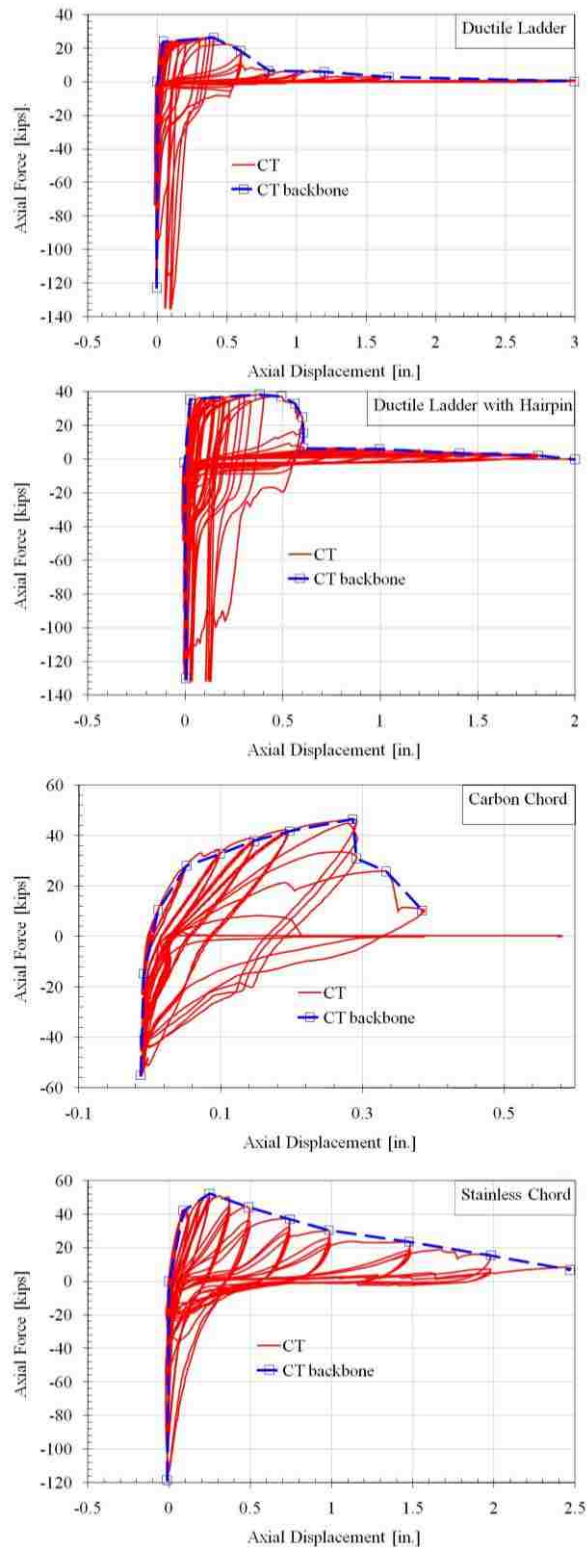


Figure 4.9. Cyclic tension response

For the splayed leg connectors (Hairpin), the capacity was estimated with the truss model to determine the PCI design strength. For the perpendicular leg connectors (carbon chord, stainless chord & ductile ladder) the capacity of the connector was based on the bar strength. In computing the design capacity of the topped connectors, it was assumed that the WWR mesh and connector are both at yield; however, for the ultimate capacity the assumption was made that the wires were already fractured. Hence the topping WWR mesh ultimate strength was not added to connector strength. In computing the design capacity of the topped connectors, it was assumed that the WWR mesh and connector were both at yield; however, for the ultimate capacity the assumption was made that the wires were already fractured. Hence the topping WWR mesh ultimate strength was not added to connector strength. The following terminology was used: cross-sectional area of one leg: A_s , bar yield or tensile strength: f_y , total cross-sectional area of WWR: A_{s_wvr} , WWR yield or ultimate tensile strength: f_{wvr} . The total cross-sectional area of ductile mesh: A_{s_wvr1} , ductile mesh yield or ultimate tensile strength: f_{wvr1} . The formulations used for design capacity and ultimate strength are summarized in Table 4.3.

Table 4.3. Connector Capacity Formulation Estimates		
Connector	Design Capacity, P_n	Ultimate Capacity, P_u
Ductile Ladder	$f_{wvr1-y} \cdot A_{s_wvr1}$	$f_{wvr1-u} \cdot A_{s_wvr1}$
Ductile Ladder w/ Hairpin	$2 \cdot (f_y \cdot A_s \cdot \cos 45^\circ) + f_{wvr-y} \cdot A_{s_wvr} + f_{wvr1-y} \cdot A_{s_wvr1}$	$2 \cdot (f_u \cdot A_s \cdot \cos 45^\circ) + f_{wvr1-u} \cdot A_{s_wvr1}$
Carbon Chord	$2 \cdot (f_y \cdot A_s)$	$2 \cdot (f_u \cdot A_s)$
Stainless Chord	$2 \cdot (f_y \cdot A_s)$	$2 \cdot (f_u \cdot A_s)$

The calculated strengths were compared to the measured responses in Table 4.4. The results from the monotonic tension, MT, and the cyclic tension-compression, CT, are presented. The mill certified material properties, presented before, were used for ultimate strength calculations when available.

Table 4.4. Connector Capacity Experimental Results				
Connector	Design Capacity, P_n [kips]	Ultimate Capacity, P_u [kips]	MT [kips]	CT [kips]
Ductile Ladder	21.25	30.03	29.41	26.35
Ductile Ladder w/ Hairpin	39.90	55.90	-	38.35
Carbon Chord	37.20	59.25	55.18	47.89
Stainless Chord	60.76	73.16	70.00	52.25

The connectors such as ductile ladder, carbon chord and stainless chord connector all met or exceeded their estimated design capacity and less than ultimate capacities. The connector ductile ladder with hairpin did not achieve their expected design or ultimate capacities due to premature failures at the welded regions.

In general, the connectors built with ductile ladder exhibited a flexible tensile response. The connectors achieved large deformations prior to strength loss due to bending of the un-welded portion of the connector front face. The straight leg chord connectors in comparison exhibited a high initial tensile stiffness, and were capable of only limited ductility. An in-depth evaluation of each connection follows.

4.7.2.1 Ductile Ladder Connector

The ductile ladder connector was evaluated under monotonic tension and cyclic tension loading separately.

Monotonic Tension

The measured capacity of the connector in pure tension was 98% of the ultimate capacity and 38% over the design capacity according to PCI design standards. The expected failure mode is fracture of the wires across the panel joint. As expected, the strands of the ductile ladder connection fractured along with several strands of the temperature and shrinkage reinforcement. The ductile ladder connector was developed in response to the brittle response with low deformability of conventional WWR topping mesh connector (Naito et al. 2006). The stiffness and strength of conventional WWR topping mesh connector matched the expected capacity. However, its deformation capacity was limited due to the cold-drawn process used for WWR strands.

The ductile ladder connector is expected to possess a high axial capacity and ductility as the “ladder”, wire configuration would act as a series of springs to resist the forces imposed on the diaphragm. The predicted axial ductility of the connector is 3-in. across the 10-in. length of the ladder cross-members since the wire has a measured elongation of 30%. Compared with the conventional topping mesh connector, there is significant improvement in deformation capacity, from 0.1-in. to 1.3-in. The connector is capable of surpassing the design capacity and matching the ultimate capacity. The damage of connector is displayed in Figure 4.10.



Figure 4.10. Damage state at 2.5-in tensile opening

Cyclic Tension

The measured tensile capacity of the connector was 88% of the ultimate capacity and 24% over the design capacity according to PCI design standards. The expected failure mode was fracture of the wires across the panel joint. As expected, the strands of the ductile ladder connection fractured at the end of test. But during the test, buckling of wires results in spalling and premature loss of cover concrete, which resulted in the force capacity loss.

Compared with the monotonic tension test, the ultimate force capacity is decreased by 10%, which may have been caused by the premature loss of concrete panel. The ductile deformation capacity is decreased from 1.1-in. to 0.4-in. for the cyclic tension test. The connector is capable of surpassing the design capacity, while the ultimate capacity is not achieved. This may be enhanced by using a thicker concrete cover, which was validated in the following ductile ladder w/ hairpin tests. The damage of connector is displayed in Figure 4.11.

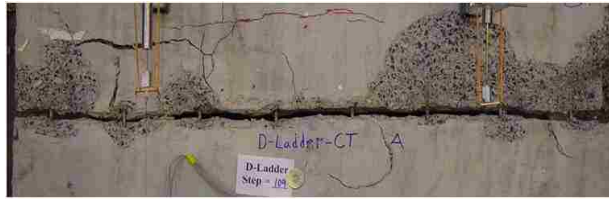


Figure 4.11. Damage state at 3.0-in tensile opening

Summary

The previously developed backbone axial force-deformation curves of the connector are presented in Figure 4.12. The ductile ladder connector exhibited a high ductility and is capable of maintain expected force capacity. A thicker concrete cover is recommended for ductile ladder connector to avoid premature loss of concrete panel.

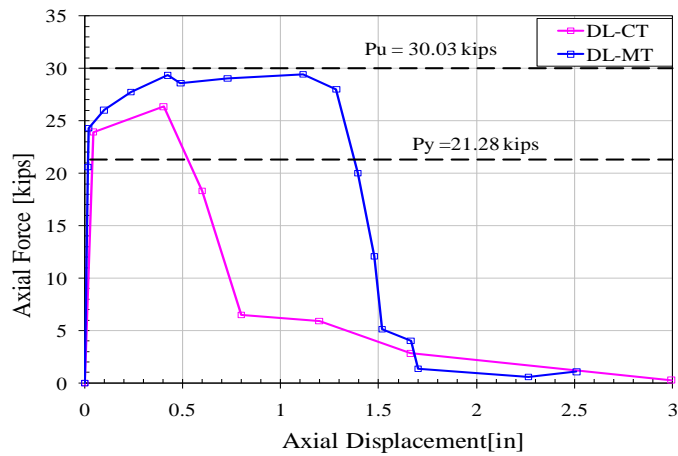


Figure 4.12. Ductile ladder (DL) tensile data

4.7.2.2 Ductile Ladder with Hairpin Connector

Cyclic Tension

The measured capacity of the ductile ladder w/ hairpin connector was 69% of the ultimate capacity and 96% of the design capacity according to PCI design standards. This was due to the connector-to-slug weld tearing of hairpin connector, despite the weld was designed to resist the bar fracture strength. Fracture of ductile ladder wires was observed at about 0.6-in, which caused the resistance strength of connector dropped down quickly to 6.38-kip. After that, weld tearing was observed at about 1.0-in. coupled with noticeable connector slug rotation, which caused the connector's strength decrease gradually until the connector lost all capacity at 2.0-in. A thicker concrete cover was used for the ductile ladder with hairpin connector, which improved the concrete spalling situation. The damage of connector is displayed in Figure 4.13.



Figure 4.13. Damage state at 2.0-in tensile opening

Summary

The previously developed backbone axial force-deformation curves of the connector are presented in Figure 4.14. The CT test data for ductile ladder is also included for comparison and discussion. The ductile ladder with hairpin connector was not able to achieve its ultimate capacity due to the premature weld failure. Compared with the cyclic tension test for ductile ladder alone, the maximum force for both case all occurred at about 0.40-in tensile joint opening, and the force capacity was increased by 12kips for the latter case. The yield all happened at about 0.05-in tensile opening, which means the ductile ladder wires yield quickly. It is indicated that the ductile ladder is able to remain for a significant joint opening before all the strands of the ladder failed.

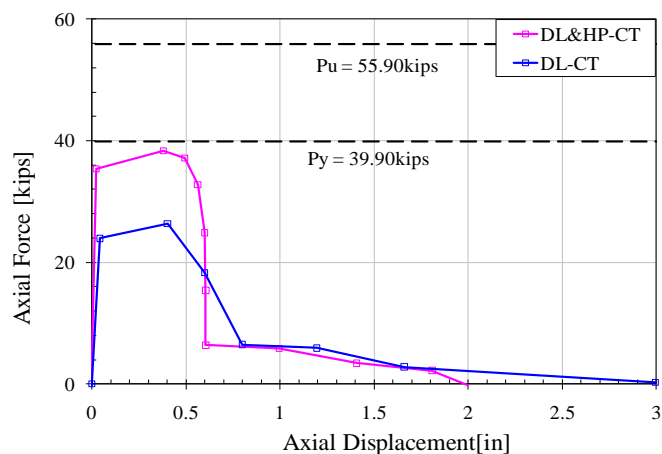


Figure 4.14. Ductile ladder w/ hairpin (DL&HP) connector tensile data

4.7.2.3 Carbon Chord Connector

Monotonic Tension

The measured capacity of the connector in pure tension was 93% of the ultimate capacity and 48% over the design capacity according to PCI design standards. The connector failed due to concrete failure through the panel connected to the fixed steel beam instead of desired anchorage bar failure. As indicated in the Section 4.2.3, the carbon chord connection utilized an unbonded region to enhance the tension ductility of the connection and to allow for shear compliance (i.e., shear movement with low force resistance).

Compared with the performance of conventional dry chord connector under monotonic tension loading, for which the connector failed due to connector-to-slug weld failure, the maximum capacity of the connection was increased by 63% of ultimate capacity and the tensile deformation capacity was increased from 0.28-in. to 0.88-in. The results proved that the enhanced design of the chord connector worked effectively to achieve the design capacity by precluding weld failed prematurely and to improve the tension deformation capacity by debonding the end of anchorage bar. The damage state of connector is displayed in Figure 4.15.



Figure 4.15. Damage state at 5.0-in tensile opening

Cyclic Tension

The measured tensile capacity of the connector was 78% of the ultimate capacity and 25% over the design capacity according to PCI design standards. The connector achieved the expected PCI design strength but did not match the ultimate strength. This was due to the fact that the connector bars did not fracture from pure tension as desired, but failed due to bar-to-faceplate weld failure, despite design of the weld to resist bar fracture strength. The connector performed well until the weld failed prematurely. The damage state of connector is displayed in Figure 4.16.



Figure 4.16. Damage state at 0.39-in tensile opening

Summary

The previously developed backbone axial force-deformation curves of the connector are presented in Figure 4.17. The enhanced carbon chord connector is able to surpass its design capacity for both load cases and achieve its ultimate force capacity under monotonic tension load. The deformation capacity of connector under monotonic loads is significantly improved compared with the bonded dry chord connector. However, the deformation capacity of connector is limited under cyclic loads even with the unbonded region designed to enhance the tension ductility performance.

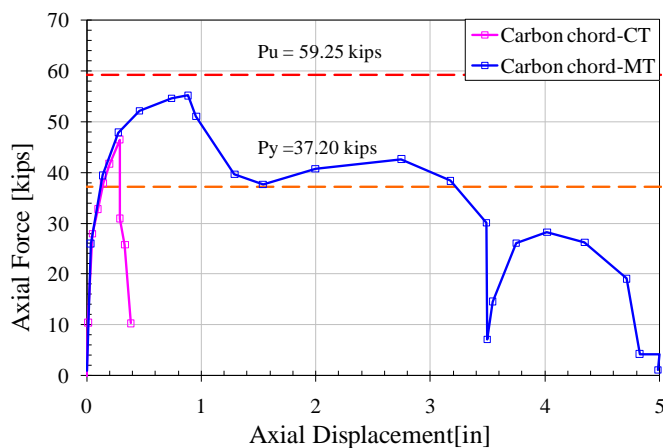


Figure 4.17. Carbon chord connector tensile data

4.7.2.4 Stainless Chord Connector

Monotonic Tension

The measured capacity of the connector in pure tension was 96% of the ultimate capacity and 15% over the design capacity according to PCI design standards. This was

due to the fact that the connector did not fail from the fracture of the connector legs as desired, but failed due to bar-to-faceplate weld failure, despite design of the weld to resist bar fracture strength. Both legs of the connector were pulled out from the weld abruptly. The connector performed well until the weld failed prematurely. As indicated in the Section 4.2.4, the stainless chord connector utilized an unbonded region to enhance the tension ductility of the connection and to allow for shear compliance (i.e., shear movement with low force resistance). It is an alternative of carbon chord connector.

Compared with the carbon chord connector tested under the monotonic tension, the failure modes of the two connectors are very different. The tensile deformation capacity was considerably decreased from 5.0-in. to 0.5-in., the damage state of connector is displayed in Figure 4.18.



Figure 4.18. Damage state at 0.5-in tensile opening

Cyclic Tension

The measured tensile capacity of the connector was 71% of the ultimate capacity and 86% of the design capacity according to PCI design standards. This was due to the fact the connector did not fail from the fracture of the connector legs as desired. The legs

of the connection yield upward during the compression cycles, which caused the WWR mesh to fracture and the concrete to delaminate. Eventually the yield of the legs of the connection caused the concrete between the legs to fail during the compression cycle. Hence the connector was not able to attain the ultimate or design strength of the connector bars. The damage state of connector is displayed in Figure 4.19.



Figure 4.19. Damage state at 2.0-in tensile opening

Summary

The previously developed backbone axial force-deformation curves of the connector are presented in Figure 4.20. The stainless chord connector was able to surpass its design capacity under monotonic tension but was not able to achieve its design capacity for cyclic tension test. The deformation capacity of connector under monotonic loads is improved compared with the bonded dry chord connector. However, the deformation capacity of connector is limited under cyclic loads even with the unbonded region designed to enhance the tension ductility performance.

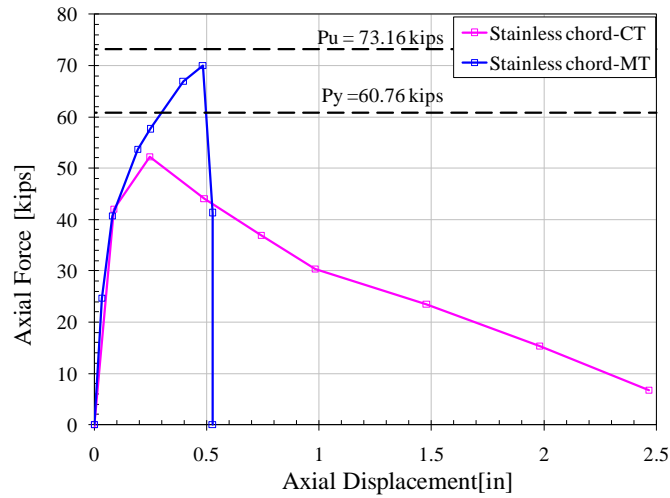


Figure 4.20. Stainless chord connector tensile data

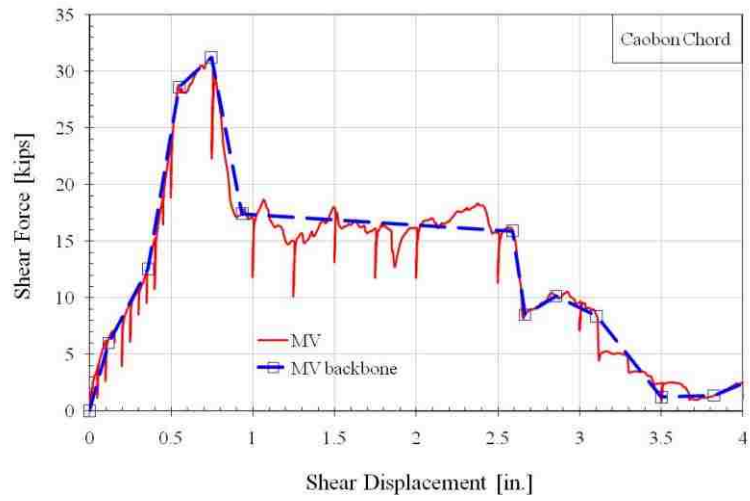
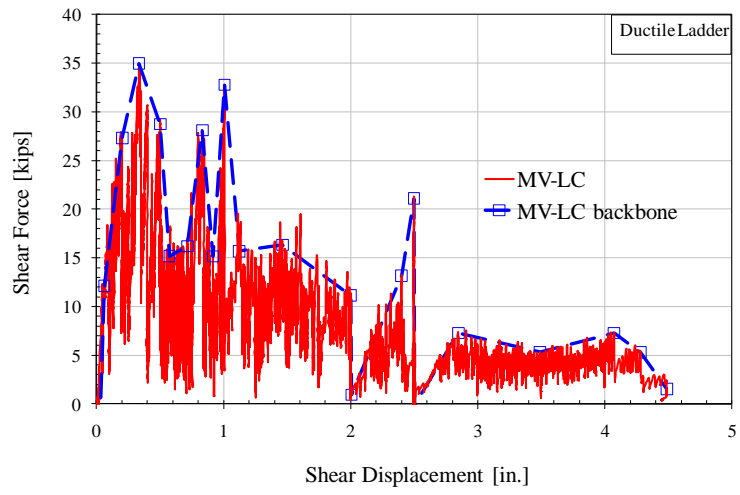
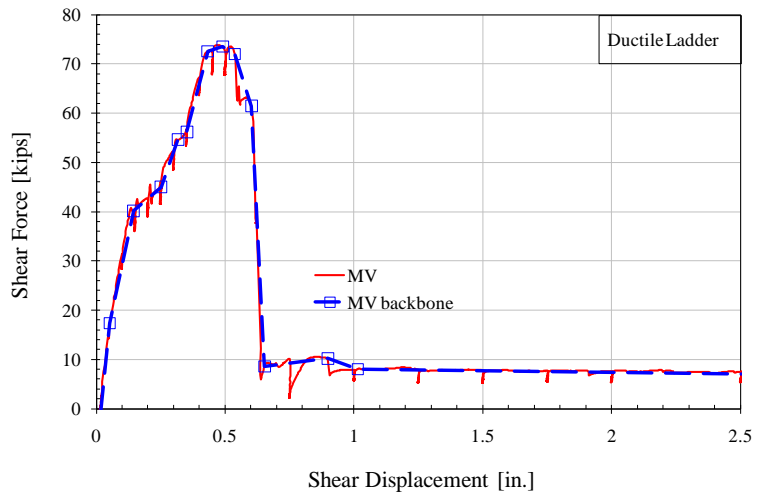
4.8 Experimental Shear Behavior

To identify the in-plane shear characteristics of the enhanced connection details, a series of shear tests were conducted on these four connection types. Monotonic shear test (MV) was conducted on three connection specimen (ductile ladder, carbon chord and stainless chord) to obtain the reference deformation for cyclic shear test. The reference deformation of the connection specimen ductile ladder with hairpin was assumed to be the same as of ductile ladder connector. Monotonic shear with axial force control test (MV-LC) was conducted on two connection specimen (ductile ladder, carbon chord) to examine the shear performance of connections under fixed levels of axial force. Cyclic tension test (CV) was conducted each connection specimen to examine the effect of load reversals. Cyclic shear with axial force control test (CV-LC) was conducted on each connection specimen to examine the shear performance of connections under fixed levels

of axial force. This section presents the performance of these connections under various shear loading patterns.

4.8.1 **Experimental Shear Results**

The connections exhibited a wide range of shear force and deformation capacities. The monotonic shear, monotonic shear with axial force control, cyclic shear and cyclic shear with axial force control responses of each connection is summarized in Figure 4.21 and Figure 4.22. The measured response and a detailed response backbone curve are presented. The web connections ductile ladder and ductile ladder with hairpin provided relatively high shear resistance while the chord connections provided a moderate shear resistance.



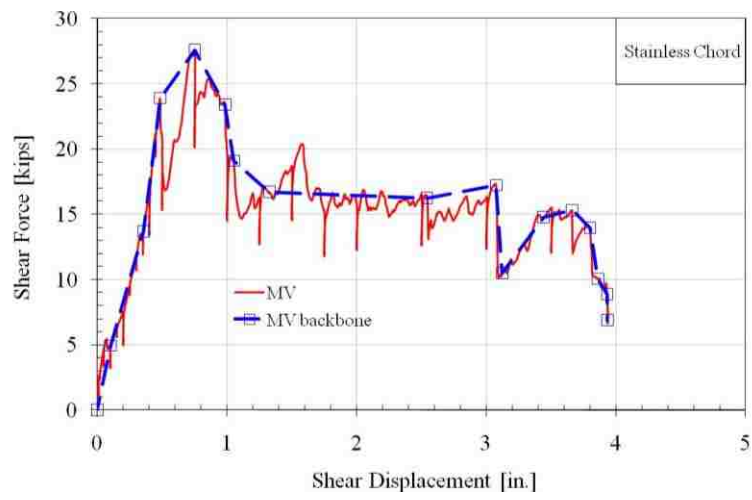
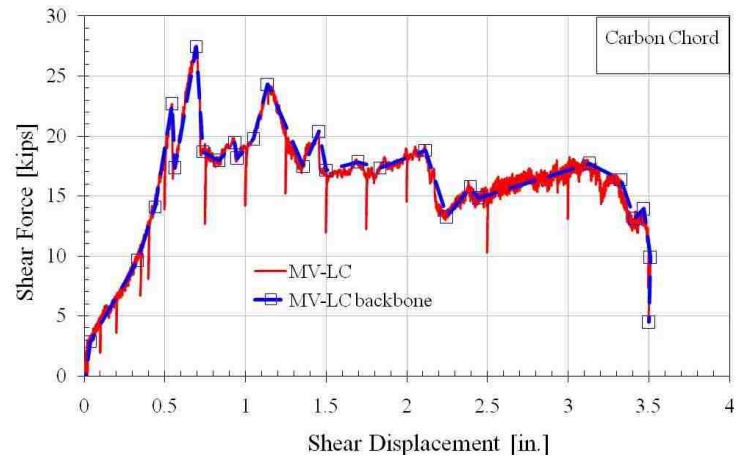
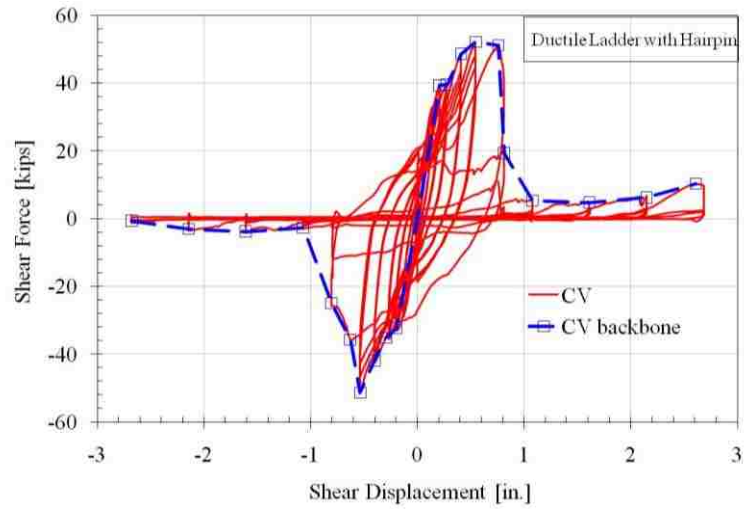
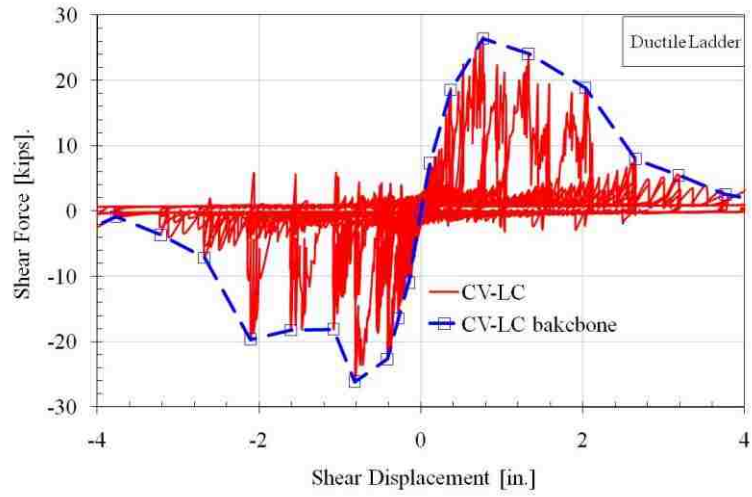
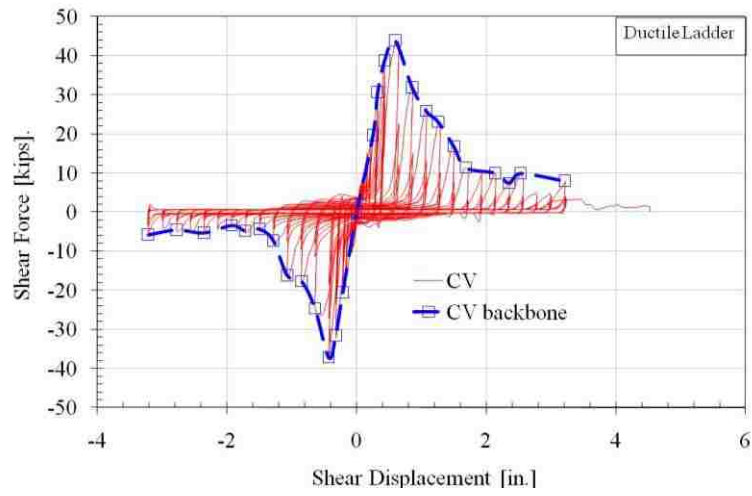
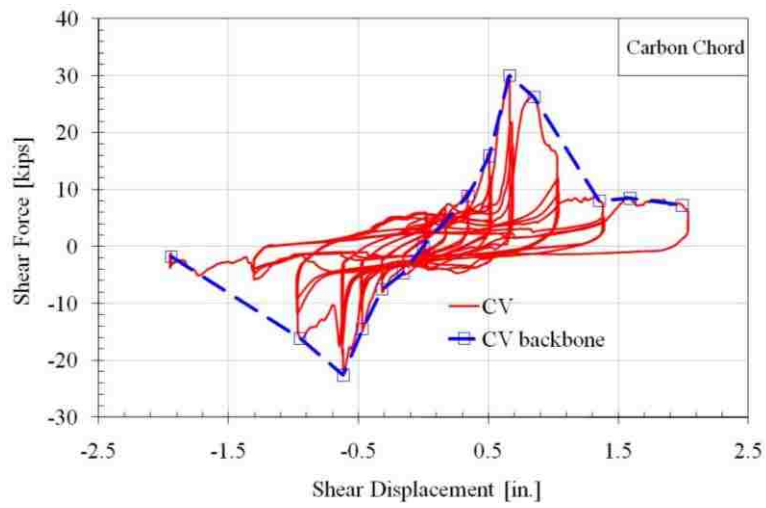
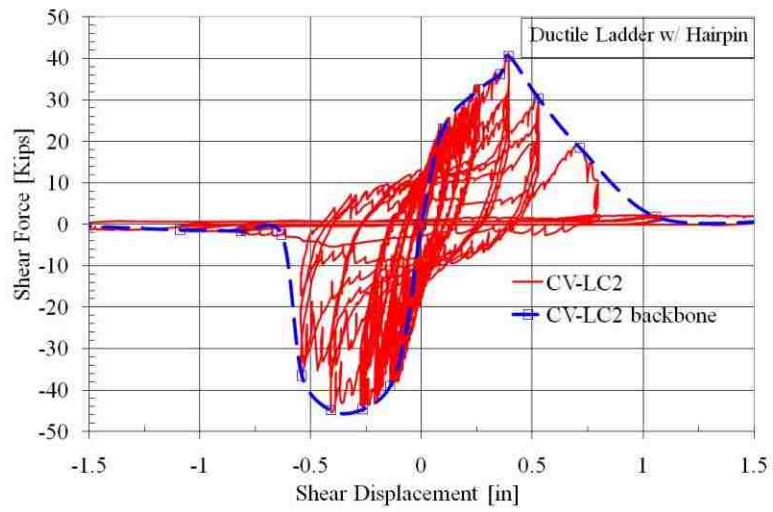
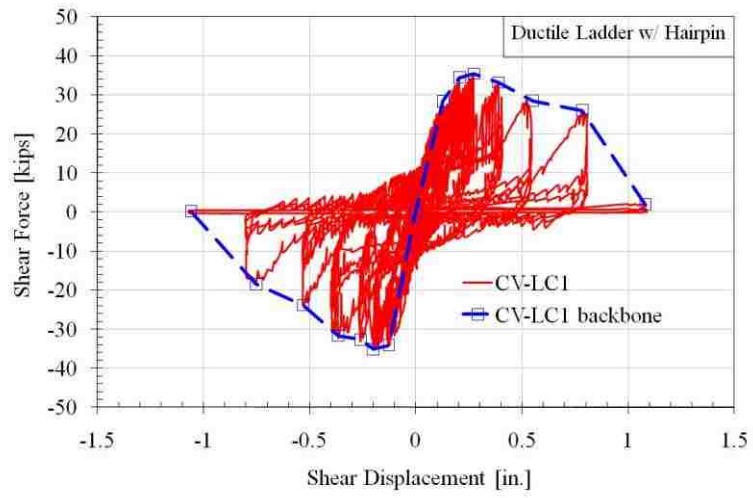


Figure 4.21. Monotonic shear response





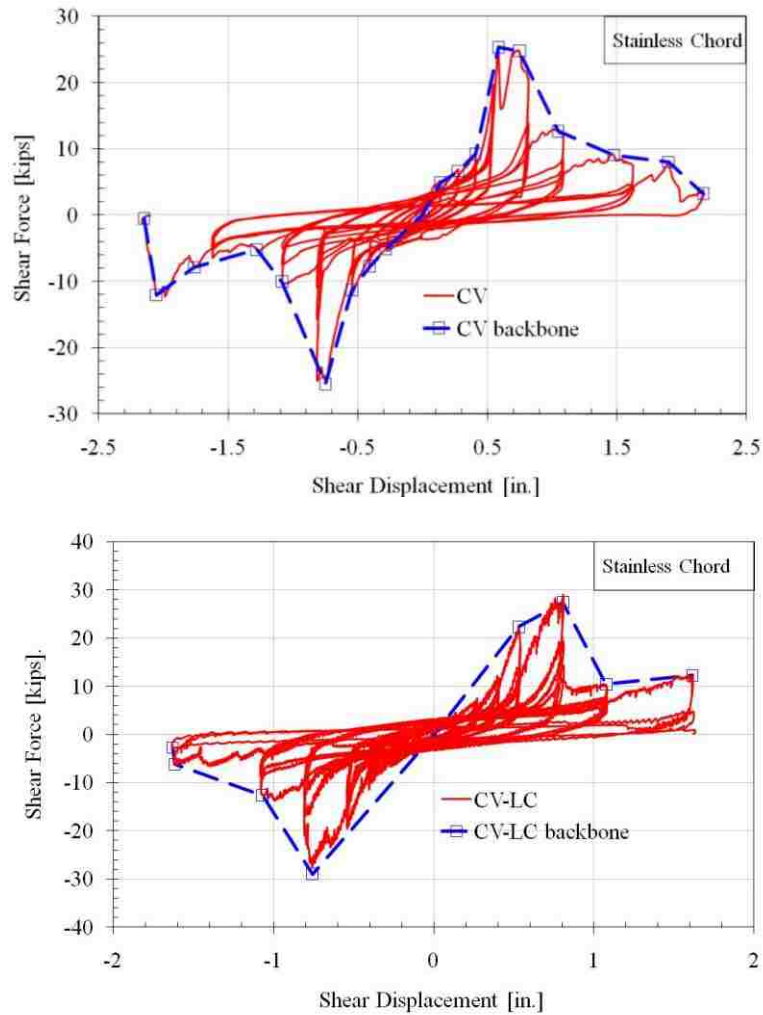


Figure 4.22. Cyclic shear response

4.8.2 Comparative Shear Behavior

The experimental data was compared to the expected connector ultimate shear strength. The shear strengths of the connectors were computed based on a simplified truss analogy in accordance with the PCI Design Handbook Section 4.8 (PCI 2010), and with an ACI shear-friction model (ACI 318-08 section 11.6 2008). This force-based design is

a simple method to estimate the available capacities by ductile failure in the connector leg coupled with shear friction. It was assumed that the weld is adequately proportioned to resist the bar fracture strength and that forces are applied uniformly and concentrically to the connector.

For the splayed leg connector such as hairpin connector, the truss analogy estimates the shear capacity based on the assumption that connector leg acts in axial tension and compression to resist shear. The tensile strength of the bar was used in conjunction with the truss model to determine the PCI design shear strength. The ultimate tensile strengths of both compressive and tensile legs provide significant resistance in the topped hairpin and were both used in determining the design shear strength.

For connectors with legs perpendicular to the joint or reinforcements spanning across the joint such as carbon chord, stainless chord and WWR mesh, the shear resistance can be computed from the ACI shear friction model. The shear capacity is determined from an effective shear-friction factor, μ , based on the interface.

For the ductile ladder connector tested in shear, two equations were used to determine the design shear strength. The first equation is the general shear friction model with the frictional contribution of the concrete included in the μ factor. The second equation (ACI 318-08 C11.6) gives more detailed calculations for the concrete contribution to the shear friction. These two equations were also applied to the strength calculation of the topped hairpin & ductile ladder connector.

Determination of which shear-friction factor to use is dependent on the interface condition. The shear friction coefficient, μ , was assumed to be 0.6 for the hairpin portion of the topped ductile ladder w/ hairpin connector, which simulating the ACI condition of “concrete placed against hardened concrete not intentionally roughened”. A value of $\mu = 1.4$ was used to simulate the ACI condition of “concrete placed monolithically” for the ductile ladder portion of the topped ductile ladder w/ hairpin connector and ductile ladder connector tests with no tensile gap. For the chord connectors $\mu = 0.7$ was used to simulate “concrete anchored to as rolled structural steel by reinforcing bars”.

Table 4.5. Capacity Formulation Estimates		
Connector	Design Capacity, P_n	Ultimate Capacity, P_u
Ductile Ladder (equation 1)	-	$f_{wvr1-y} \cdot A_{s_wvr1} \cdot \mu$ [$\mu=0.6$] / [$\mu=1.4$]
Ductile Ladder (equation 2)	-	$0.8 \cdot f_{wvr1-y} \cdot A_{s_wvr1} \cdot \mu + A_c \cdot K_1$
Ductile Ladder w/ Hairpin (equation 1)	-	$f_u \cdot A_s \cdot \cos 45^\circ \cdot \mu 1 + f_{wvr1-y} \cdot A_{s_wvr1} \cdot \mu 2$ [$\mu 1=0.6$] [$\mu 2=1.4$]
Ductile Ladder w/ Hairpin (equation 2)	-	$f_u \cdot A_s \cdot \cos 45^\circ \cdot \mu + 0.8 \cdot f_{wvr1-u} \cdot A_{s_wvr1} \cdot \mu + A_c \cdot K_1$ [$\mu=0.6$]
Carbon Chord	$2 \cdot (f_y \cdot A_s \cdot \mu)$ [$\mu=0.7$]	$2 \cdot (f_u \cdot A_s \cdot \mu)$ [$\mu=0.7$]
Stainless Chord	$2 \cdot (f_y \cdot A_s \cdot \mu)$ [$\mu=0.7$]	$2 \cdot (f_u \cdot A_s \cdot \mu)$ [$\mu=0.7$]

The formulations used for design capacity and ultimate strength are presented in Table 4.5. The following terminology was used: area of one bar leg: A_s , bar yield tensile strength: f_y , bar ultimate tensile strength: f_u , cross-sectional area of WWR: A_{s_wvr} , WWR tensile yield strength: f_{y_wvr} , cross-sectional area of ductile mesh: A_{s_wvr1} , tensile yield strength of ductile mesh: f_{wvr1-y} , ultimate tensile strength of ductile mesh: f_{wvr1-u} ; area of

concrete: A_c , $K_I=400$ psi, and shear friction coefficient: μ , the specific values of μ are also included in the table.

The calculated strengths are compared to the measured responses in Table 4.6. The results from the monotonic shear (MV), the cyclic shear (CV), the monotonic shear with axial load control (MV-LC), and cyclic shear with axial load-control (CV-LC) are presented. The mill certified material properties, presented before, were used for ultimate strength calculations when available to provide correlation with the experimental results.

Table 4.6. Connector Capacity Experimental Results							
Connector	Design Capacity, P_n [kips]	Ultimate Capacity, P_u [kips]	MV [kips]	MV-LC [kips]	CV [kips]	CV-LC1 [kips]	CV-LC2 [kips]
Ductile Ladder(eq.1)	-	14.10/32.90	73.50	34.98	43.95	26.39	-
Ductile Ladder(eq.2)		42.82					
Carbon Chord	28.47	40.93	31.23	27.46	30.04	-	-
Stainless Chord	42.53	51.21	27.58	-	25.30	22.32	-
Ductile Mesh& Hairpin (eq.1)	-	40.70	-	-	52.13	35.42	40.48
Ductile Mesh& Hairpin (eq.2)		50.60					

In general, all the connectors did not achieve their estimated ultimate capacities in most of cases. The ductile ladder connector and ductile ladder with hairpin connector achieved their expected ultimate capacities in few cases. An in-depth evaluation of each connection follows.

4.8.2.1 Ductile Ladder Connector

Monotonic Shear

The measured capacity of the connector in pure shear was approximately 123% over the ultimate capacity when using equation 1 in Table 4.6, and was approximately 72% over the ultimate capacity calculated using equation 2 according to ACI design standards, in which the first term considered the contribution of friction to shear-transfer resistance and the second term represented the sum of the resistance to shearing of protrusions on the crack faces and dowel action of the reinforcement. The connector's max load capacity was achieved at 0.49-in. where some diagonal panel cracking at the middle of the panel occurred (see Figure 4.23). These high force was mainly due to resistance to the shearing off of protrusions on the center crack face, which was released once cracking occurred. Some resistance is provided by dowel action of the WWR and concrete friction of crack interface. Connector failure was as a result of fracture of the WWR wires between 0.49-in. and 0.65-in, which was the expected failure mechanism. The equation 1 ACI shear friction model that was used to obtain the ultimate capacity does not accurately account for the concrete bearing contribution to the shear stiffness. The equation 2 ACI shear friction model includes a separate component that more accurately calculates the shear resistance provided by the concrete. Therefore, the equation 1 gives a conservative estimation of the shear capacity of the ductile ladder, and equation 2 gives a more accurate, still conservative though, estimation of the shear capacity of the ductile ladder. The damage state of connector is displayed in Figure 4.23.

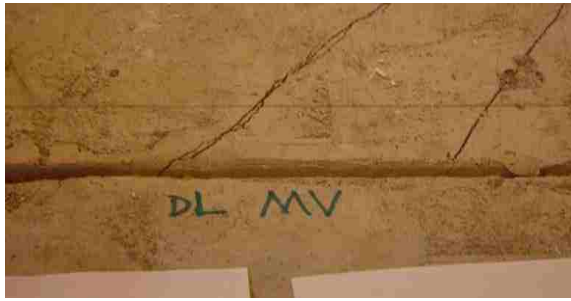


Figure 4.23. Damage state at 0.49-in shear opening

Monotonic Shear w/ Axial Force Control

The measured capacity of the connector in pure shear was approximately 6% over the ultimate capacity when using equation 1 in Table 4.6 and 82% of the ultimate capacity when using equation 2 according to ACI design standards. The connector's max load capacity was achieved at 0.33-in. where some chipping and short cracks along the edges of the joint occurred (see Figure 4.24). The resistance was mainly provided by dowel action of the WWR with some concrete contribution, which was expected by using the modified loading protocol to try to keep the axial force is zero. Only two strands of ductile ladder fractured until the shear actuator was unable to reach the desired shear deflection of 5.00-in and the test was ended. Concrete spalling and delamination occurred along the interface of the panels, and the strands of ductile ladder were exposed throughout the entire test.

The equation 1 ACI shear friction model that was used to obtain the ultimate capacity does not accurately account for the concrete bearing contribution to the shear stiffness. The equation 2 ACI shear friction model includes a separate component that

more accurately calculates the shear resistance from concrete contribution. Equation 1 provides a relative accurate estimation of shear capacity of the ductile ladder connector since the concrete cannot contribute much to the shear friction resistance in the case with axial load control.

Compared with the monotonic test with zero axial displacement, the ultimate capacity was decreased from 73.50-kip to 34.98-kip, and the shear displacement corresponding to the peak load was decreased from 0.49-in to 0.33-in. So the axial force control loading protocol decreases the ultimate capacity and makes the peak load occur at a relative smaller shear opening. This is mainly because the force control loading protocol keeps the concrete from contributing to the shear friction resistance. The damage state of connector is displayed in Figure 4.24.



Figure 4.24. Damage state at 0.33-in shear opening

Cyclic Shear

A 0.1-in pre-cracking of the topping panel joint was applied at the beginning of cyclic shear test. The measured capacity of the connector in cyclic shear was

approximately 211% over the ultimate capacity when using equation 1, and 3% over the ultimate capacity when using equation 2 according to ACI design standards. The connector's max load capacity was achieved at 0.59-in. where cracks of the panel and crushing of the concrete along the joint interface occurred (see Figure 4.25). It was also noted that the connector achieves the compression of 27.20- kips at this displacement level. The connector finally failed due to the fracture of all the strands of ductile ladder connector at 7.0-in shear opening.

Compared with the monotonic test with zero axial displacement, the ultimate capacity was decreased from 73.50-kip to 43.93-kip, and the shear displacement corresponding to the peak load was increased from 0.49-in to 0.59-in. The damage state of connector is displayed in Figure 4.25.



Figure 4.25. Damage state at 0.59-in shear opening

Cyclic Shear w/ Axial Force Control

The measured capacity of the connector in cyclic shear was approximately 87% over the ultimate capacity when using equation 1, and 62% of the ultimate capacity when

using equation 2 according to ACI design standards. The connector's max load capacity was achieved at 0.77-in. where concrete chipping and spalling over the ductile mesh wires at the joint occurred (see Figure 4.26). The resistance was mainly provided by dowel action of the WWR with almost no concrete contribution, which was expected by using the axial load control protocol. Connector failed as expected due to fracture of the WWR wires. The connector strength is higher than the estimation of equation 1 calculation model and less than the estimation of equation 2 calculation modes. The connector performance is displayed in Figure 4.26.

Compared with the cyclic test with 0.1-in axial opening, the ultimate capacity was decreased from 43.95-kip to 26.38-kip, but the shear displacement corresponding to the peak load was increased from 0.59-in to 0.77-in. Compared with the monotonic test with axial force control, the ultimate capacity was decreased from 34.98-kip to 26.38-kip, but the shear displacement corresponding to the peak load was increased from 0.33-in to 0.77-in.



Figure 4.26. Damage state at 0.77-in shear opening

Summary

The previously developed shear force-deformation backbone curves of the connectors are presented in Figure 4.27. The connectors' estimated peak performance was based heavily on the assumed center crack interface conditions. For the monotonic shear test, the interface conditions assumed as monolithically placed concrete was not very accurate since the measured shear resistance was much higher than the estimated ultimate strength. For the monotonic test with axial force control test, the interface conditions assumed as monolithically placed concrete was accurate enough so that the measured shear resistance was agree well with the estimated ultimate strength utilizing the equation 1 method, while the equation 2 method gives a higher estimate than the actual shear capacity.

The axial force control loading protocol used in the test to keep the axial force equal to zero results in a significant decrease in stiffness and the shear strength of ductile ladder connection, allowing the capacity be accurately estimated by using ACI formulations with μ of 1.4 for monotonic shear test.

For the cyclic shear test with 0.1-in. gap, the interface conditions assumed as “placed concrete against hardened concrete not intentionally roughened” was not accurate enough since the measured shear resistance was much higher than the estimated ultimate strength utilizing the equation 1 method with μ of 0.6, while the equation 2 method gives a perfect estimation. For the cyclic shear test with axial force control, the interface was

observed to be much rougher than the assumed un-roughened surface, and slightly smoother than a monolithically placed concrete, so the peak shear resistance fall in the range between estimated ultimate strength for the two assumed conditions.

Pre-cracking of the topping panel to a 0.1-in. gap results in a significant decrease in stiffness and shear strength of the connection, allowing the capacity be accurately approximated using ACI formulations and also highly improved the shear ductility of the connector.

The cyclic shear test with axial force control loading protocol results in a significant decrease in stiffness and strength of the connection, allowing the capacity to be accurately approximated using ACI formulations equation 1 method.

All tests of ductile ladder connector with no tensile gap exhibit a limited ductility with loss of significant capacity prior to 0.5-in. and almost no shear resistance after failure. The axial force control loading protocol and keep 0.1-in axial opening highly improve the connector ductility.

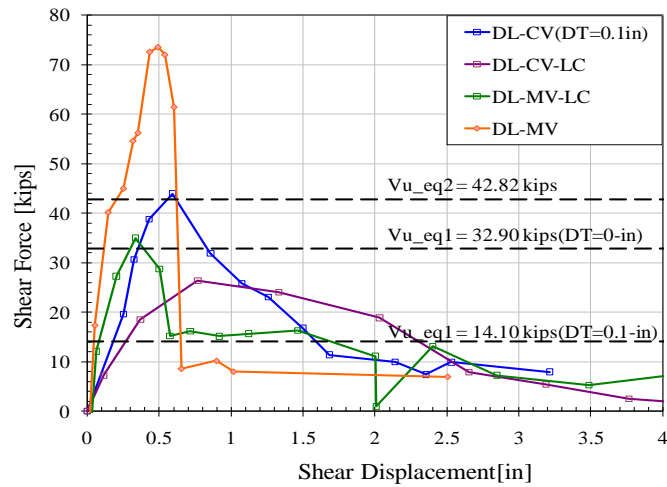


Figure 4.27. Ductile ladder (DL) shear data

4.8.2.2 Ductile Ladder with Hairpin Connector

Cyclic Shear

A 0.1-in pre-cracking of the topping panel joint was applied at the beginning of cyclic shear test. The measured capacity of the connector in cyclic shear was approximately 28% over the ultimate capacity when using equation 1, and 3% over the ultimate capacity when using equation 2 according to ACI design standards. The connector's max load capacity was achieved at 0.55-in. where cracks formed above the connector on the panel (see Figure 4.28). It was also noted that the connector achieves its maximum compression of 37.64 kips at this displacement level. Therefore it can be inferred that the increase in the connector's shear capacity was directly related to its compressive force, which was a result of friction between the concrete and the connector. Post peak behavior was characterized by a steep decline in the shear force of the

connector from 51.15 kips to 19.32 kips when the shear opening was around 0.80-in. where several strands of ductile mesh fractured. At a shear displacement of 1.00-in., the force capacity was decreased to 5.27kips, where only one strand left (see Figure 4.29). After this, the load capacity increased a little bit at the beginning of each cycle, which was most likely due to the broken rebar of the hairpin connector hanging up on the other broken pieces. The equation 1 ACI shear friction model gives a conservative estimate of the shear capacity of the ductile ladder, and equation 2 ACI shear friction model gives a more accurate estimate of the shear capacity of the ductile ladder. The damage state of connector is displayed in Figure 4.29.

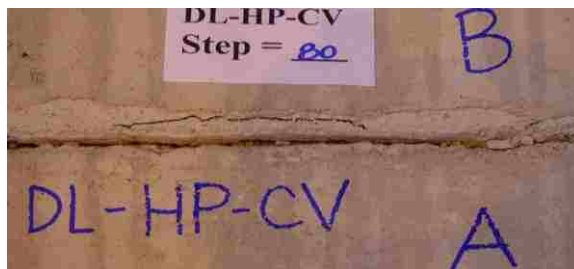


Figure 4.28. Damage state at 0.55-in shear opening



Figure 4.29. Damage state at 1.0-in shear opening

Cyclic Shear w/ Axial Force Control

Two identical cyclic shear with axial load control tests were conducted for ductile ladder with hairpin connector. The measured capacities of the connector in cyclic shear were approximately 87% of and 10% over the ultimate capacity when using equation 1, 70% and 89% of the ultimate capacity when using equation 2 according to ACI design standards. The two tests exhibited very similar load-deformation curves and failure modes, which indicates that the tests have good repeatability. The connectors' max load capacities were achieved at 0.27-in. and 0.40-in (negative direction) where concrete spalling occurred under the panel and no visible damage observed on upside of the panel. It was also noted that the compressive force in the connectors reached their maximum value of 36.55 kips and 20.66 kips respectively at this displacement level. As the compression forces in the connector decreased, so did the shear forces. Therefore it can be inferred that the increase in the connector's shear capacity was directly related to its compressive force, which was a result of friction between the concrete and the connectors. The final damage state of connector is displayed in Figure 4.30.



Figure 4.30. Damage state at 1.08-in shear opening

Summary

The previously developed shear force-deformation backbone curves of the connectors are presented in Figure 4.31.

For the cyclic shear test with 0.1-in. gap, the interface conditions assumed as “placed concrete against hardened concrete not intentionally roughened” was not accurate enough since that the measured shear resistance was much higher than the estimated ultimate strength utilizing the equation 1 method with μ of 0.6, while the equation 2 method gives a perfect estimate.

The cyclic shear test with axial force control loading protocol results in a significant decrease in stiffness and strength of the connection, allowing the capacity to be accurately approximated using ACI formulations equation 1 method.

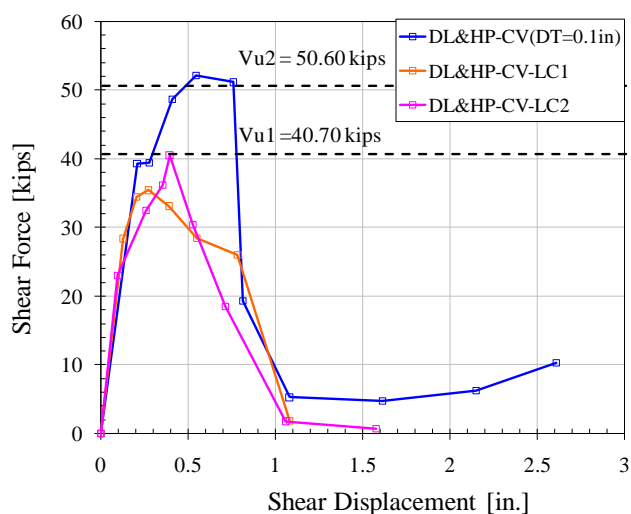


Figure 4.31. Ductile ladder with hairpin connector (DL&HP) shear data

4.8.2.3 Carbon Chord Connector

Monotonic Shear

The measured capacity of the connector in pure shear was 76% of the ultimate capacity according to ACI design standards. And the measured capacity was 10% over the design capacity according to PCI design standards. The connector's max load capacity was achieved at 0.75-in. where full length perpendicular crack occurred on the fixed panel over left chord (see Figure 4.32). It was also noted that at this point that the compressive force in the connector reached its maximum value of 16.64 kips (see Figure 4.33). Post peak behavior was characterized by a steep decline in the shear force of the connector while the concrete spall & delamination growing over the entire connection on the fixed panel. Both the axial and shear forces eventually leveled off at low load levels. The connector finally failed due to the pull out of connector legs at a 3.5-in. shear displacement (Figure 4.34).



Figure 4.32. Damage state at 0.75-in shear opening

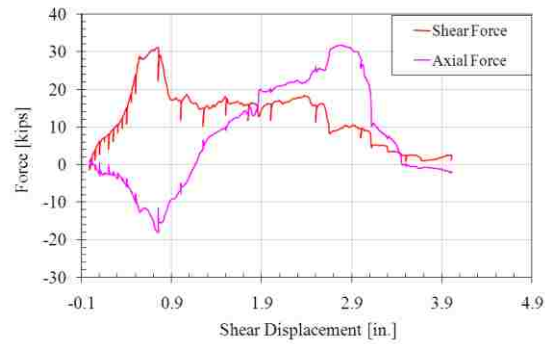


Figure 4.33. Shear & Axial force vs. shear displacement



Figure 4.34. Damage state at 3.5-in shear opening

Monotonic Shear w/ Axial Force Control

The measured capacity of the connector in pure shear was 67% of the ultimate capacity according to ACI design standards. And the measured capacity was 97% of the design capacity according to PCI design standards. The connector's maximum shear force capacity was achieved at a shear deformation of 0.69-in where the concrete panel started to bear on the connector legs, which resulted in the concrete spalling and perpendicular cracks on the panels. Post peak behavior was characterized by a steep decline in the shear force of the connector from 27.46 kips to 17.97 kips when the shear

opening increased by 0.1-in. and then followed by a steep increase of the shear force of connector from 17.97 kips to 24.31-kips, it can be inferred that the cracks caused the decrease of shear force and then the concrete bearing increase the shear resistance force again to a higher level of load. At a shear displacement of 2.5-in., one leg of the chord connection was pulled out of the weld completely, and another leg was pulled out of the weld at a shear displacement of 3.5-in (see Figure 4.35).

Compared with the monotonic shear test, the ultimate capacity was decreased from 31.23-kip to 27.46-kip, and the shear displacements corresponding to the respective peak loads were 0.75-in and 0.69-in. So the axial force control loading protocol decreased the ultimate capacity and made the peak load happen earlier at a slightly smaller shear opening.



Figure 4.35. Damage state at 3.5-in shear opening

Cyclic Shear

The measured capacity of the connector in pure shear was 73% of the ultimate capacity according to ACI design standards. And the measured capacity was 5% over the

design capacity according to PCI design standards. The connector's maximum shear force capacity 30.04 kips was achieved at a shear deformation of 0.66-in where the concrete spalling and perpendicular cracks occurred on the panels. Complete fracture of one leg of the connector occurred during the 1.32-in. deformation cycle, and the other leg was pull out of the weld during the 1.98-in. deformation cycle. The damage state at the end of test is shown in Figure 4.36.

Compared with the monotonic shear test of the carbon chord connector, the max shear force and corresponding deformation of the cyclic shear test was very close to that of the monotonic shear test. It can be inferred that the cyclic loading protocol did not have much effects on connector's force and deformation capacity.



Figure 4.36. Damage state at 1.98-in shear opening

Summary

The previously developed shear force-deformation backbone curves of the connectors are presented in Figure 4.37. In general, the enhanced carbon chord connector exhibits a stiff initial response followed by diagonal cracks causing a reduction in shear

force and a rapid softening as conventional dry chord connector did before. The unbonded region reduces the shear stiffness of the connector until plate bearing occurs, allows shear compliance and increases the shear deformation capacity.

The axial force control loading protocol decreases the ultimate shear capacity of connector and allows the peak load occur at a smaller shear opening. Cyclic action has little effect on the connector's maximum shear force and corresponding shear deformation capacity.

In all shear cases, the ultimate shear strength capacities were not achieved. One of the main reasons is premature bar-to-faceplate weld failure. In order to improve this performance, a new dry chord connector is developed and presented in Chapter 8.

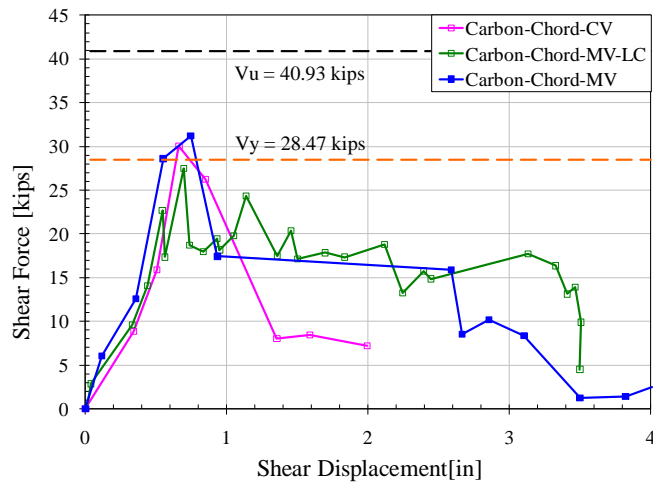


Figure 4.37. Carbon Chord shear data

4.8.2.4 Stainless Chord Connector

Monotonic Shear

The measured capacity of the connector in pure shear was 65% of the design capacity according to PCI design standards. The connector's max load capacity was achieved at 0.75-in. where cracks and delamination formed around the connection on the concrete panel (see Figure 4.38). The test was ended at a 4.5-in shear displacement without failure of the connection due to the deformation limitation of shear actuator (Figure 4.39).



Figure 4.38. Damage state at 0.75-in shear opening



Figure 4.39. Damage state at 4.5-in shear opening

Cyclic Shear

The measured capacity of the connector in pure shear was 50% of the ultimate capacity according to ACI design standards. And the measured capacity was 60% of the design capacity according to PCI design standards. The connector's maximum shear load capacity 25.30 kips was achieved at a shear deformation of 0.58-in where the connector began to bear on the concrete panels. The connector failed due to both legs being pulled out of the welds during the 2.15-in. deformation cycle (Figure 4.40).

Compared with the monotonic shear test, the max shear force and corresponding deformation of the connector was close to that of the monotonic test. It can be inferred that the cyclic loading did not have much effects on the force and deformation capacity.



Figure 4.40. Damage state at 2.15-in shear opening

Cyclic Shear w/ Axial Force Control

The measured capacity of the connector in pure shear was 44% of the ultimate capacity according to ACI design standards. And the measured capacity was 53% of the

design capacity according to PCI design standards. The connector's maximum shear load capacity was achieved at a shear deformation of 0.80-in where concrete spalling and perpendicular cracks formed on the panels (see Figure 4.41). At a shear displacement of 1.60-in., one leg of the chord connection was completely pulled out of the weld, and another leg was completely fractured at the weld region (see Figure 4.42).

Compared with the cyclic shear test, the ultimate capacity was increased from 27.58-kip to 28.98-kip, and the shear displacements corresponding to the respective peak loads were 0.75-in and 0.80-in. So the axial force control loading protocol slightly increased the ultimate force and deformation capacity.



Figure 4.41. Damage state at 0.80-in shear opening



Figure 4.42. Damage state at 1.60-in shear opening

Summary

The previously developed shear force-deformation backbone curves of the connectors are presented in Figure 4.43. The unbonded region of the enhanced stainless dry chord connection reduces the shear stiffness of the connector until plate bearing occurs, allows shear compliance and increases the shear deformation capacity.

The axial force control loading protocol increases the ultimate shear force capacity and deformation capacity, but the effect is very small. Cyclic action has little effect on the connector's shear force and deformation capacities.

In all shear cases, the measured shear strengths were generally lower than the estimated ultimate strength due to premature failure of welds. In order to improve this performance, a new dry chord connector is developed and presented in Chapter 8.

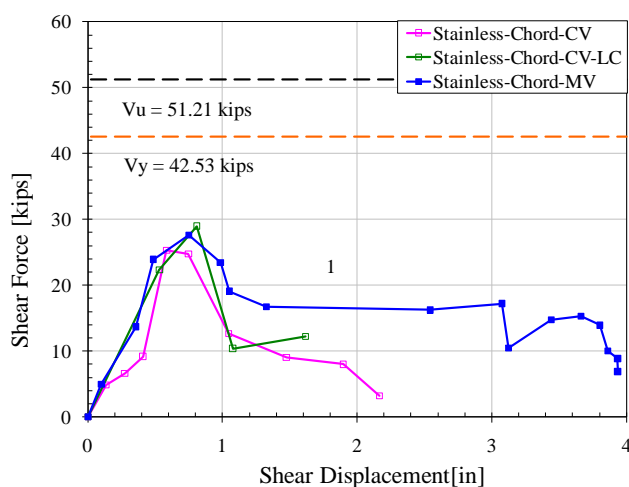


Figure 4.43. Stainless Chord shear data

4.9 References

1. American Concrete Institute (ACI) Committee 318. 2008. *Building Code Requirements for Structural Concrete (ACI 318-08) and Commentary (ACI 318R-08)*. Farmington Hills, MI: ACI.
2. Precast/Prestressed Concrete Institution. (2010). “*PCI design handbook: precast and prestressed concrete.*” Seventh Edition, Chicago IL.
3. Naito, C., W. Peter, L. Cao. 2006. Development of a Seismic Design Methodology for Precast Diaphragms - PHASE 1 SUMMARY REPORT. Advanced Technology for Large Structural Systems (ATLSS) Report No.06-03, ATLSS Center, Lehigh University.

Chapter 5 Database of Precast Diaphragm Connections

A large variety of connection details are used for providing integrity and force transfer between precast concrete panels in building floor diaphragms. A summary of DT connections details evaluated in previous research is presented. More recently developed diaphragm connections are incorporated into a connection details database to extend previous research. To assess the adequacy of these connections, over 200 tests were conducted by following the proposed evaluation method (Chapter 3) to assess the performance of precast diaphragm panel to panel connectors. A standard procedure of developing simplified response curves from original test data is used to generate simplified curves from each of the tests conducted. These characteristics are summarized in a comprehensive database. This database provides stiffness, strength and deformation properties of each connector detail examined. The connectors are divided into one of three displacement based categories: low deformation element (LDE), moderate deformation element (MDE) or high deformation element (HDE) based on the performance measured in the experiments in accordance with the acceptance criteria presented in Chapter 3. A number of connectors were found to be categorized as moderate or high flexural deformation elements; however, most of connectors were categorized as low deformation levels. In addition, the usage of performance database is discussed in this chapter.

5.1 Precast DT Connection Details Database

The Precast concrete double-tee panels are extensively used for fabrication of floor diaphragms due to the rapid field construction and reliable quality control available to the precast concrete construction industry. To ensure structural integrity and force transfer within a precast diaphragm, discrete web and chord connections are used to connect individual panels as shown in Figure 5.1.

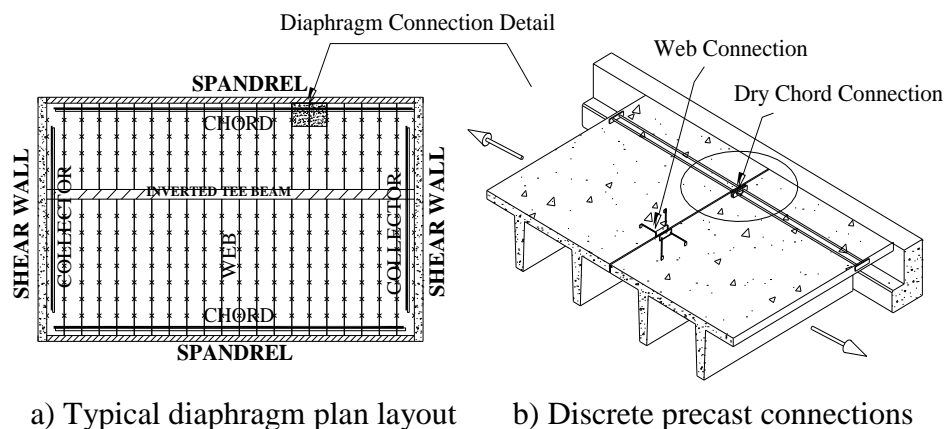


Figure 5.1. Typical diaphragm plan layout and connections

In moderate or low seismic zones, precast diaphragm systems are often constructed using mechanical connectors embedded in a 4-ft thick pre-topped double tee flange. These systems are referred to as “dry” systems since they do not require the use of a field placed topping. The connector in each double tee flange is typically welded to the adjacent connector by a round/rectangular slug between the two exposed steel plate faces. In high seismic zones, a 2-ft thick reinforced cast-in-place topping slab overlaying a 2-ft thick precast panel is typically used to ensure structural integrity. For these systems,

reinforcement is used to provide continuity over the panels. Erection requirements such as leveling of the tees often require the use of the welded mechanical connector even in high seismic regions. To provide a smooth continuous floor surface, a combination of both a mechanical connector and cast-in-place (CIP) topping is used. This system has the added advantage of enhancing serviceability and providing redundancy against seismic demands.

Connection details used for double-tee panels vary in accordance with design requirements and the preference of the precast manufacturer and erector. In current practice, discrete flange-to-flange web connectors are used to provide in-plane shear resistance, and a welded dry chord connection or a cast pour strip is used to provide in-plane flexural strength to the diaphragm.

A variety of mechanical connectors have been developed for precast DT diaphragm systems since 1970 to meet precast concrete design needs. The most traditional DT flange web connector used for precast buildings was made from a bent rebar, called “hairpin” connector (Figure 5.2). It has been widely used by precast industry since the 1970’s because of easy fabrication and low cost. Designations for each component of a hairpin connector are illustrated in (Figure 5.2). Typically for 4-in. thick DT flange, the hairpin is installed at the mid-depth of the flange with reduced concrete thickness above the front face portion. A flange depression also called “recess” (Figure 5.2) is a commonly used in construction practice to allow for more access for filed welding.

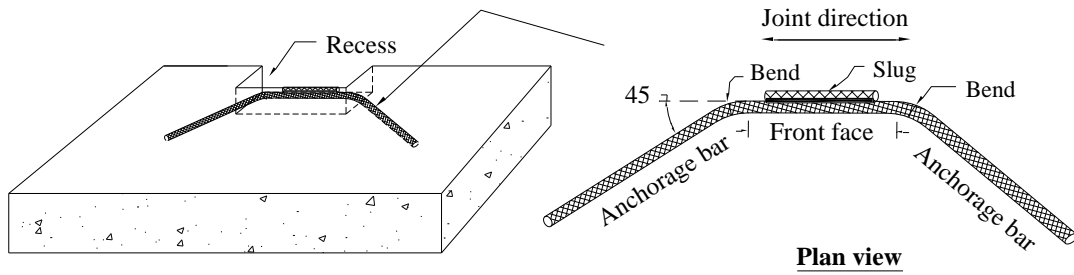


Figure 5.2. Hairpin connection details

5.1.1 Database of Connection Details in Previous Research

Table 5.1. Summary of precast concrete diaphragm connection details in previous research		
<p>Hairpin connector- Type A and B (Venuti, W. 1970)</p>	<p>Cover plate connector- Type A and B (CTC. 1974)</p>	<p>Hairpin connector (R. Spencer 1986)</p>

Table 5.1. Summary of precast concrete diaphragm connection details in previous research				
<p>Hairpin & Cover plate (Aswad 1977)</p>	<p>Hairpin & WWR Mesh (Kallros 1987)</p>	<p>Embedded rebar welded to steel plate (Pincheira 1998)</p>	<p>JVI Vector (2000,2002,2003,2004,2005)</p>	
<p>P-11</p>	<p>P-11B</p>	<p>Nelson Stud Dayton (2002)</p>	<p>Waffle</p>	<p>Channel</p>
<p>Hairpin</p>	<p>Stud-welded</p>	<p>Bent wing</p>	<p>Structural tee</p>	<p>Mesh-angle JVI vector Pincheira (2005)</p>

Research studies on a wide variety of embedded mechanical connectors have been conducted since 1968. A summary of flange-to flange mechanical connections presented in previous research, which are evaluated by using existing experimental approaches, is as shown in Table 5.1. Not all of the connectors are still commercially available however all connections have been used in practice. Most of earlier research has been focused on hairpin and other bent bar type connectors since these connectors are very popular due to

its ease of fabrication and low material cost. More proprietary connectors such as JVI vector have been recently used in new construction as web connections throughout US.

5.1.2 Connection Details Database Extension

As discussed in Chapter 4, experimental studies on various mechanical connectors have been conducted by using the new proposed evaluation methodology in this dissertation work. These connection details include existing connectors, improved ductile connectors and new proprietary connectors. A summary of the connection details evaluated in this research is as shown in Table 5.2.

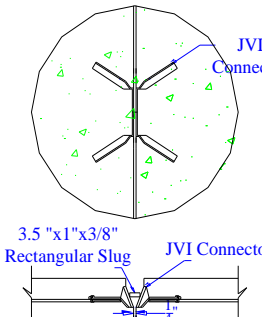
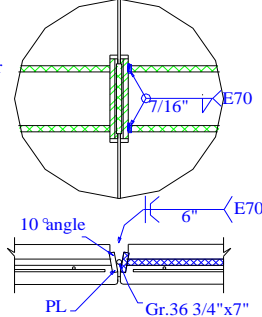
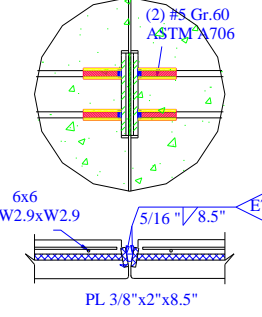
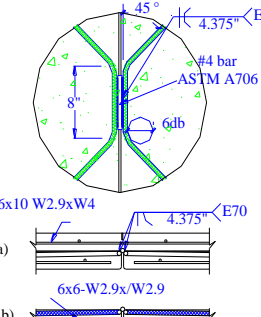
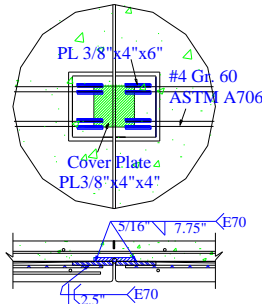
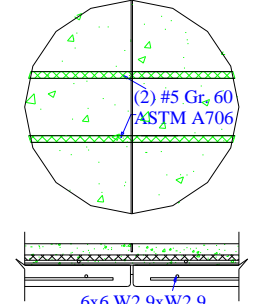
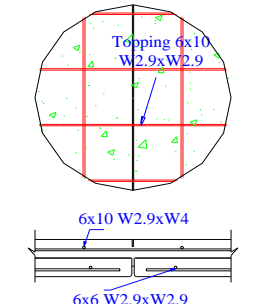
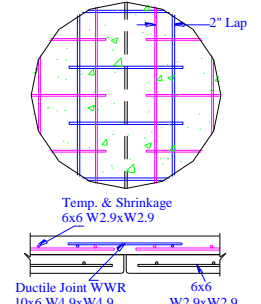
Table 5.2. Precast concrete diaphragm connection details summary			
 <p>A-1. Stainless 304 JVI A-2. A36 JVI</p>	 <p>B-1. Bonded chord</p>	 <p>B-2. Unbonded carbon chord; B-3. Unbonded stainless steel chord</p>	 <p>C-1. Pretopped hairpin C-2. Topped hairpin</p>
 <p>D. Cover plate</p>	 <p>E. Pour strip</p>	 <p>F. Topping</p>	 <p>G Ductile Ladder</p>

Table 5.2. Precast concrete diaphragm connection details summary			
<p>G&C. Topped Hairpin & Ductile Mesh</p>	<p>Type A: A to B(single weld) Type B: B to A(2 welds) <i>a. Uniform 4in panel</i> <i>b. Stepped panel</i> <i>c. ALTUS panel (3.25in thickness)</i> H-1. B-A w/ a; H-2. A-B w/ a; H-3. A-B w/ b; H-4. A-B w/ c; H-5. A-A w/ b; H-6. B-A w/ b; H-7. A w/b; H-8. B w/ b; H-9. B w/ a; H-10. A w/ c; H-11. B w/ c H. Meadow Burke Connector</p>	<p>I-1. Stainless 304 steel w/ 2in panel I-2. A36 steel w/ 4in panel I. Twister Connector</p>	
<p>J-1. 1008 steel w/ 4in panel J-2. 10B38 steel w/ 4in panel J-3. A36 steel w/ 4in panel J. Metromont Corporation Flange Connector</p>	<p>L-1. 1018 S L-2. 1018 L L-3. 304 S L-4. 304 L L-5. Rebar S L-6. Rebar L L-7. A36 L L-8. A36 S Note: S (Small), L (Large); Small connectors go w/ 2in panel; large connectors go w/ 4in panel. L. Universal Building Products Edge Connector</p>	<p>K-1. Large size w/ 4in panel K-2. Small size w/ 2in panel K. Next Gen Twister Connector by Universal Form Clamp Company</p>	

5.2 Connection Performance Database

An introduction of existing connection performance database and a discussion of its limitation are presented in this section. As part of this dissertation work, a large amount of experimental tests are conducted using new proposed evaluation methodology with more advanced techniques. The data are summarized into a comprehensive connection performance database, which can be used for design and modeling purposes.

5.2.1 Previous Connection Performance Database

To evaluate the response of diaphragm connectors, a significant amount of research has been conducted on the performance of diaphragm connections under in-plane demands in past 40 years. The first published (1970) research of experimental tests on hairpin connectors was conducted by Venuti (Venuti 1970). More research studies have been conducted on hairpin type connectors and a variety of proprietary connectors since then. The research provided extensive test data to characterize the connector behavior under prescribed force demands. As part of DSDM project, all data obtained from previous published test reports was summarized in chronological order by Cao (Cao 2006). Three typical points of the load deformation responses were tabulated into the database. Initial stiffness is calculated as the secant of strength-displacement relationship from origin to 75% peak load value. $(P1, \Delta1)$ defines the point at peak strength, $(P2, \Delta2)$ defines the point as the level of residual strength and $(P3, \Delta3)$ defines the point as the failure level (Figure 5.3). The connection performance database of previous studies is as shown in Table 5.3.

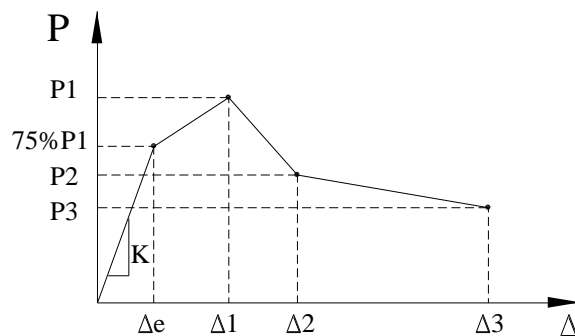


Figure 5.3. Simplified lineal curve used in previous database

Table 5.3. Previous DT/DT web connector performance database (Cao 2006)										
Ref.	Connector ID	Test ^a	Initial stiffness K (kips/in)	P1 (kips)	$\Delta 1$ (in)	P2 (kips)	$\Delta 2$ (in)	P3 (kips)	$\Delta 3$ (in)	Failure mode ^b
W. Venuti (1968)	DT1(M) ^c	MV	110	15	0.14	13	0.2	12	0.35	3
	DT1(N)	MV	180	22	0.14	15	0.25	12	0.35	
	DT1 (KK)	MV	400	53	0.11	40	0.2	25	0.35	
	DT1 (LL)	MV	335	60	0.15	55	0.2	36	0.35	
	DT2 (KK)	MV	295	60	0.17	abrupt failure at P1				
	DT2 (LL)	MV	305	55	0.23	43	0.35	33	0.5	
CTC. (1974)	DT4(A)	MV	490	20	0.06	-force control-			N/A	1 & 2
	DT4(B)	MV	1250	20	0.03	-force control-			N/A	
Aswad (1977)	DT1	MV&CV	400	10	>0.06	N/A	N/A	N/A	N/A	3
		MVT	60	10	0.8	N/A	N/A	N/A	N/A	N/A
	DT4	MV	240	20	0.2	14	0.6	13	0.96	2
		MT	N/A	5	N/A	2	N/A	N/A	N/A	N/A
R. Spencer (1986)	DT2(Aa)	(MV&)CV	345	43	0.2	N/A	N/A	18	1	4
	DT1(Ar)	(MV&)CV	915	40	0.1	N/A	N/A	26		2,4,5,6
	DT1(As)	(MV&)CV	300	33	0.17	N/A	N/A	28		2,3
	DT1(Ab)	(MV&)CV	285	25	0.12	15	0.25	12		2,3,5,6
	DT1(B)	(MV&)CV	345	26	0.2	N/A	N/A	10	1	3,4,5
Kallros (1987)	DT1(#1)	CV	820	17	0.05	14	0.05	-	-	2
	DT2(#2)	MV;CV	320	15	0.06	10	0.65	-	-	3
	DT1(#3)	MV;CV	270	20	0.11	13	0.35	10	0.55	3,8
	DT1(#4)	MV;CV	690	20	0.16	16.8	0.31	16	1	2,3,8
	Angle-mesh(a)	CV	245	15	0.07	8	0.3	8	1	2
	Angle-mesh(b)	CV	220	15	0.14	11	0.25	-	-	2
Pincheira (1998)	DT2	MV	450	16	0.05	15	0.15	2	0.2	2,4
		CV	360	17	N/A	N/A	N/A	N/A	N/A	2
		MT	210	15	0.32	2	0.36	-	-	2
		CT	265	13(T) -31(C)	N/A	N/A	N/A	N/A	N/A	2,4
		MVT-V	300	9	0.05	8	0.12	1	0.18	2
		MVT-T	330	9	0.1	8	0.16	1	0.19	
		CVT-V	320(@ T) 870(@C)	8 (@ T) 30 (@C)	N/A	N/A	N/A	N/A	N/A	2
		CVT-T ^c	535(@T)	8(@T) 30 (@C)	N/A	N/A	N/A	N/A	N/A	

Table 5.3. Previous DT/DT web connector performance database (Cao 2006)											
Ref.	Connector ID	Test ^a	Initial stiffness K (kips/in)	P1 (kips)	Δ1 (in)	P2 (kips)	Δ2 (in)	P3 (kips)	Δ3 (in)	Failure mode ^b	
JVI (2000)	DT5 (plain steel)	MV	580	20	0.06	15	0.24	13	1.5	4,8	
		CV	565	20	0.07	11	0.18	10	0.6	2	
		MT	235	10	0.81	10	1.72	6	2.7	10	
		MvV	80	7	0.19	brittle failure at ultimate load					3
		MVT	265	18	1.24	10	1.74	5	2.34	8	
		CVT	195	15	0.12	9	0.92	-	-	2	
Dayton (2002)	DT5 (P-11)	MV	100	8	0.16	7	0.78	-	-	8,9	
		MT	45	3	0.25	3	0.65	-	-	3,8	
	DT5 (Nelson)	MV	150	30	0.29	10	0.43	8	0.52	4,7	
		MT	480	15	0.11	0	0.78	-	-	5	
	DT5 (Channel)	MV	85	20	0.45	10.8	0.6	brittle failure		10	
		MT	110	9	0.47	8	0.86	7	1.05	10	
		MVT	420	20	0.14	3	0.55	-	-	2,3	
		CVT	75	17	0.25	3	0.65	-	-	2,3	
	DT3-5 (Waffle)	CV	80	17	0.28	3	0.48	-	-	2,3	
		MV	250	12	0.1	12	0.27	12	0.5	10	
	DT5 (P-11B)	MT	40	6	0.65	4	1	-	-	10	
		MV	130	10	0.17	8	0.18	6	0.63	8,9	
		MT	65	5	0.24	2	0.35	2	0.6	8	
		MVT	155	7	0.1	4	0.5	4	1	2,3	
		CVT	85	7	0.14	3	1	-	-	2,3	
Pincheira (2005)	DT2	CV	100	9	0.12	5	0.3	5	1	2,3	
		MV-nr ^d	475	19.3	0.15	11.8	0.2	12	0.44	2	
		MV-r ^d	505	21.5	0.1	20	0.4	9.2	0.8	2	
		MV-T(1/16)	205	16.2	0.26	15	0.46	10	0.7	8	
		CV-nr	380	17.9	0.1	15	0.22	12.5	0.4	2	
		CV-r	405	21.3	0.15	17	0.17	16	0.4	2	
		CV-T(1/16)	605	16.5	0.2	14	0.3	-	-	2	
	MT	70	7.8	0.46	6	0.7	-	-	2		
	DT3	MV-nr	330	13.1	0.12	-	-	-	-	4	
		MV-r	325	12.2	0.1	9.3	0.35	8	1	4	
		MV-T(1/8)	35	4.7	0.32	3.5	0.4	4	1	3	
		CV-r	315	16.5	0.09	7	0.15	4	0.5	4	
		CV-T(1/16)	225	11.3	0.05	4	0.15	2	0.66	4	
MT		130	8.6	0.18	7	0.56	3	1	4		

a. M-Monotonic, C-cyclic, T-tension, V-shear, v-vertical shear, VT-combined shear and tension
b. Failure mode: 1-cover plate or bar twisting; 2-bar fracture; 3-concrete spalling or crushing in compression; 4-weld fracture; 5-concrete splitting; 6-Bond slip; 7-concrete breakout; 8-leg pullout; 9-leg buckling; 10-faceplate rupture (bent plate connector)
c. DT1(M): No.4 bar , 2.5” thick flange; DT1(N): No.5 bar,2.5” thick flange
(KK): No.4 bar, 2” thick flange&2”topping; (LL): No.4 bar, 2.5” thick flange&2”topping
d. nr: no axial restraint, r: axial restraint, MV-T(#): monotonic shear under #-in. tensile opening

5.2.2 Discussion on Previous Connection Performance Database

The previous connection performance database made it convenient to model the connector with simplified response curve. However, the breadth of connections examined is very limited for design purpose. Furthermore, the evaluation methods used between tests are not consistent enough to give comprehensive response comparisons. Shortcomings in previous research are discussed in details as below.

- The breath of connection types examined is limited

The majority of previous experimental studies focused on the hairpin connector and the connectors with similar configuration. Many other web and chord connectors besides “hairpin” are widely used in precast diaphragm systems. Furthermore, more ductile chord and web connections are developed recently. However, little information is provided on the behavior of these connections.

- The experimental evaluation methods used need to be improved

(1)The majority loading protocols used in previous studies was monotonic shear. Recent FEM studies (Cao 2006) on diaphragm analysis found out web and chord connections are subjected to a varied combination of tension and shear demands depending upon their locations. To capture the critical deformation demands on an individual connection, a series of loading patterns should be considered in addition to monotonic shear loading protocol.

(2) Most of the loading protocols used are monotonic loading. Recent research (Cao 2006) has shown the significant effect of load reversals on the stiffness, strength degradation and ductility reduction. To characterize the connector and furthermore the diaphragm response under seismic excitement, cyclic loading and deformation combinations should be incorporated in evaluation methods as well.

(3) Most of previous studies used a single panel test configuration due to easy installation low cost. The mechanical connector was embedded in the concrete panel and then was attached to the loading beam via slug welding. The shear demand was applied via the loading beam to the welded connector with restraint in axial direction provided by bracing perpendicular to the joint. Therefore, flexibility of shear direction in the slug-to-face region of a connector pair was artificially restrained by rigidity of the additional loading beam. In addition, the axial force generated due to the restraint was not monitored in a single shear test.

(4) Most of previous tests during 1970-1980 were performed by force control with emphasis on the elastic shear behavior and the ultimate force capacity. The load control method, which is easy to conduct, can determine the max load capacity of the connections, but it is difficult to capture displacement capacity for brittle systems. The new proposed performance-based seismic design methodology of diaphragm system requires for a certain amount of ductility inherent in the connector. Limited information on ductility has been provided in previous studies.

(5) All the previous tests were evaluated under in-plane demands, the force, deformation and stiffness properties of connections under out-of-plane demands are not examined.

- The simplified backbone curve used need to be improved

In previous database, the 3-point backbone curve (Figure 5.3) was used to simplify the original test data published in literatures. The definition of initial stiffness (secant form origin to 75% of peak force) was very conservative and not able to capture the actual initial stiffness for many cases. The yield force and deformation capacity were not defined. This simplified backbone curve need to be improved.

5.2.3 New Developed Comprehensive Connection Performance Database

To extend the previous response database and provide a complete set of input data for analytical diaphragm models, a large amount of experimental research studies has been conducted on a wide variety of web and chord connections as part of this dissertation work. In this research, the new proposed experimental evaluation approach is used (Chapter 3) is used to examine the stiffness, force and deformation properties of diaphragm connections.

A comprehensive connection performance database of load-deformation responses is developed (see Table 5.4). Each individual test included in this table was conducted by following the guideline of recommended evaluation methodology. This

table incorporates the multi-linear curve (Figure 3.10) parameters previously discussed. Point ‘2’ represents the peak load. Point ‘a’ is defined as the point where the strength achieves 15% of peak resistance. Initial elastic stiffness is calculated as the secant of strength-displacement relationship from origin to point ‘a’. Point ‘b’ is on the original backbone curve at where the deformation Δ_b is computed by taking the intersection of a horizontal line at the max load and the initial elastic stiffness line at 15% of the max load. Point ‘1’ represents the occurrence of yield, which was defined by drawing a line between point ‘2’ and ‘b’ and extending back to intersect the initial elastic stiffness line at 15% of the max load. Point ‘3’ is defined as the point where the strength has decreased to 15% of the peak load. Point ‘2a’ is defined as the point where the deformation is around 50% of the summation of deformations at point ‘2’ and ‘3’. The points are defined in terms of the resistance $P_a, P_1, P_b, P_2, P_{2a},$ and $P_3,$ and the displacements $\Delta_a, \Delta_1, \Delta_b, \Delta_2, \Delta_{2a}$ and $\Delta_3.$

The connector ID is consistent with the connector details shown previously in Table 5.2. The main test types are divided into in-plane tension, in-plane shear and out of plane shear. For each test, the specific loading condition is as shown in the column of testing notation, the explanation of these notation are noted in the bottom of table. If multiple tests under same loading condition were conducted for the connector, the number of tests is also shown in the column of testing notation as “*number of tests”, and the average results of critical parameters are incorporated in the table, otherwise single test results will be shown in the table. The shear or deformation category of each tested

connector is included based on the category limits presented in Table 3.2. The tension limits are used for tension tests and shear limits for shear tests. Detailed discussion of each test can be found in the following references (Naito et al 2006a; Naito et al 2006b; Naito 2007; Naito et al 2007; Hodgson et al 2007; Naito and Hendricks 2008; Naito 2008; Naito and Ren 2009a; Naito and Ren 2009b; Ren and Naito 2010). The deformation and force presented represents that of a complete connector, which includes two connectors welded together.

The database includes three chord connectors and thirty-five varieties of web connectors. Of the web connectors, the performance ranged from LDE to HDE for both shear and tension. However the majority, 67%, of web shear response was in the LDE range. The chord connectors were all categorized as MDE in tension and two of the three were also categorized as MDE in shear. The third connector B-1 exhibited poor shear performance and was categorized as a LDE in shear. It is important to note that though the database represents a significant sample of diaphragm connectors used in current practice none of the chord connectors performed in the HDE range and only 4 of the 35 web connectors achieved the HDE category in shear.

The normalized stiffness, strength, and deformation data of connectors for both in-plane tension and shear loading case are summarized in Figure 5.4. The data are normalized based on the average value of each property listed. The mean values of stiffness, strength and deformation properties of connectors in different categories LDE, MDE and HDE are also indicated in Figure 5.4. The connectors have a considerable

variation in stiffness, strength, and deformation. From this figure, we can see that the deformation categories chosen for LDE, MDE and HDE are in line with the measured to distribution of peak deformation. As a whole the HDE elements exhibited the lowest strength and stiffness while the LDE elements resulted in the highest strength and stiffness. This correlation is most evident in the tension tests and less so in the shear tests.

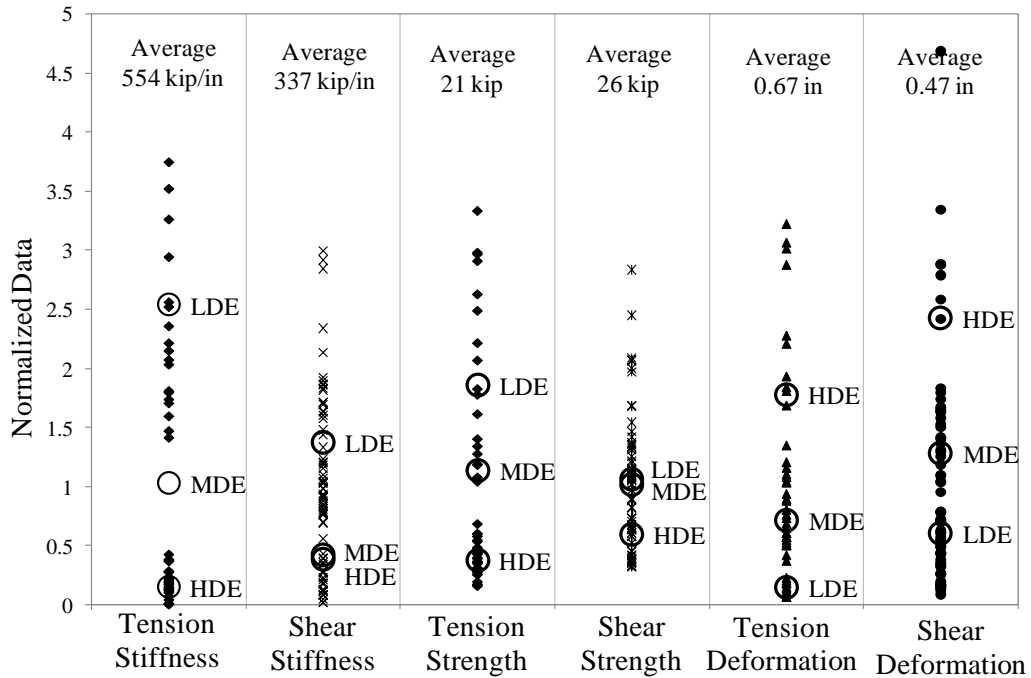


Figure 5.4. Normalized data of stiffness, strength and deformation

5.2.4 Performance Database Usage

This comprehensive performance database provides a complete set of data including stiffness, deformation capacity, yield force and ultimate force capacity, which

are important inputs for the new seismic diaphragm design methodology. In addition, it provides important information for analytical model of connections and diaphragms.

For design side, it is important to choose appropriate connections details for diaphragm system. It is well known that for high seismic regions where diaphragm ductility is required to economically resist the seismic demands, the connectors must exhibit high deformation capability. For low seismic regions where the diaphragm can be designed as elastic, connectors need only low deformation capacity. Therefore, to determine the applicability of a particular connection detail for a given seismic region, connections are categorized as LDE, MDE, or HDE relative to their deformation capacity in tension and shear. The categorization is also included in this performance database.

Overall, this performance database provides important information for model and design needs of diaphragm connection.

Table 5.4. New developed DT/DT web connector performance

ID	Test Type	Testing Notation	Δa (in)	P1 (kip)	P2 (kip)	$\Delta 2$ (in)	P2a (kip)	P3 (kip)	$\Delta 3$ (in)	Initial Stiffness K_e (kip/in)	Category	Ultimate Force (kip)
A-1	Tension	MT	0.010	4.7	10.2	1.26	9.3	1.5	2.01	158	HDE	10.2*
		CT	0.014	2.7	6.0	0.50	5.7	0.9	0.79	67		6.0*
	Shear	MV($\Delta T=0$)	0.023	10.7	35.3	0.76	22.1	5.3	2.00	232	LDE	35.3*
		MTV($\Delta T/\Delta V = 0.5$)	0.013	13.1	28.3	0.20	25.4	4.2	2.51	327		28.3*
A-2	Tension	MT	0.008	5.2	12.6	2.10	4.4	1.9	5.03	235	HDE	12.6*
		CT	0.005	2.2	7.4	0.58	7.1	1.1	1.02	209		7.4*
	Shear	MV_LC($F_t=0$)	0.006	10.0	21.4	1.11	6.3	3.2	4.58	535	LDE	21.4*
		CV($\Delta T=0$)*3	0.014	8.2	28.7	0.29	21.1	4.3	0.59	306		28.7
		CV_LC($F_t=0$)	0.007	8.2	18.5	0.08	11.9	2.8	0.35	412		18.5*
		CV_LC($F_t=10$ kip)	0.008	13.7	27.6	0.12	9.8	4.2	0.49	548		27.6*
B-1	Tension	MT	0.004	17.8	37.3	0.33	27.8	5.6	0.95	1304	MDE	37.3*
		MTV($\Delta T/\Delta V = 0.5$)	0.006	13.4	33.9	0.38	6.5	5.1	1.10	814		33.9*
	Shear	MTV($\Delta T/\Delta V = 0.5$)	0.012	15.8	31.8	0.28	15.6	4.8	0.92	402	LDE	31.8*
		MV($\Delta T=0$)	0.008	14.4	54.4	0.12	11.8	8.4	0.90	1001		54.4*
		CV($\Delta T=0.1$)	0.013	27.5	63.8	0.24	45.5	9.6	0.49	713		63.8*
B-2	Tension	MT	0.007	26.4	55.2	0.88	41.8	8.3	4.79	1189	MDE	55.2*
		CT	0.007	22.5	46.5	0.28	32.7	7.0	0.41	961		46.5*
	Shear	MV($\Delta T=0$)	0.062	4.8	31.2	0.75	16.2	4.7	3.30	77	MDE	31.2*
		MV_LC($F_t=0$)	0.068	4.1	27.5	0.69	18.7	4.1	3.51	61		27.5*
		CV($\Delta T=0$)	0.078	4.5	30.0	0.65	8.6	4.5	2.04	58		30.0*
B-3	Tension	MT	0.009	31.1	70.0	0.48	62.2	10.5	0.50	1125	MDE	70.0*
		CT	0.008	25.0	52.2	0.24	23.7	7.9	1.99	1001		52.2*
	Shear	MV($\Delta T=0$)	0.035	4.1	27.6	0.75	16.1	4.1	3.94	120	MDE	27.6*
		CV($\Delta T=0$)	0.062	3.8	25.3	0.58	8.5	3.8	2.16	62		25.3*
		CV_LC($F_t=0$)	0.121	27.6	29.0	0.80	9.9	4.2	1.63	36		29.0*

Table 5.4. New developed DT/DT web connector performance												
C-1	Tension	MT	0.017	2.7	7.7	1.44	6.7	1.2	1.85	71	HDE	7.7*
	Shear	MV($\Delta T=0$)*2	0.012	3.8	8.7	1.28	2.3	1.3	2.29	114	HDE	8.7
C-2	Tension	MT	0.003	4.1	25.0	0.05	23.0	3.8	0.16	1395	LDE	25.0*
		MTV($\Delta T/\Delta V=0.5$)	0.003	5.5	22.7	0.05	22.0	3.4	0.15	1147		22.7*
	Shear	MV($\Delta T=0.1$)*2	0.015	22.3	51.3	0.28	25.3	7.7	2.32	544	LDE	51.3
		MTV($\Delta T/\Delta V=0.5$)	0.008	7.2	29.8	0.20	23.4	4.5	0.75	566		29.8*
		CV($\Delta T=0.1$)	0.014	20.1	53.8	0.48	30.8	8.2	0.69	573		53.8*
D	Tension	MT	0.003	12.4	43.4	0.15	25.8	6.5	0.57	2072	LDE	43.4*
		MTV($\Delta T/\Delta V=0.5$)	0.003	4.3	28.2	0.12	14.3	4.2	1.02	1628		28.2*
	Shear	MV($\Delta T=0.1$)	0.017	21.2	53.9	0.32	18.2	8.1	2.84	481	LDE	53.9*
		MTV($\Delta T/\Delta V=0.5$)	0.009	11.2	34.1	0.16	8.4	5.1	0.93	573		34.1*
		CV($\Delta T=0.1$)	0.011	12.5	26.5	0.16	17.4	4.0	0.69	356		26.5*
E	Tension	MT	0.005	29.2	62.3	0.14	46.5	9.3	2.23	1948	LDE	62.3*
		MTV($\Delta T/\Delta V=2.0$)	0.005	25.0	61.1	0.12	55.7	9.2	2.17	1805		61.1*
		CT	0.009	13.0	62.6	0.10	55.6	9.4	1.25	994		62.6*
	Shear	MV($\Delta T=0.1$)	0.013	16.1	34.6	0.36	12.9	5.2	3.50	404	LDE	34.6*
		MTV($\Delta T/\Delta V=2.0$)	0.006	1.4	9.4	0.04	4.0	1.4	1.08	235		9.4*
		CV($\Delta T=0.1$)	0.007	4.8	17.1	0.09	7.3	2.6	2.60	350		17.1*
F	Tension	MT	0.004	11.6	24.9	0.09	22.9	3.7	0.19	883	LDE	24.9*
		MTV($\Delta T/\Delta V=0.5$)	0.004	10.2	21.9	0.08	21.0	3.3	0.15	782		21.9*
	Shear	MV($\Delta T=0.1$)	0.018	3.8	11.0	0.36	1.9	1.7	3.29	96	LDE	11.0*
		MV($\Delta T=0$)	0.011	18.9	43.8	0.24	14.3	6.6	1.58	622		43.8*
		CV($\Delta T=0$)	0.006	3.5	19.0	0.07	15.9	2.9	0.70	445		19.0*
G	Tension	MT	0.004	5.2	29.5	1.10	21.0	4.4	1.65	1225	MDE	29.5*
		CT	0.004	4.1	26.8	0.40	7.7	4.0	1.22	944		26.8*
	Shear	MV($\Delta T=0$)	0.032	32.4	73.9	0.48	67.6	11.1	0.65	342	MDE	73.9*
		MV_LC($F_t=0$)	0.020	19.5	35.0	0.33	14.3	5.3	2.02	262		35.0*
		CV($\Delta T=0$)	0.046	16.7	44.0	0.59	12.9	6.6	2.59	145		44.0*
		CV_LC($F_t=0$)	0.044	4.0	26.6	0.77	5.1	4.0	2.66	91		26.6*

Table 5.4. New developed DT/DT web connector performance												
C&G	Tension	CT	0.004	5.8	38.4	0.38	7.7	5.8	1.04	1417	MDE	38.4*
	Shear	CV($\Delta T=0.1$)	0.012	19.3	52.1	0.54	51.3	7.8	0.85	634	LDE	52.1*
		CV _{LC} (Ft=10)*2	0.009	17.0	38.3	0.33	25.5	5.7	0.82	608		38.3
		CV($\Delta T/\Delta V=0.5(p) \Delta T=0.10(n)$)	0.006	12.7	37.0	0.23	14.7	5.6	1.94	975		37.0*
H-1	Tension	MT	0.086	3.5	3.6	1.18	2.9	0.6	2.22	6	HDE	3.6*
		MTV($\Delta T/\Delta V=0.5$)	0.020	1.7	11.3	0.68	9.5	1.7	2.02	85		11.3*
	Shear	MV($\Delta T=0$)	0.012	9.8	23.4	1.19	6.5	3.5	3.00	293	HDE	23.4*
		MTV($\Delta T/\Delta V=0.5$)	0.008	6.3	15.2	1.32	9.0	2.3	3.59	308		15.2*
H-2	Shear	CV($\Delta T=0$)	0.008	8.2	16.8	0.70	11.5	2.5	1.58	329		16.8*
		MV($\Delta T=0$)	0.075	8.3	21.4	0.84	6.1	3.2	4.24	43	HDE	21.4*
H-3	Shear	CV($\Delta T=0$)	0.103	16.7	19.2	0.73	16.1	2.9	1.14	29		19.2*
		MV	0.074	13.0	13.6	0.63	8.8	2.0	1.76	28	MDE	13.6*
		CV($\Delta T=0$)*4	0.052	7.8	11.8	0.50	6.2	1.8	1.72	39		
H-4	Shear	MV	0.155	2.4	15.9	0.83	6.7	2.3	4.25	15	MDE	15.9*
		CV($\Delta T=0$)*4	0.048	6.3	15.8	0.65	5.5	2.4	1.70	71		15.8
		CVT($\Delta T/\Delta V=0.5$)*4	0.056	8.4	9.3	0.50	6.9	1.4	1.57	27		9.3
H-5	Tension	MT	0.440	1.0	6.5	1.88	5.7	1.0	1.92	2	HDE	6.5*
		CT*3	0.690	1.0	6.6	2.00	4.9	1.0	2.52	2		6.6
	Shear	MV	0.255	1.6	10.7	1.33	5.9	1.6	4.17	6	HDE	10.7*
		CV($\Delta T=0$)*4	0.253	3.3	9.5	1.53	3.5	1.4	4.00	6		9.5
H-6	Tension	MT	0.006	1.8	4.1	0.71	2.0	0.6	1.56	112	MDE	4.1*
		CT*4	0.007	1.4	3.3	0.43	1.5	0.5	0.77	77		3.3
	Shear	MV	0.007	8.3	16.9	2.15	8.7	2.5	4.00	347	LDE	16.9*
		CV($\Delta T=0$)*4	0.005	2.5	9.1	0.12	5.6	1.4	0.49	265		9.1
		CVT($\Delta T/\Delta V=0.5$)*3	0.005	1.8	8.4	0.08	4.7	1.2	1.02	279		8.4
H-7	Out of Plane Shear	OV*4	0.010	0.8	2.0	0.48	1.8	0.3	0.75	46	N/A	2.0
H-8	Out of Plane Shear	OV*4	0.019	1.6	2.8	0.84	2.7	0.4	1.02	48	N/A	2.8
H-9	Out of Plane Shear	OV*4	0.019	4.5	6.8	0.32	6.3	1.0	0.45	91	N/A	6.8
H-10	Out of Plane Shear	OV*5	0.045	1.9	4.5	0.42	3.0	0.7	0.82	38	N/A	4.5

Table 5.4. New developed DT/DT web connector performance

Table 5.4. New developed DT/DT web connector performance												
H-11	Out of Plane Shear	OV*5	0.018	2.5	4.8	0.29	4.5	0.7	0.53	54	N/A	4.8
I-1	Tension	MT	0.009	2.7	7.6	1.49	2.6	1.1	3.52	127	HDE	7.6*
	Shear	MV	0.005	2.4	10.0	0.08	2.5	1.5	2.62	302	LDE	10.0*
		CV($\Delta T=0$)	0.005	2.7	9.9	0.07	9.3	1.5	0.26	286		9.9*
I-2	Tension	MT	0.006	3.5	8.4	0.33	1.9	1.3	2.25	212	MDE	8.4*
	Shear	MV	0.010	17.8	40.2	0.25	8.0	6.0	3.50	625	LDE	40.2*
		MTV($\Delta T/\Delta V = 0.5$)	0.005	5.9	29.6	0.08	14.5	4.4	0.78	951		29.6*
		CV($\Delta T=0$)	0.007	16.2	35.7	0.15	8.5	5.4	1.02	783		35.7*
J-1	Tension	MT	0.018	1.7	11.5	1.97	4.1	1.7	3.03	96	HDE	11.5*
		CT	0.016	2.2	8.2	1.20	6.2	1.2	1.32	79		8.2*
	Shear	MV	0.004	2.7	17.6	0.08	14.1	2.6	2.95	613	LDE	17.6*
		CV($\Delta T=0$)	0.004	2.6	16.8	0.06	14.8	2.5	0.30	643		16.8*
	Out of Plane Shear	OV*2	0.022	3.0	4.6	0.49	1.7	0.7	0.97	32	N/A	4.6
J-2	Tension	MT	0.007	3.6	9.2	0.53	7.2	1.4	1.35	203	MDE	9.2*
		CT	0.010	4.3	9.9	0.40	2.0	1.5	0.79	155		9.9*
	Shear	MV	0.009	14.5	29.9	0.33	21.7	4.5	2.42	527	LDE	29.9*
		CV($\Delta T=0$)	0.009	11.1	23.0	0.23	10.4	3.5	0.56	395		23.0*
	Out of Plane Shear	OV*2	0.014	1.5	4.1	0.41	3.0	0.6	1.52	46	N/A	4.1
J-3	Tension	CT*2	0.010	1.4	3.6	0.76	1.1	0.5	1.40	57	HDE	3.6
	Shear	CV($\Delta T=0$)*2	0.004	1.3	8.3	0.06	7.0	1.2	0.28	313	LDE	8.3
	Out of Plane	OV*2	0.008	1.2	2.7	0.78	1.8	0.4	2.02	58	N/A	2.7
K-1	Tension	MT*2	0.009	2.7	5.7	0.79	5.1	0.9	1.54	97	HDE	5.7
	Shear	MV*2	0.007	5.2	11.8	0.20	6.6	1.8	0.84	254	LDE	11.8
	Out of Plane Shear	OV*2	0.013	3.8	6.5	1.25	4.3	1.0	2.88	81	N/A	6.5
K-2	Tension	MT*2	0.035	3.9	5.4	0.72	3.5	0.8	2.15	23	HDE	5.4
	Shear	MV*2	0.008	4.4	10.1	0.15	3.8	1.5	2.10	187	LDE	10.1
	Out of Plane Shear	OV*2	0.009	1.1	2.5	0.24	1.9	0.4	1.83	42	N/A	2.5
L-1	Tension	MT	0.006	2.1	5.4	0.38	5.2	0.8	0.44	130	MDE	5.4*
	Shear	MV*2	0.024	10.3	16.7	0.33	11.9	2.5	0.75	131	MDE	16.7
	Out of Plane Shear	OV*2	0.013	1.4	3.1	0.69	2.4	0.4	1.55	36	N/A	3.1

Table 5.4. New developed DT/DT web connector performance												
L-2	Tension	MT	0.019	2.0	9.0	0.45	5.6	1.3	0.88	72	MDE	9.0*
	Shear	MV*2	0.008	13.8	28.0	0.25	26.7	4.2	0.38	495	LDE	28.0
	Out of Plane Shear	OV*2	0.006	2.5	6.6	0.31	5.6	1.0	1.02	182	N/A	6.6
L-3	Tension	MT	0.009	1.9	6.0	0.35	3.6	0.9	2.23	103	MDE	6.0*
	Shear	MV*2	0.027	12.2	15.2	0.26	6.7	2.3	2.13	92	LDE	15.2
	Out of Plane Shear	OV*2	0.014	1.4	3.2	1.24	3.1	0.5	1.61	37	N/A	3.2
L-4	Tension	MT	0.036	2.2	14.4	0.59	11.0	2.2	1.38	60	HDE	14.4*
	Shear	MV*2	0.012	12.2	28.5	0.60	20.0	4.3	1.57	368	MDE	28.5
	Out of Plane Shear	OV*2	0.007	3.1	6.4	0.25	5.5	1.0	2.24	151	N/A	6.4
L-5	Tension	MT	0.013	2.9	9.3	0.33	5.9	1.4	0.74	108	MDE	9.3*
	Shear	MV	0.022	15.8	19.0	0.18	16.9	2.9	0.22	130	LDE	19.0*
L-6	Tension	MT	0.012	3.8	12.6	0.36	4.4	1.9	1.55	152	MDE	12.6*
	Shear	MV	0.013	14.7	32.7	0.20	16.5	4.9	0.65	386	LDE	32.7*
L-7	Tension	MT*2	0.015	3.3	12.2	0.68	9.9	1.8	0.91	120	HDE	12.2
	Shear	MV*2	0.018	18.0	27.7	0.44	27.1	4.2	0.68	271	MDE	27.7
L-8	Tension	MT*2	0.034	1.9	7.4	0.61	5.7	1.1	1.22	39	HDE	7.4
	Shear	MV*2	0.013	9.0	16.5	0.36	15.9	2.5	0.58	258	MDE	16.5
<p>a. M-Monotonic, C-Cyclic, O-Out of plane, T-Tension, V-Shear, TV-Combined Tension and Shear, Δ-Deformation, LC-Load Control; Ft-Axial Force</p> <p>b. * Value based on one test, shown for comparison only, not recommended for design.</p>												

5.3 References

1. Venuti, W. J. (1970). "Diaphragm Shear Connectors between Flanges of Prestressed Concrete T-Beams." *PCI Journal*, 15(1), 67-78.
2. Concrete Technology Corporation (1974). "Tests of Shear Connectors Report." CTA-74-B8/9, 55-62.
3. Spencer, R. A., and Neille, D.S. (1976), "Cyclic Tests of Welded Headed Stud Connections," *PCI Journal*, 21(3), 70-83.
4. Aswad, A. (1977). "Comprehensive Report on Precast and Prestressed Connections Testing Program." Research Report, Stanley Structures, Inc, Denver, Colorado.
5. Spencer, R. (1986). "Earthquake Resistant Connections for Low-Rise Precast Concrete Buildings", Proceedings for Seminar on Precast Concrete Construction in Seismic Zones, V.1, NSF/Japan Society for the Promotion of Science, Tokyo, Japan.
6. Kallros, M.K. (1987). "An Experimental Investigation of the Behavior of Connections in Thin Precast Concrete Panels under Earthquake Loading", M.S. Thesis, Civil Engineering Department, University of British Columbia, British Columbia, Canada.
7. Pincheira, J. A., Oliva, M.G., and Kusumo-Rahardjo, F. I. (1998). "Tests on Double Flange Connectors Subjected to Monotonic and Cyclic Loading" *PCI Journal*, 43(3) 82-96.

8. Oliva, M.G. (2000). "Testing of the JVI Flange Connector for Precast Concrete Double-tee Systems." Test Report, Structures and Materials Test Laboratory, University of Wisconsin, Milwaukee, Illinois.
9. Oliva, M.G. (2001). "Testing of JVI mini-V Flange Connector for Precast Concrete Double-tee Systems." Test Report, Structures and Materials Test Laboratory, University of Wisconsin, Milwaukee, Illinois.
10. Shaikh, A.F., and Feile, E.P. (2002). "Testing of JVI Vector Connector." Test Report, Structural Engineering Laboratory, Milwaukee, Illinois.
11. Wiss, Janney, Elstener Associates, Inc. (2002). "Dayton/Richmond Flange-to-Flange Connector Tests" Test Report, Northbrook, Illinois.
12. Shaikh, A.F., and Feile, E.P. (2003). "J.W.Peters and Sons Tee Flange Connector for Precast Concrete Applications" Report on the Results of Laboratory Testing, Structural Engineering Laboratory, Milwaukee, Illinois.
13. Shaikh, A.F., and Feile, E.P. (2004). "Additional testing of JVI vector connector in 4" slabs" Report on the Results of Laboratory Testing, Structural Engineering Laboratory, Milwaukee, Illinois.
14. Pincheira, J.A., Oliva, M.G., and Zheng, W. (2005). "Behavior of Double-Tee Flange Connectors Subjected to In-Plane Monotonic and Reversed Cyclic Loads" PCI Journal, 50(6), 32-54.
15. Cao, L. (2006). "Effective Design of Precast Concrete Diaphragm Connections Subjected to In-Plane Demands", Ph.D dissertation, Lehigh University, Bethlehem, PA

16. Naito, C., Peter W., Creek J. (2006a). "T.C.S. Twister Connector Universal Form Clamp Company In-plane Performance", ATLSS Report No. 06-08, ATLSS Center, Lehigh University.
17. Naito, C., Peter W., Creek J. (2006b). "T.C.H.D. Twister Connector Universal Form Clamp Company In-plane Performance", ATLSS Report No. 06-09, ATLSS Center, Lehigh University.
18. Naito, C. (2007). "Erector Connector Meadow Burke Company In-plane Performance", ATLSS Report No. 06-22, ATLSS Center, Lehigh University.
19. Naito, C., Ren, R., Jones, C., Cullen, T. (2007). "Development of a Seismic Design Methodology for Precast Diaphragms - PHASE 1B SUMMARY REPORT", ATLSS Report No.07-04, ATLSS Center, Lehigh University.
20. Hodgson I, Naito, C., Stokes F., Bowman C. (2007). "Erector Connector Meadow Burke Company In-plane and out-of-plane Performance", ATLSS Report No. 07-12, ATLSS Center, Lehigh University.
21. Naito, C., Hendricks R. (2008). "In-plane and Out-of-plane Performance of the MC Flange Connector", ATLSS Report No. 08-08, ATLSS Center, Lehigh University.
22. Naito, C. (2008). "Universal Form Clamp Company Next Generation Twister Connector Performance", ATLSS Report No. 08-14, ATLSS Center, Lehigh University.
23. Naito, C., Ren, R. (2009a). "In-plane and Out-of-plane Performance of Building Products Edge Connector System," ATLSS Report No. 09-02, ATLSS Center, Lehigh University.

24. Naito, C., Ren, R. (2009b). “In-plane and Out-of-plane Performance of the Mini-MC Flange Connector”, *ATLSS Report* No. 09-05, ATLSS Center, Lehigh University.
25. Ren, R., Naito, C. (2010). “In-plane and Out-of-plane Performance of MC Flange Connector.” *ATLSS Report* No. 10-02, ATLSS Center, Lehigh University.

Chapter 6 Response Estimation Approach of Diaphragm System based on Performance Database

In this chapter, a simplified pushover modeling approach is developed to estimate the maximum midspan flexural deflection and shear sliding of a diaphragm subjected to a statically applied uniform load. This method begins with developing shape functions of joint moment-rotation and shear-sliding deformation responses using along with the information included in the performance database, and then estimate the in-plane flexural and shear resistance-displacement responses of the diaphragm system. The application of this method was conducted on the three cases of diaphragm system designed with web connectors in LDE, MDE and HDE categories.

6.1 Precast DT Diaphragm Joint

A precast double tee diaphragm joint is referred as the region between precast concrete panels, where the mechanical connections are used across to connect the adjacent panels together. The typical diaphragm joint, which are parallel to the lateral-force-resisting system, must contain web connections to resist the diaphragm shear forces as well as chord connection to resist tension/compression forces at the edges of the diaphragm. The types of connections used to connect precast concrete double tee panels together to form diaphragms vary depending on the required connection strength, strain capacity to accommodate expected joint movement, and the preference of the precast

concrete supplier manufacturing and erecting the precast concrete units. A typical layout of double tee diaphragm joints is shown in Figure 6.1.

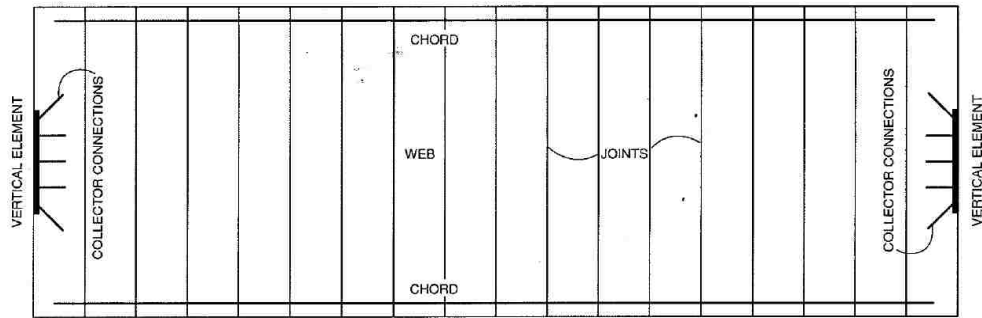


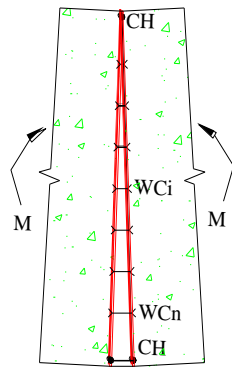
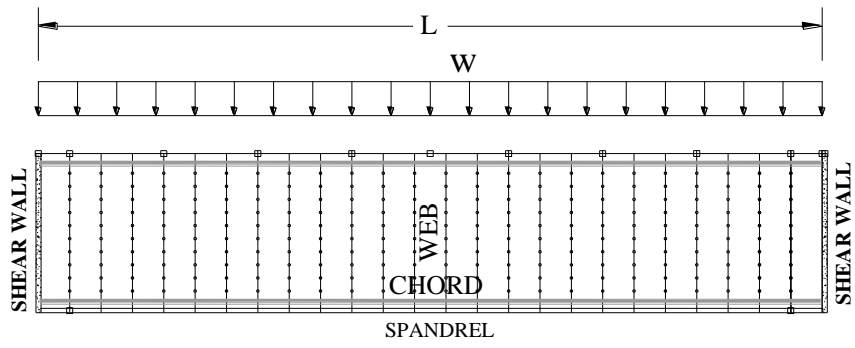
Figure 6.1. Typical double tee diaphragm joints

6.2 Simplified Diaphragm Response Estimation Approach

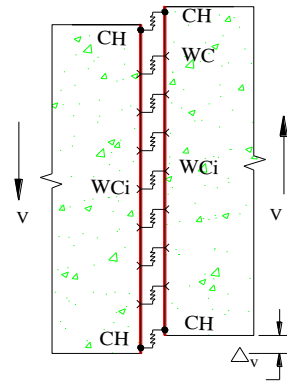
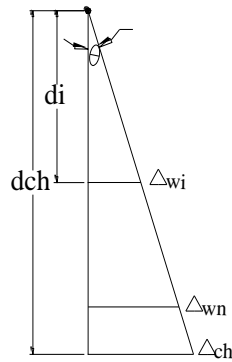
Three-dimensional finite element (FE) analyses have illustrated the significance of diaphragm in-plane flexibility on the seismic performance of precast concrete structures (Zhang et al. 2009). However, developing a detailed FE analysis is cumbersome for practicing engineers and not practical for most design projects. A simplified method is presented here which can be used to model diaphragm response quickly by utilizing the database information provided. The method builds on the PCI girder analogy to estimate the maximum midspan flexural deflection and shear sliding of a diaphragm for a statically applied uniform load. By using this model, the simplified multi-linear strength and deformation curve of various connectors included in the performance database can be used to create a shear or flexure pushover curve for the diaphragm system. The results generated by this simple pushover method gives design

engineers a rough estimation of flexural and shear responses of diaphragm. Furthermore, varying the connector used can be helpful to provide guidance about choosing appropriate connector types for diaphragm to meet design requirements.

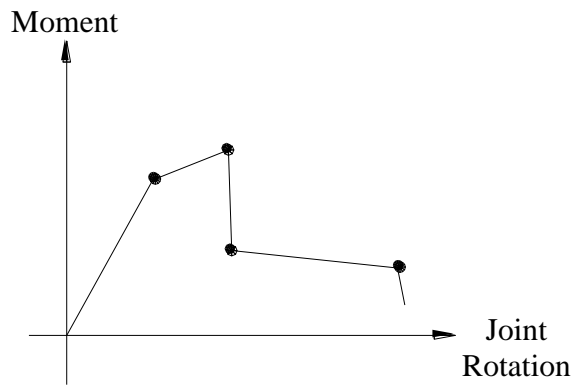
The girder analogy assumes that the first mode (single curvature) is the dominant response under seismic demands. Flexural demands will be the largest at the center of the diaphragm and the shear demands will be highest at the end of the diaphragm. The flange-flange joint at the midspan of the diaphragm and the joint adjacent to the diaphragm lateral boundaries are critical joint locations for flexure and shear, respectively. Assuming that each panel is rigid and deformation compatibility exists along the joint, the opening and shear deformations at each connector can be determined as illustrated in Figure 6.2a and Figure 6.2b.



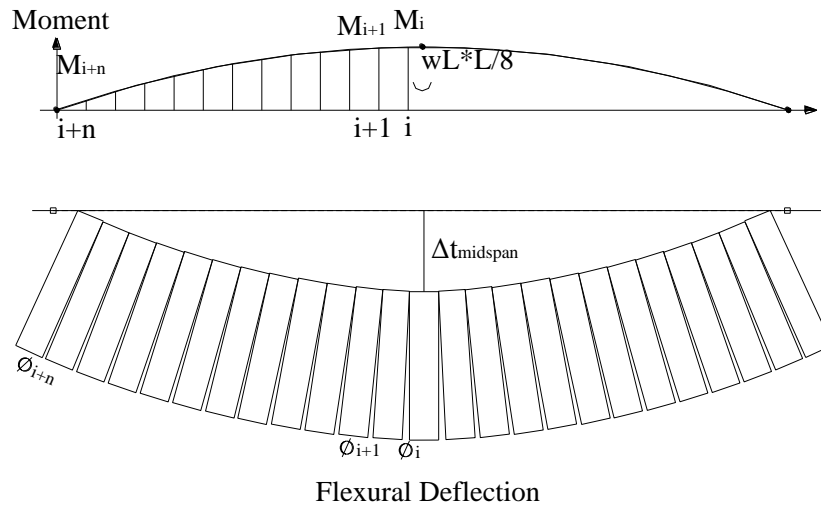
a) Flexural joint analysis



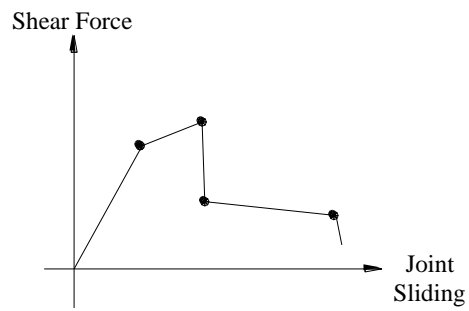
b) Shear joint analysis



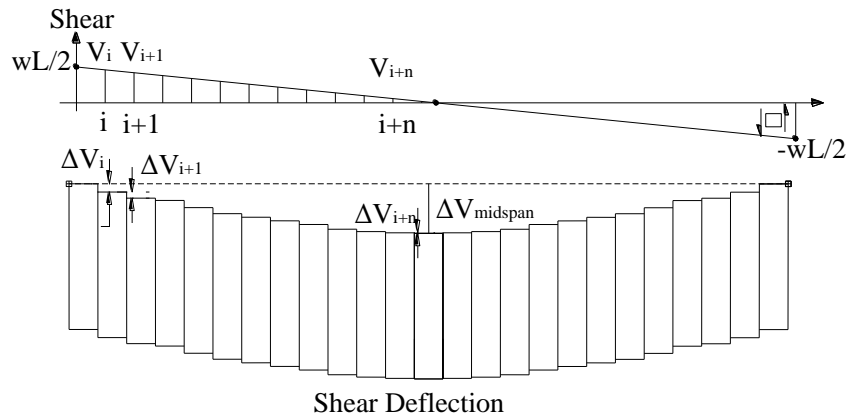
c) Joint Moment-rotation response



d) Midspan flexural deflection



e) Joint shear force-sliding response



f) Midspan shear sliding

Figure 6.2. Flexural deflection/shear sliding response of diaphragm

6.2.1 Joint Flexure/Shear Response

The moment-rotation and shear-sliding deformation is determined for each joint. If all the joint reinforcement is identical in the diaphragm the procedure shall be applied once. For diaphragms with varying connector types and numbers the procedure must be applied to each joint. The joint moment-rotation response is computed for increments of joint rotation. For each increment the deformation of each discrete chord and web element can be calculated by compatibility. The joint is assumed to rotate about the compression chord. The tensile resistance provided by each web connector, F_{wci} , and chord connector, F_{ch} , are found using the database information. At a given step, j , the moment resistance of the joint, M_j , is equal to the sum of each connector tensile force multiplied by its distance from the compression chord, d_i for the web connectors and d_{ch} for the tension chord as shown in Eq. 6-1:

$$M_j = (F_{ch})_j * d_{ch} + \sum_i (F_{wci})_j * d_i \quad \text{Eq. 6-1}$$

For joint shear analysis, joint sliding is incremented at small step size. For each step, the shear force of each web connector V_{wci} and Chord connector V_{ch} are found using the database information. At a given step j , the shear resistance of the joint, V_j , is computed in accordance with Eq. 6-2. Where n_{ch} is the number of chords and n_{wc} is the number of web connectors.

$$V_j = (V_{ch})_j * n_{ch} + (V_{wci})_j * n_{wc} \quad \text{Eq. 6-2}$$

6.2.2 Diaphragm Flexure/Shear Response

To determine the diaphragm response a deformation based analysis method is used. For each increment, j , the moment and rotation at each joint, i , is computed. For flexural resistance-deflection response of the diaphragm, steps of joint rotation, ϕ_{ij} , at the joint closest to midspan are incremented and the moment resistance, M_{ij} , of the joint is determined from the joint moment-rotation previously determined. The load level, w_j , at this step is computed from statics and the moment at the joint. The moment at the other joints along the span (M_{ij} to $M_{(i+n)j}$) are computed based on statics and the corresponding rotations (ϕ_{ij} to $\phi_{(i+n)j}$) are then determined from the moment-rotation relationship. The midspan deflection at a given step, j , is computed in accordance with Eq. 6-3:

$$\Delta mid_j = b * [\sin (\phi_{ij}) + \sin (\phi_{ij} + \phi_{(i+1)j}) + \dots + \sin (\phi_{ij} + \phi_{(i+1)j} + \dots + \phi_{(i+n)j})]$$

Eq. 6-3

Where b is the width of each panel, n is the number of joints from support to the midspan, and $\phi_i, \phi_{i+1}, \dots, \phi_{i+n}$ are the rotation of joints along the span.

To compute the shear resistance-deflection response of the diaphragm the joint sliding deformation, ΔV_j at the joint closest to support are incremented. For each increment the shear resistance, V_{ij} , of the joint is computed from the shear force-sliding relationship developed. The load level w_j is computed from statics and used to determine the shear force at the remaining joints along the span (V_{ij} to $V_{(i+n)j}$). The sliding of joints along the span (ΔV_{ij} to $\Delta V_{(i+n)j}$) can be found from the joint shear-sliding response. The midspan sliding at a given step j is estimated with the following equation Eq. 6-4:

$$\Delta V_{midspanj} = \Delta V_{ij} + \Delta V_{(i+1)j} + \dots + \Delta V_{(i+n)j}$$

Eq. 6-4

Where n is the number of joints from support to the midspan, and $\Delta V_i, \Delta V_{i+1} \dots, \Delta V_{i+n}$ are the sliding of joints along the span.

6.3 Numerical Examples

A series of examples are conducted using the methodology presented in previous section. The flexural and shear resistance-deflection response of diaphragms designed

with web connectors corresponding to LDE, MDE and HDE tension categories from the performance database are examined. A 300-ft by 60-ft sub-diaphragm is selected from a representative prototype structure diaphragm (Figure 6.3) (Fleischman et al. 2005). The sub-diaphragm is designed to resist a bending moment of 13,000 kip-ft and a shear reaction of 350 kip. The number of connectors is chosen based on the girder analogy and the measured connector capacity from the database and are evenly spaced along the joint.

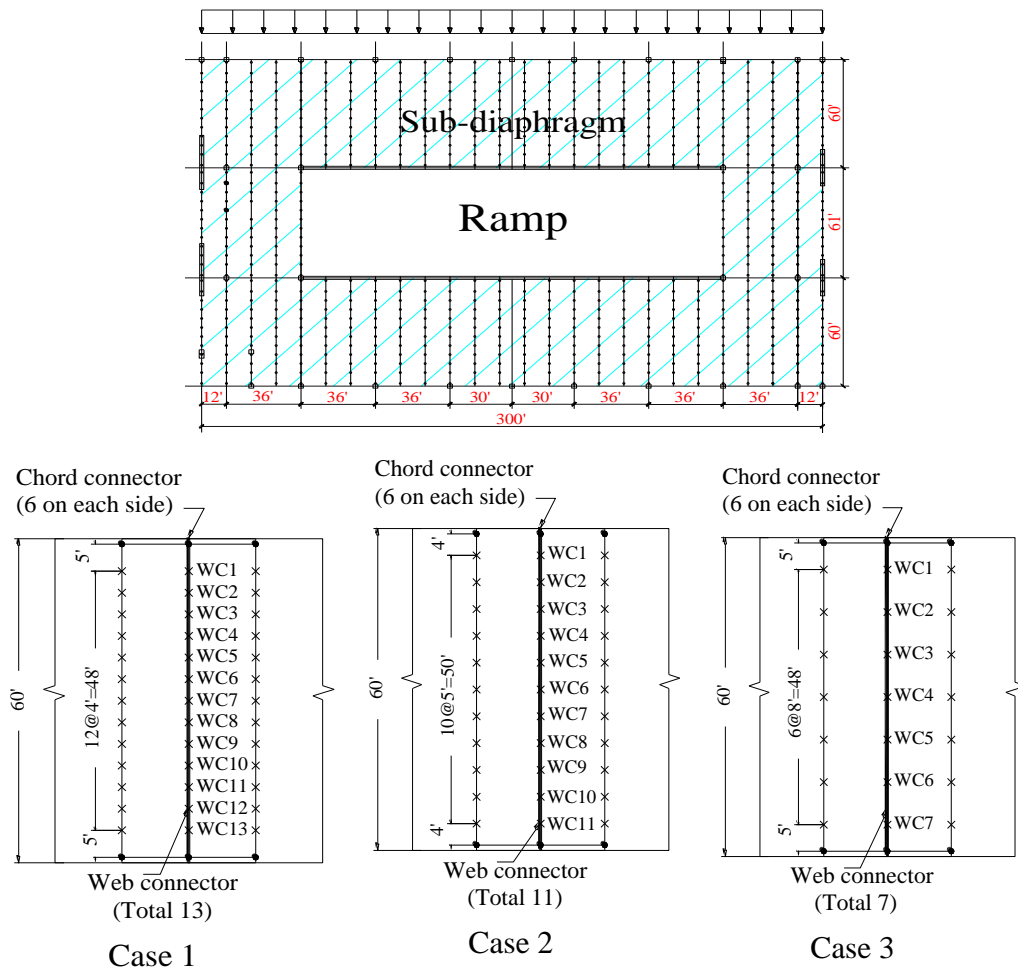


Figure 6.3. Prototype structure diaphragms and joint design cases

As indicated in Figure 6.3 and Table 6.1, three representative joints with web connectors categorized in LDE, MDE and HDE tension categories are examined. Due to the varying strength of the chosen web connectors the number and spacing of connectors vary in each case. Due to the limited chord variety the same chord type was used for each case. Chord connector B-1, an MDE tension connector, was used for each case. For simplicity, the number of chord and web connectors used in each joint is kept constant throughout the diaphragm for each case studied. The number and type of connector, and the moment, M, and shear, V, capacity of each diaphragm is summarized in Table 6.1.

Table 6.1. Joints design with different tension category connectors							
Case	Tension Category	Web connector ID	Chord connector ID	#of Chord connector	#of Web connector	M [kip-ft]	V [kip]
1	HDE	L-4	B-1	12	13	13025	370
2	MDE	L-6	B-1	12	11	13025	360
3	LDE	D	B-1	12	7	13025	377

The joint moment-rotation and shear force-deformation of individual joints is computed using the simplified multi-linear curves included in the database. The three tension categories, HDE, MDE, and LDE, are used to estimate the typical joint responses for each case as illustrated in Figure 6.4.

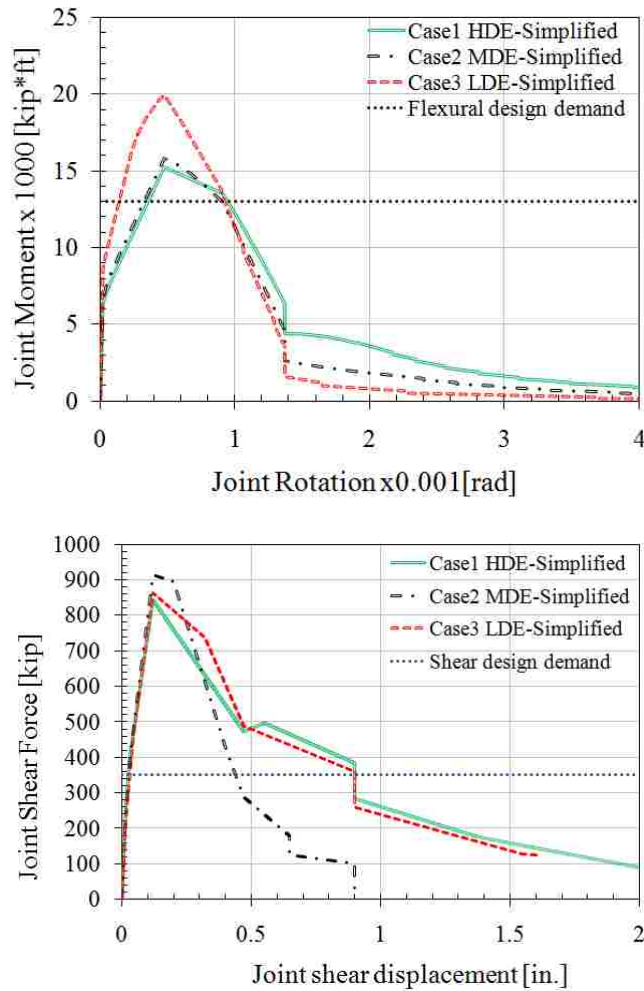
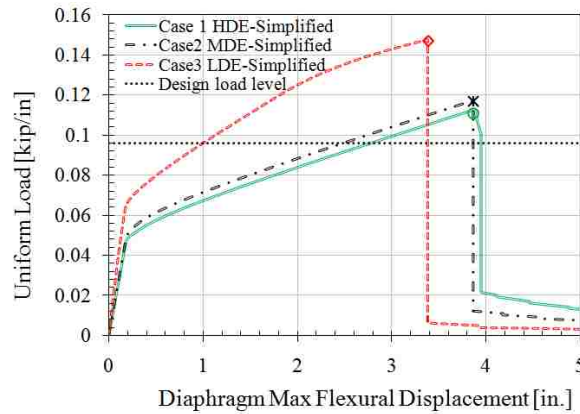


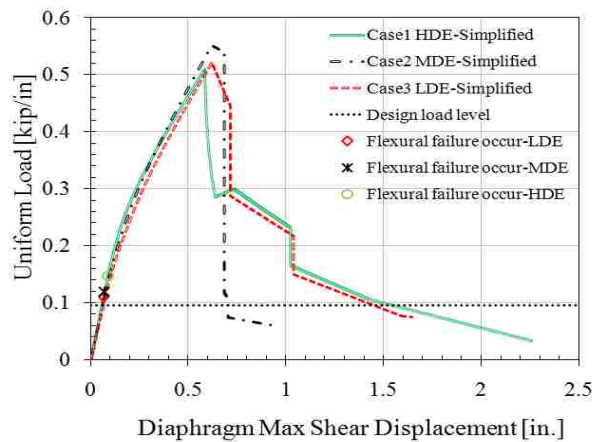
Figure 6.4. Joint moment-rotation and shear-sliding responses

The multi-linear connector responses and resulting joint response are used to estimate the flexural and shear resistance-deformation performance of the overall diaphragm using the developed simple shape function pushover modeling approach. The results are illustrated in Figure 6.5. Unlike standard design methods, the modeling approach used accounts for the shear strength of the chord connectors. Consequently the shear resistance of the diaphragm is much greater than the design requirement this

ensures a ductile flexural failure mode of diaphragm. This ductile flexural failure mode will occur for all three cases before the ultimate shear capacities are achieved as shown in Figure 6.5b. Diaphragm designed with connectors in different tension categories ends up in different global flexural force and deformation capacities, i.e. the diaphragm with LDE elements has the highest stiffness and force capacity but the lowest deformation capacity. It is important to note that the variation in global response is not too significant due to the use of the same MDE category chord connector in each case.



a) Flexural resistance-deflection response



b) Shear resistance-sliding response

Figure 6.5. Diaphragm resistance-deformation response

As presented in this chapter, the database is utilized to conduct a simplified pushover modeling approach for the estimation of the maximum midspan flexural deflection and shear sliding of a diaphragm subjected to a statically applied uniform load. This method begins with developing the shape functions of joint moment-rotation and shear-sliding deformation responses by using the database information of connectors used in the specific joint, then the flexural and shear load-deformation responses of diaphragm system can be estimated by using a deformation based analysis technique. This estimation model is simple and easy to use for practicing engineers who do not have time to develop detailed FE models. This chapter also illustrates case-by-case examples of determining flexural and shear response of diaphragm systems designed with LDE, MDE and HDE connectors. The results show that the ductile flexural failure modes occur for all three cases before ultimate shear capacities are achieved, and the diaphragm designed with connectors in different deformation categories influence the global diaphragm response.

6.4 References

1. Zhang, D., Fleischman, R.B., Naito, C., and Ren, R. (2010) "Pretopped precast diaphragm critical flexure joint under seismic demands, Part I: Analytical modeling." *J. Struct. Eng.*, Accepted
2. Fleischman, R.B., Naito, C., Restrepo, J., Sause, R. et al. (2005) "Seismic Design Methodology for Precast Concrete Diaphragms", Part2: Research Program, *PCI Journal* 50(6), 14-31.

Chapter 7 Experimental Program of Precast Concrete Diaphragm Critical Joint with Multiple Connections

This phase of the dissertation research pertains to the experimental program associated with integrated experimental and analytical evaluation of the seismic behavior of critical multi-connection joints of precast concrete diaphragm system. The analytical component was developed by research collaborators at the University of Arizona. This chapter mainly presents the experimental portion of this research effort. The analytical portion and joint performance is out of the dissertation scope. The detailed information regarding the analytical component and behavior of the multi connection joint was discussed by the research team member in University of Arizona (Zhang 2010).

A multi-directional test fixture is developed to allow for simultaneous control of shear, axial and bending deformations at the panel joint. The test is conducted at a half-scale. Two specimens of critical flexural and shear joints are designed and fabricated for evaluation. The test specimens are detailed using diaphragm connections intended to meet deformability requirements. The load protocols applied to the test specimens are provided by project members in University of Arizona.

The critical flexural joint is evaluated under predetermined displacement histories (PDH) derived from nonlinear transient dynamic analysis (NLDTA) of 3D analytical model (Zhang 2010). The critical shear joint is evaluated using hybrid testing techniques

in which the experiment testing and NLTDA are performed simultaneously, with the physical test specimen acting as a substructure of the analytical model superstructure.

This chapter presents the experimental program including test setup, specimen design and details, material properties of major components, instrumentation design and control algorithm used in PDH and Hybrid test.

7.1 Test Setup

A multi-directional test fixture is developed to allow for simultaneous control of shear, axial and bending deformations exhibited at the panel joint during earthquake simulations. The fixture utilizes three actuators with the capacity of 281-kips, two in axial displacement and one in shear displacement as shown in Figure 7.1. Actuators 1 and 2 control displacement perpendicular to the joint at the specimen top and bottom (producing opening/closing of the joint); Actuator 3 controls displacement parallel to the joint (producing joint sliding displacement). The test specimen is connected to a restraint beam (W30x326 steel sections) on either end of the panel. One beam is fastened to the lab floor, providing a fixed end, while the other beam rests on a pair of Teflon coated steel plates, providing mobility with minimal frictional forces. Independent control of the three actuators allows for application of shear, axial and bending deformations. The connections between panels and restraint beams consists of: (1) a total of 7 grouted through-rod bolts along the angle fixed to the restraint beam; (2) welding of the chord connector back end face plate to the restraint beam. Vertical movement of the panel was

restricted by Teflon coated bearing pads under the center of each panel. This eliminates sag of the test specimen due to self-weight, while still allowing for free, near frictionless motion in the horizontal plane.

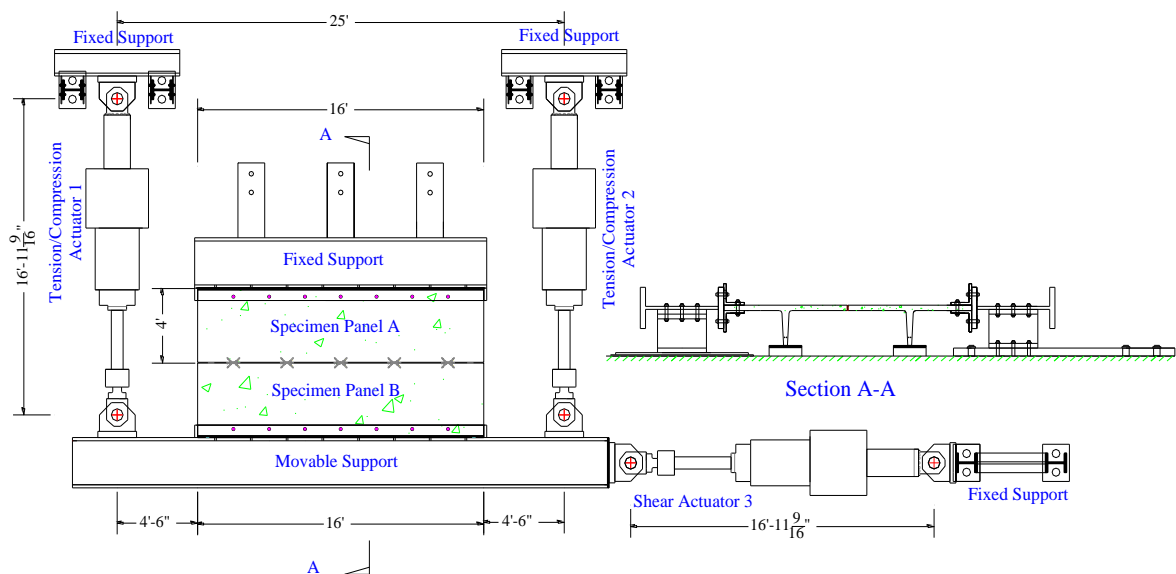


Figure 7.1. Multi-directional test fixture

The panels are installed in the following sequence: (1) Specimen Panel A is placed in the fixture and welded to the fixed support; (2) Through-bolts are inserted into the anchor holes, fully tightened, and then grouted; (3) Specimen Panel B is attached to

the movable support in identical fashion; (4) The actuators are attached to the movable support and brought on-line (hydraulic pressure is then maintained until completion of testing); and, (5) The panels are welded to each other. The welding procedure follows typical field construction practice (Figure 7.2): (1) a steel rectangular slug is tack welded between connectors, moving from top to bottom; (2) the sequence is repeated with the appropriate size fillet weld as specified in the detail drawings (Figure 7.2).



Figure 7.2. Field welding of connections between panels

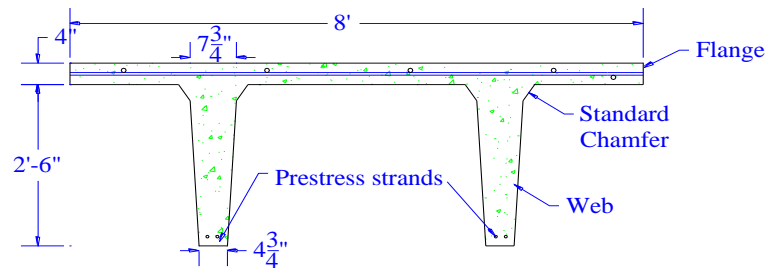
7.2 Test Specimen

The test specimen is composed of two pretopped precast floor units, connected across their joint with chord and web connections. The full scale specimen replicated a typical joint from a prototype building system. The Specimen dimensions are consistent through the collaborative research program between UCSD, University of Arizona and Lehigh University. A DT panel with 8-ft wide 32-ft long geometry is assumed for the full-scale size. In order to fit specimen with the facilities (actuators and strong floor) of

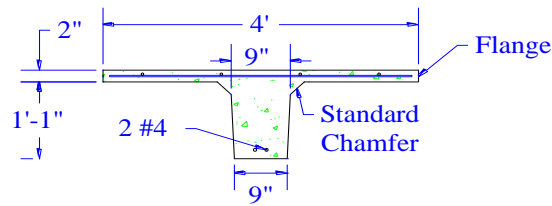
the laboratory (NEES @ ATLSS Research Center) and allow industry partners to produce identical units for a half-scale shake table test (Schoettler et.al. 2009), half-scale test specimen is designed and used for evaluation.

7.2.1 **Scaling of Specimens**

To ensure that stress remains consistent, the physical dimension of DT panels, individual connections and all other reinforcing details were scaled down by a length factor of 0.5. Figure 7.3a shows the DT cross-section for the full-scale specimen. The 4-in flange represents a typical existing pre-topped floor diaphragm system used in low seismic zones. The specimens are built to replicate current practice. The tees are fabricated at a precast concrete manufacturing facility on a standard double tee form. The half scale DT panels with 2-in thick flange is measured 4-ft wide by 16-ft long. The full scale DT panel cross section and corresponding approximate half scale panel cross section are illustrated in Figure 7.3. Important actions occur in the plane of DT flange, thus the specimen stem geometry is chosen for ease of forming and load handling, rather than complete verisimilitude. In addition, as prestressing steel is typically well within the DT stem, leading to low prestress level in the flange, the test specimens used in this dissertation work are not prestressed.



(a). Full scale



(b). Half scale

Figure 7.3. Scaling of DT Section

The unbonded dry chord connector (for flexural joint), bonded chord connector (for shear joint) and common DT flange-to-flange JVI vector connector are chosen as embedded chord and web connections of the experimental panels. The full scale and corresponding half scaled chord and JVI connection details are illustrated in Figure 7.4 and Figure 7.5. These details exhibited excellent behavior in isolated connector tests (Naito et al, 2007).

To provide tension ductility to the chord, mechanical debonding of the anchorage bars is used for chord connection in flexural joint specimen. The mechanical debonding technique allows significant amount of inelastic bar deformation, and hence joint opening, prior to bar fracture. In addition, the compressible filler material surrounding the

bars significantly reduces the high stresses associated with dowel action, therefore delays bond-slip and the associated flange cracking.

The full scale connector using a dual #5-bar configuration, while the half-scale connection detail used in the test specimen is a six #3-bar configuration. Debonding is provided through 1/8-in padded foam encircling the anchor bars from the back of the faceplate over the unbonded length.

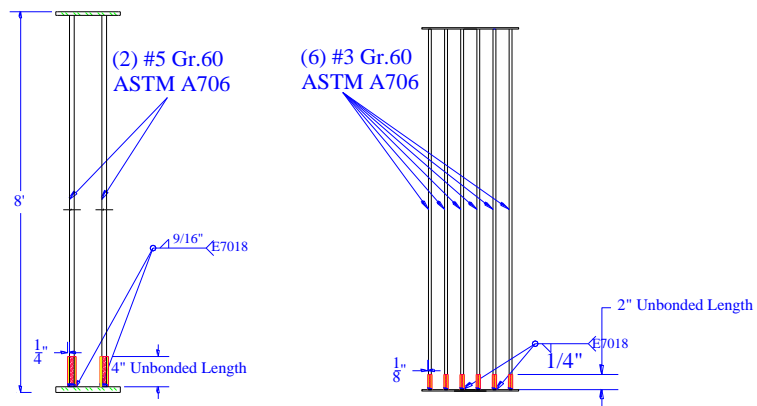


Figure 7.4. Full scale and half scale unbonded chord connection



Figure 7.5. Full scale and half scale JVI Vector

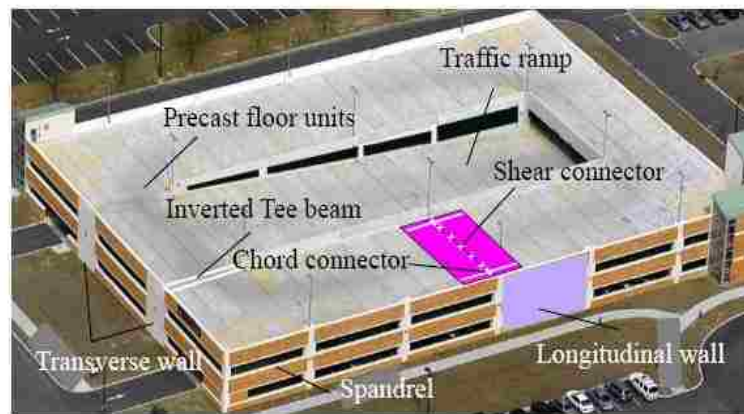
The scaled JVI Vector connector (see Figure 7.5) is a special-made piece developed and fabricated specifically for the testing program by JVI Inc. The results of half-scale connector tests showed good similitude to full scale connector tests (Naito and Ren 2008). The strength of half scale connectors is approximately one quarter of full scale connectors, the elastic stiffness and deformation capacity of half scale connector are about half of the full scale connector.

Table 7.1. Half scale connector strength hierarchy			
Connection Type	Over strength factor		
	Weld	Slug	Faceplate
Dry Chord	1.64	3.98	3.87
JVI Vector	1.83	2.69	-

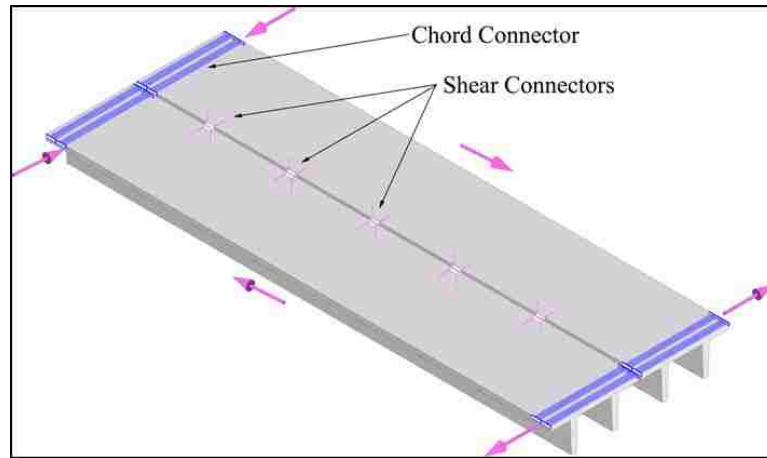
The connector strengths are controlled by yielding of chord bars and JVI legs. To achieve this desired controlling mechanism, overstrength factors are provided to the plates, welds, and slug relative to the yield mechanism (see Table 7.1).

7.2.2 Flexure Joint Specimen Design

The flexure joint specimen (Figure 7.6b) replicates the critical flexural joint in a pretopped precast concrete diaphragm, where the critical flexural joint refers the joint undergoing the highest in-plane flexural demands in the diaphragm (shaded region in Figure 7.6a).



(a) Typical parking structure



(b) Close up of shaded area

Figure 7.6. Critical flexural joint in a typical parking structure

Table 7.2 summarizes the required and nominal strengths for full-scale and half-scale critical flexural joint designs. It is important to note that the current code required moment resistance $M_u = 2700$ kip-ft is increased to 4050 kip-ft through the use of a diaphragm force amplification factor Ψ_d of 1.5 (BSSC TS4 2009). In according to the scale rule of moment strengths, which should be reduced by the cubic of the scale factor, the required moment strength is reduced by 2^3 at half-scale, i.e., $M_u = 506$ kip-ft. The nominal flexural capacity M_n is determined using an analytically-based design procedure (BSSC TS4 2009) and considers the tension contribution of the web connections.

Table 7.2. Critical flexural joint design								
Case	M_u [kip-ft]	V_u [kip]	Detailing	Tension Strength [kip]	Shear Strength [kip]	# of required	M_n [kip-ft]	V_n [kip]
Full scale	4050	0	#6 bar	26.5	0	6	4685	65
			JVI	3.15	13	5		
Half Scale	506	0	#3 bar	6.6	0	6	586	16
			JVI	0.79	3.26	5		

Since this specimen is selected to represent the flexural joint, which is under high flexural demanding with low shear demanding, the # of web connections (JVI vector) is controlled by maximum spacing limits from construction practice (6-ft for full scale) resulting in a specimen layout of five half-scale JVI Vector connectors, spaced at 3-ft. The tension and shear design strengths of individual connectors are determined from experiments (Naito and Ren 2008). Note that while the design is based on flexure alone,

the critical flexure joint is subjected to combinations of flexure, shear and axial during the experiment, particularly for the bidirectional earthquake loading.

In addition to primary connection reinforcement details, temperature and shrinkage reinforcement (ACI 318-08 2008) in the form of welded wire reinforcement is used in each precast panel. Two conventional #4 reinforcing bars are placed at the bottom of the stem instead of prestressing steel (see Figure 7.7). Seven additional L-shaped No.4 bars are installed to strengthen the boundary of the test subassembly. The specimen details are shown in Figure 7.7.

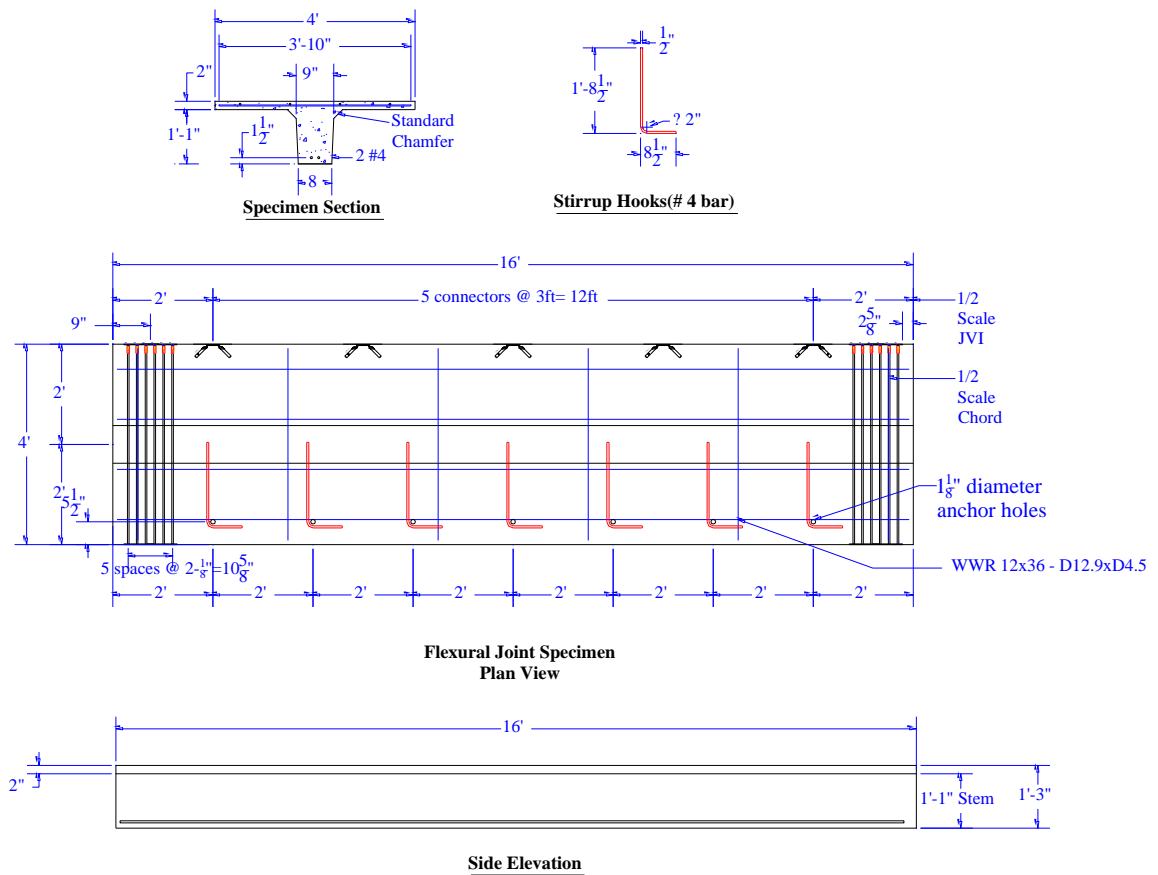


Figure 7.7. Flexural joint specimen plan view & side elevation

7.2.3 Shear Joint Specimen Design

The shear joint specimen replicates the critical shear joint in a pretopped precast concrete diaphragm, where the critical shear joint refers the joint undergoing the highest in-plane shear demands in the diaphragm.

The design of shear joint specimen is similar as flexural joint discussed in section 8.2.2. The difference is that the shear joint specimen employs three #3 bars bonded bars for chord connection and 8 JVI vector as web connections. The layout of shear joint specimen is shown in Figure 7.8.

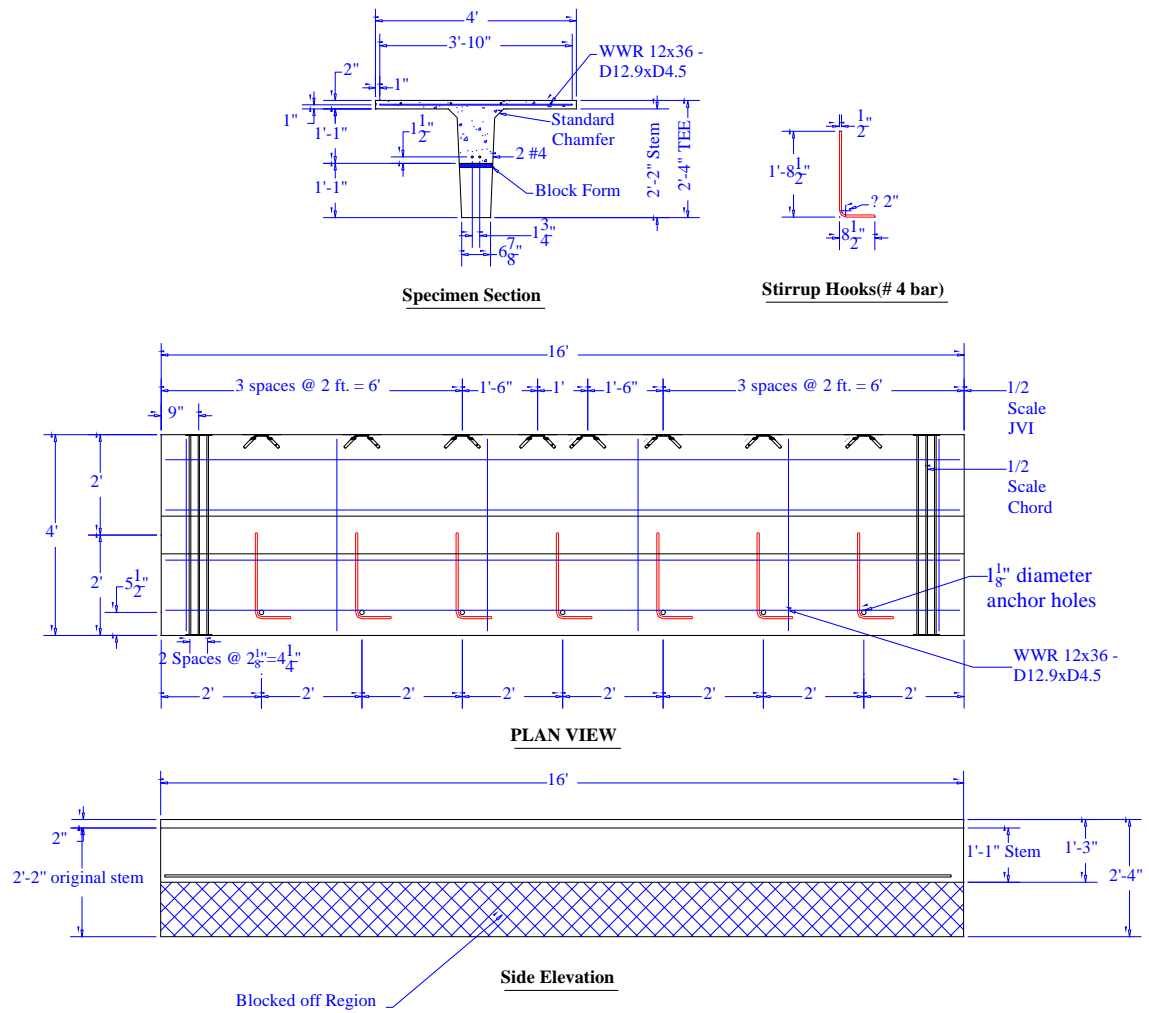


Figure 7.8. Shear joint specimen plan view & side elevation

7.3 Material Properties

Test specimens were constructed in accordance with current practice at an industry partner manufacturing facility. Materials used for fabrication of the test specimens replicate typical precast construction. A standard single tee form was modified

to create the half-scale cross section. Self-consolidating concrete with design strength of 7000psi was used for the precast sections. Actual concrete compressive strength were measured from cylinder tests conducted according to ASTM C39 (ASTM 2008), the compressive strengths are averaged 7860+/-100psi. The reinforcing details embedded in the panels include: (1) mild steel reinforcement #3 and #4 rebar; and, (2) welded wire reinforcement (WWR) conforming to ASTM A185 (ASTM 2008). The WWR possessed a measured tensile strength of 105-ksi and ultimate strain capacity of 0.03. Reinforcement bars were made of ASTM A706 Grade 60 steel. Mill certified yield and fracture strengths are 65.6-ksi and 94.3-ksi for #3 bars, 65.8-ksi and 91.4-ksi for #4 bars, respectively. Bar ultimate elongation was measured in tests as approximately 0.16. All connector plates and slugs were fabricated from ASTM A36 steel. All welds were conducted using the shielded metal arc welding (SMAW) process using E7018 in accordance with AWS standards.

7.4 PDH Test of Diaphragm Critical Flexural Joint

Experimental test is conducted on flexural joint specimen to evaluate the seismic performance of a critical flexural joint in a pretopped precast concrete diaphragm. This testing program is a collaborative integrated experimental and analytical effort. The test load histories are derived from analytical simulation conducted by University of Arizona.

The seismic loadings are applied to test specimen as predetermined displacement histories (PDHs), which represents the interface displacements between the analytical

superstructure and physical substructure (Figure 7.9). This loading condition is realized through a test fixture developed to simultaneously provide shear, axial and moment to the joint (Figure 7.1).

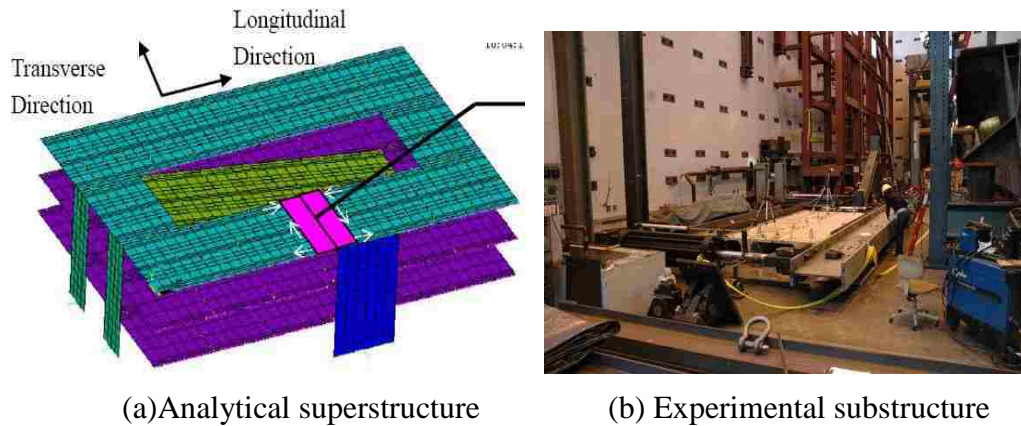


Figure 7.9. PDH test program

The analytical component of this test program is developed at University of Arizona (Zhang 2010). This section focuses on the experimental program including instrumentation design, control algorithm and flexure joint response.

7.4.1 Instrumentation

Tension and compression are applied to the specimen through two 281 kip capacity actuators attached between the fixed and movable support beams. Shear is applied with a 281 kip capacity actuator attached to the movable load beam. Seventeen panel and joint deformations are measured directly on the precast specimen using a series of Linear Voltage Displacement Transducers (LVDT) as illustrated in Figure 7.10. The opening displacement at the joint is measured across each embedded connector (labeled

D1 through D7). The shear deformations between the panels are measured along the joint at three equal spaces (labeled D8, D9 and D10). The overall deformation between the fixed and free supports is measured at the centerline, C3, and in line with the chords, C1 and C2. The slip of the panels from the supports is measured at each chord in LVDT C4 through C7. The actuator deformations (labeled Disp 1, 2, and 3) are captured by a series of feedback LVDT centered pin to pin of each actuator (labeled Act 1, 2, and 3). Restoring forces are measured using load cells in line with each actuator.

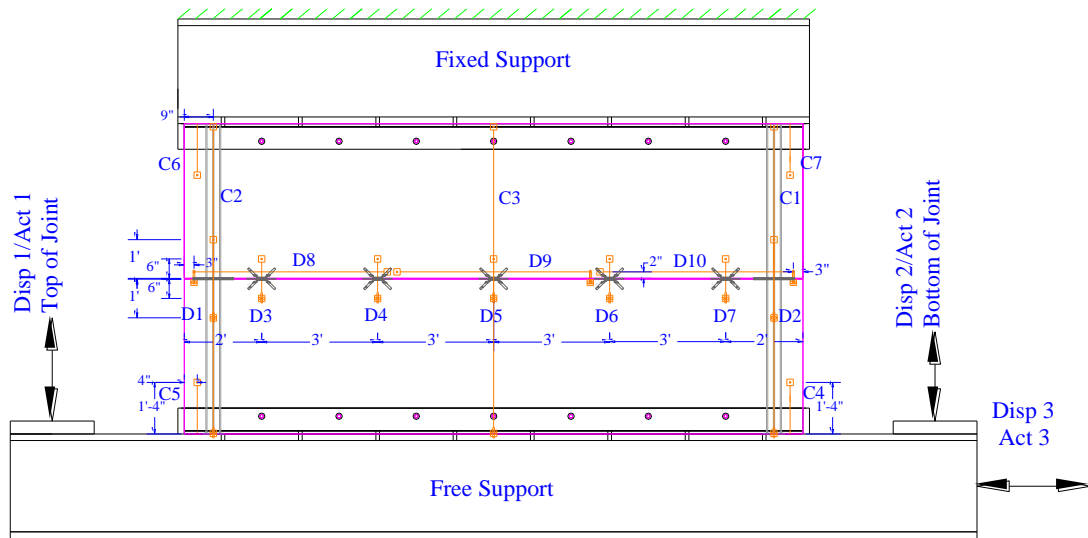


Figure 7.10. Instrumentation layout of PDH test

Six video cameras are placed at different location to record the response of overall system and detailed connection regions. One is placed on the top of the test module to observe the behavior of entire system. Three individual cameras are placed on the left, middle and right region of panel. The other two cameras are placed on the lab floor to have a close up observation of chord connections at two ends of test panels. Additional

pictures are taken at the end of loading cycles and when sound and failure occurred. A real time control system of these cameras is as shown in Figure 7.11.

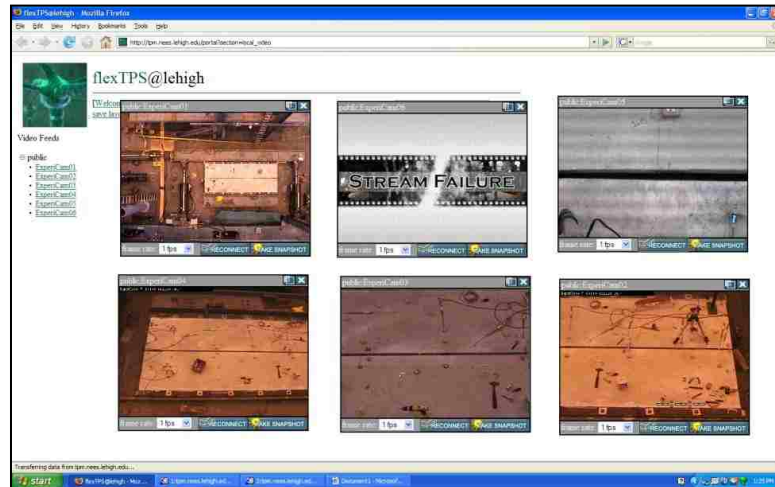


Figure 7.11. Control system of video Camera

7.4.2 Loading Control Algorithm

The loading history PDHs are derived from the chosen prototype structure (Figure 7.6) response to a sequence of increasing intensity ground motions. Five ground motions are selected for the PDH test sequence (Table 7.3). The first three motions represent seismic hazard for Charleston SC corresponding to service (SVC), design basis earthquake (DBE), and maximum consider. The fourth ground motion is a bi-directional motion at Charleston DBE level. The flexural joint is subjected to combined axial, shear and flexure effects due to the transverse flexure in conjunction with in-plane twisting and collector forces from the longitudinal component. The final ground motion is corresponding to Berkeley MCE level.

Table 7.3. PDH test sequence			
Loading Histories	Earthquake	Intensity	Direction
PDH 1	Charleston (CH)	SVC	Transverse
PDH 2	Charleston (CH)	DBE	Transverse
PDH3	Charleston (CH)	MCE	Transverse
PDH 4	Charleston (CH)	DBE	Bi-direction
PDH 5	Berkeley (BK)	MCE	Transverse





The interface PDHs applied to critical flexural joint under each ground motion are determined as the same discretization as the analytical model. As the high elastic stiffness of test panels, the displacement commands associated with low force levels are of the same order of magnitude as in the actuator. Therefore, actuator displacement commands which include axial deformation of the top chord, axial deformation of the bottom chord and shear deformation along the joint are controlled through a multiple loop architecture using external LVDTs C5, C1 and D9 located on the panels (Figure 7.10). The outer loop consists of application of one step of the predefined joint displacement history. Each outer loop displacement step is divided into small sub-steps (started at 0.006-in, changed to 0.002-in after PDH2) at approximately the resolution of the actuators (0.004-in). In the inner loop each sub-step was applied through the actuator displacement commands Disp 1, Disp 2, and Disp 3 until the displacement targets are achieved at C1, C2 and D9 within an error tolerance (originally 0.002-in, changed to 0.003-in after PDH1). If the target displacement is exceeded on any actuator it is then retracted, and if the target is not achieved the actuator is extended. The inner loop steps are continued until the full outer loop step was achieved on all feedback channels.

7.4.3 Flexure Joint Performance

The performance of critical flexure joint is evaluated under the predefined displacement histories. The experimental results indicate that the test specimen successfully survives the CH MCE but fails in the BK MCE, which implies that the diaphragm under proposed design will survive the MCE level earthquake while the diaphragm under current design cannot. The failure progress in the chord and web connections are summarized in this section.

7.4.3.1 Chord Connection

The response of the top and bottom chord connections is indicated in Table 7.4. The progression of damage in the chord connections is: (1) hairline cracks occur in the chord region during the essentially elastic response to the SVC earthquake; (2) moderate cracks form on the top chord region during the DBE earthquake, where chord strength is reached but no large inelastic deformation demand observed; (3) major cracking occurs in the bottom chord region in the MCE where the chord incurs significant inelastic opening deformation; (4) major cracking/crushing is exhibited in the top chord region for the Bi-Dir DBE, in which inelastic opening occurs in combination with significant compression cycles; and, finally, (5) fracture of the slug of the bottom chord connector at a maximum deformation capacity of 0.4-in.



Table 7.4: Chord connection response of PDH test		
Loading Histories	Top Chord Connection	Bottom Chord Connection
PDH 1 CH SVC	 Hairline cracking	N/A
PDH 2 CH DBE	 Moderate cracking	N/A
PDH3 CH MCE	N/A	 Major cracking
PDH 4 CH Bi DBE	 Major cracking/crushing	N/A
PDH 5 BK MCE	N/A	 Slug weld fracture

7.4.3.2 JVI Vector Connection

The response of the JVI vector connections is indicated in Table 7.5. The progression of damage in the JVI connection near the bottom chord is: (1) No damage observed during the SVC earthquake; (2) Cracking forms during the DBE earthquake; (3) the surrounding concrete start minor spalling during the MCE earthquake after 0.15-in shear displacement; (4) Major spalling occurs during the Bi-Dir DBE earthquake; and (5) the JVI connector fractures under tension with significant shear during the BK MCE at approximately 0.35-in opening.

7.4.3.3 Summary

In a summary, the critical flexural joint survives its designated MCE earthquake by using the new design methodology proposed by DSDM research group. While the joint will likely fail during its designated MCE earthquake under current design method. The joint rotational stiffness degrades to approximately half its original values at flexure critical joint under expected earthquake loading. The experimental responses of flexure joint and local connections show good agreement with the 3D NLTA analytical model. The unbonded enhanced dry chord connector exhibited good inelastic tensile deformation capacity corresponding to a joint rotation of 0.0025 rad (0.4-in opening in half-scale). The JVI Vector connector exhibited good inelastic tension compliance, achieving 0.35-in opening (half-scale) before pulling out from the surrounding concrete.

Table 7.5: JVI Vector connection response of PDH test	
Loading Histories	JVI Vector Connection
PDH 1 CH SVC	 Undamaged
PDH 2 CH DBE	 Cracking
PDH3 CH MCE	 Concrete pop-out
PDH 4 CH Bi DBE	 Major spalling
PDH 5 BK MCE	 JVI fracture

7.5 Simplified Estimation of Joint Performance

As discussed in Chapter 6, the proposed simplified estimation approach can be used to conduct joint analysis. This approach is adopted for the joint analysis of the critical flexure joint specimen used in PDH test, and the calculated results are compared with the measured experimental results and the 3D NLTDA analytical results as shown in Figure 7.12. The results indicate that the simplified estimation approach provides a conservative estimation than the measured joint response. This may be caused by the assumption used in the simplified estimation approach, which assumes that joint rotates about the compression chords. The actual rotation center may lower than the assumed position.

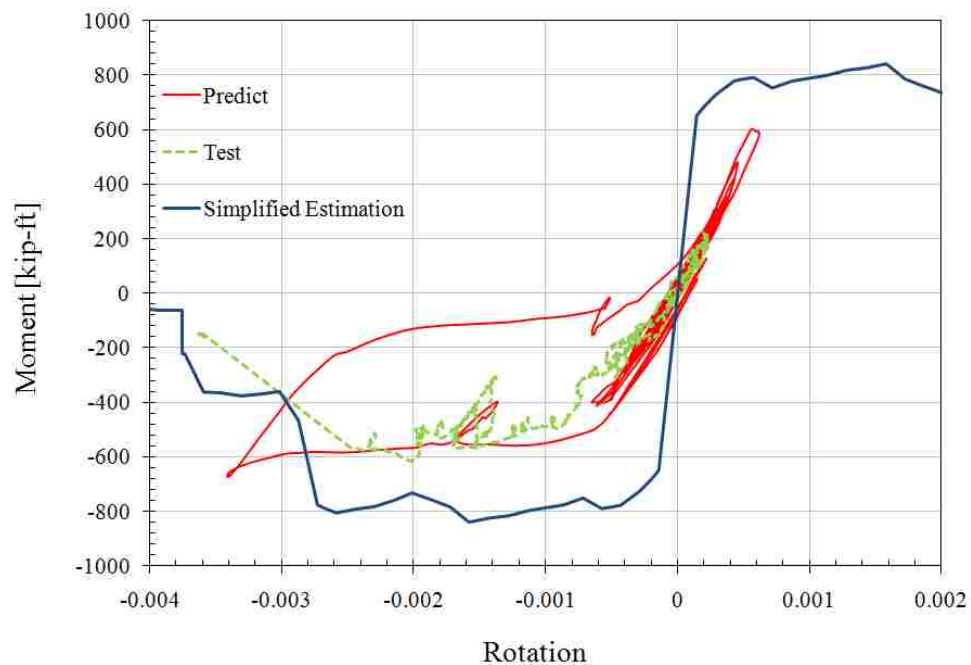


Figure 7.12. Flexure joint performance

7.6 Hybrid Test of Diaphragm Critical Shear Joint

Experimental test is conducted on shear joint specimen to evaluate the seismic performance of a critical shear joint in a pretopped precast concrete diaphragm. In this case, the hybrid testing techniques are used in simulating the expected seismic demands on the critical shear joint. The experiment is also conducted at half-scale. The analytical structure is a three-story precast concrete shear wall building with single diaphragm bay and the experimental substructure represents the critical shear joint(Figure 7.8). This test is also a collaborative integrated experimental and analytical effort. The analytical superstructure is developed by University of Arizona. This section focuses on the experimental program including instrumentation design, control algorithm and shear joint response.

7.6.1 Instrumentation

The instrumentation design for hybrid test is similar to the PDH test. Seventeen panel and joint deformations are measured directly on the precast specimen using a series of Linear Voltage Displacement Transducers (LVDT), the layout is indicated in Figure 7.13.

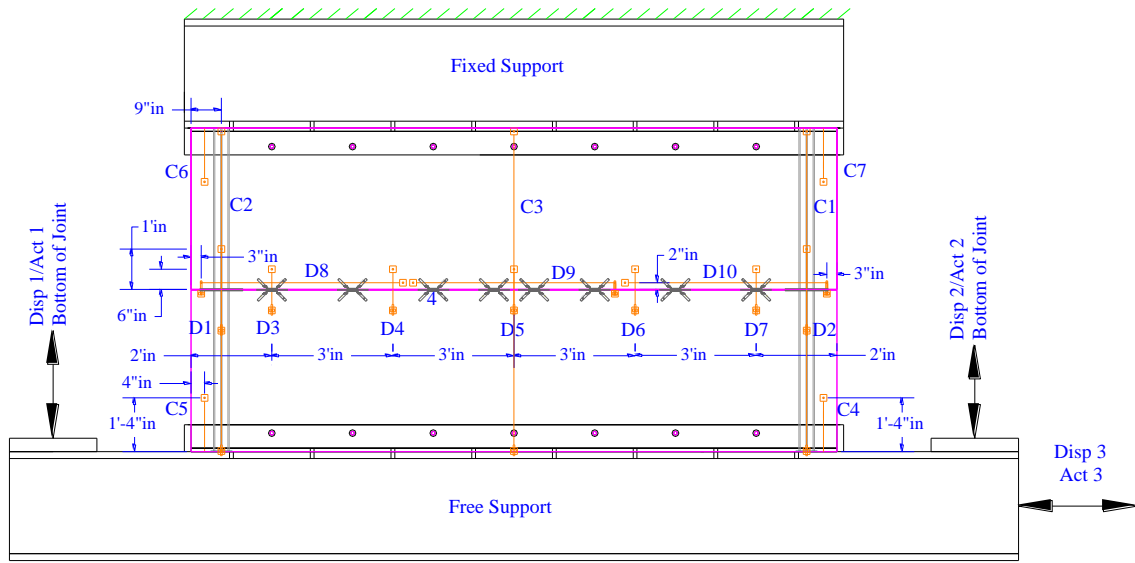


Figure 7.13. Instrumentation layout of hybrid test

7.6.2 Control Algorithm

A MATLAB based time integration control algorithm is used for the hybrid test. This program generates a displacement vectors at each time step. The displacement demands are applied to the analytical model and experimental test and then the static restoring forces from the FE model and physical test are sent back to the control program to calculate the displacement vectors for the next time step. The detailed control algorithm is indicated in Figure 7.14.

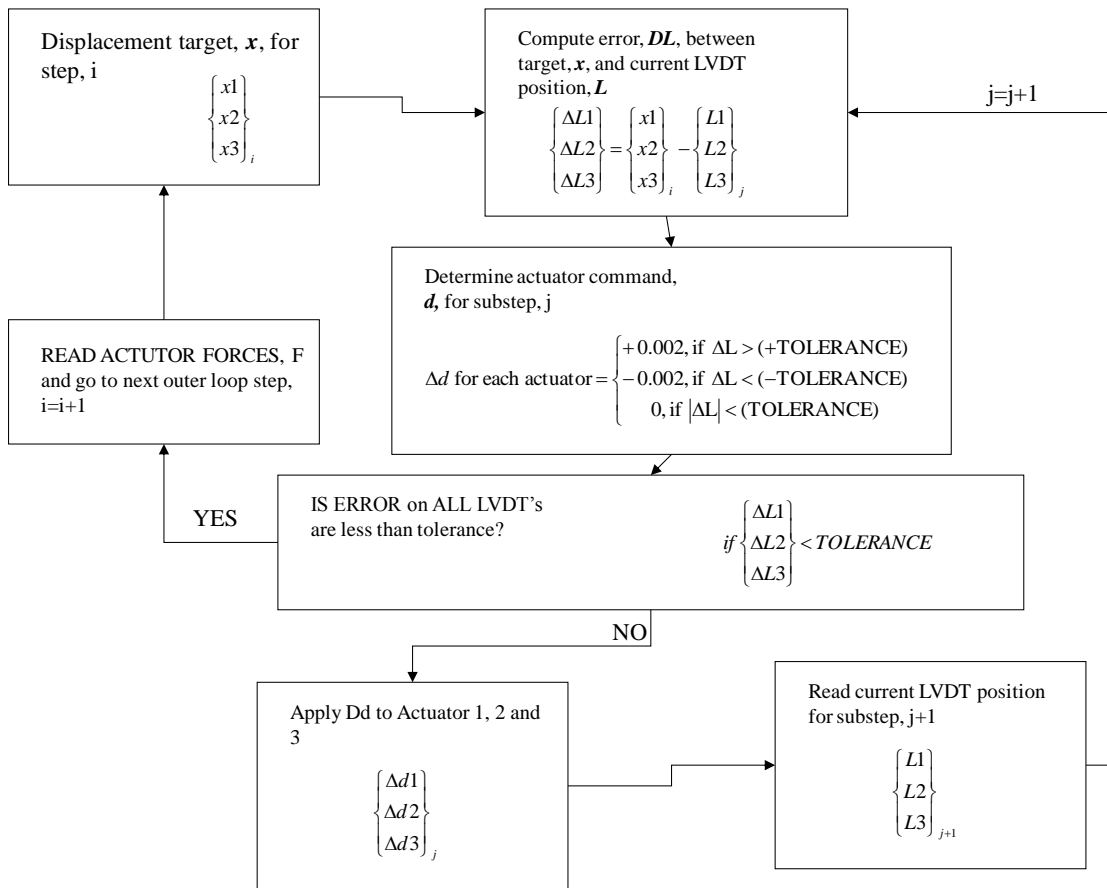





Figure 7.14. Control algorithm of hybrid test

7.6.3 Shear Joint Performance

The seismic performance of critical shear joint in a pretopped precast concrete diaphragm is evaluated by using the hybrid (adaptive) testing techniques. The failure progress in the chord and web connections are summarized in this section. The entire test is divided into three stages: stage 1(1 to 400 steps), stage 2(401 to 800 steps) and stage 3(801 to 1600 steps).


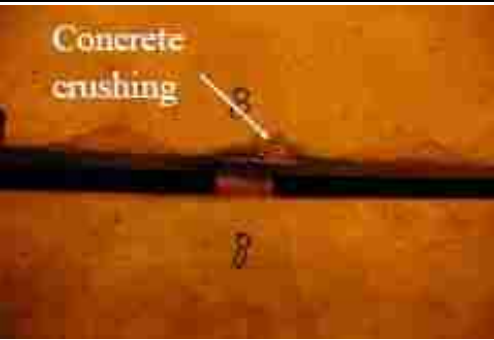
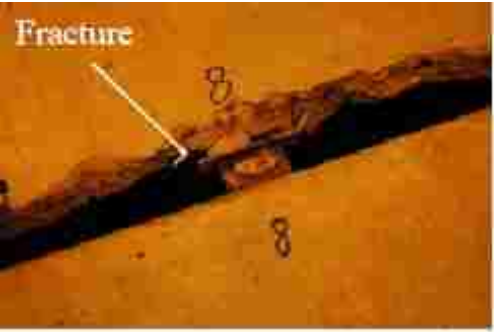
7.6.3.1 Chord Connection

The response of the chord connections is indicated in Table 7.6. The progression of damage in the chord connections is: (1) minor crack occurs in the top and bottom chords region during the first stage; (2) concrete cracking and crushing occur in the bottom chord region during the second stage; (3) loss of concrete in the chords region during stage 3.

Table 7.6: Chord connection response of hybrid test	
Loading Histories	Chord Connection
Stage 1	
Stage 2	
Stage 3	

7.6.3.2 JVI Vector Connection

The response of the JVI vector connections is indicated in Table 7.7. In stage 1, the joint is in elastic condition and only micro cracks are observed. In stage 2, the shear reinforcements start to yield, local concrete crushing occurs around each of the JVI vector connections. In stage 3, fracture of the JVI connections are observed.

Table 7.7: JVI Vector connection response of hybrid test	
Loading Histories	JVI Vector Connection
Stage 1	 A photograph showing a cross-section of a concrete joint with a horizontal reinforcement bar. A white arrow points to a small crack in the concrete above the bar, labeled "Micro crack". The number "4" is written on the concrete surface below the bar.
Stage 2	 A photograph showing a cross-section of a concrete joint with a horizontal reinforcement bar. A white arrow points to a localized area of concrete crushing above the bar, labeled "Concrete crushing". The number "8" is written on the concrete surface below the bar.
Stage 3	 A photograph showing a cross-section of a concrete joint with a horizontal reinforcement bar. A white arrow points to a fracture in the concrete above the bar, labeled "Fracture". The number "8" is written on the concrete surface below the bar.

7.6.3.3 Summary

In a summary, the critical shear joint in a pretopped concrete diaphragm is evaluated at half-scale by using hybrid “adaptive” algorithm. The critical shear joint designed with shear overstrength factor of 1.1 will likely fail in the expected earthquake after the significant shear strength loss. Thus higher shear overstrength factor is required for the diaphragm shear design to prevent non-ductile shear failure. The experimental responses of shear joint and local connections show good agreement with the analytical model. The shear reinforcement (JVI vector) shows strength and stiffness degradation with increasing inelastic shear sliding loading.

7.7 References

1. Zhang, D. (2010). “Examination of precast concrete diaphragm seismic response by three-dimensional nonlinear transient dynamic analyses”, Ph.D dissertation, the University of Arizona, Tucson, AZ.
2. Schoettler, M.J., Belleri, A., Zhang, D., Restrepo, J., and Fleischman, R.B. (2009). “Preliminary results of the shake-table testing for development of a diaphragm seismic design methodology.” *PCI Journal*, 54 (1), 100-124.
3. Naito, C., Ren, R., Jones, C., Cullen, T. (2007). “Development of a Seismic Design Methodology for Precast Diaphragms - PHASE 1B SUMMARY REPORT”, ATLSS Report No.07-04, ATLSS Center, Lehigh University.

4. Naito, C., Ren, R., “Development of a Seismic Design Methodology for Precast Diaphragms - PHASE 1C REPORT”, ATLSS Report No.08-09, Lehigh University, September, 2008.
5. Building Seismic Safety Council, Committee TS-4. (2009). “Seismic design methodology for precast concrete floor diaphragms,” Part III, 2009 NEHRP Recommended Seismic Provisions, Federal Emergency Management Agency, Washington, D.C.
6. American Concrete Institute (ACI) Committee 318. 2008. *Building Code Requirements for Structural Concrete (ACI 318-08) and Commentary (ACI 318R-08)*. Farmington Hills, MI: ACI.
7. ASTM (2008). *Annual Book of ASTM Standards, A706 – 93*, West Conshohocken, Pennsylvania

Chapter 8 Design and Development of Ductile Dry Chord Connection

A precast panel-to-panel dry chord connection with considerable ductility and predictable strength is required for buildings located in moderate and high seismic regions in accordance with the new proposed diaphragm design methodology. Research on the conventional dry chord connection and enhanced dry chord connection (Cao 2006) indicated that welds used between the bars and between the faceplates are sensitive to premature yielding and fracture. The premature weld failure modes were observed again during the evaluation of critical flexure multi-connection joint under predefined displacement histories (Chapter 7). Due to these failure modes the chord bar strength is not reliably achieved and the connection fails with limited ductility. An innovative dry chord connection with high ductility is developed in the dissertation research.

This Chapter presents the experimental and analytical performance evaluation of existing dry chord connections, which includes conventional dry chord and enhanced dry chord. In addition, the design concept, design goal, design details, expected performance and final design layout of the new developed ductile dry chord connection are presented as well.

8.1 Background

In precast concrete diaphragm systems, chord connections are utilized at extreme edges of the diaphragm to resist in-plane diaphragm forces generated during seismic events. This is achieved through a force couple in which the chords provide tension and compression resistance. Conventional construction chord construction is considered “wet” in that it utilizes a field cast element. These wet chords can be fabricated by creating a reduced section, pour strip, at the edge of the double tee panel in which longitudinal chord bars can be placed and ready mix concrete is placed. While this method of construction has been shown to perform well, it requires the use of field cast concrete. In some cases the use of field cast concrete can detract from the quality, increase the construction schedule, and raise the cost of the building.

To eliminate the use of field cast concrete in the precast building a “dry” chord detail is required. A dry chord consists of a connection installed in the panel during precast operation. These chords are then interconnected through welding. No cast-in-place concrete is used to complete the anchorage.

Although the dry chord connection may ease construction schedule and cost, the effectiveness is dependent on the integrity of a potentially brittle weld. Proper design of the connection is critical for ductile response of the diaphragm.

The current existing dry chord connection consists of bars welded to a faceplate and embedded in a precast double tee (DT) flange. The faceplates in adjacent DT flanges

are welded using a steel slug to span the gap and a weld to create a force path (Figure 8.1).

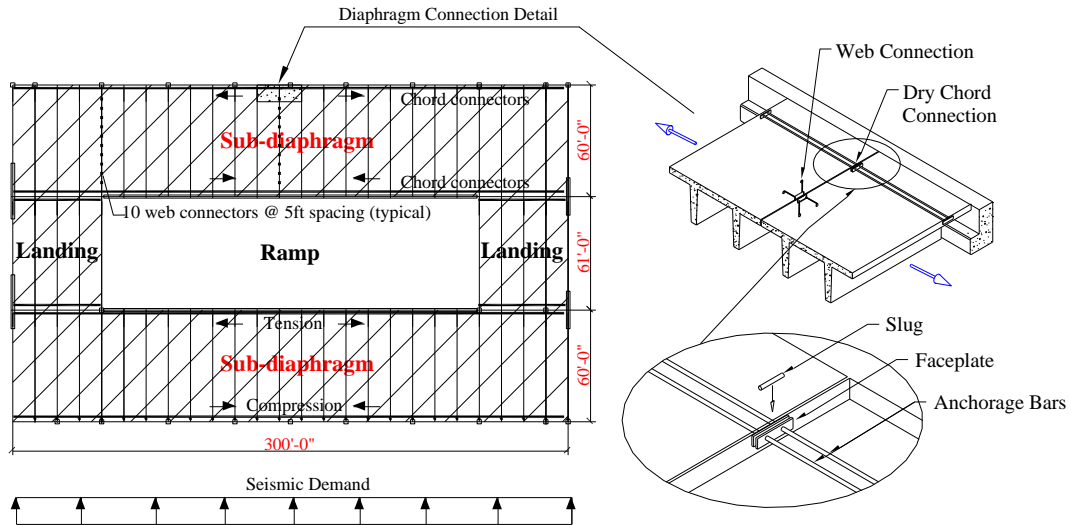


Figure 8.1. Dry chord connection in typical precast diaphragm

The previous research conducted on the pre-topped dry chord connections indicated that the resisting force and deformation capacity are reduced significantly due to premature failure of the weld. This section provides a brief background on the issues identified and the research conducted.

8.1.1 Experimental Performance of Conventional Dry Chord Connection

Experimental studies were conducted on conventional bonded dry chord connections (Naito, C., et al. 2006). The test specimen detail is shown in Figure 8.2. The specimen was fabricated from two #5 bars fillet welded to the exposed face plate and installed in the panel prior to precast operations. During erection, a round or square solid

slug was installed between the adjacent face plates and welded in place. To prevent the slug from dropping through to the floor below, the face plate was angled backward at 10-degrees. A slug of varying size was used in the field with the diameter chosen based on the gap available between the adjacent tees. The tested connection contains a 0.75-in. round stock with an effective throat of 0.2 times the bar diameter in accordance with AWS [AWS 1992].

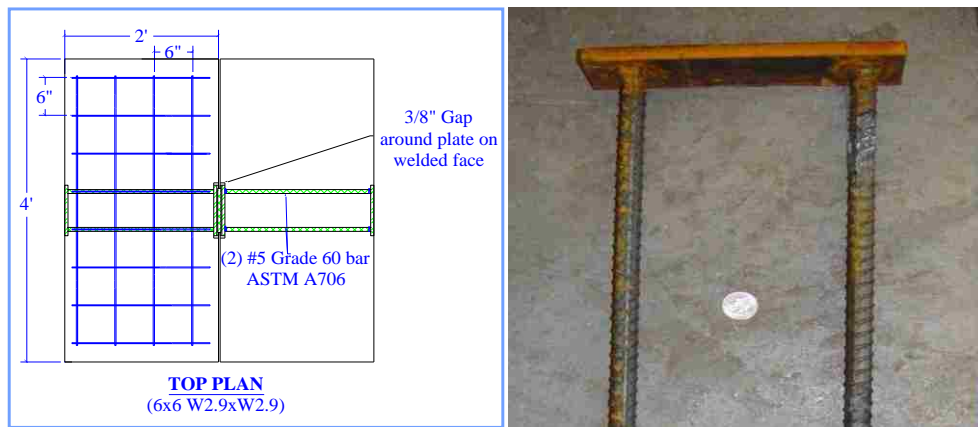


Figure 8.2. Test specimen detail of conventional dry chord connection

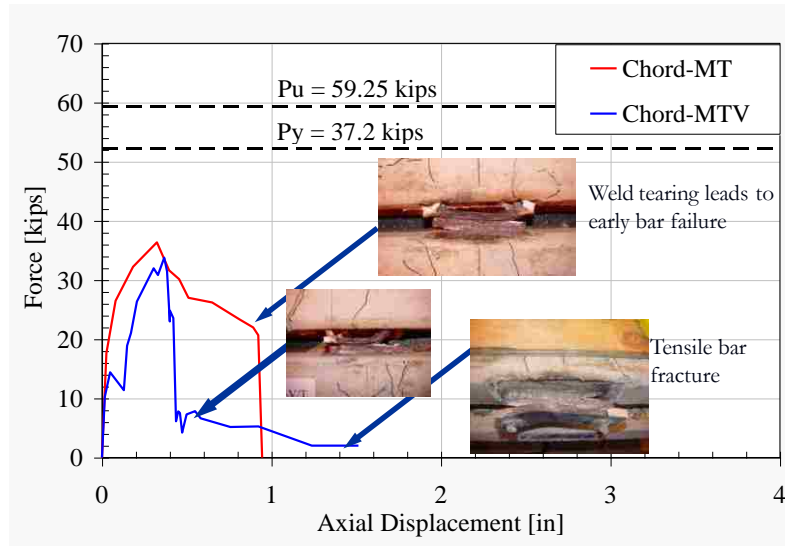


Figure 8.3. Tension performance of conventional dry chord connection

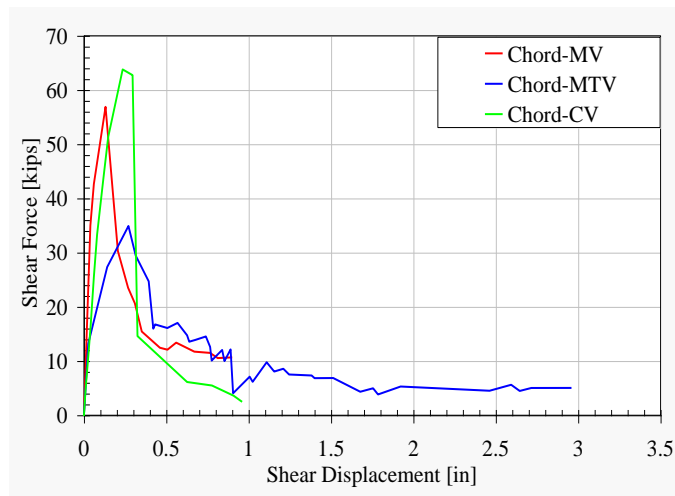


Figure 8.4. Shear performance of conventional dry chord connection

The performance of the conventional dry chord connection under monotonic and cyclic tension loading cases is indicated in Figure 8.3, the test results showed that the conventional dry chord connections were not able to attain their design capacity due to the premature failure of the weld details. In addition due to the bonded detail the

connections were very stiff resulting in limited deformation capacity under both tension and shear loadings (Figure 8.4). The various failure mechanisms of the conventional dry chord connection under the tension and shear demands include yield of the anchorage bars, flexure or torsion of the faceplate, fracture of the welds as illustrated in Figure 8.5.

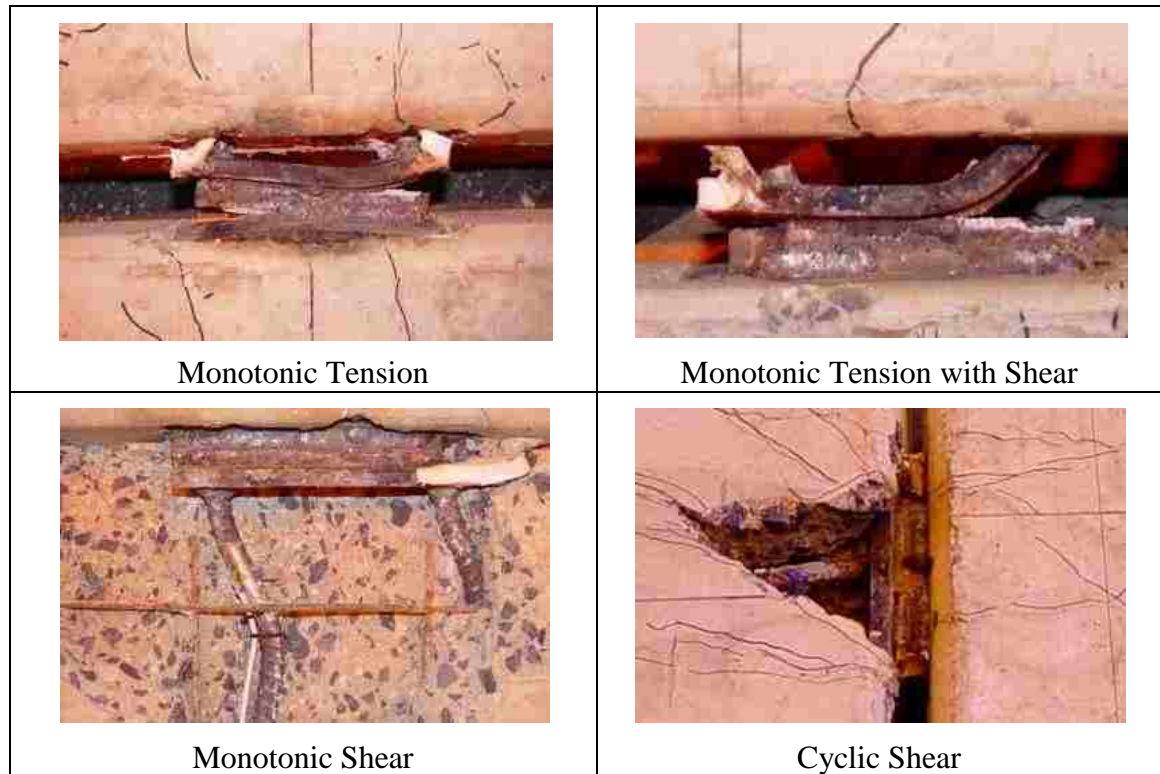
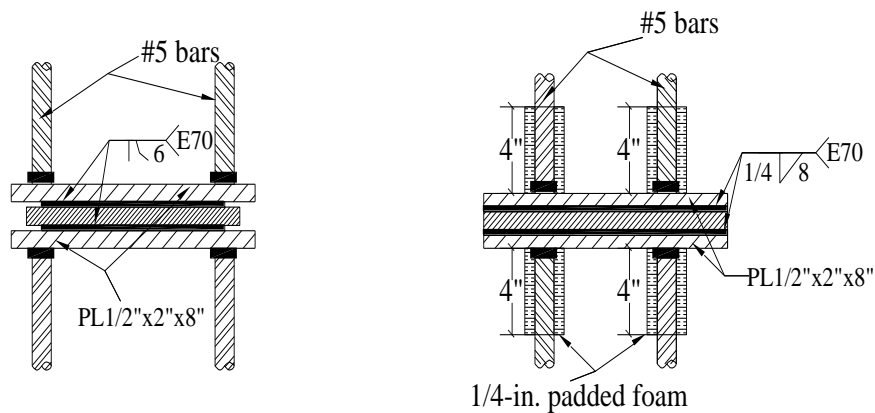


Figure 8.5. Failure mechanisms of conventional dry chord connections

8.1.2 Performance Evaluation of Enhanced Dry Chord Connection

To enhance the strength and deformation capacity of the connection a finite element (FE) model was developed and a parametric examination of weld details was undertaken by Cao (2006). The FE model was verified with experimental data and used to evaluate the sensitivity of the connection to geometry variations and changes in the

welding details. To develop the intended ductile failure mechanism of anchorage bars, a parametric study was conducted to investigate the sensitivity of faceplate thickness, weld cross-section, and weld location. Preliminary design recommendations based on the evaluation results were proposed to allow the connection to achieve the desired failure mechanism. These design recommendations included the extension of weld length and mechanical debonding of anchorage reinforcement bars (Figure 8.6).



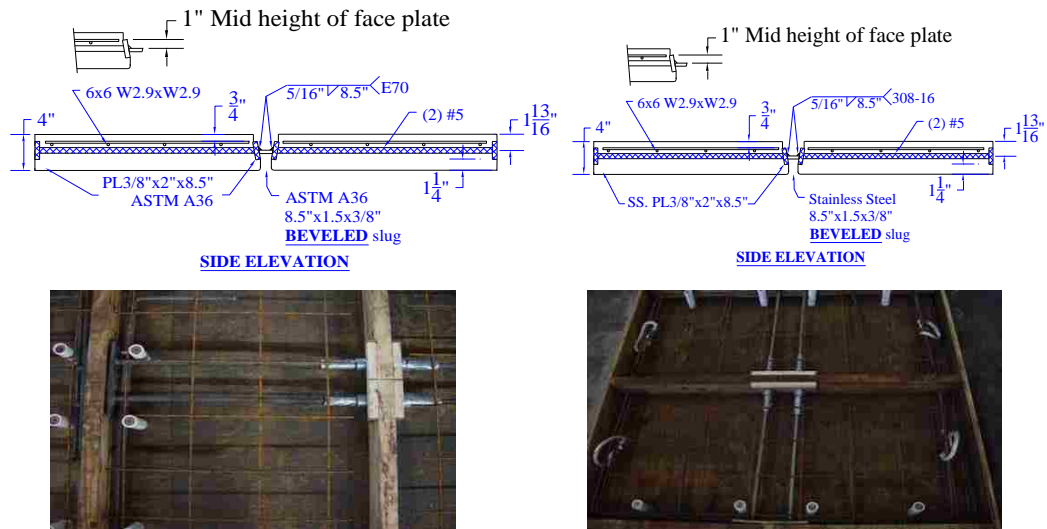
a). Conventional dry chord connection b) Enhanced dry chord connection

Figure 8.6. Development and improvements of dry chord connection

According to the design recommendations, typical examples of enhanced dry carbon chord connection details were developed and evaluated experimentally (Naito, C., Ren, R. et al 2007). The test specimen details of pre-topped carbon chord connection and stainless chord connection are shown in Figure 8.7.

Both the stainless steel chord connection and the carbon steel chord connection were developed in response to the poor performance of the conventional pre-topped dry

chord connection. Both connections utilized an unbonded region to enhance the tension ductility and to allow for shear compliance i.e., shear movement with low force resistance. The “Carbon” chord was fabricated from ASTM A36 plate and ASTM A706 reinforcement. The “Stainless” chord was fabricated from type 304 stainless plate, type 316LN reinforcing bar, and 308-16 weld electrodes, which was used as an alternate to the carbon steel chord in the regions where corrosion may be a concern. All welds were conducted at room temperature using the SMAW process in accordance with AWS procedures. The welds were sized to produce failure of the reinforcement prior to the welds.









a) Pre-topped Carbon Chord Connection b) Pre-topped Stainless Chord Connection

Figure 8.7. Test specimen details of typical enhanced dry chord connections

The experimental results (Naito, C., Ren, R. et al 2007) indicated that the enhanced dry chord connections had a better performance than the conventional dry chord connections, the enhanced design of a length of unbonded region worked

effectively to reduce the shear stiffness of the connection until plate bearing occurs, which allowed shear compliance and increased the shear deformation capacity. However, the connections under most loading cases were not able to achieve their ultimate strength capacity. This situation was particularly apparent under a shear condition. It was attributed to failure of the connection at the bar-to-faceplate weld (see Table 8.1).

Table 8.1: Enhanced dry chord connection failure mechanisms	
Tension Loading Case	
<i>Carbon Chord Connection</i>	<i>Stainless Chord Connection</i>
 <p style="text-align: center;">CT</p>	 <p style="text-align: center;">MT</p>
Shear Loading Case	
<i>Carbon Chord Connection</i>	<i>Stainless Chord Connection</i>
 <p style="text-align: center;">MV</p>	 <p style="text-align: center;">CV</p>
 <p style="text-align: center;">MV-LC</p>	 <p style="text-align: center;">CV-LC</p>

To improve the strength and ductility capabilities of the enhanced dry chord connections, an innovative design concept of ductile dry chord connection is proposed.

This design uses a prefabricated module instead of a built-up welded detail between the faceplate and rebar. This design avoids potential weld failure issues previously observed. A three dimensional FE model is developed based on the new design concept and analytical studies are conducted to evaluate the performance and develop effective design details for these connections.

8.2 Design Concept

The goal of the dry chord connection design is to achieve a ductile tension response of the anchorage bars. The desired ductile mechanism cannot be formed unless each component of the connection is designed to maintain the load path without premature failure. A typical diaphragm connection consists of anchorage bars, faceplate, slug, and weld components. To ensure that ductile modes of failure occur, a general rule should be followed. Design the connection to develop a predictable yield mechanism in the targeted yield region while protecting the other components, through over-strength factors, against premature failure. For example, designing the weld, slug, faceplate and anchorage bar to have strength greater than the capacity of the yield shaft will typically provide a ductile connection with a predictable strength. An acceptable hierarchy of strengths is illustrated in Figure 8.8.

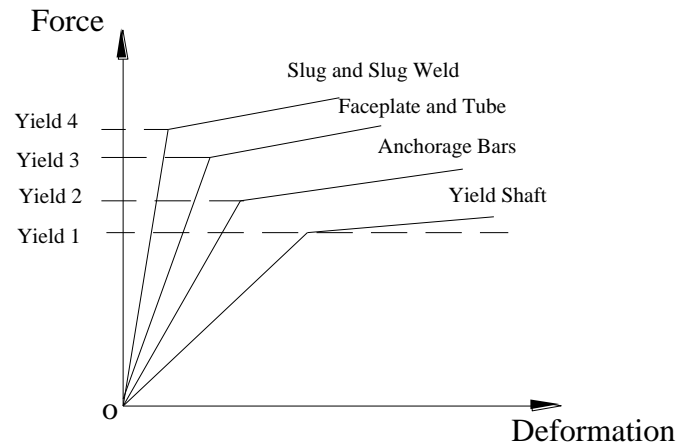


Figure 8.8. Ductile design concept

8.3 Design Goal

The objective of the chord connection design is to achieve the targeted yield and ultimate tensile strength capacity while developing a high ductility with low cost.

Strength

A modular system with single anchorage rebar will be developed, which can be stacked laterally to resist the design loads for particular diaphragm system. In order to ensure its applicability in both moderate and high seismic regions, an appreciate strength capacity of the modular system should be designed. According to industry advices, the yield and ultimate strength capacity developed in the single modular system should be in the range of 10-kip to 20-kip.

Ductility

As discussed in Chapter 6, all of the existing dry chord connections exhibited a moderate deformability level, which could not meet the ductile demands of buildings in high seismic zones. Therefore, the new dry chord connector is targeted to fall in the high deformability category by developing a minimum 0.6-in deformation capacity (a pair of chord connector).

8.4 Design Detail

The design details of the new dry chord connection are presented in this section. The design utilizes several special features to achieve the expected strength and deformation performance. These innovative features are discussed in this section. A layout of new connection is presented.

8.4.1 Standard Module

In order to avoid the premature failure of welds located between faceplate and anchorage bars, a standard module system which serves as the connection piece between faceplate and anchorage bars is used instead of conventional weld technique. This piece can be prefabricated using cast steel and installed easily. The detail of the cast piece is illustrated in Figure 8.9.

Faceplate serves the same function as a conventional dry chord connection, it will be welded with slug and then connect two chords together at joint. The front flange and

tube are designed to stay elastic when the anchorage bar yields. The yield shaft is designed to yield first and develop ductile deformation capacity. It is targeted to achieve 90% of its ultimate force capacity at the time when anchorage bar yields. Two slots are set on the tube to weld the anchorage rebar with the casting piece. To avoid stress concentration, transition regions are used when the diameters change dramatically. A mechanical debonding is used in the front flange and yield shaft region to reduce the stiffness and provide shear compliance.

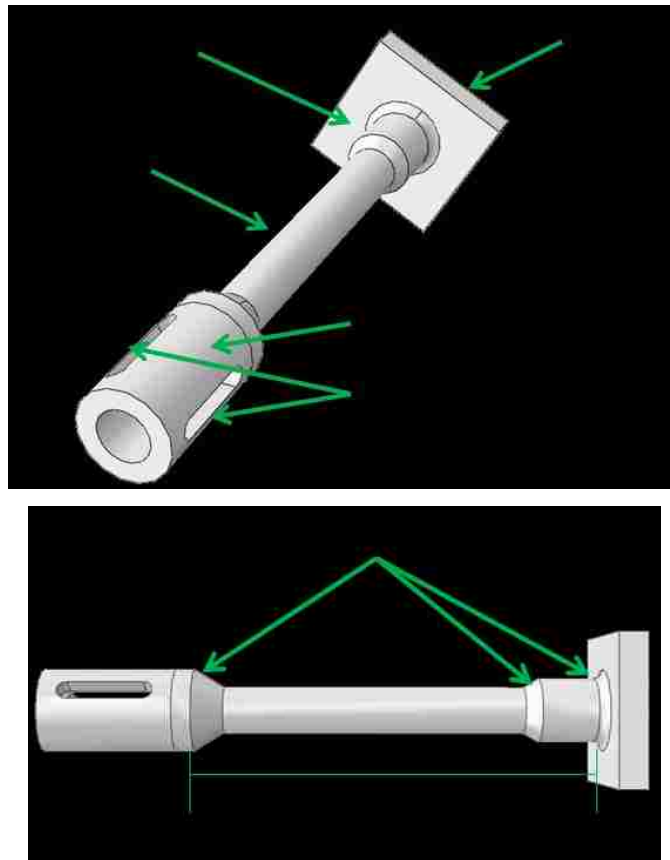


Figure 8.9. Detail of standard casting module

8.4.2 New Connection Layout

A single bar chord connection is shown in Figure 8.10. The anchorage bar is inserted into the tube and welded together using plug welds performed through the slotted end regions of the tube. A fillet weld is used between the faceplate and the slug at the joint to connect two panels together. This portion of the connector is similar to standard chord connections. The number of rebar used in the panel is dependent on the force demands applied to the diaphragm system. The standard module of casting piece makes it easy and flexible to fabricate and install the chord connection with multiple bars. An example of 3-Bar chord connection embedded in the concrete panel is as shown in Figure 8.11.

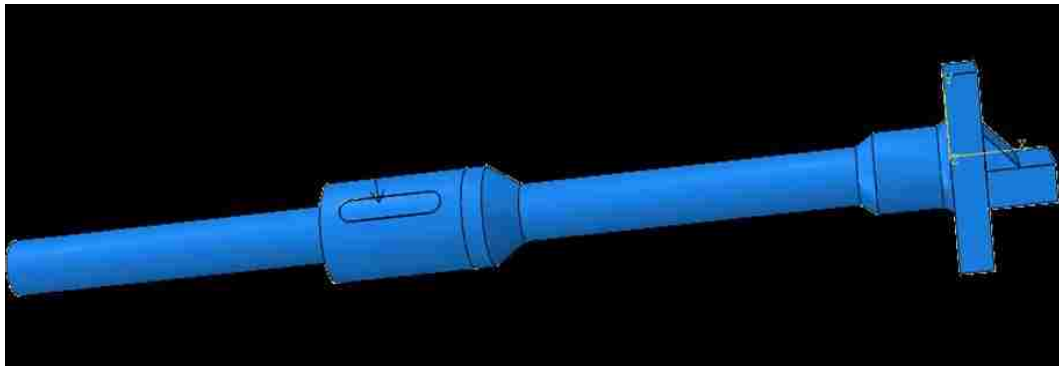


Figure 8.10. Lay out of new developed dry chord connection

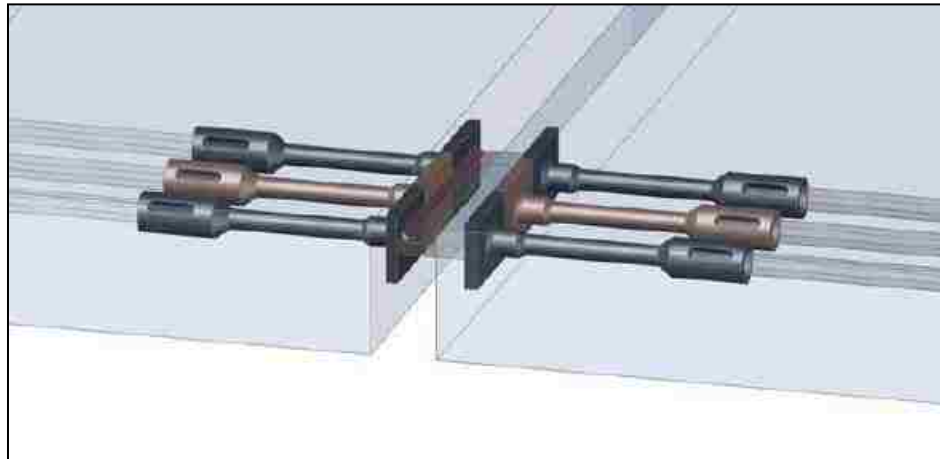


Figure 8.11. A typical panel-to-panel 3-Bar chord connection

8.4.3 Design Details

The dimensions of various pieces shown in Figure 8.10 are sized based on the ductile design concept (Figure 8.8). The design detail and recommendation are presented in this section.

8.4.3.1 Anchorage Bar

To achieve the strength capacity of design goal, No.5 rebar with yield strength of 60-ksi is recommend to use for design. The low alloy steel ASTM A706 is recommended since it limits chemical composition and carbon equivalent to enhance the weldability of the material. The rebar should have a minimum yield strength of 60-ksi, the tensile strength of the rebar should be at least 1.25 times the actual yield strength. The minimum elongation of the rebar is 0.14. The ASTM A615 Grade 60 steel is applicable as well only if the carbon equivalent is limited to 0.55. The anchorage rebar in the design

example of this dissertation research is the ASTM A706 #5 rebar with a yield strength of 60-ksi and tensile strength of 80-ksi. The nominal strength capacity of the anchorage bar is 18.6-kip.

8.4.3.2 Cast Modular System

The layout of the cast modular system is illustrated in Figure 8.9. A cast steel material with good ductility is used for design of the modular system. The desired yield strength of this portion is around 40-ksi. There are several cast steel material candidates which have been used in recent building constructions. These options are ASTM A958 grade SC 8630, ASTM A27 grade 70-40 and ASTM A352 grade LCC. All of these options have qualification to meet the yield strength requirement. However, the first two options are not recommended due to their high carbon equivalents (>0.55), since high carbon equivalent makes the material tend to have potential weld cracks in heat affected zone according to recent research (Zimpher et al, 2008). The carbon equivalent (CE) of material can be calculated as indicated in Eq. 8-1.

$$CE = C + \frac{Mn + Si}{6} + \frac{Cr + Mo + V}{5} + \frac{Ni + Cu}{15} \quad \text{Eq. 8-1}$$

The ASTM A352 grade LCC is chosen for final design to develop the maximum ductile behavior. The minimum yield strength is 40-ksi, the minimum tensile strength is 70-ksi and the maximum tensile strength is 95-ksi. The elongation should be greater than 0.22. The supplementary requirement S23 that restrict the carbon equivalent of LCC down to 0.55 should be applied for better weldability.

The skinny part in the cast modular system is called yield shaft, which is designed to yield before anchorage bar under tension load and develop ductile deformation capacity. This portion is expected to achieve 90% of the minimum tensile strength of cast material when the rebar yields. The material with a yield strength of 40-ksi and tensile strength of 70-ksi is used. The calculated minimum diameter of the yield shaft is 0.61-in to develop expected strength capacity, the minimum length of yield shaft needed to develop a 0.3-in deformation capacity (for half of dry chord connection) is determined from elastic-hardening bilinear material property of cast material. The length should be larger than 1.90-in. A length of 4-in and a diameter of 0.62-in are chosen for the yield shaft in this design example. The yield strength capacity of this portion is around 12.0-kip and the ultimate strength capacity is 19.0-kip.

To prevent other elements of the connection from failure and ensure the desired ductility, capacities of other components are designed to exceed the bar design capacity ΩR_n , where Ω is the overstrength factor and R_n is the nominal strength capacity of the anchorage bar, which is equal to 18.6-kip for single No.5 anchorage bar.

An overstrength factor of $\Omega=1.25$ is used for the design of this cast modular system except the skinny part. The front flange has a diameter of 0.86-in and a fillet with a radius of 0.17-in is used at the end tip of front flange to smooth the stress flow. The length of the front flange is set as equal to the diameter of 0.86-in according to Saint-Venant's Principle. A transition cone region with a length of 0.2-in is used to connect the yield shaft and front flange. The interior diameter of the tube is set as 0.75-in, which is

able to accommodate No.5 rebar properly. The minimum exterior diameter of the tube is 1.1-in based on calculation. An exterior diameter of 1.2-in and a length of 2.5-in are used for tube in the design. A transition region is used to connect tube and yield shaft. This region can be divided into two parts. One part is a solid cylinder with a diameter of 1.2-in and length of 0.25-in, it is placed right next to the tube. The other part is a cone region with a top diameter is 0.62-in and bottom diameter of 1.2-in to connect the yield shaft and the solid cylinder. The length of this part is 0.4-in. These transition regions are used wherever the dimension changes dramatically to avoid stress concentration.

8.4.3.3 Faceplate

The faceplate is premade with the modular system. Its strength is computed according to the base metal strength as shown in Eq. 8-2.

$$R_p = f_p t_p L_p \quad \text{Eq. 8-2}$$

Where L_p is the plate length and t_p is thickness of the plate. f_p is the strength of plate which is equal to 60% of the tensile strength of plate, $0.6 f_{up}$, for the fillet weld. The tensile strength used for faceplate is 70-ksi, same overstrength factor of 1.25 is used for faceplate design. The required plate length L_p should be larger than fillet weld length. It is assumed to be 3-in, therefore the minimum thickness should be determined according to the Eq. 8-3, where ϕ_p is the resistance factor for the faceplate, which is 0.75 for fillet weld. The determined minimum faceplate thickness is 0.25-in. A thickness of 3/8-in is

used for this design. The faceplate height can be considered as half of the panel thickness, which is 2-in. Therefore, a dimension of 3x2x3/8-in is used for faceplate design.

$$t_p \geq \frac{\Omega R_n}{\phi_p f_p L_p} \quad \text{Eq. 8-3}$$

8.4.3.4 Slug

The slug is used to connect a pair of dry chord connector at the joint. Similar to faceplate, the slug strength is also computed according to the base metal strength as shown in Eq. 8-2. The material ASTM A36 is recommended for slug plate, the minimum yield strength is 36-ksi and minimum tensile strength is 58-ksi. The elongation should be greater than 0.20. An overstrength factor 1.50 is used for slug design. The slug length is assumed to be the same as faceplate length of 3-in. The required minimum thickness of slug determined from Eq. 8-3 is 0.35-in. A thickness of 3/8-in is chosen for design. The width of slug is assumed as 1.5-in cross the joint. Therefore, a dimension of 3x1.5x3/8-in is used for slug design.

8.4.3.5 Welds

Rebar to tube weld design

Two slots are designed on the tube to perform plug welds between rebar and tube. The relative slots location on the tube is illustrated in Figure 8.12. In this design, the two

slots are located at the left and right side of vertical axis with an angle of 60 degree separately.

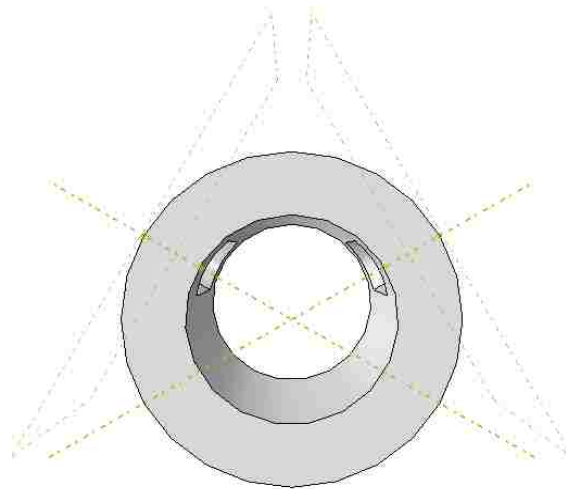


Figure 8.12. Slots location on the tube

The strength capacity of plug weld is computed as the product of the faying surface (nominal cross section) and the stress on that area (Eq. 8-4).

$$T_w = 0.75 * 0.6 * F_{EXX} A_{faying} \quad \text{Eq. 8-4}$$

An overstrength factor of 1.5 is used for weld design. The electrode E7018 with a tensile strength of 70-ksi is recommended for weld material. According to the specification in LRFD weld section (AISC 2006), a slot width of 3/8-in is chosen and the minimum required length is calculated as 0.89-in at both sides. The final design chooses a plug weld go through the thickness of cast tube with a base width of 3/8-in and a length

of 1-in. Two semicircular with a diameter of weld width are required at the two ends. The top width of the slug weld is extended to 1/2-in for ease fabrication according to industry advises.

Faceplate to slug weld design

Fillet weld is used to connect faceplate and slug. The electrode E7018 with a tensile strength of 70-ksi is recommended for weld material. According to the specification in LRFD weld section (AISC 2006), the required minimum thickness is 3/16-in. For this design, a thickness of 3/8 -in is assumed and an overstrength factor of 1.50 is used. The calculated required fillet weld length is 1.89-in. A fillet weld length of 3-in is chosen for design. The final design of the fillet weld used is 3/8@3-in with E7018 electrode. The desired location of fillet weld is that the center of slug is placed in line with the center of other connection components such as faceplate, tube and rebar etc, since no additional flexural demand will be generated in the yield shaft based on simple free body diaphragm (FBD) analysis. An elevation view is shown in Figure 8.13.

Vertical eccentricity often occurs when the slug is improperly placed in the field. This weld offset produces additional tension demand on all the components of connector due to the generation of flexure. The additional tension has the potential to initiate premature fracture of the connector at a tension demand less than ultimate capacity. The sensitivity of connector performance to the offset will be evaluated through the FE analysis in Chapter 9. To avoid significant offset of weld location in field work, two tabs

prefabricated with the faceplate could be used to locate the slug in the acceptable position.

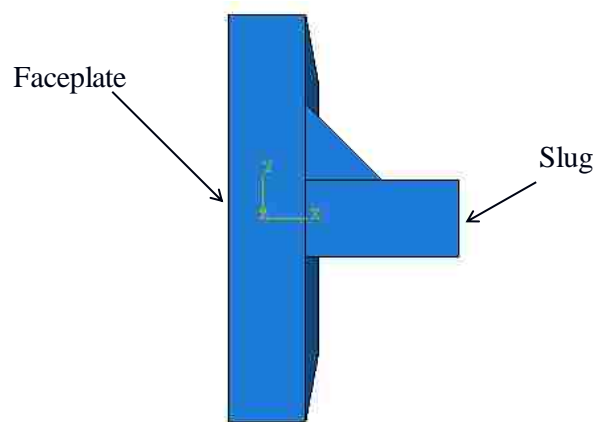


Figure 8.13. Location of faceplate to slug weld

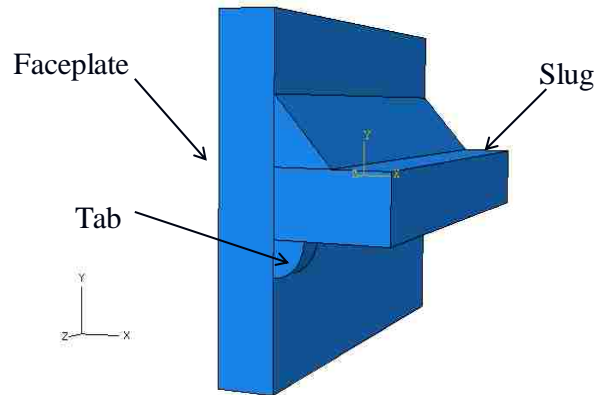


Figure 8.14. Tabs prefabricated with the faceplate to locate slug

8.5 Expected Performance

As discussed in section 8.3, the design goal of new dry chord connection strength capacity is in the range of 10-kip to 20-kip, and the design goal of connection

deformation capacity is in HDE category with at least 0.6-in for a connection pair. The dimensions of an example new dry chord connection are presented in section 8.4. Based on the design detail of this example, the expected performance is that the yield shaft yields first before rebar yield, the strength of yield shaft is close to 90% of its ultimate strength when the rebar yield, and the connection failed by the failure of yield shaft. The faceplate, tube, slug and welds are in elastic region when the failure occurs. The expected yield strength capacity is 12.0-kip and the expected ultimate strength capacity is 19.0-kip. At the time when the rebar yields, the total strain developed in the yield shaft is about 0.15. Therefore a 0.6-in deformation capacity is expected to develop in the 4-in length yield shaft for half of a connection pair.

8.6 References

1. Cao, L. (2006). "Effective Design of Precast Concrete Diaphragm Connections Subjected to In-Plane Demands", Ph.D dissertation, Lehigh University, Bethlehem, PA
2. Naito, C., Peter, W., Cao, L. (2006), "Phase 1A Summary Report," PCI-NSF Project Development of Seismic Design Methodology for Precast Diaphragms, Internal Report.
3. AWS Structural Welding Committee(1992), *AWS D1.4-92 Structural Welding Code*, American Welding Society, Miami, FL, 1992

4. Naito, C., Ren, R., Jones, C., Cullen, T. (2007), "PCI/NSF Development of a Design Methodology for Precast Concrete Diaphragms: Connector Performance Phase 1B," ATLSS Report 07-04, Lehigh University, Bethlehem, PA.
5. Zimpfer, J., Naito, C., Sause, R., and Kaufmann, E. (2008), "Investigation of the Impact of Environmental Conditions on Field Welding of Precast Concrete Connections," ATLSS Report No. 07-03.
6. ASTM (2008). *Annual Book of ASTM Standards, A706 – 93*, West Conshohocken, Pennsylvania
7. AISC (2006). *Load and Resistance Factor Design*, American Institute of Steel Construction, Chicago

Chapter 9 Analytical Studies of New Proposed Precast Concrete Dry Chord Connection

Most of previous research identified strength and deformation capacities of the existing chord connections through experimental studies. Limited information was provided on the contribution of various connector components, the local stress flow, development of concrete cracking and the interaction between the interface of connector and the concrete.

To effectively develop the design details and recommendations of new dry chord connection the local mechanisms in the connection must be understood and be predictable. To accomplish this, an analytical model of the chord connection is developed. This approach provides an understanding of the connection behavior allowing further improvements in the design.

This chapter presents the background of the connection modeling approaches used in recent research. In section 9.2, the constitutive material models and solution strategies are presented for development of 3D FE model of the new proposed dry chord connection.

Section 9.3 identifies the analytical tension behavior of the new dry chord connection in pre-topped precast concrete diaphragm systems. Detailed finite element models of dry chord are developed. The deformed shape, local stress state, failure

mechanism and global force-deformation performance of connection under tension demands are examined. A parametric investigation is conducted to evaluate the sensitivity of connection behavior to various cases with different vertical locations of faceplate-to-slug weld.

9.1 Simplified Models

Previous experimental tests on connection used in diaphragm system (Aswad 1977) have shown that concrete spalling and cracking typically occurred within a relative small region around the connector compared to the dimension of a DT panel. Hence the connections are commonly represented by simplified models to save computational efforts in analytical diaphragm analysis. The simplified connection models used in recent research included the PCI truss/spring model, truss-spring connection model and 2D connection model developed in DSDM project.

9.1.1 PCI Truss/Spring Model

In un-topped precast diaphragm systems, two adjacent double-tee panels are connected by discrete connectors. The tension and shear resistance of a connection can be modeled by truss (spring) elements in orthogonal directions. One truss (spring) element is oriented normal to the joint to model the axial behavior, and one truss (spring) element is oriented parallel to the joint to model the connection shear behavior (Figure 9.1). The axial truss (spring) element is modeled with flexible tensile response under

tensile opening and rigid compressive response under joint closing. Both the axial and shear input is obtained from connection test results.

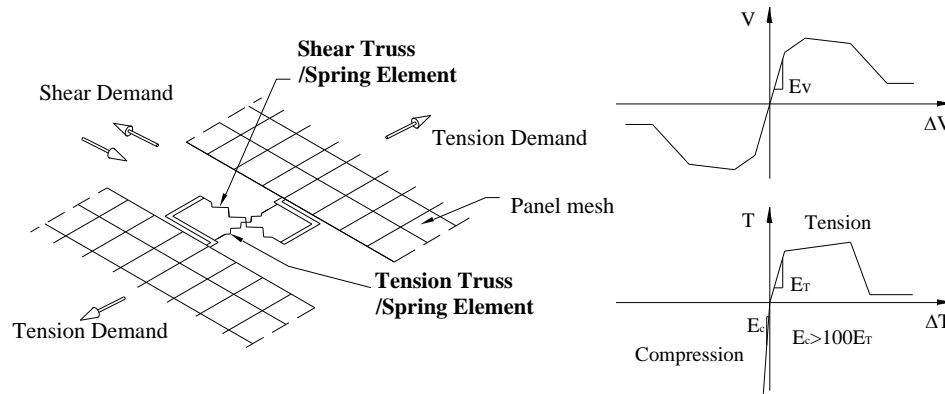


Figure 9.1. Idealized truss/Spring model

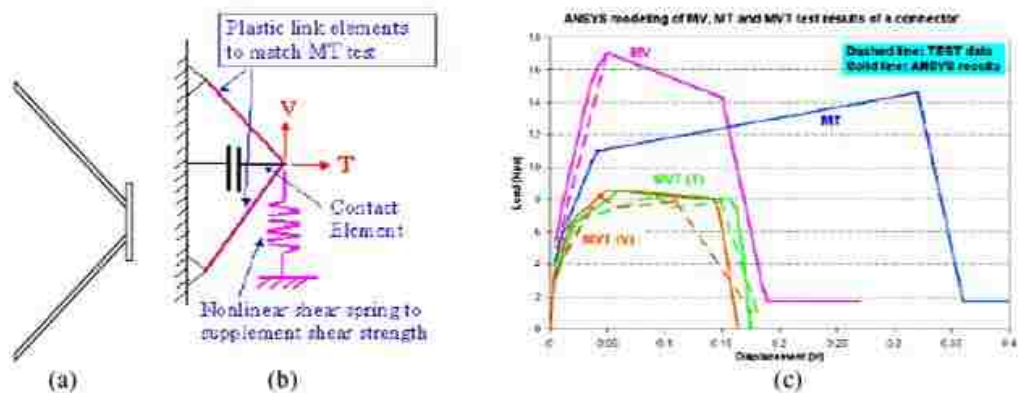
This model provides a simplistic method to capture the connection behavior in axial and shear directions in advanced diaphragm analysis. An implicit assumption is made in this approach that the tensile and shear responses are not coupled under combined load demands. In other words, the effect of the tension demand on degradation of shear strength and the effect of compression on an increase of shear capacities are not considered in this model. This may overestimate the shear connection capacity in diaphragm tension region and underestimate the shear strength in compression region. To address this, an advanced DSDM truss-spring model is developed.

9.1.2 DSDM Connection Model

A detailed connection model was developed by the University of Arizona research group [Wan & Fleischman 2006] to provide an enhanced representation of

response. For an angled bar-plate connector (Figure 9.2a) [Pincheira et.al. 1998], two diagonal plastic link elements are used to model the tension response of the connection and one spring element is used to model the connection shear behavior. A contact element is attached to model the compression contribution from concrete (Figure 9.2b). This idealized connection model is calibrated with existing experimental results from the shear and tension tests. An interactive action of the element components is generated under combined load demands, resulting in shear and tension resistance to the joint. A comparison with the combined shear with tension test result in Figure 9.2c shows a reasonably good accuracy of the connection modeling.

The advancement made in this DSDM connection model is that the model is capable of capturing the coupled shear and tension behavior which was ignored in conventional truss/spring models. Once verified by test results, this advanced model can be used to characterize the actual connection capacities under varied load conditions.



(a). Angled bar connection; (b). Idealized connection model; (c). Comparison of idealized model with test results

Figure 9.2. DSDM connection model [Wan, G. and Fleischman, R.B 2006]

Previous research shows that connection shear and tension behavior vary depending upon the connector configuration. The DSDM simplified connection model can accurately characterize the behavior of angled bar-plate connectors; however, whether this modeling technique is applicable for all the precast concrete diaphragm connections needs to be further evaluated. Sensitivity of the simplified model to physical connection details must be studied. To accomplish this, the load path and state of stress inside the common connector components is investigated through detailed finite element analysis.

9.1.3 Previous 2D FE Connection Model

A two-dimensional (2D) finite element model of conventional dry chord connection was developed and executed in DIANA FEA software (Cao 2006). The analysis was intended to estimate the load-deformation response of the connection as well as provide detailed results of the stress state and failure mechanism. The FE model configuration is presented in Figure 9.3. Parametric studies were conducted and design recommendations were proposed based on analysis. The experimental research conducted on enhanced dry chord connection showed that the 2D FE analysis may not capture the real behavior of connection embedded in concrete panels due to assumption and limitation inherent in the models and software used. Therefore, to develop effective design details, it is necessary to simulate the physical connection more accurately by using three dimensional (3D) models.

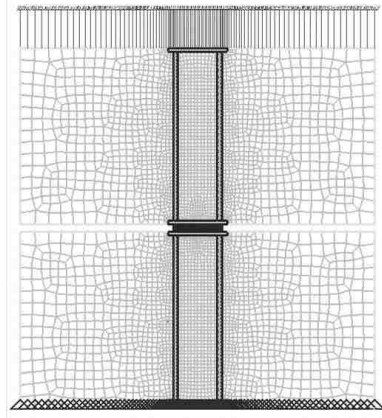


Figure 9.3. 2D FE dry chord model (Cao 2006)

9.2 3D FE Connection Model

The FE program ABAQUS (Version 6.9) is used for the FE analysis. The finite element model is developed for the new proposed dry chord connection embedded in the concrete panel. The detailed model analysis is intended to evaluate the global behavior of connections under tension loading, and investigate the stress transfer path, plastic strain development and failure mechanism. Details of the models are discussed below.

9.2.1 Model Geometry

3D detailed connection model is developed based on the new designed chord connection configuration. To evaluate the connection behavior in the physical precast concrete diaphragm system, the model is composed of chord connector embedded in a concrete panel with a rectangular slug welded to the faceplate. As discussed previously, the interaction of concrete and connector typically occurred within a relative small region around the connector compared to the dimension of entire concrete panel. Therefore a

partial 6x12x4-in concrete panel is used in the FE model to represent concrete behavior (Figure 9.4). To save on computational effort, one single bar chord connector is used with half of the slug. Assuming symmetry this detail represents half of the joint (Figure 9.5). The dry chord connector is designed using #5 bar inserted into the tube, which has exterior diameter of 1.2-in and interior diameter of 0.75-in.

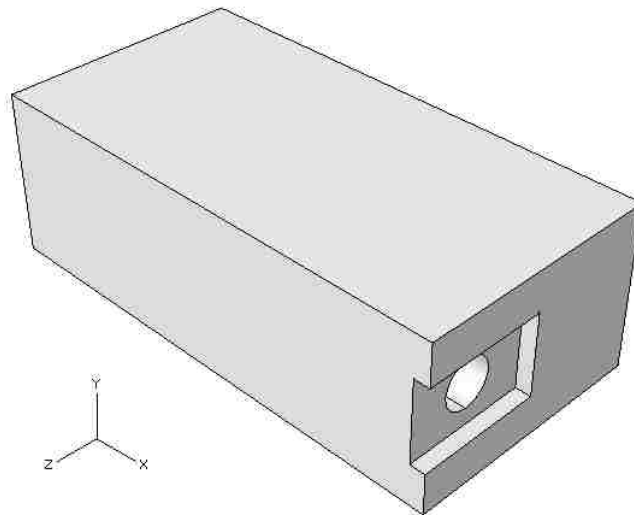


Figure 9.4. Partial concrete panel region around connector (6x12x4-in)

There are 2 slots set on the tube, which are for plug welds between rebar and tube. The plug weld is fit with the tube with a thickness of 0.225-in, the layout of two plug welds are shown in Figure 9.6. The front flange has a diameter 0.86-in and yield shaft has a diameter 0.62-in. The unbonded region has a length of 5.5-in covered from front flange to tube. The entire model which represents dry chord connection embedded in the concrete panel is indicated in Figure 9.7, the chord connector is embedded in the concrete panel, and the slug (3/8x3/4x3-in) is connected with faceplate (3/8x2x3-in) via a 3/8@3-in fillet weld.

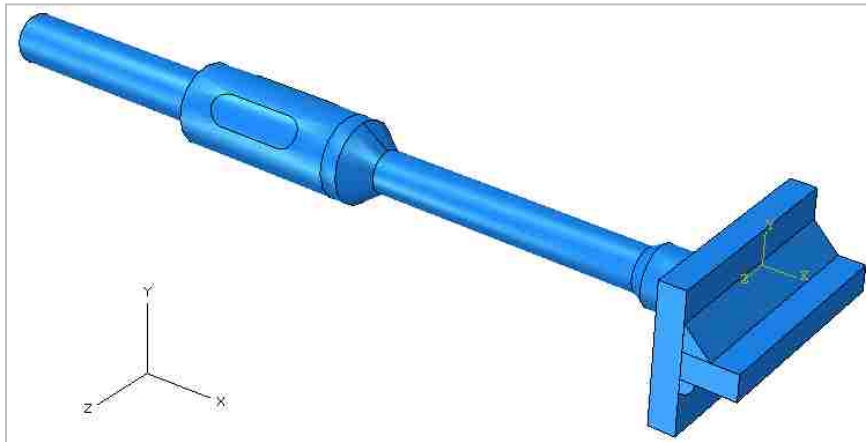
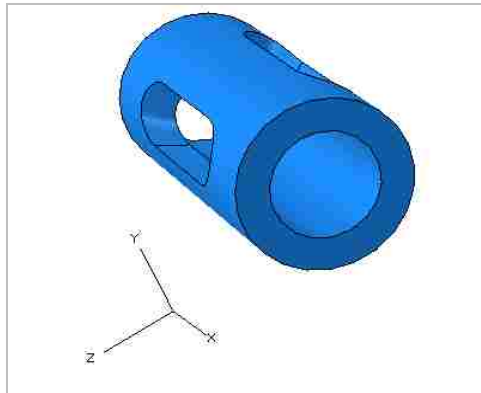
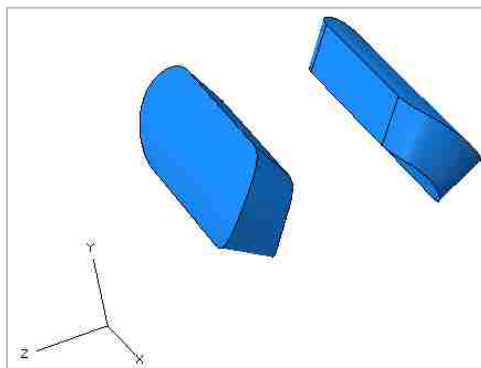


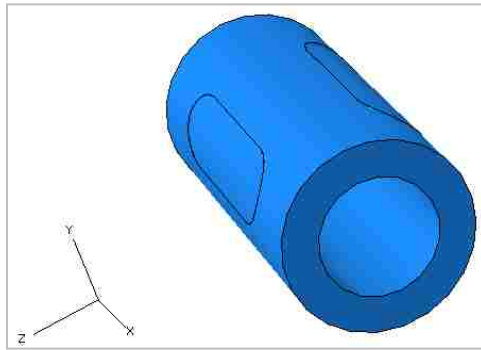
Figure 9.5. Chord connector with slug and slug weld



(a) Tube with two slots

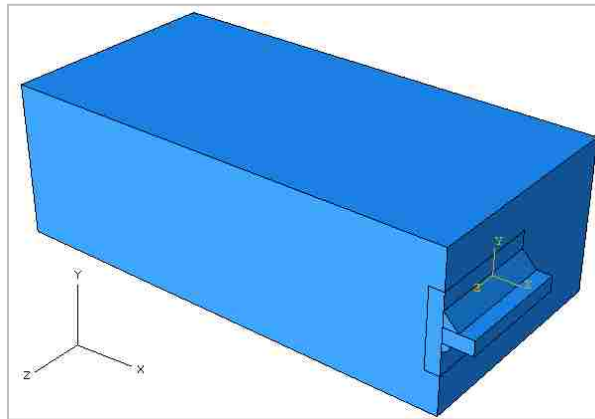


(b) Plug welds performed in the two slots

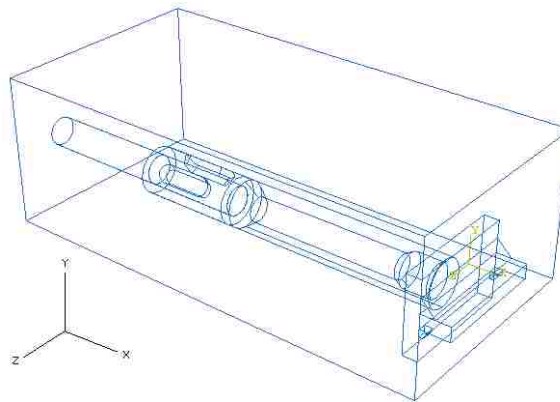


(b) Tube with plug welds

Figure 9.6. Tube and plug welds



(a) Shaded View



(a) Wireframe View

Figure 9.7. Chord connector embedded in the concrete panel

9.2.2 Material Models and Properties

A linear elastic isotropic material model is used for steel and weld components in the elastic range, with Young's modulus of 29000-ksi and Poisson's ratio of 0.3. The ABAQUS classical metal plasticity material model is used for rebar, slug and casting piece in the inelastic range. This model uses the Von Mises yield criterion to define yielding, the elastic-hardening behavior is used to capture the events of yielding and fracture (Figure 9.8). An abrupt degradation in the stress can lead to difficulty in numerical convergence; therefore, a stress plateau is assumed for computation purpose when the strain exceeds the fracture strain. Failure of connection is assumed when the response reaches fracture point, as a result, the post-fracture results are not used in the analysis.

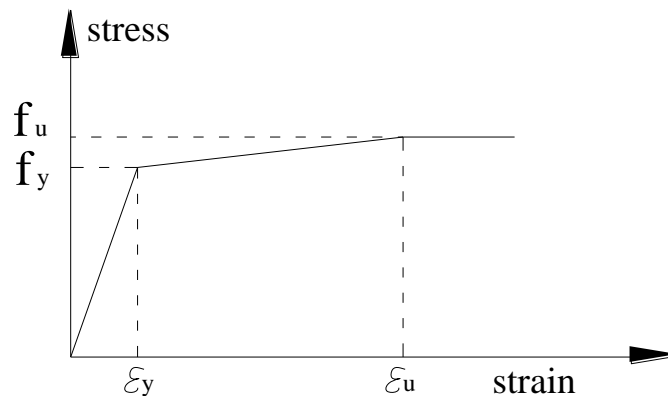


Figure 9.8. Constitutive steel model

Concrete materials used for components of this FE model replicate typical precast construction. No additional direct loads is applied to the concrete panel in this case

besides the force transferred through the contact action, therefore no cracks is expected in the concrete panel and the concrete is assumed in elastic range, with Young's modulus of 4.415-ksi, compressive strength of 6-ksi and Poisson's ratio of 0.2. The #5 rebar is made using ASTM A706 steel with a yield strength of 60-ksi and ultimate strength 80-ksi. The slug plate is ASTM A36 steel with a yield strength of 36-ksi and ultimate strength of 58-ksi. The casting carbon steel is ASTM A352 LCC plus a condition that the carbon equivalent is less than 0.55. The fillet weld and slug weld in the model are to be fabricated using E7018 electrodes in accordance with American Welding Society standards [AWS 2004].The elastic-hardening –plastic tri-linear model is indicated in Table 9.1and Figure 9.9.

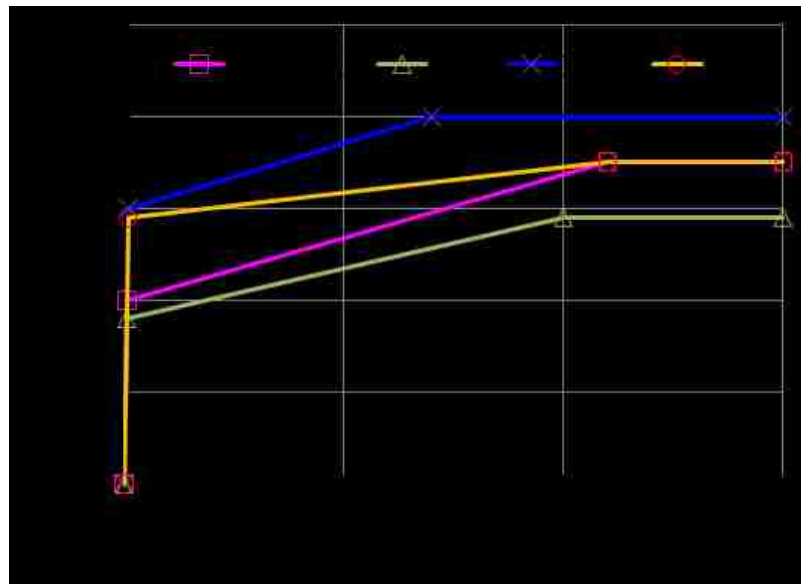


Figure 9.9. Constitutive material model for casting steel, rebar, slug and welds

Table 9.1. Material properties of connector model				
Material	Type	Yield Strength [ksi]	Ultimate Strength [ksi]	Ultimate Strain
Cast Steel	ASTM A352	40	70	0.22
Rebar	ASTM A706	60	80	0.14
Slug	ASTM A36	36	58	0.20
Fillet Weld	E7018	58	70	0.22
Plug Weld	E7018	58	70	0.22

9.2.3 Mesh and Elements

Due to the complex geometry of the connector model, it is difficult to use the solid hex element and have good element perspective. Therefore, the three-dimensional, 10-node modified quadratic tetrahedron with hourglass control, continuum element C3D10M used to model the concrete panels, casting piece, rebar, slug and welds (Figure 9.10). This modified element is recommended for problem involving contact analysis and large plasticity because of its excellent contact properties. Therefore it is the best element candidate for the FE model developed in this dissertation research. A negative issue with the use of this C3D10M element is longer run times and computational efforts.

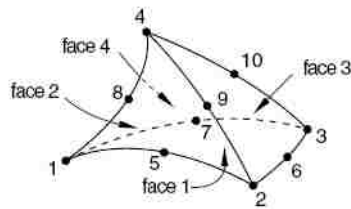


Figure 9.10. Modified second-order element C3D10M (ABAQUS, 2009)

In order to get accurate simulation results while saving computational effort, very fine meshes are used for components of dry chord connector, same fine meshes are used in the region of concrete panel around connector, and relative coarse meshes are used in the other region of concrete panel. The detailed model is indicated in Figure 9.11.

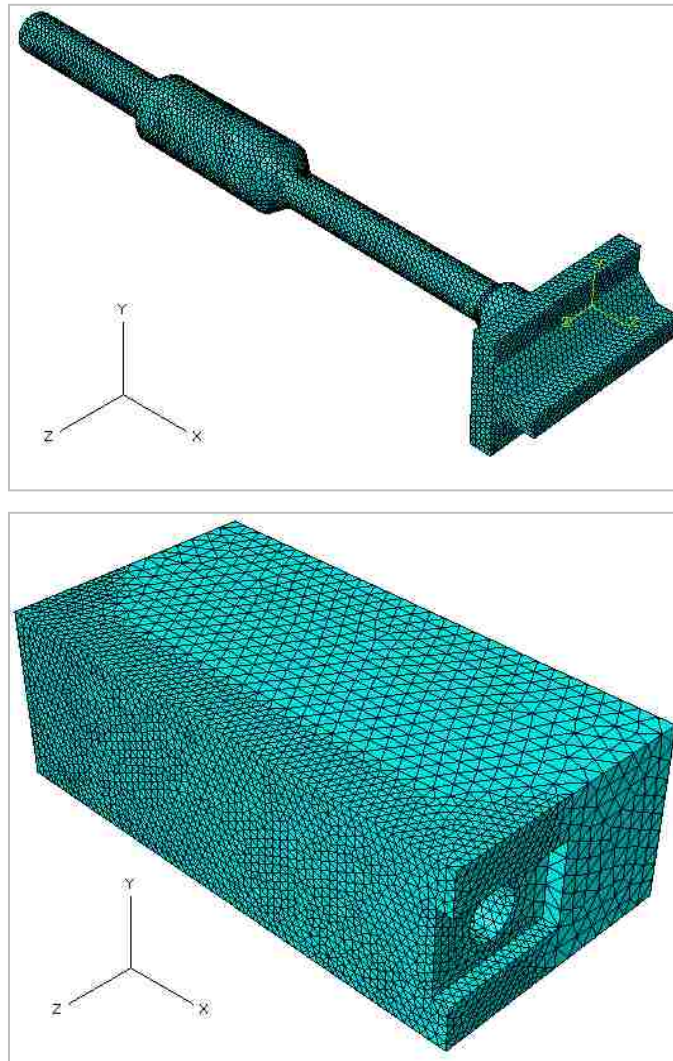


Figure 9.11. Meshes of the dry chord connector and surrounding concrete panel

9.2.4 Interface Contact Modeling

When the connection is subjected to loading, an interaction is activated at the interface between the bar surface and surrounding concrete. In this investigation, the concrete to steel interactive actions exist between concrete panel with connector components, which includes the concrete and tube interface, concrete and rebar interface, and concrete and faceplate interface. In addition, the steel to steel interaction behavior occurs inside the connector, such as the tube and rebar interface. These interactions (Figure 9.12) are modeled through surface-to-surface contact analysis.

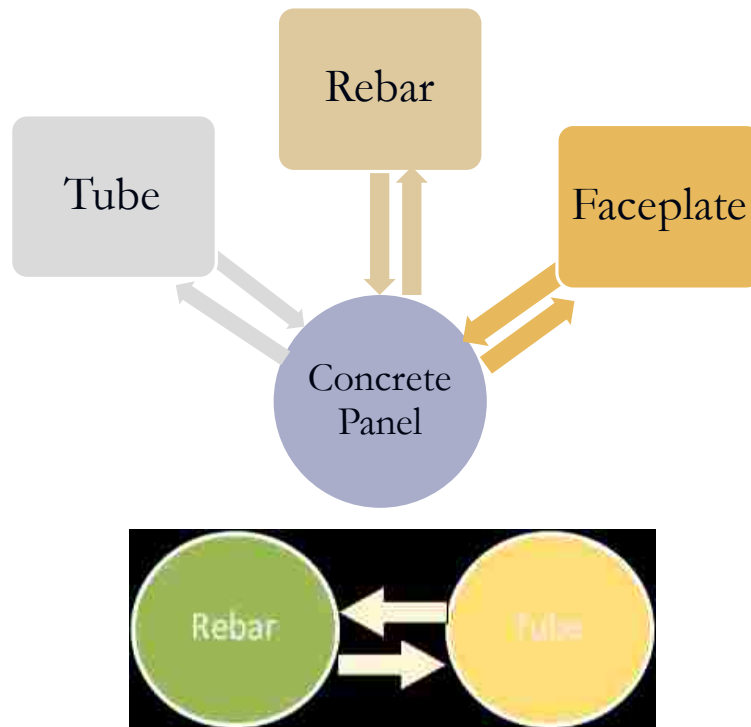


Figure 9.12. Interactive action in the FE model of connector and concrete panel

9.2.4.1 Surface-to-surface Contact Pairs

A quote regarding the surface contact pair form ABAQUS is presented as follows
“When a contact pair contains two surfaces, the two surfaces are not allowed to include any of the same nodes, the master and slave surface must be defined. Some general roles must be followed when choosing the master and slave roles in a two-surface contact pair. When both surfaces in a contact pair are element-based and attached to either deformable bodies or deformable bodies defined as rigid.

- If a smaller surface contacts a larger surface, it is best to choose the smaller surface as the slave surface.
- If that distinction cannot be made, the master surface should be chosen as the surface of the stiffer body or as the surface with the coarser mesh if the two surfaces are on structures with comparable stiffnesses. The stiffness of the structure and not just the material should be considered when choosing the master and slave surface.”

The assignment of master and slave roles can have a significant effect on performance with surface-to-surface contact. If the two surfaces have dissimilar mesh refinement; the solution can become quite expensive if the slave surface is much coarser than the master surface. In this analysis, for concrete steel interactive actions, the surfaces on concrete panel are chosen to be the master surface, while the surfaces on faceplate,

tube and rebar are slave surfaces. The surface on the rebar is chosen to be the master surface for steel-to-steel interface interaction between casting tube and rebar.

9.2.4.2 Interaction Properties

The interaction behavior can be decomposed to a tangential behavior and a normal behavior. The tension load path is transferred from the connector to surrounding concrete through the bond stress of tangential behavior. An isotropic penalty friction model is used to simulate the tangential behavior of concrete-to-steel interaction. This stiffness (penalty) method permits some relative motion of the surfaces (an “elastic slip”) when they should be sticking. While the surfaces are sticking (i.e., $\bar{T} < \bar{T}_{crit}$), the magnitude of sliding is limited to this elastic slip. The program will continually adjust the magnitude of the penalty constraint to enforce this condition. The friction ratio used is 0.45. For steel-to-steel interaction exist between tube and rebar, the friction ratio is set to be 0.3. The interaction behavior on the normal direction for both concrete-to-steel interaction and steel-to-steel interaction are modeled with the “hard” contact pressure-overclosure relationships (Figure 9.13). This “hard” contact relationship minimizes the penetration of the slave surface into the master surface at the constraint locations and does not allow the transfer of tensile stress across the interface.

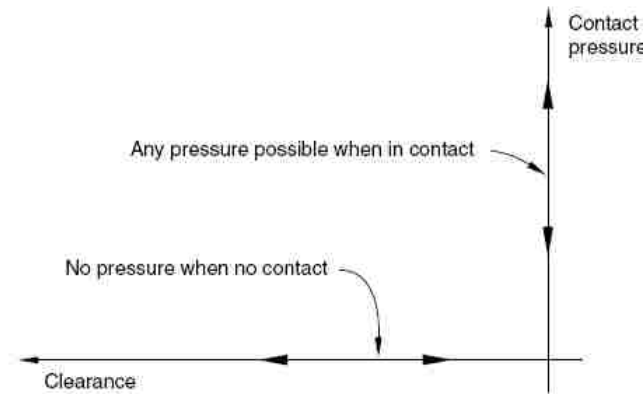


Figure 9.13. Normal “hard” contact pressure-overclosure relationship (ABAQUS, 2009)

9.2.5 Boundary and Loading Conditions

The FE model includes only half of the entire joint model which consists of a pair of dry chord connector and two concrete panels due to symmetry of the geometry, the model is loaded at the mid-span of slug. The boundary conditions are illustrated in Figure 9.14, where u_x , u_y , u_z , ϕ_x , ϕ_y and ϕ_z are the displacements and the rotations about the global X-, Y-, and Z- axes respectively. To simulate the connection embedded in the concrete panel and subjected to tension loading, all the nodes on 3 faces (back and sides) of concrete panel are restrained from moving and rotating in all the directions. The end face of rebar is also fixed in all directions. The front face of concrete panel is set free to move. The longitudinal displacement in Z direction (u_z) and the rotation (ϕ_x and ϕ_y) about the X-axis and Y-axis are restrained for all the nodes on the side face of the faceplate, slug and fillet weld because of symmetry. A uniform tensile displacement loading is applied along the nodes on the front face of the slug in X-axis.

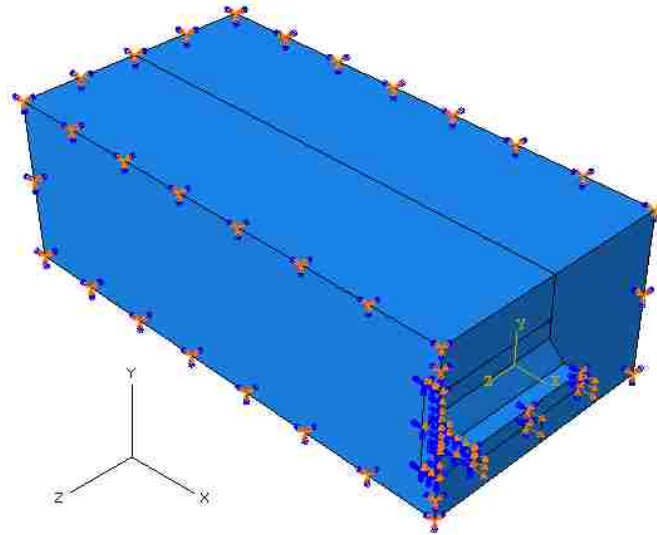


Figure 9.14. Model boundary and loading conditions

9.2.6 Iteration Methods

The solution strategies used for the finite element analysis are full Newton-Raphson, Newton-Raphson method uses a direct approach to determine the iterative displacement increment, δu_i , using Eq. 9-1.

$$\delta u_i = K_i^{-1} \cdot g_i \quad \text{Eq. 9-1}$$

where K_i is the stiffness matrix used at every iteration and g_i is the out-of-plane force vector at the start of iteration i . The stiffness matrix used for Newton method is recalculated at each iteration step with regard to the initial un-deformed shape. As a result, this method converges to the final solution with only a few iteration steps. However, iteration is relatively time consuming since the stiffness needs to be assembled at each step.

The quasi-Newton method essentially uses the information of previous solution vectors and out-of-balance force vectors during the increment to set up the new stiffness matrix. Unlike regular Newton-Raphson method, the stiffness matrix is calculated based on the previous step. Secant Broyden method yields the new stiffness at step $i+1$ as shown in Eq. 9-2:

$$K_{i+1}^{-1} = K_i^{-1} + \frac{(\delta u_i - K_i^{-1} \delta g_i) \delta u_i^T K_i^{-1}}{\delta u_i^T K_i^{-1} \delta g_i} \quad \text{Eq. 9-2}$$

For structural behavior with minimal damage such as concrete cracking or plasticity, regular Newton-Raphson method is used for solving the problem. For structural behavior with considerable concrete cracking, quasi-Newton method is used instead. In analysis of precast concrete diaphragm dry chord connections, the tension response of the connection is analyzed using regular Newton-Raphson iteration. An automatic step size based on deformation increments is used.

9.2.7 Analyses

The nonlinear load-displacement analyses, including both material inelasticity and contact behavior, are conducted to evaluate the performance of new developed dry chord connection.

9.3 Analytical Tension Behavior

In precast diaphragm systems, chord elements are used at the ends of the DT members to resist flexural in-plane demands. Therefore, the strength and deformation capacities of chord connector under tension load are critical criteria to evaluate the connector. As discussed in Chapter 8, the connector performance under tensile loading may be affected by the vertical location of faceplate-to-slug weld. The ideal position will be the center of slug is in line with the center of standard modular system based on simply free body diaphragm (FBD) analysis. However, the actual connector behavior is complex when subjected to incremental tensile loading and may not be well represented by the simple FBD analysis. Hence the performance of new dry chord connector subjected to uniform tensile loading is analyzed using the FE model described in section 9.2.

In addition, the connector behavior may be sensitive to the vertical weld offset due to the design involves a very flexible and thin portion” yield shaft”. To develop the intended tensile mechanism of yield shaft, a parametric study is conducted with the goal of minimizing flexure and maximizing ductility in the yield portion of standard casting modular system. The sensitivity of faceplate-to-slug weld location is investigated.

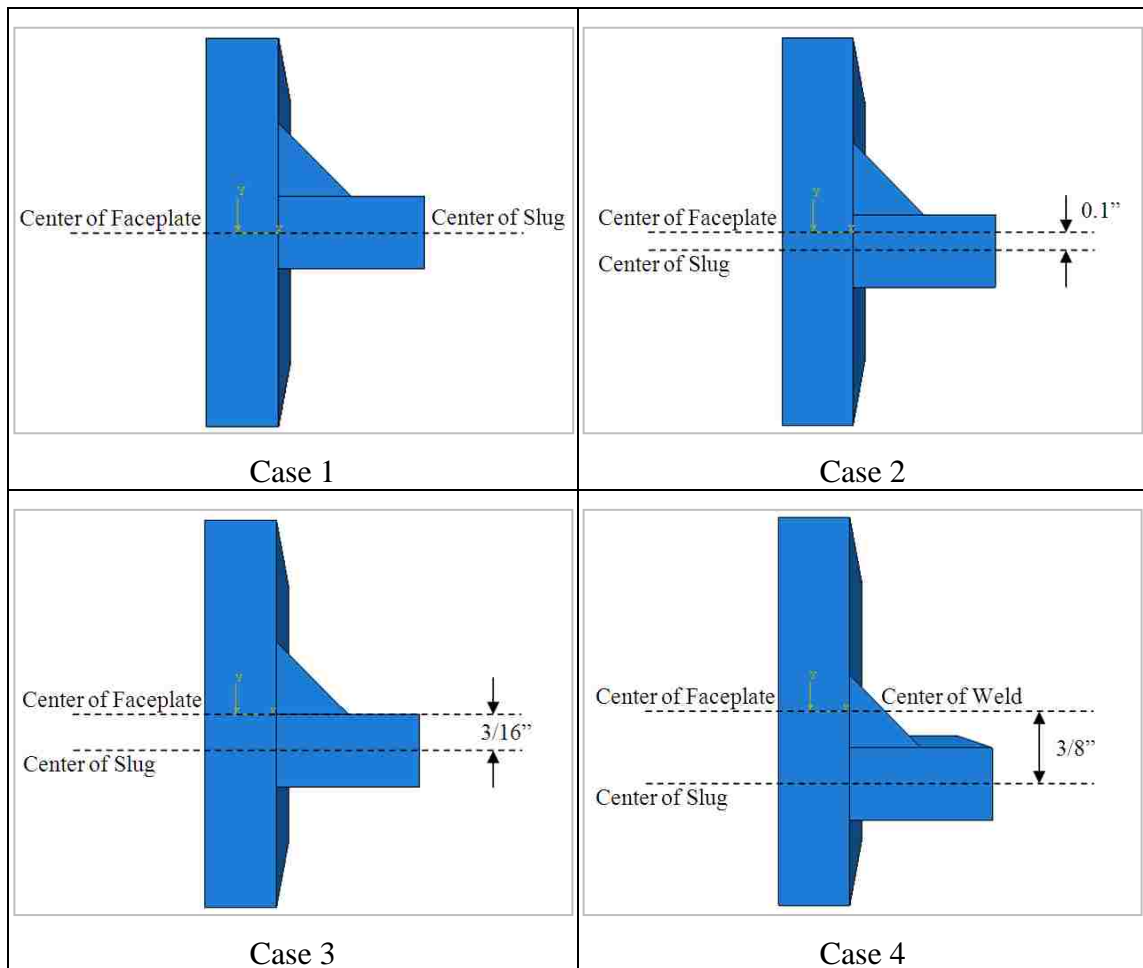


Figure 9.15. Location of faceplate-to-welds in various cases

The weld location alters the deformation demands on the connection components. To illustrate this effect, connection performance of four cases with different weld locations are examined. The center of faceplate is line with the center of slug in case 1, the vertical offset in downside direction is 0.1-in for case 2, considering the location in case 1 is the reference location. The center of faceplate in case 3 is in line with the bottom of weld, which means the vertical offset in downside direction is 3/16-in. The center of faceplate in case 4 is in line with the center of faceplate-to-slug weld, which

means the vertical offset in downside direction is 3/8-in. The vertical location of faceplate-to-slug weld for each case is illustrated in Figure 9.15.

9.3.1 Deformed Shape

The response of chord connector embedded in the concrete panel varies with different cases. In all of the cases, no visible deformation occurred in the concrete panel and anchorage bar.

A comparison of undeformed and deformed shape of embedded connector in each case is indicated in Figure 9.16. A scale factor of 1.0 is used for all cases. As illustrated, a considerable plastic elongation occurred in the connector under the tensile loading in all of the cases.

The response of yield shaft and faceplate varies with the different cases. In the first case, significant flexure occurs in the casting modular system, and the bottom portion of faceplate is rotated relative to the bottom of faceplate-to-slug weld. Very slight flexure and rotation occurs in the second case and no visible flexure and rotation occurred in the third and fourth case.

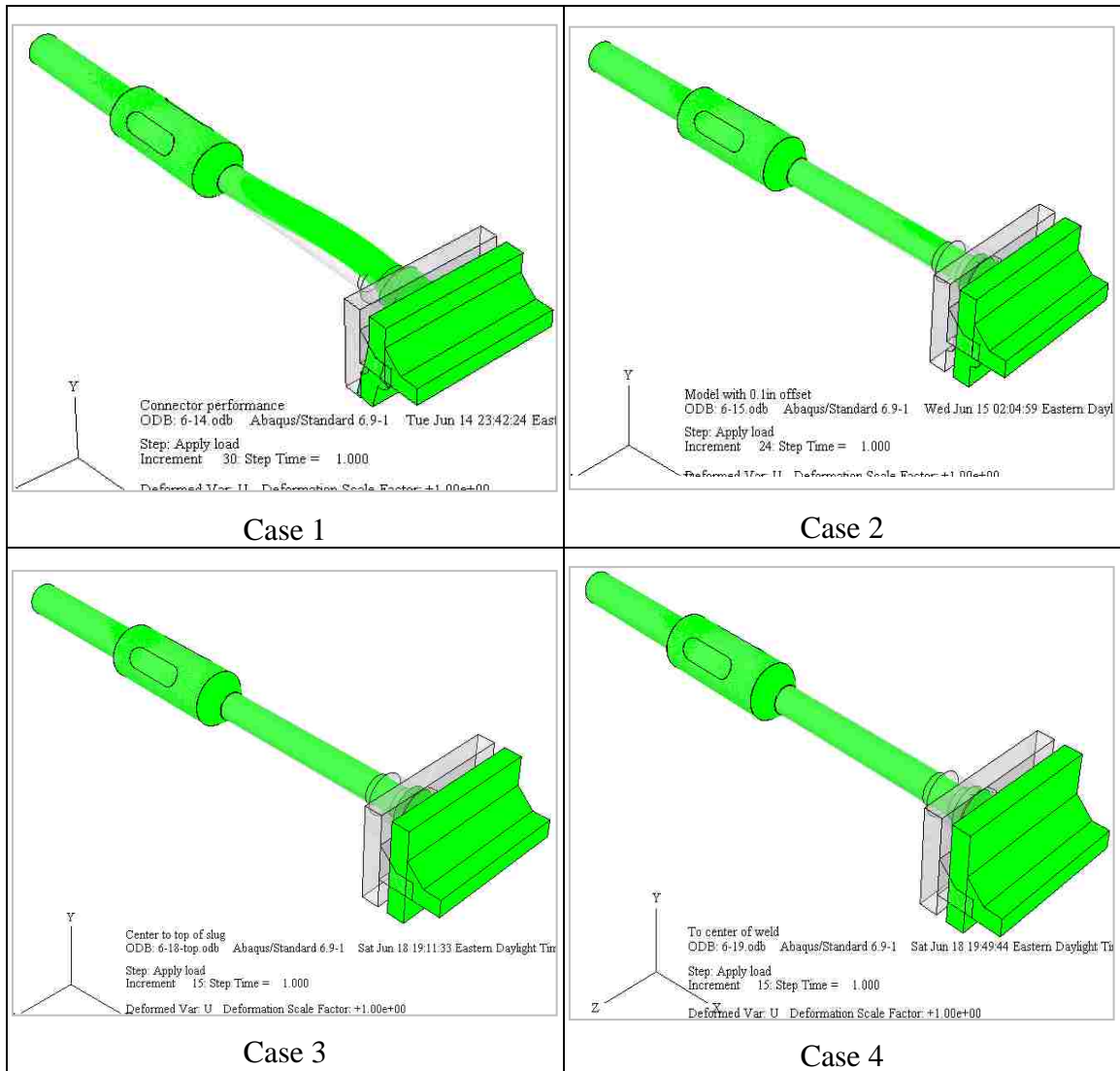


Figure 9.16. Undeformed and deformed shape comparison of connector in various cases

9.3.2 Stress State

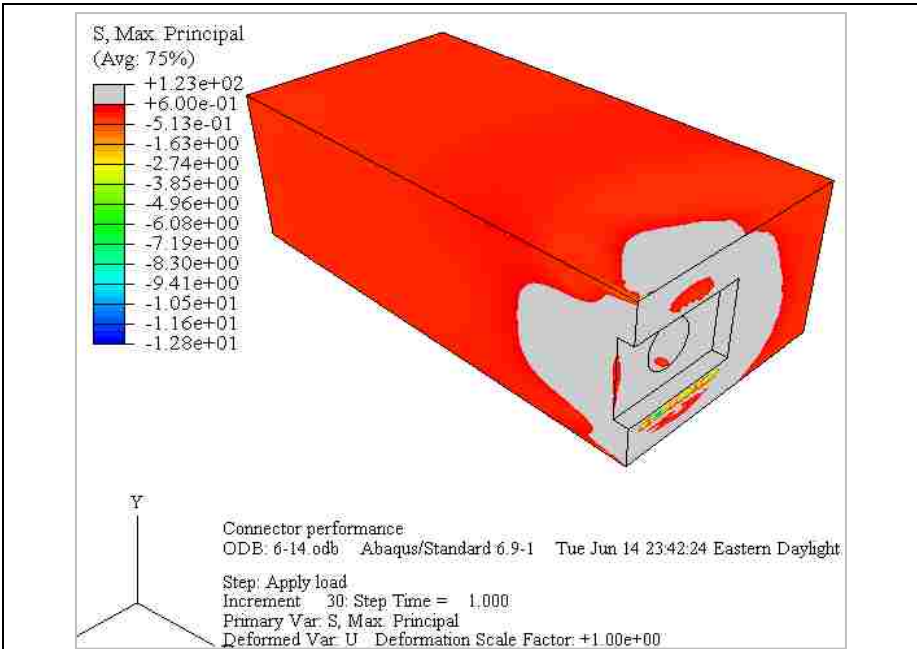
The stress state of connection varies with different cases. The stress distribution of connection components and surrounding concrete panel in all of the cases are presented in this section.

9.3.2.1 Concrete panel

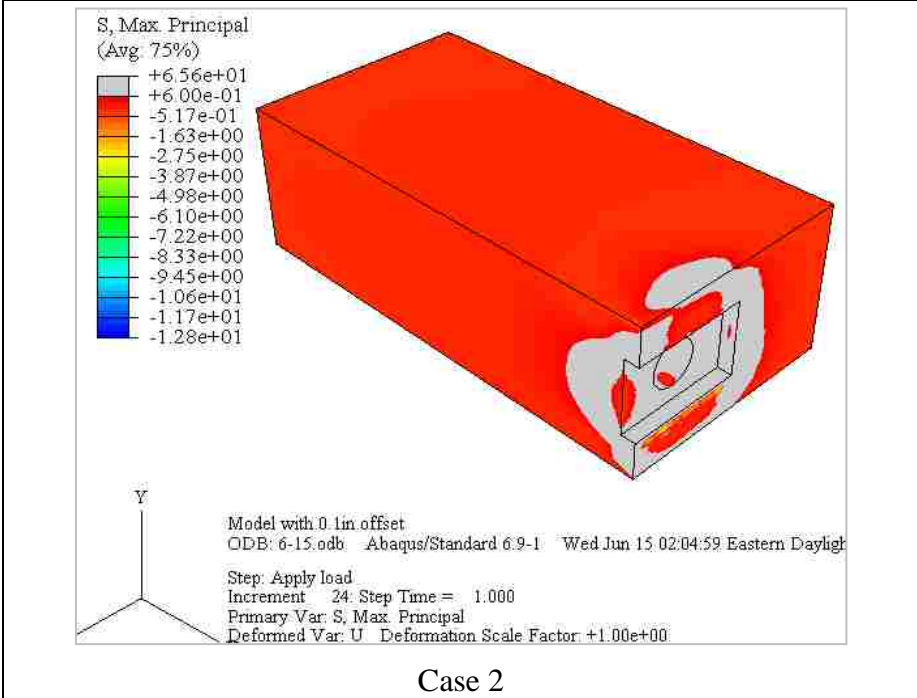
The concrete was assumed to be in the elastic range during the FE analysis to solve the divergence issue and reduce computational load. The actual principle tensile stress distributions in the concrete panel of all cases are indicated in Figure 9.17. To get a better comparison of various cases, the maximum limits of the stress contour in all of the cases are set to be 0.6-ksi, which is the rupture strength of concrete material with a compressive strength of 6-ksi. Thus stresses in the grey regions shown in the figure are greater than 0.6-ksi, which means concrete cracking may occur in the grey regions.

It is indicated that maximum principle stress in a small portion of concrete panel is higher than the critical rupture strength of concrete in each case. No significant cracking occurs in majority parts of the panel. The assumption that the concrete panel is in the elastic range is reasonable to use.

Stress concentration of all of the cases occurs in the contact surface between the faceplate and the concrete panel. The situation of stress concentration in the panel is improved as the vertical offset increases in the downside direction. A bearing pad around bottom of the faceplate may be used to reduce the stress concentration.



Case 1



Case 2

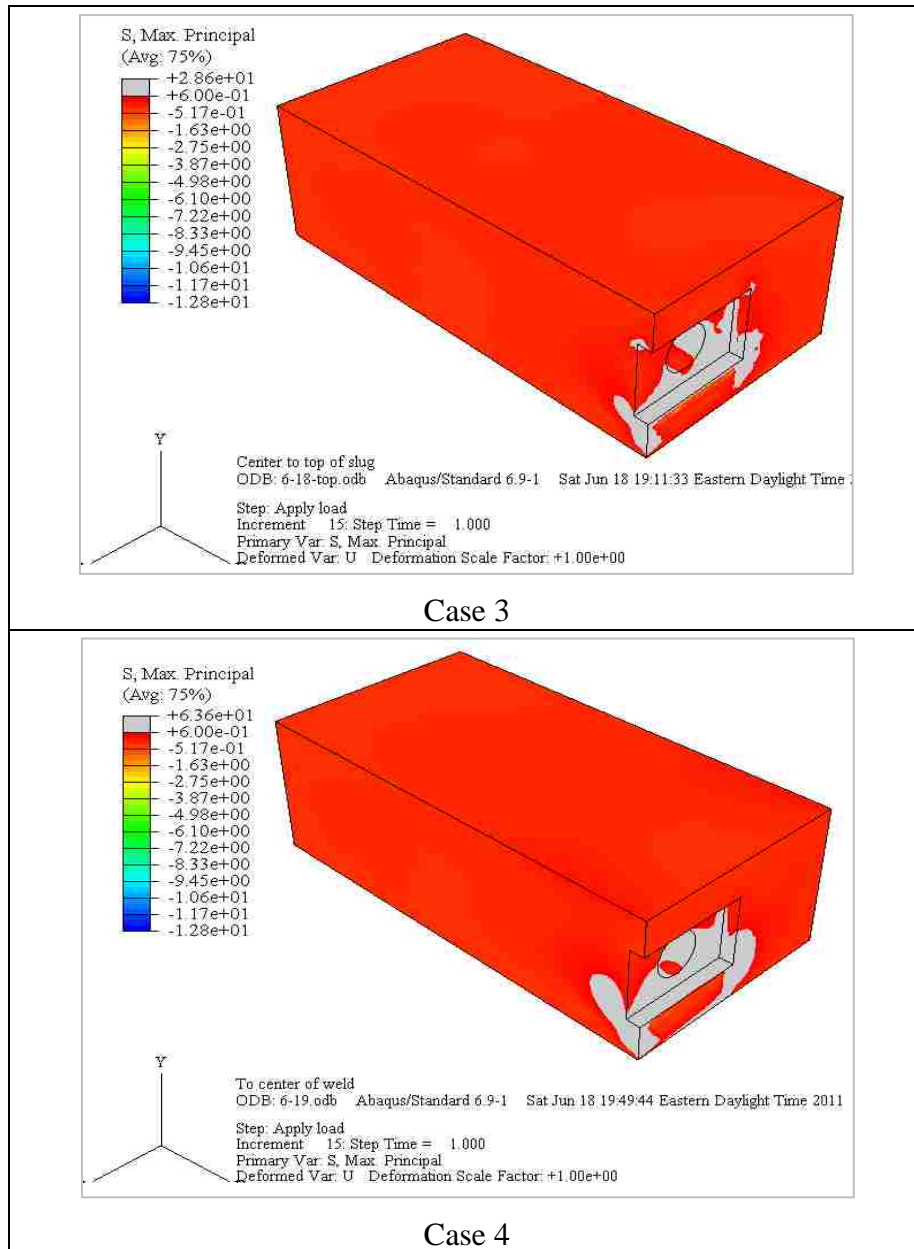


Figure 9.17. Maximum principal stress contour of concrete panel in various cases

9.3.2.2 Casting modular system

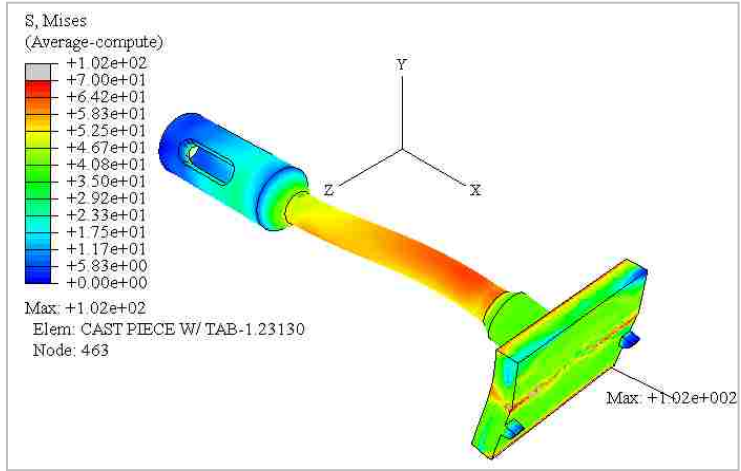
The Von Mises stress distributions of the casting modular system in all of the cases are indicated in Figure 9.18. To get a clear illustration and comparison, the

maximum limits of contour in all of the cases are set to be the 70-ksi, which is the ultimate strength of carbon casting steel.

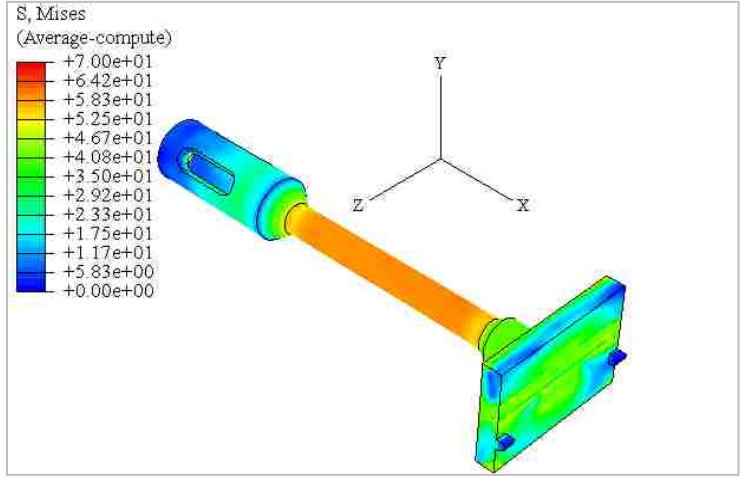
In the first case, the maximum Von Mises stress occurs in the bottom tip region of faceplate surface which bears on the concrete panel. A bearing pad around bottom of faceplate could be used to reduce the bearing stress. Stress concentration occurs in the yield shaft region as expected and the stress distribution is not uniform because of considerable flexural deformation of yield shaft. Failure of faceplate may occur as well because of the high stress concentration caused by flexural deformation. The front flange may yield due to flexural deformation while the tube is in elastic stage.

In the second case, the stress in the entire casting modular system is lower than the ultimate strength of casting material. Similar to the first case, the stress in the yield shaft is close to its ultimate strength. However, the tensile stress distribution in the yield shaft is uniform and no significant tensile/compressive stress caused by addition flexural deformation. The stress in the faceplate is generally smaller than that of the first case because less flexural deformation involved in the faceplate.

In the third and fourth case, the stress in the entire casting modular system is lower than the ultimate strength of casting material as well. Similar to the second case, the tensile stress distribution in the yield shaft is uniform, no significant tensile/compressive stress caused by addition flexural deformation. The stress in the faceplate is reduced as the vertical offset of weld increases.



Case 1



Case 2

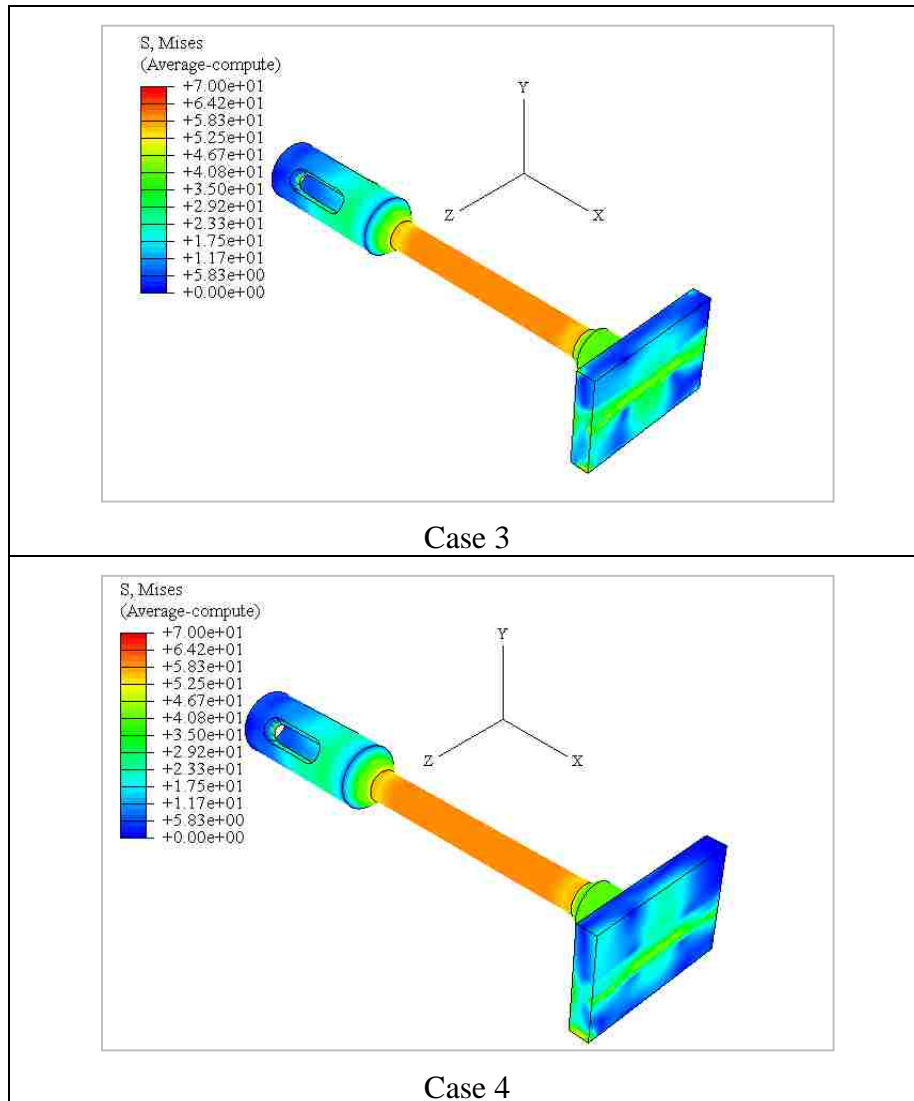


Figure 9.18. Von Mises stress contour of casting modular system in various cases

9.3.2.3 Anchorage Bar

The Von Mises stress distributions of anchorage bar in all of the cases are indicated in Figure 9.19. To get a clear illustration and comparison, the maximum limits of contour in all of the cases are set to be the 60-ksi, which is the yield strength of A706 Gr.60 steel rebar.

It is indicated that the performance of anchorage bar in all of the cases is very similar. The stresses in the anchorage bar of each case are all less than its yield strength, no yield or failure occurs in the rebar. The stress concentration of anchorage bar in all of the cases occurs at the same location in the interface region between rebar and plug weld. Generally, the rebar has a good performance in each case and the performance is not sensitive to the vertical location of faceplate-to-slug weld.

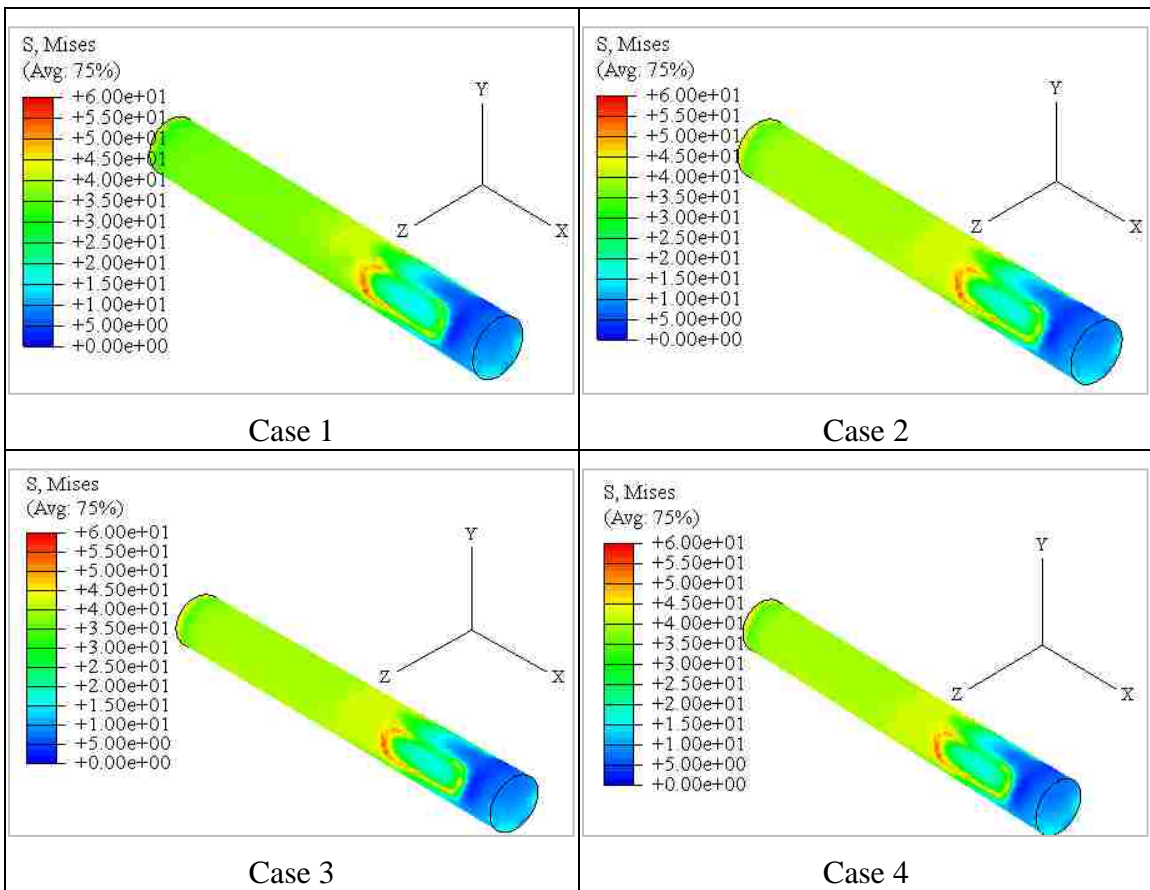


Figure 9.19. Von Mises stress contour of anchorage bar in various cases

9.3.2.4 Tube-to-Rebar Plug Weld

The Von Mises stress distributions of tube-to-rebar plug weld in all of the cases are indicated in Figure 9.20. To get a clear illustration and comparison, the maximum limits of contour in all of the cases are set to be the 70-ksi, which is the ultimate strength of E7018 electrode used for plug weld.

As illustrated in Figure 9.20, the stress distributions in the plug welds of all of the cases are very similar. The maximum stresses occur at the exact same locations, which is the bottom end edge of the interface region. The majority part of the plug welds perform well. The performance of plug weld is not sensitive to the location of faceplate-to-slug weld.

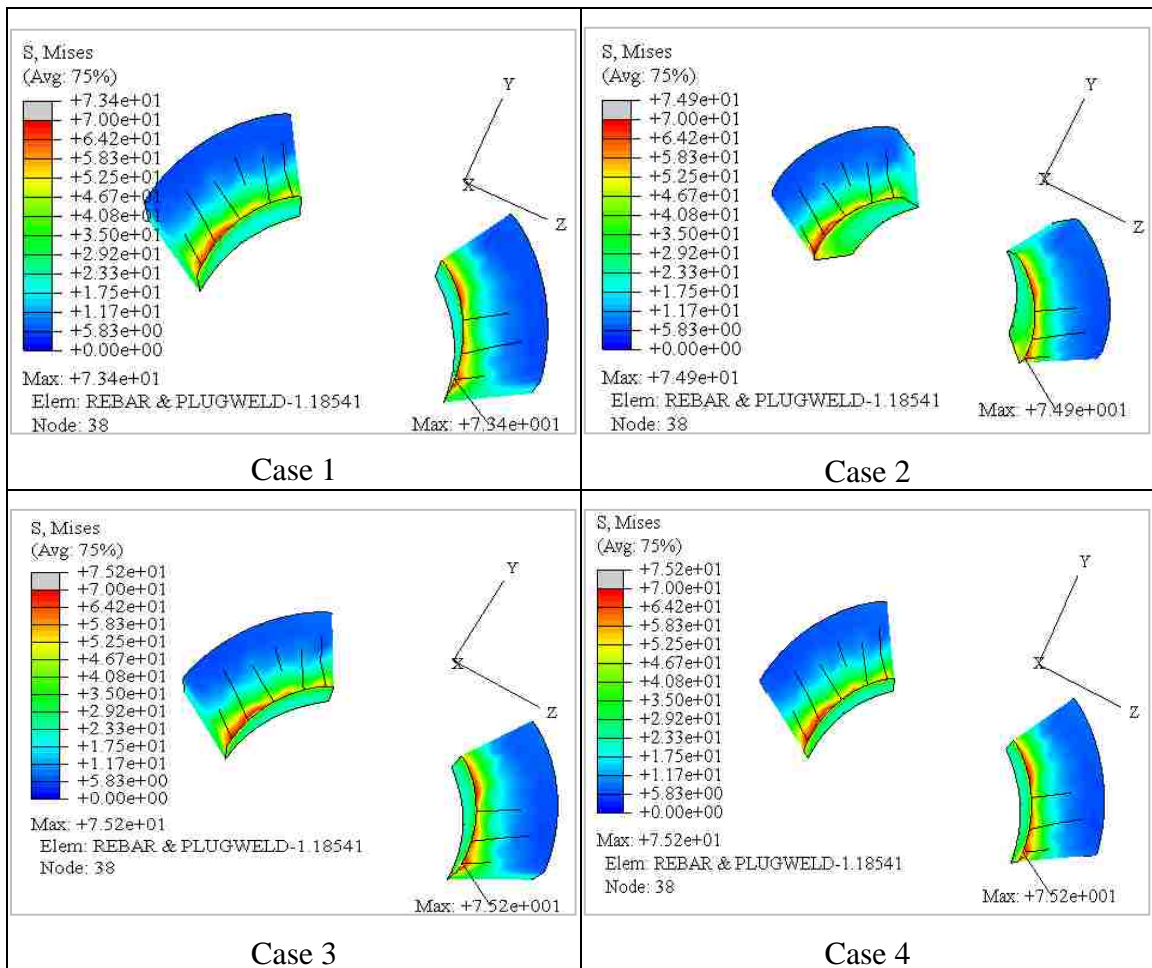


Figure 9.20. Von Mises stress contour of tube-to-rebar plug weld in various cases

9.3.2.5 Faceplate-to-Slug Fillet Weld

At a joint opening of 1.2-in

The Von Mises stress distributions of faceplate-to-slug fillet weld at a joint opening of 1.2-in in all of the cases are indicated in Figure 9.21. To get a clear illustration and comparison, the maximum limits of contour in all of the cases are set to be the 70-ksi, which is the ultimate strength of E7018 electrode used for fillet weld. As illustrated

in Figure 9.21, the stress distribution of faceplate-to-slug weld varies with different location.

In the first case, high stress concentration occurs in the faceplate-to-slug, the addition moment due to the faceplate flexural deformation and eccentricity of loading amplifies the tensile demand on the weld. Most of the weld region has a stress higher than fracture strength of weld, premature faceplate-to-slug weld failure may occur before the other components of connector fails.

Although the situation of the second case is better than the first case, concentration of stress which is higher than the weld fracture strength still occurs in the center region of weld. The addition moment due to the faceplate flexural deformation and eccentricity of loading amplifies the tensile demand on the weld, premature faceplate-to-slug weld failure may occur before the other components of connector fails.

In the third case, only a very small portion of weld has a stress higher than the weld fracture strength while the other portions perform well. The performance of the fourth case is even better. Most region of weld is in elastic stage while stress of the bottom edge is close to the weld fracture strength. Generally, the stress distribution of weld is very sensitive to its vertical location.

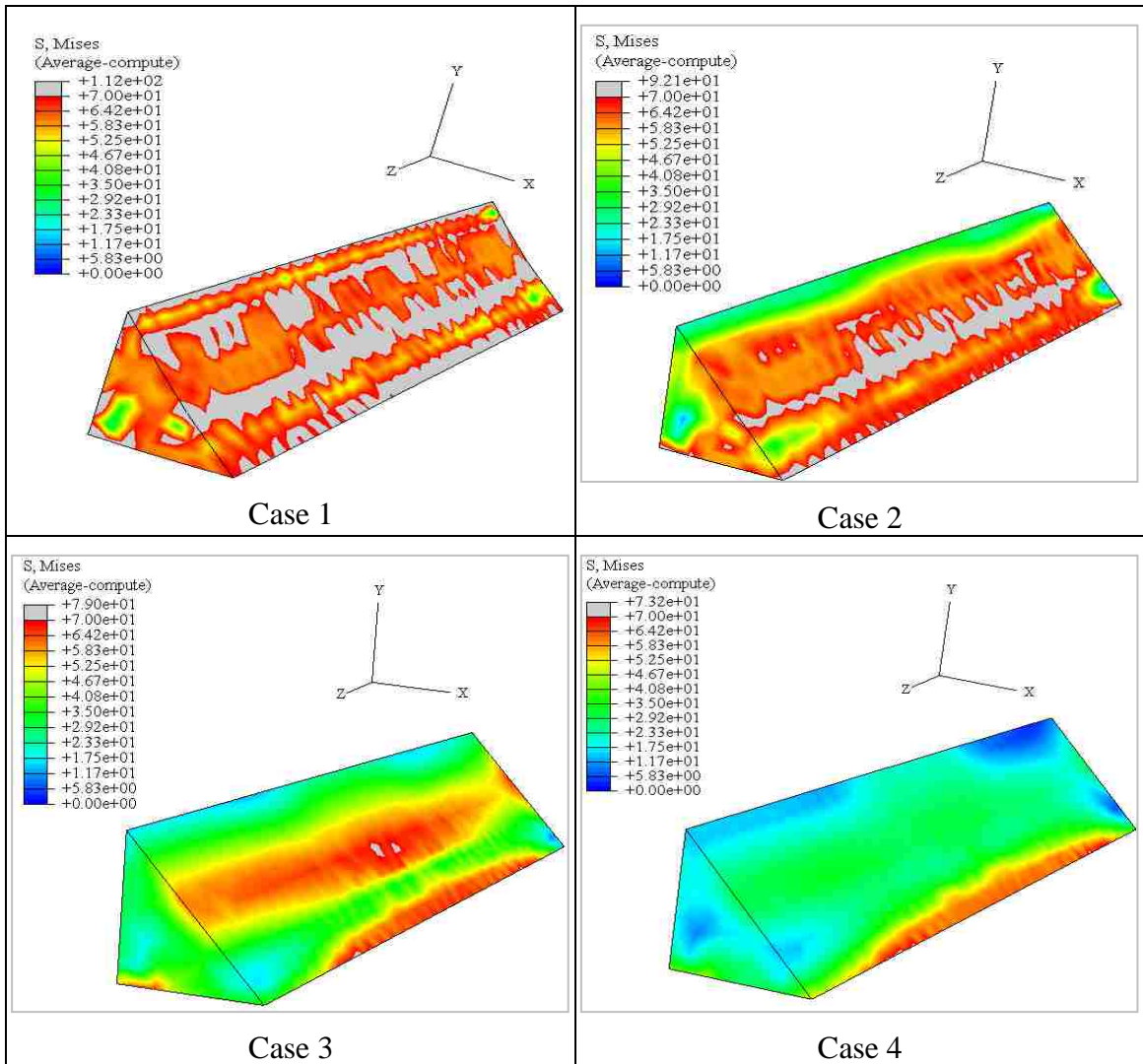


Figure 9.21. Von Mises stress contour of faceplate-to-slug fillet weld in various cases at a joint opening of 1.2-in

At the targeted joint opening of 0.6-in

The Von Mises stress distributions of faceplate-to-slug fillet weld at the targeted joint opening of 0.6-in in all of the cases are indicated in Figure 9.22. To get a clear illustration and comparison, the maximum limits of contour in all of the cases are set to

be the 70-ksi as well, which is the ultimate strength of E7018 electrode used for fillet weld. The results indicate that the no premature fillet weld failure occurs in case 2, case 3 and case 4 at the targeted deformation capacity of 0.6-in.

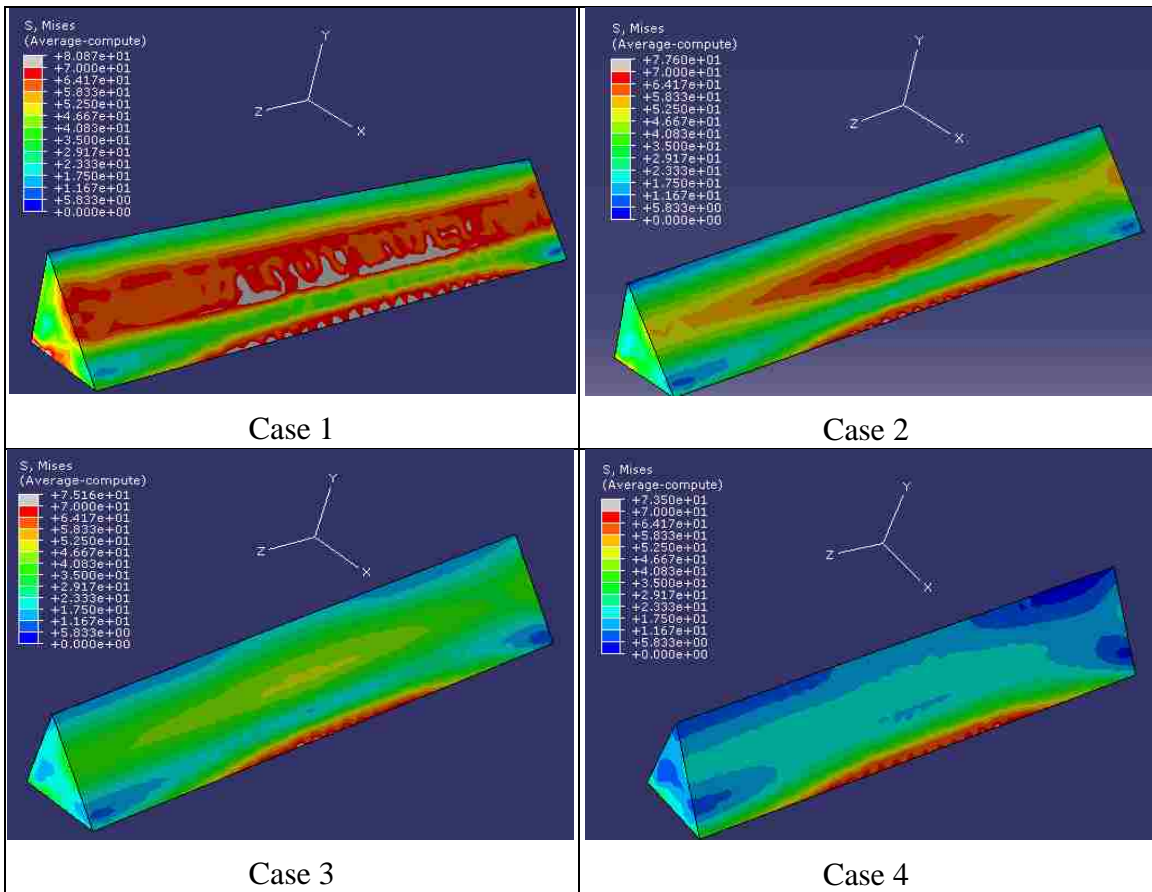


Figure 9.22. Von Mises stress contour of faceplate-to-slug fillet weld in various cases at a joint opening of 0.6-in

9.3.2.6 Slug

The Von Mises stress distributions of slug in all of the cases are indicated in Figure 9.23. To get a clear illustration and comparison, the maximum limits of contour in

all of the cases are set to be the 58-ksi, which is the ultimate strength of A36 plate used for slug.

As illustrated in Figure 9.23, in the first case, high stress concentration occurs in the interface region between fillet weld and top surface of slug. Failure may occur in the high stress region. A very small portion of slug has stress higher than the ultimate strength capacity of slug in the case 2 and case 3 while the other portions perform well. The stress of entire slug in the fourth case is less than its ultimate strength capacity. The performance of slug is also affected by the vertical weld location.

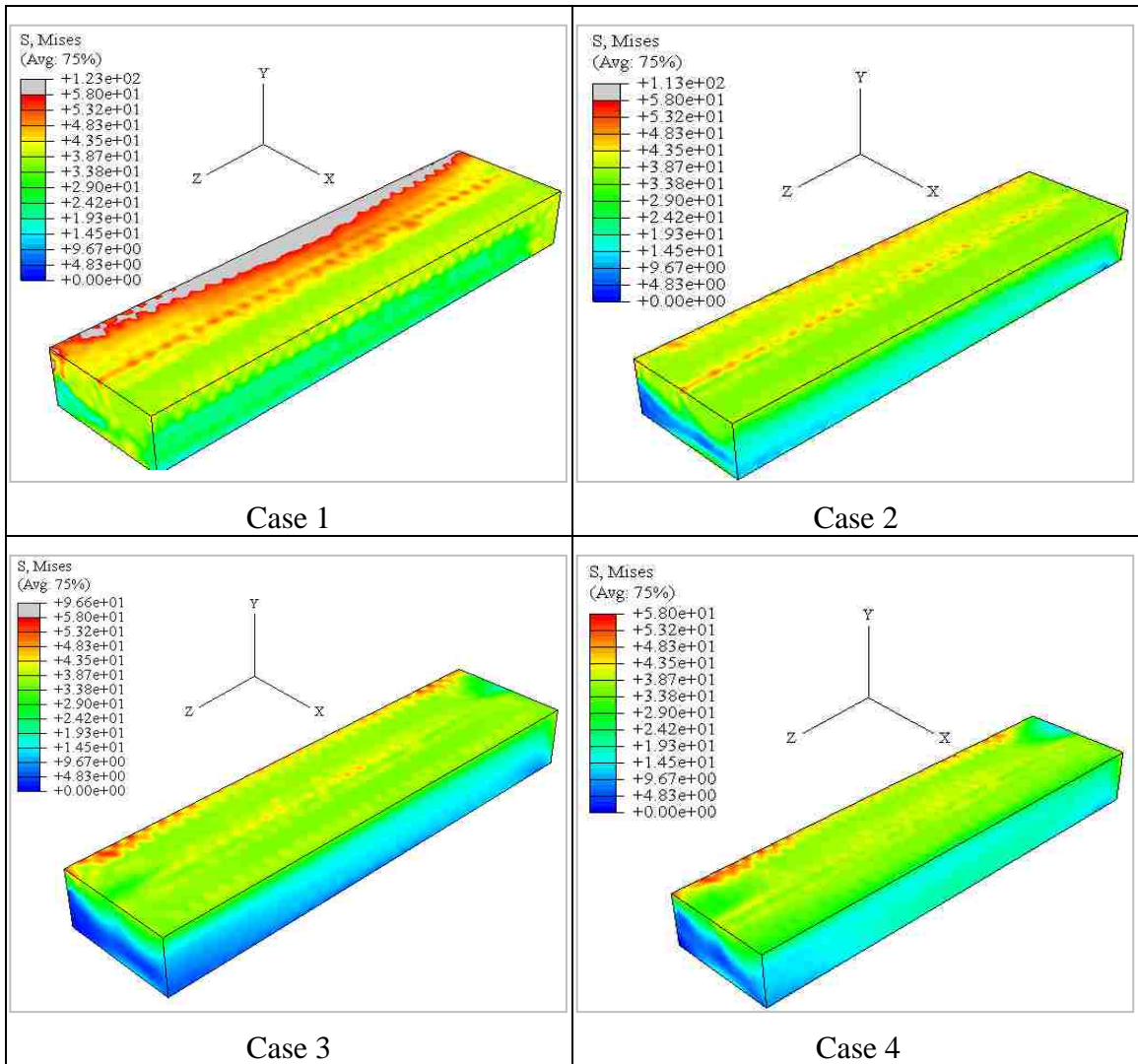


Figure 9.23. Von Mises stress contour of slug in various cases

9.3.3 Global Force-displacement Performance

The global axial force-displacement relationships of the new dry chord connector in all of the cases are indicated in Figure 9.24. The expected yield strength, ultimate strength capacity and the targeted deformation capacity of the connection are also shown in the figure for comparison. It is noted that the axial displacement illustrated in the

figure is the result of a pair of dry chord connector by using an amplification factor of 2 for the FE analysis results.

Generally, the global load-deformation response of the FE analysis correlated well with the expected strength performance. As for the targeted deformation capacity, the joint openings in all of the cases are able to reach 0.6-in before failure occurs. The new developed dry chord connector can be categorized in the high deformability element (HDE) category. In the first case, the weld hits its strength limit and starts to exhibit hardening behavior right after 0.6-in joint opening, no further ductility could be developed. Therefore this case is not recommended to use. All the other three cases exhibit high ductility, of which the case 4 has the best performance.

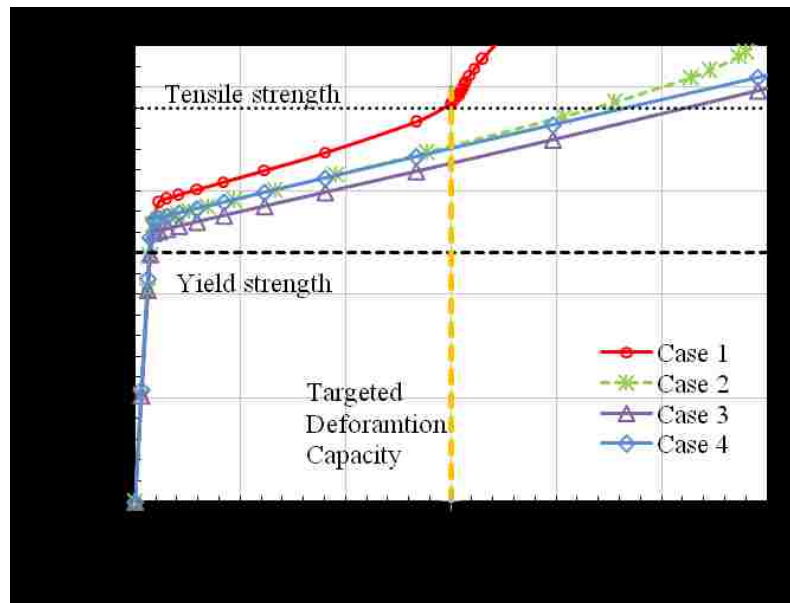


Figure 9.24. Axial force-displacement performance of a pair of dry chord connector

9.3.4 Discussion

As discussed previously, the ideal position will be the center of slug is in line with the center of standard modular system based on simply free body diaphragm (FBD) analysis. However, the results of FE analysis show that adding vertical eccentricity between the slug and the anchorage bar does not necessarily initiate premature failure.

The performance of connector assembly which includes rebar, standard modular system, fillet weld and slug in all of the cases at a same time step during loading is shown in the Figure 9.25. Both deformed shape and undeformed shape are shown for comparison. A deformation scale factor of 100 is used in all of the cases for better illustration. It is noted that concrete panel is also analyzed with the connector, however the performance of the concrete panel is not shown here due to the deformation of connector is limited in the gap between yield shaft and concrete panel. The results show that adding vertical eccentricity between the slug and the anchorage bar causes flexural moment in the anchorage bar, which can be illustrated by the stress distributions of anchorage bar in all of the cases. No flexural stress caused in the anchorage bar for the first case while the case 4 has the highest flexural stress in the rebar. This effect is not significant though. However, the performance of standard modular system is not controlled by this mode because of its high ductility. For the local modular system, the performance of yield shaft is controlled by deforming of faceplate. In the first case, the rotation of faceplate is largest, which cause the maximum flexural deformation in the

yield shaft. While in the case 4, the rotation of faceplate is smallest, in turn developing minimum flexural deformation in the yield shaft.

Since the design philosophy of the new dry chord connection is to develop yielding and plastic deformation in the yield shaft instead of anchorage bar as in the conventional chord connection, therefore the performance of local components should be evaluated carefully by using FEM techniques.

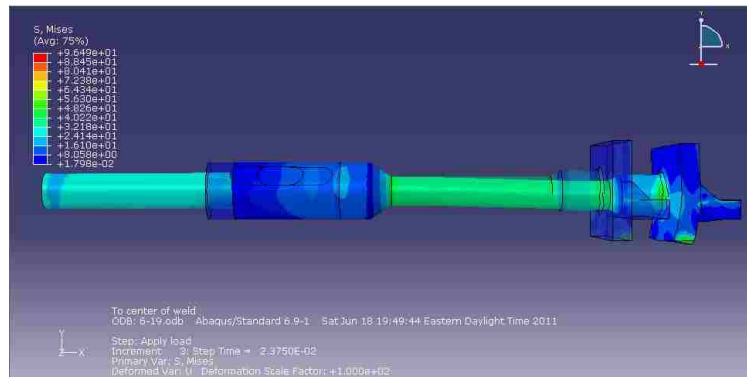
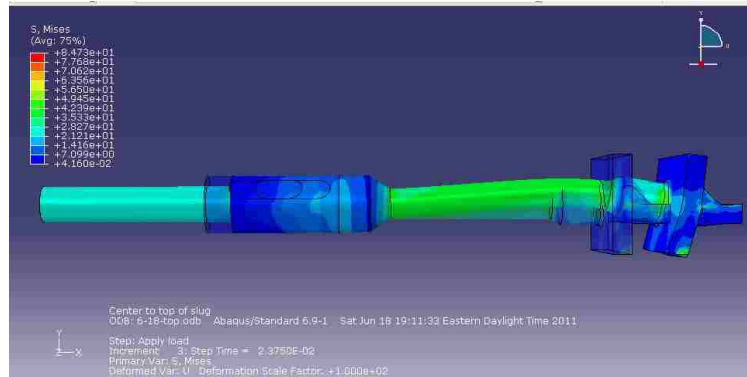
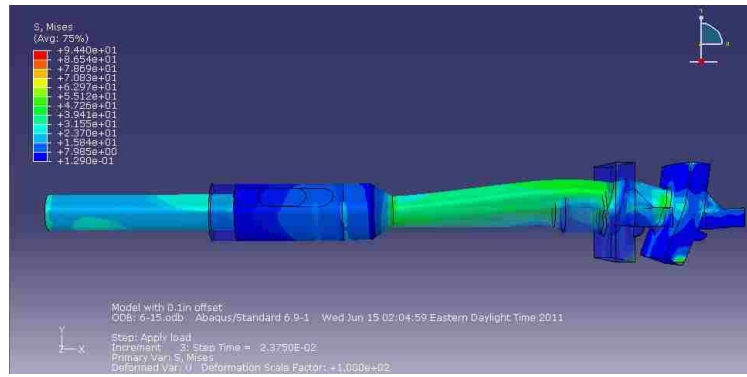
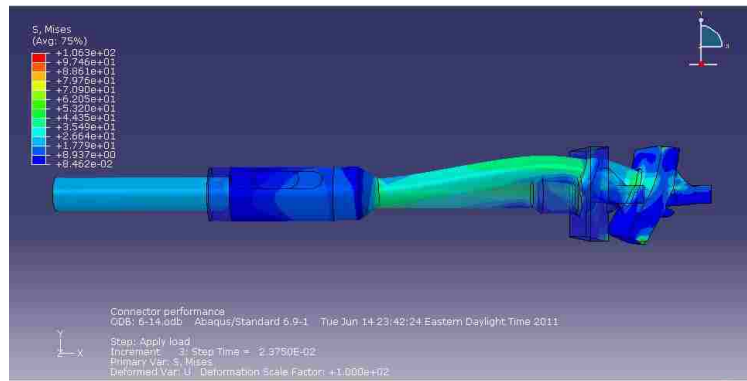


Figure 9.25. Performance of connector at same time step in various cases

9.3.5 Summary of Tension Behavior

A dry chord connection for the precast systems is advantageous from both an economic and construction scheduling perspective. A new dry chord connection is developed in this research to improve the brittle response of existing dry chord connections.

To examine the strength and deformation capacity of the new developed connection a finite element model is developed and a parametric study of vertical weld location is undertaken. The following conclusions can be made:

- The actual response of various components of the new developed dry chord connector is complex and cannot be accurately predicted by the simple FBD analysis. The connector has the best global and local behavior when the center of faceplate is line with the center of weld, while the performance is worst in the case when the center of faceplate is line with the center of slug.
- The deformed shape of connector varies with the vertical location of faceplate-to-slug weld. Significant flexure and rotation occurs in the faceplate and yield shaft if the center of faceplate is in line with the center of slug. An increase of offset in downside direction reduces the flexure deformation demands.
- Stress concentration of concrete panel occurs in the contact surface between the faceplate and the panel. The situation of stress concentration in the panel is

improved as the vertical offset increases in the downside direction. A bearing pad around bottom of faceplate may be used to reduce the stress concentration.

- Stress concentration and distribution of faceplate and yield shaft is sensitive to the vertical weld location, a more uniform and lower stress occurs in these regions as the weld offset increase. A premature failure of faceplate may occur in the case when the center of faceplate is line with the center of slug.
- Stress concentration of anchorage bar and plug weld occurs in the interface region between rebar and plug weld, the behavior of anchorage bar and plug weld is not sensitive to the vertical weld location. No premature failure occurs in the rebar and plug weld.
- Stress distribution of faceplate-to-slug fillet weld is very sensitive to its vertical location. Stress concentration of fillet weld occurs in its center and boundary regions. A premature failure of weld failure may occur in all cases. Additional tensile demands on the weld are caused by the faceplate flexural deformation and eccentricity of tensile loads applied. The situation is significantly improved in the case when the center of faceplate is in line with the center of weld. More attention should be paid to the design of faceplate-to-slug weld. It is recommended that the weld is detailed by considering the additional flexural demands caused by the tensile loading to prevent premature weld failure.

- Stress concentration of slug occurs in the interface region between fillet weld and top surface of slug. The situation of stress concentration in the slug is improved as the vertical offset increases in the downside direction.
- The global load-deformation relationship of the new dry chord connector is not sensitive to the weld location as long as it is located in an appropriate region. The proposed allowable offset is (0.1-in, 3/8-in) from the center of faceplate to the center of slug when moving the weld in the downward direction.
- With appropriate locations of faceplate-to-slug weld, the new developed dry chord connector is able to develop desired failure mechanism and achieve the expected strength and deformation capacities.

9.4 Design Recommendation

The design procedure and details of the new proposed dry chord connection is presented in Chapter 8. Additional design recommendations based on the FE study of connection tension behavior are discussed in this section. The following suggestions are recommended.

- A bearing pad around faceplate is recommended to use in order to reduce the bearing stress concentration in the concrete panel and faceplate.
- The faceplate-to-slug weld is better to be sized by considering additional flexural demands caused by load eccentricity.

- The center of faceplate-to-slug weld is recommended to be located in line with the center of faceplate to achieve a desired connection performance.
- An allowable offset of fillet weld in field construction is (0.1-in, 3/8-in) from the center of faceplate to the center of slug when moving the weld in the downward direction.

9.5 References

1. Aswad, A. (1977). "Comprehensive Report on Precast and Prestressed Connections Testing Program." Research Report, Stanley Structures, Inc, Denver, Colorado.
2. Wan, G. and Fleischman, R.B. (2006). "Parametric Study on the Overstrength of Shear Reinforcement in Untopped Precast Concrete Diaphragms." *Proceedings of the 8th US National Conference on Earthquake Engineering*, San Francisco, CA.
3. Pincheira, J. A., Oliva, M.G., and Kusumo-Rahardjo, F. I. (1998). "Tests on Double Flange Connectors Subjected to Monotonic and Cyclic Loading." *PCI Journal*, 43(3) 82-96.
4. Cao, L. (2006). "Effective Design of Precast Concrete Diaphragm Connections Subjected to In-Plane Demands", Ph.D dissertation, Lehigh University, Bethlehem, PA
5. ABAQUS (2009), *ABAQUS/Standard User's Manual: Volume I – III*, version 6.9, Hibbitt, Karlsson, and Sorenson, Inc., Pawtucket, Rhode Island.

Chapter 10 Conclusions and Future Work

A comprehensive study of precast concrete diaphragm DT connection is conducted in this dissertation. The connection studies include development of a standard experimental approach to evaluate any existing or new developed DT connections, experimental investigations of representative improved ductile connections, establishment of a connection details database and connection performance database, development of numerical estimation approach for multi-connection joint performance, experimental program developed for investigation of multi-connection joint, design of new ductile dry chord connection, and analytical investigations of the new developed dry chord connection.

This chapter summarizes the conclusions of the work presented. Suggestions on future work are also presented.

10.1 Summary

The primary objective of the dissertation research is to examine the behavior of precast concrete diaphragm DT connections and develop enhanced connection details to ensure a desired ductile performance. To accomplish this objective, a comprehensive experimental and analytical investigation is conducted. Summary of each phase is presented as follows.

First, an experimental evaluation approach for assessing the mechanical properties of embedded connections used in conventional precast concrete panel systems is developed. Adherence to this evaluation method allows connection properties to be determined in a repeatable, reproducible, and consistent manner so that existing and new connections can be quantified and utilized effectively in the diaphragm system. The proposed evaluation method provides a detailed test procedure for determination of stiffness, deformation capacity, and force capacity. The test procedure includes details on developing a test module, loading setup, instrumentation, load protocols, testing guidelines, testing observations, data acquisition and test report. A procedure of developing a four point multi-linear backbone curve is developed to simplify the measured experimental data, and then the performance characteristics of the connector are quantified from the backbone response. The measured connector deformation capacities are tied to performance levels which are used to categorize connectors into low-deformability element (LDE), a moderate-deformability element (MDE), or a high-deformability element (HDE).

An experimental program is conducted on representative connection details in accordance with the proposed experimental evaluation approach. Based on a review of previous research, four discrete improved precast diaphragm chord and web connections are selected for evaluation. These connections were developed by previous researcher to improve the poor performance of conventional diaphragm connections. The test subassembly is developed to represent condition of the connection embedded in the precast concrete element. The connection behavior under in-plane tension, shear, and

combined tension with shear is examined with a multi-directional test fixture utilizing three displacement-controlled actuators. The test fixture allows for the simultaneous control of shear, axial, and potential bending deformations at the panel joint. Six loading protocols are used to represent the spectrum of demands a local individual diaphragm connector could experience under lateral loading. These loading protocols include monotonic tension, cyclic tension and compression, monotonic shear, cyclic shear, monotonic shear with target axial force and cyclic shear with targeted axial force. Twenty monotonic and cyclic tests are conducted on the four representative connection specimens to identify the stiffness, strength and deformation capacity of individual connections under in-plane demands. The measured test results are compared to design expectations, and failure mechanisms of individual connections are identified. Effect of cyclic loading and axial force control for shear test is examined. The effectiveness of improved design details is evaluated.

In addition to the four improved connections presented in the dissertation, experimental evaluation is also conducted on various existing diaphragm connections. A total of over 200 tests are conducted in the dissertation research program. Each individual test is conducted by following the guideline of recommended evaluation methodology. A diaphragm connection details database is established by incorporating all the existing mechanical connections in use and the new improved connections. The proposed four point multi-linear backbone curve is used to simplify the measured connection response. The backbone curves of all the connections are incorporated into a comprehensive connection performance database. The database includes three chord connectors and

thirty-five varieties of web connectors. This database provides stiffness, strength and deformation properties of each connector detail examined. The connectors are divided into one of three displacement based categories: low deformation element (LDE), moderate deformation element (MDE) or high deformation element (HDE) based on the performance measured in the experiments. The connection performance database provides important information for model and design needs of DT connection and diaphragm system.

To provide a simple method for practicing engineers to estimate the flexural and shear responses of diaphragm system instead of using FEM techniques. A simplified pushover modeling approach is developed to estimate the maximum midspan flexural deflection and shear sliding of a diaphragm for a statically applied uniform load by utilizing the connection performance database information. This method begins with developing shape functions of joint moment-rotation and shear-sliding deformation responses using along with the information included in the performance database, and then estimate the in-plane flexural and shear resistance-displacement responses of the diaphragm system. The results generated by this simple pushover method gives design engineers a rough estimation of flexural and shear responses of diaphragm. Furthermore, varying the connector used can be helpful to provide guidance about choosing appropriate connector types for diaphragm to meet design requirements. The application of this method is conducted on the three cases of diaphragm system designed with web connectors in LDE, MDE and HDE categories.

As part of the collaborative DSDM project, an experimental program associated with integrated experimental and analytical evaluation of the seismic behavior of critical multi-connection joints of precast concrete diaphragm system is developed in this dissertation work. A multi-directional test fixture is developed to allow for simultaneous control of shear, axial and bending deformations at the panel joint during earthquake simulations. The test fixture utilizes three actuators with the capacity of 281-kips, two in axial displacement and one in shear displacement. Two specimens of critical flexural and shear joints are designed and fabricated for evaluation. The test specimens are detailed using diaphragm connections intended to meet deformability requirements. The test is conducted at a half-scale. The critical flexural joint is evaluated under predetermined displacement histories (PDH) and the critical shear joint is evaluated using hybrid testing techniques. The load protocols applied to the test specimens are provided by project members in University of Arizona.

The findings related to the experimental study of conventional dry chord and improved dry chord connection indicates these connections cannot achieve their strength capacity and the connection fails with limited ductility due to premature weld failure. To provide a ductile dry chord connection for diaphragm system in high seismic zone, an innovative dry chord connection is developed. A ductile design concept is used for development of design details. The new dry chord connection is targeted to achieve the expected strength capacity with high ductility at a low cost. In order to avoid the premature failure of welds located between faceplate and anchorage bars, a standard module system which serves as the connection piece between faceplate and anchorage

bars is used instead of conventional weld technique. This piece can be prefabricated using cast steel. The modular system with single anchorage rebar can be stacked laterally to resist the design loads for particular diaphragm system.

To evaluate the performance of the new dry chord connection and further improve the design details, analytical examination of the connections is conducted by developing detailed 3D FE model. To properly model the connection performance, appropriate modeling techniques are established. Detailed numerical models are developed to capture characteristics of the concrete, connector and the concrete-connector interactions. Using these techniques new dry chord connector and surrounding concrete element are modeled. The behavior of the connector under tension loading is investigated, a parametric study on vertical weld location is conducted and design recommendations are provided.

10.2 Conclusions

Conclusions made in this dissertation research are divided by topics.

On the basis of the study that develops an evaluation method for precast DT connections based on structural testing, the following conclusions can be made:

1. The stiffness, strength and deformation properties of diaphragm connector are important inputs of the new developed performance based diaphragm design methodology.

2. Connection deformation capacity under in-plane tension and shear is contingent on a series of inelastic failure modes, which include concrete breakout, yield of the anchorage bars, flexure or torsion of the faceplate, yield of the slug or jumper plate, fracture of the welds, or fracture of the faceplate or anchorage.
3. Connection stiffness and strength capacity is dependent on the details of the connector, amount of embedment, and welding techniques used to attach the two connectors.
4. Due to the variety of connections in use, it is not practical to assess connection performance based on generalized analytical response formulations. Proper determination of the strength and deformation capacity of connections is best determined through experimental evaluation.
5. A standard experimental evaluation approach can be used to assess in-plane strength, stiffness, and deformation properties in a repeatable, reproducible, and consistent manner.
6. To evaluate the performance of a precast concrete connection a test module representing the connection and the precast concrete element it is embedded in shall be fabricated and tested.
7. For each connection test a multi-directional test fixture shall be used to allow for the simultaneous control of shear, axial, and potential bending deformations at the panel joint. At a minimum instrumentation shall consist of displacement and force transducers.

8. An in-plane monotonic tension test shall be conducted to determine the initial reference deformation for use in the cyclic tension tests. Two alternative (non-experimental) methods may be used for determination of the reference deformation if applied.
9. In-plane cyclic tension tests shall be conducted to failure to determine stiffness, strength capacity and deformation capacity of connection under tension loading. The measured tension deformation capacity shall be used to establish the performance category of the connection.
10. An in-plane monotonic shear test shall be conducted to determine the initial reference deformation for use in the cyclic shear tests. Two alternative (non-experimental) methods may be used for determination of the reference deformation if applied.
11. In-plane cyclic shear tests (with a constant 0.1 in. axial opening) shall be conducted to failure to determine stiffness and strength capacity of connection under shear loading.
12. In-plane monotonic shear with proportional tension tests may also be conducted for the connections used in intermediate diaphragm regions. In-plane cyclic shear with a target axial load tests could be conducted if needed.
13. For in-plane tests the data of axial and shear force, and deformations should be recorded. Photographs shall be taken to illustrate the condition of the test module at the initiation and completion of testing as well as points through the testing history.

14. A four point multi-linear backbone curve can be used to represent a simplistic approximation of the load-deformation response of the connection. Determination of this simplified backbone curve is presented in Eq. 3-7 to Eq. 3-12.
15. The initial elastic stiffness of the connection shall be determined from the secant to yield point 1.
16. The yield deformation shall be defined at Δ_1 , the max deformation at Δ_2 , and the residual deformation at Δ_3 . For deformation-controlled connections the deformation capacity shall correspond to Δ_2 . For force-controlled connections the deformation capacity shall correspond to Δ_1 . The connection deformation capacity shall be determined as the mean value of each test deformation capacity for deformation-controlled elements and the mean minus one standard deviation for force-controlled connections if multiple tests conducted.
17. The connection shall be classified as a low-deformability element (LDE), a moderate-deformability element (MDE), or a high-deformability element (HDE) based on its deformation capacity in tension.
18. The tension force capacity of the connection is defined as the maximum force, P_2 for deformation controlled connections and as P_1 for force controlled connections.
19. The shear force capacity shall be computed at force level P_1 for all connections due to the intention of the diaphragm system to remain elastic under shear demands. Due to the existence of low stiffness connections limits are placed on the allowable deformation at which the force capacity, P_1 , can be determined slightly differently.

20. To provide accurate stiffness, strength, and deformation capacity multiple tests for shear and tension are recommended. The connection performance shall be tied to the number of tests conducted.

On the basis of the study that evaluates the behavior of improved diaphragm connections in accordance with the proposed evaluation method, the following conclusions can be made:

1. The improved connections exhibit a wide range of strength and ductility under tension loadings. The carbon chord and stainless chord connections provide relatively high tension resistance while the web connections ductile ladder and ductile ladder with hairpin provide a moderate resistance.
2. The majority of these improved diaphragm connections are unable to meet their expected ultimate tensile strength capacities. Failure of the field welds and fracture of the anchorage bars are the primary failure modes.
3. As fabricated from the special type of WWR without cold-drawn process, the ductile ladder connector exhibits a high ductility and is capable of maintain expected force capacity. A thicker concrete cover is recommended for ductile ladder connector to avoid premature loss of concrete panel.
4. The ductile ladder with hairpin connector is not able to achieve its ultimate capacity due to the premature weld failure. The tension performance of the ductile ladder with hairpin connector is similar to ductile ladder connector, the yield

occurs at 0.05-in tensile opening and the maximum force capacity occurs at 0.4-in tensile opening for both connectors.

5. The enhanced carbon and stainless chord connector is able to achieve its tensile design strength capacity. The ductility of connection is improved by using the unbonded techniques compared with the conventional dry chord connection, however, is still not able to meet the design demands.
6. Cyclic tension loading alters the failure mechanism and reduces the connection strength and deformation capacity. The majority of connections fail at a smaller deformation level than the monotonic test. The initial stiffness, however, is not affected.
7. The improved connections exhibit a wide range of shear strength and ductility under shear loadings. The web connections ductile ladder and ductile ladder with hairpin provided relatively high shear resistance while the chord connections provided a moderate shear resistance.
8. The shear strength of diaphragm connections can be estimated by neglecting any bearing mechanism and relying on ACI shear friction model. ACI Formulations are presented and shown to compare with experimental results. Appropriate shear friction coefficient need be used to simulate the interface condition and achieve accurate strength estimations.

9. The majority of these improved diaphragm connections are unable to meet their expected ultimate shear strength capacities. Failure of the bar-to-faceplate weld and fracture of the anchorage bars are the primary failure modes.
10. Cyclic shear action has little effect on the connection's ultimate shear strength capacity and corresponding deformation capacity.
11. The monotonic/cyclic shear with targeted axial force control loading protocol loading reduces the stiffness and strength capacity of connection. The majority of connections have a higher level of strength capacity than the standard monotonic/cyclic shear test. However, the deformation capacity is rarely affected.

On the basis of the study that develops database of precast diaphragm connections and estimation modeling approach of diaphragm response based on database information, the following conclusions can be made:

1. Over 200 tests are conducted on three chord connectors and thirty-five varieties of web connectors. Of the web connectors, the deformation capacity of connections ranges from LDE to HDE for both shear and tension.
2. The majority, 67%, of web shear response is in the LDE range. The dry chord connectors are all categorized as MDE in tension. The conventional dry chord is categorized as LDE in shear and improved dry chords are categorized as MDE in shear.

3. The HDE connections exhibit the lowest strength and stiffness while the LDE connections result in the highest strength and stiffness. This correlation is most evident in the tension tests and less so in the shear tests.
4. The moment-rotation and shear-sliding deformation response can be determined for the multi-connection joint by using a simplified procedure presented in Eq. 6-1 and Eq. 6-2 based on database information.
5. The diaphragm flexural and shear resistance-deformation response can be estimated by using the method presented in Eq. 6-3 and Eq. 6-4 based on database information.
6. The diaphragm designed with connectors in different deformation categories influence the global diaphragm response.

On the basis of the studies on development of a ductile dry chord connection and analytical investigation of the new developed dry chord connection, the following conclusions can be made:

1. The conventional dry chord connection is unable to attain the expected design capacity due to the premature failure of the weld details. The bonded detail resulted in a limited deformation capacity.
2. The improved dry chord connection exhibits a better ductility than conventional chord connection by introducing a length of unbonded region. However, the desired ductile failure mechanism is not achieved due to failure of bar-to-faceplate weld.

3. A ductile design concept is used to develop ductile mechanism in the connector through overstrength factors.
4. A standard casting modular system which serves as the connection piece between faceplate and anchorage bars is used instead of conventional weld technique to avoid premature bar-to-faceplate weld failure.
5. 3D finite element modeling can be used to simulate the new developed dry chord connection subjected to in-plane tension demands. Accurate modeling techniques involve appropriate constitutive models of the connection components. Steel behavior modeled using Von Mises yield criteria and the interface relation modeled with surface-to-surface contact behavior can identify the chord connection tension characteristics.
6. The actual response of various components of the new developed dry chord connector is complex and cannot be accurately predicted by the simple FBD analysis.
7. Stress concentration and distribution of faceplate, yield shaft, faceplate-to-slug weld and slug is sensitive to the vertical weld location. The local performance of these components can be improved as the vertical offset increases in the downside direction.
8. The behavior of anchorage bar and plug weld is not sensitive to the vertical weld location.
9. The global load-deformation relationship of the new dry chord connector is not sensitive to the weld location as long as it is located in an appropriate region.

With the appropriate weld locations, the expected strength and deformation capacities could be achieved.

Based on the analytical studies, the following recommendations on the new dry chord connection design are made:

1. A bearing pad around faceplate is recommended to use in order to reduce the bearing stress concentration in the concrete panel and faceplate.
2. The faceplate-to-slug weld is better to be sized by considering additional flexural demands caused by eccentricity of load applied to the connection.
3. The center of faceplate-to-slug weld is recommended to be located in line with the center of faceplate to achieve a desired connection performance.
4. An allowable offset of fillet weld in field construction is (0.1-in, 3/8-in) from the center of faceplate to the center of slug when moving the weld in the downward direction.

10.3 Unique Contribution

The dissertation work is part of a multi-university research project to develop an industry-endorsed seismic design methodology for precast concrete floor diaphragms.

The dissertation work has made the following unique contributions:

1. Develop a standard experimental evaluation methodology to assess connector stiffness, strength capacity and deformation capacity in a repeatable, reproducible and consistent manner.
2. Perform over 200 experimental tests on existing and improved individual diaphragm chord and web connections. The connections are evaluated under in-plane tension, shear and combined tension with shear demands.
3. Establish a comprehensive connection performance database for use in model and design of diaphragm system.
4. Develop a simplified pushover modeling approach to estimate the diaphragm flexural and shear resistance-deformation response based on database information.
5. Design a full scale multi-direction test fixture which allows simultaneous control of shear, axial and bending deformations exhibited at the panel joint during earthquake simulations to evaluate the performance of critical multi-connection joints.
6. Design the test specimen of critical joints, instrumentation and perform the PDH and hybrid tests of joints.
7. Design and development of an innovative ductile dry chord connection.
8. Develop a detailed 3D finite element model for examining the behavior of the new developed dry chord connection subjected to in-plane tension demands.
9. Develop design recommendation for the new dry chord connection based on the analytical studies.

10.4 Future Work

This section proposes some suggestions and ideas on possible future work that could be conducted on topics related to the precast concrete diaphragm double tee connections.

While the database of connection detail and database of connection performance incorporated a significant amount of existing and new developed connections used in current practice, the connection detail database should be extended by adding more connection types when available. Most of the connections in the performance database are not evaluated using multiple test approach due to financial reason, the ultimate force capacities labeled with * are not recommended for direct design use. This issue can be improved by conducting multiple tests on these connections to get reliable design strength.

Analytical studies should be conducted to examine the performance of the new developed dry chord connection under in-plane shear, combined shear with tension and out-of-plane shear load demands. Parametric studies should be conducted to improve the understanding of the connection behavior and further optimize the design details. Experimental studies on the new dry chord connection should be conducted to verify the analytical results. These findings can be used to finalize the design details.

Vita

Ruirui Ren was born on the day of December 14th in the Chinese lunar calendar in 1981. She is the daughter of Fujun Ren and Aili Ren. She grew up happily with her beloved younger brother Kaikai in Luoyang, Henan Province of China.

She received a Bachelor of Science degree in Civil Engineering with honors and a Master degree in Structural Engineering with honors from Xi'an University of Technology in 2003 and 2006, respectively. Ruirui began to pursue her Ph.D. in structural engineering at Lehigh University in August, 2006. At the same time, she worked as a Research Assistant at the ATLSS research center. Her research work focused on the precast concrete diaphragm connections.